Inter-penetrating Polymer Network (IPN) Tissue Expanders

Thesis submitted to the University of Oxford for the degree of Doctor of Philosophy

Yun Zhu
Trinity Term 2015
St Anne's College

Abstract

Inter-penetrating Polymer Network (IPN) Tissue Expanders

Thesis submitted for the degree of Doctor of Philosophy, Trinity Term 2015

Yun Zhu, St Anne's College

Self-inflating hydrogel tissue expanders have drawn great interest for generating new soft tissue in plastic and reconstructive surgeries. However, their over-rapid expansion rate can lead to tissue necrosis. Additional coatings or membranes can provide controlled swelling, but will be damaged upon crafting. This study is concerned with developing a novel inter-penetrating polymer network (IPN) tissue expander with controlled expansion and the ability to be crafted by surgeons as well.

Firstly, VP/MMA-PLGA IPN has been prepared by crosslinking a secondary PLGA network in the presence of a primary VP/MMA network. The incorporation of PLGA effectively decreases the initial swelling rate and extends the swelling period. It is the only self-inflating tissue expander at present with controlled swelling and the ability to be crafted by surgeons. However, the equilibrium swelling ratio is sacrificed with increased PLGA weight fraction, which will limit the application of this IPN expander to surgeries that only need small tissue expansions, such as anophthalmia, eyelid, lip or nose reconstructions.

Secondly, PLGA has been replaced with alternative secondary polymer networks, PLA and PCL to prepare IPN hydrogels. The swelling behaviour of VP/MMA-PLA IPN and VP/MMA-PCL semi-IPN is closely linked with the hydrophobicity and weight fraction of the secondary network, regardless of its glass transition temperature or crosslinking condition. At a similar weight fraction, the more hydrophobic the secondary network, the lower the initial swelling rate and the equilibrium swelling ratio, and the longer the swelling period.

Thirdly, HEMA, VP/HEMA, and HEMA/SA bulk hydrogels have been prepared as alternative primary networks. Hydrogels show an increased swelling capacity with increased content of VP or SA, but at the expense of mechanical properties at the swollen state. Both HEMA and VP/HEMA show a low swelling, which might not be enough to induce tissue expansion. HEMA/SA shows superior swelling in distilled water but minimal swelling in non-polar solvents.

Finally, the in vivo study of VP/MMA-PLGA IPN has been performed in a sheep model. The IPN hydrogels successfully generate tissue growth with the same quality as natural skin tissue and without any signs of serious inflammation or tissue necrosis. The rapid degradation of PLGA in vivo can cause the loss in mechanical integrity, leading to hydrogel collapsing under the restorative force of the skin. But this could be solved by tuning the ratio of lactide to glycolide in PLGA.

Acknowledgements

First of all, I would like to thank my supervisor, Professor Jan Czernuszka for his supervision, support and patience throughout those years. I would also like to thank my group members Jessica, Michelle, Xuan, Chen, Kerem, Rabia and Narjes. I could not have arrived here without their help.

NMR experiments were done by Dr Tim Claridge(Chemistry Department, Oxford). And I would like to thank him for the kind help.

SANS experiments were done by Dr Stephen King and Dr Sarah Rogers(ISIS, Didcot, UK). And I would like to thank them and Dr Mark Telling for their help with the experiments and SANS interpretations.

The in vivo study was done by University of Malaya(Kuala Lumpur, Malaysia). And I would like to thank Zamri, Sze, Elia, Fadhil for their kind help with the animal test.

And I would like to thank my friends, Yisu Wu, Jingjing Le, Min, Haibo, Xiaohe for their help, support and suggestions, especially in the final year of my DPhil life. And my housemates, Anne, Barbara, Emilie, Jiajun for their caring and loving.

Finally, I really want to thank my parents and Yuan Yuan, for their understanding and caring through those years.

List of Abbreviations

AA	Acrylic acid
AIBN	Azobisisobutyronitrile
BIS	N, N'-methylenebisacrylamide
DCM	Dichloromethane
DMA	Dynamic Mechanical Analysis
DSC	Differential Scanning Calorimetry
EGDMA	Ethylene glycol dimethacrylate
EWC	Equilibrium water content
HEMA	2-hydroxyethyl methacrylate
KPS	Potassium persulfate
MMA	Methyl methacrylate
NMR	Nuclear Magnetic Resonance
PAA	Polyacrylic acid
PAAm	Polyacrylamide
PBS	Phosphate buffer saline solution
PCL	Polycaprolactone
PCL semi-IPN	VP/MMA-PCL semi-IPN hydrogels
PEG	Polyethylene glycol
PGA	Polyglycolic acid
PHEMA	Poly(2-hydroxyethyl methacrylate)
PLA IPN	VP/MMA-PLA IPN hydrogels
PLGA	Poly(lactic-co-glycolic acid)
PLGA IPN	VP/MMA-PLGA IPN hydrogels
PMMA	Poly(methyl methacrylate)
PNIPAAm	Poly(N-isopropylacrylamide)
PVP	Poly(vinyl pyrrolidone)
SA	Sodium acrylate
SANS	Small angle neutron scattering
SEM	Scanning Electron Microscopy
VP	Vinly pyrrolidone
VP/MMA	Poly(vinly pyrrolidone-co-methyl methacrylate)

List of Symbols

ξ	mesh size
φ_s	polymer volume fraction
Q_v	volume swelling ratio
Q_∞	equilibrium swelling ratio
R_i	initial volume swelling rate
T_e	swelling period(time taken to reach equilibrium)
γ_e	effective crosslinking density
χ	Flory-Huggins interaction parameter
M_c	average molecular weight between crosslinks
f	crosslinker functionality
V_1	molar volume of water
R	universal gas constant
T_g	glass transition temperature
E	compressive modulus
E_d	specific modulus (E divided by density)
E_n	normalized modulus (E times $1-\varphi_s$)
E_s	modulus of cell wall solid material(in a cellular structure)
ϕ	fraction of solid contained in cell edges

List of Figures

List of Tables

Contents

Chapter One: Introduction

1 Introduction

1.1 Objectives

Self-inflating hydrogel tissue expanders are opening a new way for the treatment of congenital defects or diseases that need soft tissue expansion. VP/MMA(poly(vinyl pyrrolidone-co-methyl methacrylate)) hydrogels have been used as the primary tissue expander. However, the application of VP/MMA is limited by its over-rapid expansion rate and a lack of control on the overall expansion which might lead to tissue necrosis. To obtain new skin tissue, numerous devices have specially prepared coatings or silicone envelopes to control the rate expansion. Unfortunately, they fail to be crafted by surgeons to fit the specific void volume on the patients as it will damage the coating or membrane and result in a local burst of expansion.

The objective of this study is to devise alternative methods for the delayed and controlled swelling of tissue expanders and particularly, with the ability to be crafted into various shapes and sizes by surgeons.

This study focuses on developing a self-inflating osmotic interpenetrating polymer network (IPN) hydrogel tissue expander which has an inherent controlled swelling with the introduction of a biocompatible, biodegradable polymer (e.g. PLGA) into an existing primary network (e.g. VP/MMA hydrogel). By tuning the composition ratio between VP/MMA and PLGA, the initial swelling rate, equilibrium swelling ratio, swelling period can all be varied and controlled. VP/MMA-PLGA IPN devices will be implanted in a sheep model and we aim to demonstrate the efficacy of the IPN hydrogel in vivo.

The construction of an interpenetrating polymer network offers various combinations of primary and secondary polymer networks. This study also searches for alternative

primary networks (such as HEMA, VP/HEMA, HEMA/SA) and alternative secondary networks (such as PLA, PCL) for the complementary properties of the IPN hydrogel. The primary requirements for a desirable tissue expander is good swelling capacity and the ability to maintain its mechanical integrity and original shape at the swollen state. This approach saves the trouble of preparing a permeable membrane or coating and gives the tissue expander an inherent controlled swelling, making it convenient for surgeons to craft it to serve complicated medical needs. IPN provides a new way to prepare tissue expanders with the possibility of acquiring combined desirable properties.

1.2 Thesis Outline

The thesis starts with a literature review related to this study. Tissue expansion and tissue expanders are reviewed in terms of the history, the materials and methods used, and the problems and limitations. Hydrogels are reviewed focusing on their swelling behaviour, the factors that affect the swelling and potential hydrogels to be used as tissue expanders. Inter-penetrating polymer networks are then reviewed pointing out their superiority over traditional hydrogels and the most widely studied IPN hydrogels at present.

Chapter 3 demonstrates the preparation and characterization of VP/MMA-PLGA IPN hydrogel tissue expanders. The swelling behaviour, mechanical properties and the internal structure will be examined as a function of PLGA weight fraction. The potential of controlling the expansion will be discussed.

Chapter 4 concerns alternative secondary polymer networks, PLA and PCL, for the preparation of IPN hydrogels. The swelling behaviour, the mechanical properties, the internal morphology of VP/MMA-PLA IPN and VP/MMA-PCL semi-IPN hydrogels will be discussed and compared with those of VP/MMA-PLGA IPN hydrogels. The

influence of the properties of the secondary polymer network on the swelling behaviour of the IPN hydrogels will be discussed.

Chapter 5 explores the alternative primary networks, HEMA, VP/HEMA and HEMA/SA hydrogels. The synthesis methods of bulk, crack-free hydrogels and their swelling behaviour and mechanic properties will be demonstrated. Their possibility to be used as the primary network of IPN hydrogels will be discussed.

Chapter 6 describes the in vivo study of the VP/MMA-PLGA IPN hydrogels. IPN hydrogels will be sterilized and implanted in a sheep model and their swelling behaviour and the histology results will be discussed.

Finally, Chapter 7 draws the conclusions of this study and Chapter 8 concerns with the future work.

Chapter Two: Literature Review

2 Literature Review

2.1 Definitions

2.1.1 Tissue Expansion

Additional soft tissue, especially skin tissue, is highly needed in plastic and reconstructive surgeries. The traditional method of using free grafts or flaps are not ideally suitable because of a lack of free grafts and the mismatch of colour and texture. The idea of growing new soft tissue locally would be convenient to solve those problems.

Skin is the largest organ of our body, which has the ability to generate new cells under chronic and proper stretch[1]. Normally, the skin is in a natural state of resting tension[2], at its biological equilibrium. Once stretched beyond the physiological limit, a series of stretch-induced signalling pathways are triggered[3]. Cells will convert mechanical stimulus into electro-chemical activity that will bring a cascade of changes in cytoskeletal structure, extracellular matrix, enzyme activity[1]. The skin cells will then replicate itself to restore the state of resting tension, thus generating additional soft tissue.

Using this particular ability of skin tissue, researchers have placed a rubber balloon beneath the skin to grow new tissue by adding air or fluids into the balloon via an injection point. This process is called tissue expansion and the materials implanted beneath the skin are called tissue expanders. Tissue expansion is a relatively new method to grow additional soft tissue that can be subsequently used to cover a permanent implant or a nearby defect.

2.1.2 Silicone Balloon Tissue Expander

The first tissue expander was introduced by Neumann[4] in 1957. Neumann inflated a

rubber balloon with air several times a week over 2 months. Skin had been observed to expand from 12 square inches to 18 square inches, which was sufficient to cover the cartilaginous graft in the repair of an avulsed ear. Later Radovan[5] used tissue expanders in post mastectomy breast reconstruction by intermittent injections of saline into silicone balloons. The saline water inflated silicone balloons can be produced in various sizes and shapes and are now widely used in the medical world. However, these manually inflated silicone balloons cause immediate tensions that compress blood supply and cause tissue hypoxia, resulting in skin necrosis and perforation[6]. The existence of the percutaneous filling port largely increases the incidence of infection and complications and manual inflation discomforts the patients[7]. Moreover, any leakage, rupture, or malfunction of the balloons or injection ports can cause serious problems[8].

2.1.3 Osmotic Tissue Expander

Because of the disadvantages of traditional silicone balloons, some researchers began to look into self-inflating tissue expanders made of biocompatible hydrogels using osmotic as a driving force in body fluids. In 1982 Austad and Rose[9] introduced a silicone balloon filled with sodium chloride wrapped with a semi-permeable silicone membrane. But the inflation periods were too long (8-14 weeks) and there were high risks of leakage and membrane rupture which would lead to saline exposure inside the body. Later in 1993 Wiese[10, 11] introduced a solid, self-inflating hydrogel expander using the copolymer of methylmethacrylate(MMA) and vinylpyrrolidone(VP). He verified the biocompatibility and swelling pressure of the VP/MMA hydrogel and suggested it had desirable properties in clinical applications. The swelling ratio of VP/MMA hydrogels was 250-300% when implanted in the body[10]. Higher swelling ratio could be achieved by replacing the $-CH_3$ groups in the copolymer chains with -COOH groups

which can dissociate into COO^- and H^+ leading to a higher osmotic pressure[11]. Figure 2.1 is the comparison between a conventional silicone balloon expander and a self-inflating hydrogel tissue expander with the same final volume. Conventional silicon balloon is much more cumbersome than the solid anhydrous hydrogel, requiring a much larger incision on the patient.

Figure 2.1 A conventional silicon balloon expander and a solid self-inflating hydrogel with the same nominal final volume (reproduced from [11])

2.1.4 Current Problems and Limitations

The use of tissue expanders not only regenerates skin tissue with the perfect colour and texture match for the patients but also provides possibilities for treatments that require soft tissue augmentation first. Osmotic tissue expander has been used in congenital anophthalmia[12], breast reconstruction[13], burnt skin reconstruction[14] and showed promising results. However, the over-rapid expansion rate and the lack of control on the expansion remain a big problem. Skin necrosis occurs if the expansion proceeds too rapidly. Excess tension may compress the blood supply of the local tissue that results in necrosis. The first generation of osmotic tissue expander lacked a permeable membrane and reached its maximum swelling one or two days after implantation, which caused skin ischemia and necrosis. The second generation of osmotic tissue expander was equipped with a semi-permeable silicone membrane which is 0.2 to 0.5 mm thick and

achieves slower swelling over 6-8 weeks[13]. Clinical tests[13, 14] have demonstrated the need to slow down the expansion rate to allow enough time for wound heal and tissue growth, and avoid wound dehiscence and tissue ischemia which will eventually lead to implant extrusion. A more gradual and delayed expansion not only decreases the rate of complications but also facilitates tissue expansion with more tissue grown as verified in a porcine model[15].

A desirable hydrogel tissue expander should have the following properties:

1. Self-inflating with good swelling capacity
2. Good biocompatibility, elasticity and mechanical integrity during expansion
3. Delayed initial expansion to allow enough time for wound heal and controlled expansion over time to avoid tissue necrosis and complications
4. The convenience to be easily crafted by the surgeon to best fit into the desired void volume of the defects

2.2 Hydrogels

2.2.1 Definition of Hydrogels

Hydrogels are physically or chemically crosslinked three-dimensional networks which are able to absorb and contain large amounts of water or biological fluids[16, 17]. The term hydrogel was first introduced by Wichterle and Lim in 1960 on crosslinked HEMA hydrogels[18].

Hydrogels have been widely studies in drug delivery and tissue engineering because they resemble the biological tissues[19]. The high water content and rubbery nature of hydrogels guarantee minimal tissue irritation[20]. Hydrogels have been widely used in drug delivery because of their ability to respond to external stimuli by swelling and de-swelling in various physiological conditions. For example, one of the most widely used

thermal-responsive hydrogel poly(N-isopropylacrylamide) (PNIPAAm) is highly developed for drug delivery system because of its unique volume phase transition in water around 32℃[21]. It means the hydrogel swells below this temperature and deswell or collapse above this temperature. This enables PNIPAAm-based hydrogels to control drug release in response to temperature change.

Hydrogels have the benefits of being biocompatible, easy to modify, sensitive to various stimulus and providing controlled release of drugs. But they also have the limitations of being fragile (low mechanical strength) and difficult to sterilize, non-adhesive to cells and costly to manufacture.

2.2.2 Classification of Hydrogels

Hydrogels are kept from dissolving in water because of the existence of physical or chemical crosslinks in their networks. Thus hydrogels can be divided into chemically crosslinked and physically crosslinked hydrogels. Physical hydrogels, are held together by physical interactions, such as molecular entanglements, ionic interaction, hydrogen bonding and hydrophobic bonding[22]. Chemically cross-linked hydrogels are called permanent hydrogels because they are crosslinked by covalent bonds. Chemical cross-linking uses a cross-linking agent (crosslinker) to link two polymer chains. The cross-linking is achieved by their functional groups (such as –C=C) with cross-linkers such as N, N-methylenebisacrylamide(BIS), potassium persulfate(KPS), ethylene glycol dimethacrylate(EGDMA).

Hydrogels can also be classified based on the natural or synthetic monomers used during preparation, the method of preparation(homopolymeric hydrogels, copolymeric hydrogels or multipolymer interpenetrating polymeric hydrogels) and the network electrical charge(such as nonionic, anionic, and cationic).

2.2.3 Synthesis of Hydrogels

Hydrogels can be made from natural polymers like hyaluronic acid, carrageenan, pectin, chitosan, collagen and gelatine, or from synthetic polymers like polycaprolactone, poly(hydroxyethyl methacrylate), poly(vinyl pyrrolidone) and poly(acrylamide).

Synthetic polymers have several advantages, such as easy control of monomer ratios, tuneable swelling and mechanical properties, but many synthetic hydrogels are non-adhesive to cells such as PEG[23]. Natural polymer hydrogels have the advantages of being hydrophilic, having abundant natural sources and similar structure to biological macromolecules[24]. So it is better to combine natural and synthetic polymers for the synthesis of hydrogels.

In general, hydrogel preparation involves use of monomers, initiator and crosslinker. The final properties of the hydrogel depend on the concentration ratios as well as the preparation method. There are many methods of preparing hydrogels, and the main two ways are thermal polymerization and radiation crosslinking. Thermal polymerization technique has been widely used to synthesize hydrogels [25, 26]. Radiation cross-linking uses high energy source such as gamma ray, X-ray or electron beam on the polymer to produce free radicals for polymerization. Radiation induced hydrogels have gained high interest because it does not need chemical additives (cross-linker or initiator, many of which are toxic) and can combine hydrogel formation and sterilization in one step. In this way, the biocompatibility is largely increased.

2.2.4 Hydrogel Swelling

Swelling in hydrogels occurs when water molecules get absorbed by the gel. When water molecules enter a hydrogel network, they firstly bound to the polar groups of the polymer chains(bound water), then form freezing bound water(clusters around bound

water) and finally exist as free water(mobile in the void volume) after bound and freezing bound water have reached their maximum contents[27]. It was later proved that free water also exists in the early stage of swelling but at the initial stage, the fraction of non-freezing water(relative to its equilibrium value) Q_1 is greater than that of freezing water Q_2. Q_1/Q_2 decreased with swelling time or a higher content of the hydrophilic component[28]. The more hydrophilic the hydrogel network, the more binding sites it provides for water molecules and the more water molecules are attracted in to reside as free water, expanding the polymer chains as shown in Figure 2.2.

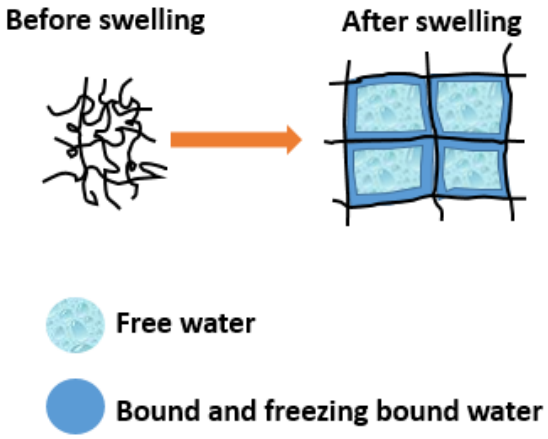

Figure 2.2 States of water in a hydrogel network

According to the Flory-Rehner theory[29], the swelling process of a non-ionic hydrogel can be described by the free energy of mixing ΔG_{mix} and the elastic free energy $\Delta G_{elastic}$ from the crosslinked network, as shown in equation(2.1):

$$\Delta G_{system} = \Delta G_{mix} + \Delta G_{elastic} \quad (2.1)$$

At the beginning of swelling, the $\Delta G_{mix} << 0$, $\Delta G_{elastic} > 0$, $\Delta G_{mix} + \Delta G_{elastic} < 0$, so solvent molecules diffuse into and expand the hydrogel network. As swelling increases, the ΔG_{mix} and $\Delta G_{elastic}$ both increase until $|\Delta G_{mix}| = |\Delta G_{elastic}|$ and $\Delta G_{system} = 0$, then swelling reaches the equilibrium state and maintains the balance.

Thus the swelling pressure of a non-ionic gel can be described as the sum of an osmotic pressure Π_{os} which tends to uncoil the polymer chains and expand the network and an

opposing pressure Π_{el} which acts against the expansion as shown in equation (2.2):

$$\Pi = \Pi_{os} + \Pi_{el} \tag{2.2}$$

The swelling stops when $\Pi_{os} + \Pi_{el} = 0$. The swelling pressure depends on the hydrophilicity/hydrophobicity of the polymer network, the crosslinking or ionisation degree, polymer-solvent interactions, and the environmental conditions such as temperature and pH. Hydrophilic groups and dissociated ions will increase the osmotic pressure Π_{os} while higher effective crosslinking density (as a result of increased crosslinker content or hydrophobic bonding) will increase the elastic pressure Π_{el}.

The swelling pressure of an ionic hydrogel[30] is more often written as in equation (2.3) because of an additional pressure generated from the mixing of ions with the solvent:

$$\Pi = \Pi_{os} + \Pi_{el} + \Pi_{ion} \tag{2.3}$$

The osmotic pressure of a polymer hydrogel Π_{os}, is also described[29] as shown in equation (2.4):

$$\Pi_{os} = -\frac{RT}{V_1}[\ln(1-\varphi_s) + \varphi_s + \chi\varphi_s{}^2] \tag{2.4}$$

Where φ_s is the polymer volume fraction, V_1 is the molar volume of the solvent, R is the universal gas constant, T is the absolute temperature, $\boldsymbol{\chi}$ is the Flory-Huggins Interaction Parameter. $\boldsymbol{\chi}$ characterizes the thermodynamic interaction between the polymer network and the solvent during the mixing. According to Flory-Huggins theory[29], $\boldsymbol{\chi}$ takes a higher value when the interaction between the polymer and solvent is weak, which also means the polymer network is more hydrophobic. The value of $\boldsymbol{\chi}$ [31] can be calculated using equation (2.5), where γ_e is the effective crosslinking density of the hydrogel, f is the functionality of the crosslinker used in the preparation of the hydrogel:

$$\chi = -\frac{\ln(1-\varphi_s)+\varphi_s+\gamma_e V_1\left(\varphi_s{}^{\frac{1}{3}}-2\varphi_s f^{-1}\right)}{\varphi_s{}^2} \tag{2.5}$$

For a glassy hydrogel, the swelling is mainly composed of three steps:

1. Water molecules diffuse into the polymer network due to osmotic pressure
2. Water molecules act as a plasticizer and uncoil the polymer chains
3. The glassy state becomes a rubbery state, causing the network to expand with the free volume occupied by water molecules

Numerous mathematical models[32, 33] have been proposed to describe the kinetics of hydrogel swelling but the most widely used and well accepted are the Fickian diffusion models which are based on Fick's laws. Fick's first law assumes that flux diffuses from the high concentration region to low concentration region and the rate depends on the concentration gradient. Fick's first law[34] is shown in equation (2.6), where J is the diffusion flux per unit area per unit time, D is the diffusion coefficient, ∅ is the concentration per unit volume, x is the position:

$$J = -D\frac{\partial \emptyset}{\partial x} \tag{2.6}$$

Diffusion processes that are described by equation (2.6) are called Fickian diffusion, which is common in rubbery polymers or when the experimental temperature is above the T_g of the polymer network. In this case, the polymer chains are mobile enough to allow immediate penetration of water molecules, i.e. the solvent diffusion rate, R_{diff}, is much slower than the polymer chain relaxation rate, R_{relax}. Fickian diffusion shows a linear relationship between the solvent uptake and the square root of time.

Diffusion processes that don't obey equation (2.6) are called non-Fickian diffusion. This always happens in a glassy polymer, or when the experimental temperature is below the T_g of polymer. Thus the polymer chains do not allow immediate penetration of the solvent and the rate of chain relaxation is much slower or comparable to the rate of

solvent diffusion. When R_{relax} is much slower than R_{diff}, it is called Case II diffusion. When $R_{diff} \approx R_{relax}$, it is called anomalous diffusion.

Different diffusion processes correspond to different relationships between solvent uptake and time. An empirical equation, called power law equation is widely used to determine the diffusion mechanism of the hydrogels, as shown in equation(2.7)[34], where M_t is the water uptake at time t and M_∞ is the water uptake at the equilibrium state, k is a constant and n is the diffusion exponent:

$$\frac{M_t}{M_\infty} = kt^n \tag{2.7}$$

The exponent n shows the type of diffusion mechanism. When n≤0.5, it is Fickian diffusion, which is also called diffusion controlled swelling. When n equals 1.0, it is Case II diffusion which is relaxation controlled swelling. When n is between 0.5 and 1.0, it is anomalous diffusion, where swelling is both diffusion and relaxation controlled. The diffusion mechanism, diffusion exponent, time dependence and rate difference are summarized in Table 2.1:

Table 2.1 Diffusion Mechanism, diffusion exponent, their time dependence and rate difference

Type of Diffusion	Diffusion Exponent n	Time Dependence	Rate
Fickian Diffusion	0.5 or smaller	$t^{1/2}$	$R_{diff} \ll R_{relax}$
Anomalous Diffusion	0.5<n<1	t^{n-1}	$R_{diff} \approx R_{relax}$
Case II Diffusion	1	t	$R_{diff} \gg R_{relax}$

2.2.5 Factors Affecting Hydrogel Swelling

The swelling of a hydrogel is mainly affected by the following factors:

1. Innate properties of the polymer network such as the hydrophilicity/hydrophobicity, effective crosslinking density (can be affected by crosslinker content and monomer ratios), ionisation degree of the network, the interactions between individual monomer components.

2. Environmental conditions such as pH, temperature, the polarity of the solvent, the presence of electric or magnetic field.
3. The interactions between the polymer and the solvent, for example, an ionic polymer network shows good swelling in distilled water because of the dissociated ions that increase the osmotic pressure. But it will not swell in non-polar solvents because ions prefer to form ion pairs and multiplets in less polar solvent.

For tissue expanders, it is important to tune the innate properties for delayed and controlled swelling. Also, tissue expanders will be implanted in animal or human bodies. In vitro studies are always performed in distilled water or phosphate buffer solutions. Thus it is important to know how hydrogels will actually behave in living mammals. The local change in the temperature, pH or ion concentrations will cause drastic changes to the swelling of a hydrogel.

2.2.5.1 Monomer Ratios (i.e. Hydrophilicity/Hydrophobicity)

The swelling rate and equilibrium swelling ratio of a hydrogel depends on the polymer and solvent interactions. And the monomer ratios used in the preparation determine the final property of the hydrogel network. A hydrophilic polymer network tends to have strong interactions with water or other polar molecules and attract them through hydrogen bonding. A hydrophobic network tends not to bond with water or polar molecules and only interact with non-polar molecules.

The hydrophilicity/hydrophobicity of a polymer network is determined by measuring its water contact angle. The contact angle measures the wettability of a solid surface by a liquid or vapour via the Young's equation shown in Figure 2.3:

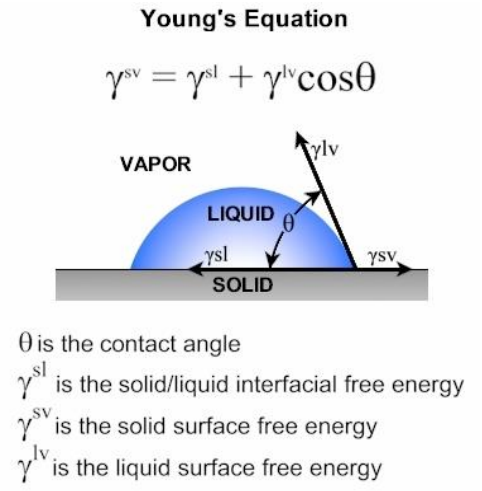

Figure 2.3 Young's equation measuring the contact angle

The contact angle can be measure directly by a telescope-goniometer[35] or by advanced imaging techniques like AFM(atomic force microscopy)[36]. A small contact angle(less than 90°) corresponds to a relatively more hydrophilic surface that favours wetting with the liquid. While a large contact angle (greater than 90°) corresponds to a more hydrophobic surface which prefers minimized contact with the liquid. The more hydrophobic the surface, the higher the contact angle. In biomaterials and tissue engineering, researchers tend to define a surface as hydrophobic when its water contact angle is higher than 65°, considering the biological activity such as cell adhesion on the surface[37].

Davis and Huglin have done a lot of research on N-vinyl-2-pyrrolidone(VP) based copolymeric hydrogels. They prepared VP/MMA(methyl methacrylate) copolymeric hydrogels[38] using γ irradiation and found the equilibrium water content(EWC) to increase from less than 5% to over 80% when VP content was increased from 5% to 85%, whether in the presence or absence of a crosslinker. They also prepared VP/HEMA(hydroxyl ethyl methacrylate) copolymeric hydrogels[39] and found the EWC to increase from 40.4% to 85.4% when VP content was increased from 5% to 70% in the absence of a crosslinker. The difference in EWC is a result of the hydrophilic/hydrophobic difference between the hydrogel networks due to varied

monomer ratios. VP has been reported to have a contact angle of around 5°[40], while MMA and HEMA have been reported to have a contact angle of 71.5°[41] and 60°[42], respectively. This shows VP is highly hydrophilic while HEMA and MMA are relatively more hydrophobic. More hydrophilic groups on the polymer chains provide more binding sites for water molecules, while hydrophobic groups repel water molecules and act as a steric hindrance at the same time, preventing them from binding with hydrophilic components[43].

VP has been widely accepted and used as a highly hydrophilic polymer to modify other polymers to lower their water contact angles[44]. EWC of VP/BA(butyl acrylate) copolymeric hydrogels was shown to increase at almost the same magnitude as the increase in VP content[45]. VP modified poly(vinylidene fluoride) (PVDF) membrane was shown to have a contact angle of 24° compared with the unmodified PVDF membrane of 84°[46]. The contact angle of P(VP-co-HEMA) was found to decrease from 75% to 15% when VP content was increased from 0% to 90%[47].

2.2.5.2 Type and Concentration of Initiator and Crosslinker

Most research shows that an increased initiator or crosslinker concentration leads to an increased crosslinking degree (number of crosslinks per unit space), thus a stronger network with less chain mobility. This will further lead to a slower water uptake and lower equilibrium swelling ratio.

PDMAA/Clay(poly N,N-dimethylacrylamide/clay) hydrogels prepared with AIBN (azobisisobutryonitrile) as the initiator were shown to be 2000% higher in the swelling ratio than those prepared with KPS(potassium peroxodisulfate)[48]. An extended swelling period and improved mechanical properties were observed as well.

Davis and Huglin[49] prepared PVP hydrogels crosslinked with EGDMA. They increased EGDMA content 0.5wt% to 5wt%, and found the EWC to decrease from

95.7% to 77.4% and the free water fraction to decrease from 85.7% to 66.5% as confirmed by DSC. They also prepared VP/MMA hydrogels and found the EWC to decrease around 30% when EGDMA content was increased from 0.4% to 4%[31].

Haldon and Lee[50] prepared PHEMA hydrogels with three different crosslinkers, EDMA, TPT(trimethylol propane trimethacrylate), PETMA(pentaerythritol tetramethacrylate) and found the EWC to decrease with increased crosslinker molar content in each case. The difference in the functionality of the crosslinker did not seem to affect the EWC at the same crosslinker molar content, as shown in Figure 2.4.

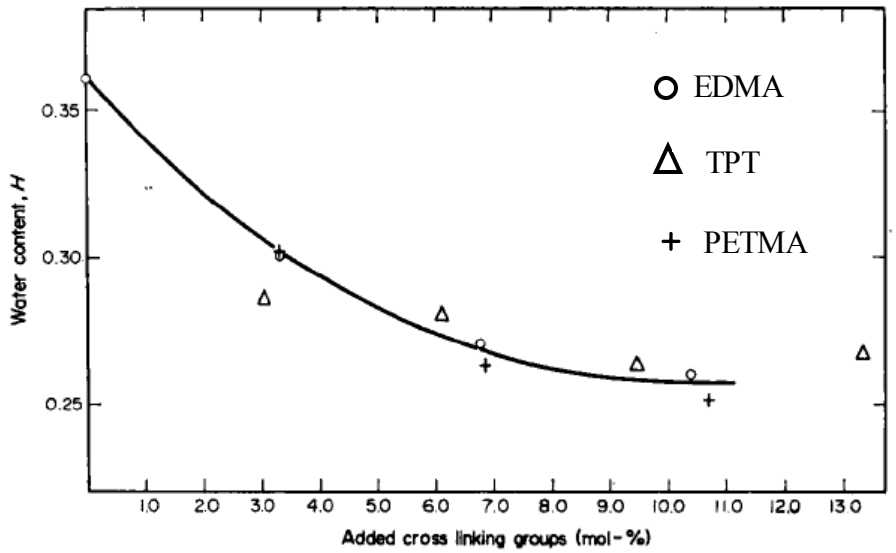

Figure 2.4 Equilibrium water content of PHEMA prepared with EDMA, TPT, and PETMA (reproduced from [50])

The swelling ratio of poly(methacrylic acid) hydrogels was found to decrease by half when the crosslinker content was increased from 0.003(mol%) to 0.006 and by one third when the initiator content was increased from 0.06(mol%) to 0.1[51].

Different crosslinker or initiator concentrations change the number of crosslinks per unit volume as well as the average distance between two consecutive crosslinks, i.e. the mesh size, as shown in Figure 2.5. The mesh size ξ was introduced by Peppas[52] to measure the free volume(nanometer scale) in the polymer network that could provide

accommodation for water molecules or other solvents. The molecular weight between two consecutive crosslinks is defined as M_c. ξ is indicative of the swelling capacity and the swelling rate as it shows effective space for diffusion and accommodation of water molecules. Mesh size ξ can be described using equation(2.8)[53], where Q is the volume swelling ratio, C_n is the polymer characteristic ratio, M_r is the molecular weight of repeating units, l is the carbon-carbon bond length(1.54A):

$$\xi = Q^{1/3}\left(\frac{2C_nM_c}{M_r}\right)^{1/2} l \tag{2.8}$$

Thus a higher crosslinker or initiator concentration results in an increased number of crosslinks per unit volume. This then leads to a decreased mesh size, which means less effective space for water diffusion and less free volume for water molecules accommodation, i.e. a smaller equilibrium swelling ratio Q_∞. The existence of more crosslinks also acts as barriers for water diffusion, leading to a decreased swelling rate.

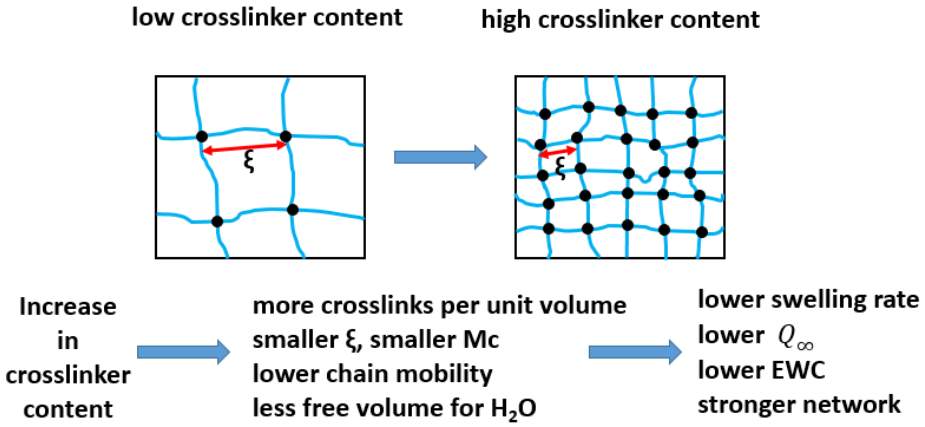

Figure 2.5 Changes brought by increased crosslinker content

Changing crosslinker concentration to control the drug release rate has been applied on PHEMA hydrogels[54]. Drug release rate was decreased by over 80% when the concentration of EGDMA was increased from 0% to 40% in the solution where PHEMA had been soaked.

2.2.5.3 Intensity of Irradiation

The mesh size can be affected by the change in crosslinker concentration as well as the intensity of irradiation. In both cases, the number of crosslinks per unit volume will be changed and the corresponding change in mesh size will affect the swelling behaviour of hydrogels. Increased irradiation (either increased dose or treating time) will lead to an increased number of crosslinks and a decreased mesh size.

UV treated PHEMA hydrogels were found to have a decreased drug release rate by 30% when UV irradiation time was increased from 0 to 60 minutes[54]. The swelling ratio of PVA(polyvinyl alcohol)/PVP hydrogels was decreased from around 20 to 12 when γ irradiation dose was increased from 20kGy to 40kGy[55]. The swelling ratio of kappa-carrageenan/acrylamide hydrogels could be decreased by 300 when γ irradiation dose was increased from 7.5kGy to 12.5kGy depending on the composition ratio[56].

In contrast to these works, Lee & Bucknall[57] found the equilibrium swelling ratio of VP/HEMA hydrogels to increase from around 8 to 11 when UV intensity was increased from 0.0075 to 2.65mW/cm^2. They explained that it was attributed to the over-rapid reaction rate generated by increased UV intensity that left inadequate time for crosslink formation. Thus more dangling chains were left in the hydrogel network, leading to an increased molecular weight between consecutive crosslinks and a decreased mesh size, as shown in Figure 2.6.

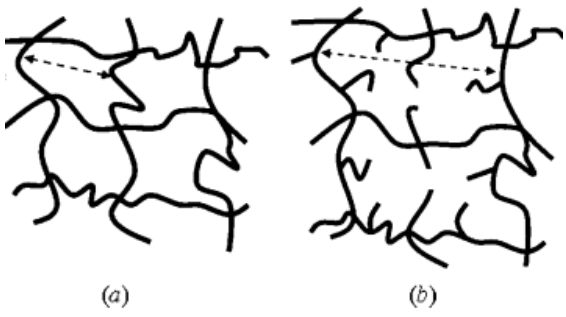

Figure 2.6 Schematic of VP/HEMA hydrogel network prepared at (a) lower (b) higher UV intensity (reproduced from[57])

Hydrogel tissue expanders need to be sterilized before the implantation in animals or humans. Generally a minimum dose of 25kGy is required for various medical implants[58].

2.2.5.4 Effect of ions and pH

The swelling of a hydrogel can be affected by ions and pH of the swelling medium. VP/AA hydrogels were prepared which showed volume transition with pH change and a transition point of pH=4[59]. The swelling ratio Q of VP: AA 60:40 remained unchanged under pH=2 or over pH=6. Q increased from 20 to 110 when pH was increased from 2 to 6. The volume transition was observed for all VP/AA hydrogels with different VP: AA ratios, which was attribute to the dissociation of ions when pH approached the dissociation constant pK_a of AA (4.25) that increased the osmotic pressure of the hydrogels.

Wiese[11] has studied the swelling of VP/MMA in a variety of solutions. They modified VP/MMA by changing –CH3 groups into –COOH groups for higher swelling. The swelling ratio (Q) of the modified VP/MMA was 30 in distilled water. Q decreased to around 8.8 in 0.9% NaCl solution (~150mmol/L) and a further 5.8 in equimolar Ringer solution (Na^+ 147mmol/L, K^+ 4mmol/L, Ca^{2+} 2.3mmol/L, Cl^- 155.5mmol/L). Q was 9.5 in 15% mannitol solution and 7.6 in a mixture of 15% mannitol and 0.9% NaCl. These demonstrate that the swelling ratio decreased with increased concentration and ion content in the swelling medium.

AAm/CA(acrylamide/crotonic acid) and AAm/IA(acrylamide/itaconic acid) hydrogels were prepared under γ irradiation[60]. The swelling ratio of AAm/CA decreased from 18 in distilled water to 14 in 0.9% NaCl solution, while that of AAm/IA decreased from 16 to 10. They explained that with the diffusion of Na^+ into the hydrogel, there would be increased interactions between Na^+ and the carboxyl groups on the polymer chains,

leading to a decreased amount of $-COO^-$ to bind with water molecules.

The osmotic pressure generated by ions is described in equation (2.9)[29], Where C_i^g is the mobile concentration of ion i inside the hydrogel network, C_i^s is the mobile concentration of ion i in the solvent, R is universal gas constant and T is temperature:

$$\pi_{ion} = RT \sum_i \left(C_i^g - C_i^s\right) \tag{2.9}$$

Equation (2.9) demonstrates that the greater the difference of ion concentrations, the higher the swelling pressure generated by mixing the ions with the solvent, and the higher the swelling rate and equilibrium swelling ratio.

2.2.6 Inverse Relationship between Swelling Capacity and Mechanical Strength of Hydrogels

To be used as a desirable self-inflating tissue expander, the hydrogel needs to be highly expandable, controllable and also capable of withstanding the compressive pressure exerted by the skin when implanted under the subcutaneous layer. Thus it is important to maintain its mechanical integrity and original shape during swelling and at the fully swollen state as well. However, in the history of hydrogel preparation, there seems to be an inverse relationship between the swelling capacity and the mechanical properties of the hydrogels. As has been discussed above, the swelling capacity of a hydrogel can be affected by monomer ratios, crosslinker content and irradiation intensity. Higher proportion of hydrophilic components, lower crosslinker content or less irradiation will result in a higher swelling ratio, leading to a mechanically weaker hydrogel at the swollen state.

Hydrogels could rupture or collapse during expansion when the ratio of hydrophilic component is too high. VP/MMA hydrogels with VP:MMA 85:15 weight ratio were found to break up during expansion[38]. The compressive modulus of swollen VP/MMA hydrogels was decreased from 13.1MPa to 0.15MPa when EWC was

increased from 32.9% to 82.6%[38]. The compressive modulus of VP/HEMA hydrogels were found to decrease from 220kPa to 10kPa when equilibrium swelling ratio was increased from around 8 to 80[57]. The inverse relationship between swelling capacity and the mechanical properties (swollen states) can be found in various reports [61-63]. The reason is that when a hydrogel absorbs water, water molecules get inside the gel network and act as plasticizers, decreasing the glass transition temperature of the network and promoting the chain mobility. Thus, the more water molecules the hydrogel contains, the less energy it needs to unfasten the polymer chains for deformation.

In recent years, novel hydrogels with extremely high mechanical strength have been developed, but they all come at the expense of swelling abilities. Nanocomposite(NC) hydrogels composed of NIPA(N-isopropyl acrylamide) and inorganic clay were prepared with superior tensile properties than traditional hydrogels[64]. But the swelling ratio decreased from 110 to 48 when tensile modulus was increased from 1.5kPa to 9.9kPa. Gong et al.[65] prepared super-tough IPN hydrogels using different combinations of primary and secondary networks as shown in Table 2.2. Table 2.2 shows that the incorporation a loosely crosslinked secondary network can effectively increase the fracture stress but it comes at the expense of EWC. For example, EWC of Agarose/HEMA decreased from 96% to 66% when fracture stress was increased from 0.02MPa to 2.4MPa. However, there were some combinations that show an insensitive decrease in EWC with significantly increase in fracture stress. For example, PAMPS/PAAm hydrogels could withstand 17.2MPa compression while maintaining around 90% of water content. The swelling process was not shown but it is worth into this kind of hydrogels for use as tissue expanders.

Table 2.2 Compressive and swelling properties of IPN hydrogels (reproduced from[65]) (PAMPS- poly(2-acrylamido-2-methylpropanesulfonic acid), PAAm-polyacrylamide, TFEA-2,2,2-trifluoroethyl acrylate, PAA-polyacrylic acid, PDMAAm-poly(N, N'-dimethyl acrylamide))

First network	Second network	Water content [wt.-%]	Fracture stress σ_{max} [MPa]	Fracture strain λ_{max} [%]	$\sigma_{max}^{DN}/\sigma_{max}^{SN}$
PAMPS-1-4 [a]	–	92	0.4	41	–
	PAMPS-2.2-0.1	93	3.0	80	7.5
	PAA-1-0.1	92	2.3	75	5.8
	PAAm-2-0.1	90	17.2	92	43
PAMPS-1-8	–	98	0.006 [b]	0.13 [b]	–
	TFEA-1-0.1	52	1.6 [b]	4.9 [b]	267
PAA-1-4	–	99	0.1	65	–
	PAA-1-0.1	95	0.7	77	7.0
	PAAm-1-0.1	89	2.1	95	21
PAAm-1-1	–	93	0.7	98	–
	PAAm-1-0.1	92	5.4	92	7.7
P(AMPS-*co*-TFEA)-1-4	–	98	0.03	73	–
	AAm-1-0.1	93	21.0	97	700
Collagen [c]	–	93	0.26	52	–
	PDMAAm-1-0.1	87	2.9	53	11
Agarose [c]	–	96	0.02	20	–
	HEMA-2.5-0.1	66	2.4	87	120
Bacteria cellulose	–	–	–	–	–
	Gelatin	78	3.7	37	31 [d]

[a] *P-x-y*: *P*, *x*, and *y* denote the abbreviated polymer name, molar monomer concentration, and the crosslinker concentration in mol-% with respect to the monomer, respectively. [b] Stretching properties. [c] Physically cross-linked gel prepared from 2 wt.-% solution. [d] Relative to gelatin SN gel.

Hydrogels with extensive swelling capacity, i.e. superabsorbent hydrogels (SAH) have also been widely studied but most of them are not mechanically strong enough to be used as tissue expanders. For example, a polyrotaxane gel could absorb water up to 400 times its dry weight while maintaining its original shape. But its elastic modulus was only 500Pa[66]. DMAA(N, N-dimethylacrylamide) hydrogels could swell up to 70 times its original size but the tensile modulus at swollen state was only 1000Pa which may not be enough to be used as tissue expanders[67]. Polyacrylamide-sodium alginate IPN hydrogels showed a swelling ratio of 40-50 while being able to be stretched to 2-3 times its original length and also resist a static mechanical pressure of at least 10N at its swollen state[68]. But the increase in mechanical properties was shown to be a result of increases Ca^{2+} concentration (for crosslinking alginate) and also decreased with swelling capacity. Thus the swelling can be largely offset when implanted in vivo because of the existence of ions in physiological conditions.

2.3 Potential Hydrogels Used as Tissue Expanders

2.3.1 PVP (polyvinyl pyrrolidone) Based Hydrogels

PVP has been widely used in the biomedical world because of its good biocompatibility and non-toxicity[69]. It was used as a safe plasma expander in the 1940s[70]. PVP is highly hydrophilic because it contains the amide groups on its polymer chains[71], as shown in its chemical structure in Figure 2.7. PVP based hydrogels have the potential to be used as tissue expanders because of their non-toxicity and good swelling capacity.

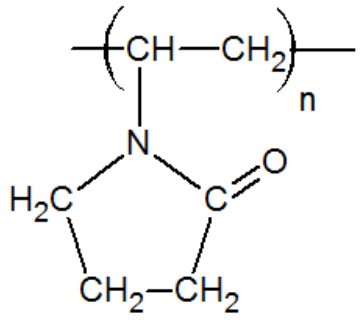

Figure 2.7 Chemical structure of PVP

Controlled swelling of PVP based hydrogels can be achieved by copolymerization, changing crosslinker content or irradiation dose. VP/BA(butyl acrylate) copolymeric hydrogels with a wide range of swelling and mechanical properties were prepared with varied monomer ratios[72]. EWC ranged from 1% to 89% with a corresponding compressive modulus from 0.12MPa to 0.05MPa. PVP hydrogels crosslinked with 1-2wt% EGDMA under γ irradiation were found to rupture and lose their original shapes upon swelling due to a lack of formed crosslinks, while those with 3-5% EGDMA remained intact[73]. But those with 6-7% EGDMA collapsed again because of the inhomogeneous distributed crosslinks. The swelling behaviour of PVP hydrogels was found to change with γ irradiation dose[74], as shown in Figure 2.8. The swelling ratio decreased from 80 to less than 5 when irradiation dose was increased from 3kGy to 30kGy. PVP prepared under 3kGy reached the equilibrium state in 8 days, showing

potential to be used as tissue expander. But its mechanical properties at the swollen state were not shown.

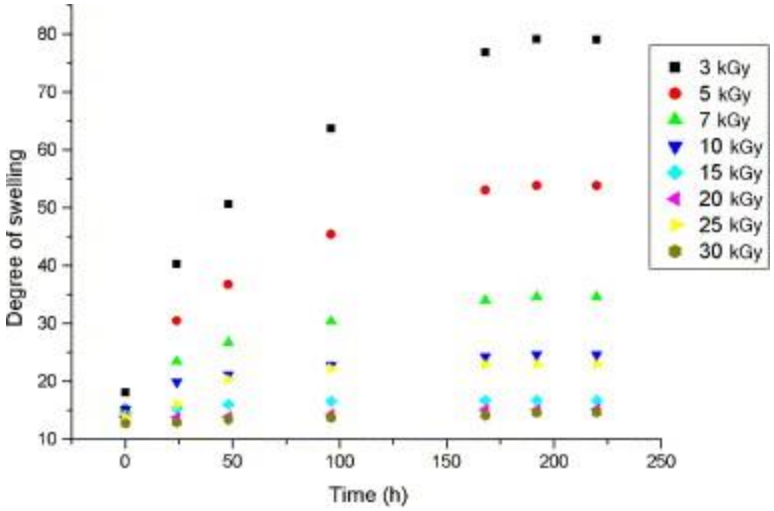

Figure 2.8 Swelling behaviour of PVP hydrogels as a function of time under varied irradiation doses(reproduced from[67])

Despite its high swelling capacity, the application of PVP hydrogel is limited by its weak mechanical property[75, 76]. The mechanical properties of PVP hydrogels can be enhanced through copolymerization[45], or formation of IPN hydrogels[77] with other polymers. The compressive modulus of swollen VP/HEMA hydrogels increased from 0.083MPa to 0.813MPa when VP content decreased from 60% to 5%[78]. At a fixed VP:HEMA ratio(70:30), the compressive modulus increased from 1MPa to 3MPa with increased crosslinker(EDMA) content from 0.25% to 4%[78][78][78][78][78][78].

2.3.2 PMMA Based Hydrogels

The chemical structure of PMMA is shown in Figure 2.9. Poly(methyl methacrylate) (PMMA) has been used as a major material as intraocular lenses for treating cataracts[79]. PMMA was used as contact lenses materials but was later replaced by MMA/HEMA and VP/MMA hydrogels which are softer and have better oxygen permeability and less protein adsorption[80]. PMMA has a glass transition temperature of 108°C[81] and its biocompatibility has been well established[82]. MMA is more

hydrophobic than VP as has been verified by their water contact angles (section 2.2.5.1). Thus it is usually copolymerized with other hydrophilic monomers such as HEMA[83] and VP[84] to prepare materials with better water content and swelling abilities. Its non-toxicity, biocompatibility, and relatively hydrophobic nature make itself a useful component in preparing hydrogels tissue expanders.

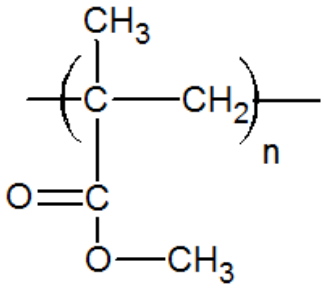

Figure 2.9 Chemical structure of PMMA

2.3.3 VP/MMA Hydrogels

The chemical structure of VP/MMA is shown in Figure 2.10. VP/MMA has been long used as a contact lens material[85]. Wiese[10] first used VP/MMA as a tissue expander and proved its biocompatibility. Since then it has been used as the major material as self-inflating tissue expanders[86]. VP/MMA hydrogel can generate an in vitro swelling pressure of approximately 235mmHg(31.3kPa)[10]. The swelling capacity of VP/MMA ranged from 5 to 50 depending on the ionization degree of –CH3 groups to –COOH groups[11] and also on the ion concentration in the swelling medium as discussed in section 2.2.5.4. In clinical trials, VP/MMA prepared with a perforated silicone membrane has been proved to have better controlled swelling than VP/MMA alone, which results in more effective tissue growth and less incidence of complications and implant extrusions[87-89].

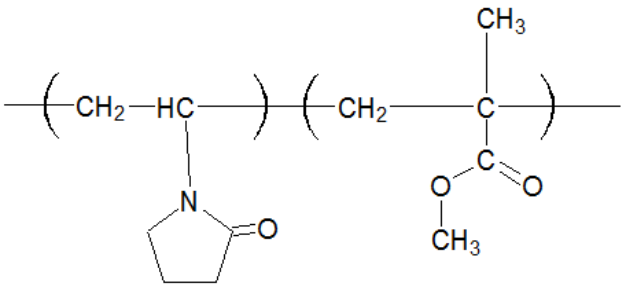

Figure 2.10 Chemical structure of VP/MMA

2.3.4 PHEMA (polyhydroxyethyl methacrylate) Based Hydrogels

The chemical structure of PHEMA is shown in Figure 2.11. PHEMA hydrogels have been long and widely used in the biomedical field such as soft contact lenses[90], wound dressings[91], surgical prostheses[92]. However, the application of PHEMA hydrogels is restricted because of its low water absorption[93], and its weak mechanical strength[94]. The swelling capacity can be improved when copolymerized with a hydrophilic polymer such as acrylic acid[93] or polyethylene glycol(PEG)[95]. As with other copolymer hydrogels, the swelling ratio can be tuned with monomer ratios and crosslinker content. Pure PHEMA hydrogels have been reported to reach equilibrium swelling in approximately 100 hours[96]. With proper copolymerization, good swelling capacity and controlled swelling of HEMA hydrogels could be achieved.

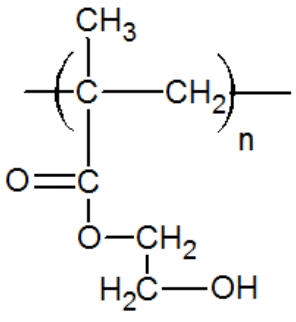

Figure 2.11 Chemical structure of PHEMA

2.3.5 Other potential biocompatible hydrogels

VP/MMA has been used as the primary self-inflating hydrogel tissue expander but researchers are looking into other biocompatible hydrogels as well.

Polyacrylamide(PAAm) hydrogels have been widely used in tissue engineering and drug delivery because of its hydrophilicity and biocompatibility[97]. Acrylamide-based hydrogels such as AAm/CA(acrylamide/crotonic acid) and AAm/IA(acrylamide/itaconic acid) have been prepared using γ irradiation and their biocompatibility was shown[60]. These acrylamide-based hydrogels were proved to be biocompatible and exhibit good swelling capacity in water (18 for AAm/CA and 16 for AAm/IA) and 0.9% NaCl solution (14 for AAm/CA and 10 for AAm/IA) as well. But the swelling reached equilibrium within 7 hours and their mechanical properties under compression was not shown. Later AAm/CA and AAm/IA were implanted in a rat model as tissue expanders[98]. Tissue necrosis or serious infection was not shown in both cases, but AAm/IA hydrogels tended to break into pieces in vivo after 6 weeks. AAm/IA hydrogels were able to swell and maintain their original shapes in vivo during the 10 weeks of implantation.

Acrylamide(AAm), acrylic acid(AA) and N-isopropylacrylamide(NIPAAm) hydrogels were prepared and implanted in a rat model[99]. The histology analysis showed serious tissue damage caused by AA because of its over-rapid expansion rate at the initial stage (Q reached around 18 in 4 days). AA and AAm hydrogels could not retain their original shapes during expansion. NIPAAm expander showed promising results with the maximum swelling ratio of 4-5 reached within 5 days. But the swelling ratio tended to fluctuate and decrease after that. Serious shrink of NIPAAm was observed after 15 days of implantation.

Poly sodium acrylate-PEC(pectin) hydrogels were prepared as orbital implants which

exhibited good swelling in water and mechanical strength at the swollen state as well[100]. The compressive modulus at the fully swollen state ranged between 40-64kPa depending on the composition of the hydrogels. The volume swelling ratio could be as high as 4.5 in water but it decreased sharply(less than 0.5) in phosphate buffer solution or physiological saline water because of the decrease in Na^+ concentration difference. Thus it may not have enough swelling capacity as a tissue expander.

2.4 IPN (Inter-penetrating Polymer Network)

2.4.1 Definition

Interpenetrating polymer networks (IPNs) are composed of two or more polymer networks that at least one is crosslinked in the presence of another. The component networks are entangled and interlaced at a molecular level but not covalently bonded to each other[101-103]. The interpenetrating on the molecular level is an ideal situation, and actually only limited penetration could be achieved due to phase separation[104].

Sperling[105] compared the difference of various ways to mix two kinds of polymer molecules in Figure 2.12. Polymer blend is formed by simple mixing as shown in Figure 2.12a, while graft(Figure 2.12b) or block copolymers(Figure 2.12c) results when the chains are covalently bonded with each other. A full IPN(Figure 2.12e) is formed when both polymer networks are crosslinked and at least one is crosslinked in the presence of another. A semi-IPN(Figure 2.13f) is obtained when one network is crosslinker and the other is linear and one is crosslinked in the presence of the other. In Figure 2.12, polymer structures a-c are thermoplastic while d-f are thermoset.

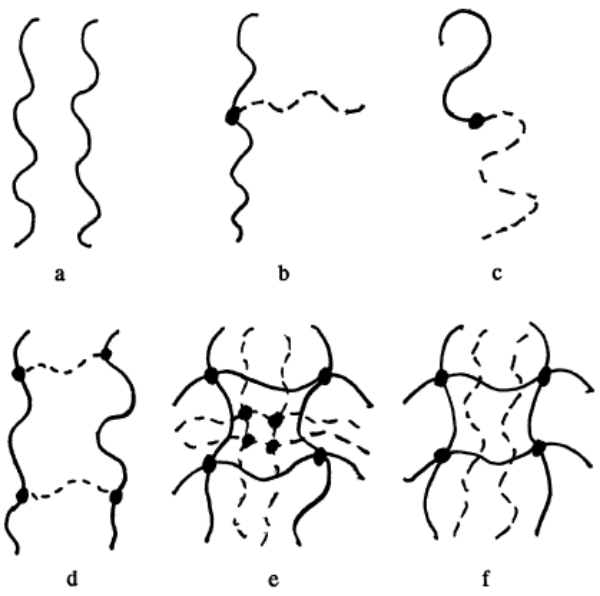

Figure 2.12 Various combinations of two polymers. a: polymer blend; b: a graft polymer; c: a block copolymer; d: an AB-graft copolymer; e: a full IPN; f: a Semi IPN (reproduced from [105])

2.4.2 History and Types of IPN Hydrogels

The first IPN was a patent by Aylsworth in 1914[106], and it was not called IPN until in 1960 when Millar prepared polystyrene/polystyrene IPHs to be used as ion exchange resin matrices[107]. Frisch[108] and Sperling and Friedman[109] have made the most contributions to this field. They established that IPNs are two or more independently crosslinked polymer networks held together by topological interactions and the entanglements and interlacing are permanent because component networks cannot be separated until fracture happens. The interpenetrating on the molecular level is an ideal situation, and actually phase separation is quite common in the preparation of IPNs[110, 111]. For example, Sperling and Friedman[109] observed two separate glass transition temperatures, one corresponding to the T_g of poly(ethyl acrylate) and the other corresponding to the T_g of polystyrene. This indicated the presence of two polymer phases.

According to the synthesis methods, IPNs can be defined as the following types[112]:

(1) Sequential IPN: Generally the first crosslinked network is swollen in a solution that

dissolves the monomer of the second network, crosslinker and initiator. Then the second network is crosslinked under appropriate conditions in the presence of the first network[113].

(2) Simultaneous IPN: The monomers of both networks, and crosslinker and initiators are mixed together. The crosslinking of both networks are performed at the same time but neither would interfere with the other[114].

(3) Latex IPN: Both networks are above their glass transition temperature in a latex form. After crosslinking latex IPN always form a core and shell structure[115].

(4) Gradient IPN: Gradient IPNs are IPNs whose concentration or crosslinking degree depends on the position[116].

(5) Thermoplastic IPN: A normal IPN is composed of chemically crosslinked networks. But thermoplastic IPN is composed of physically crosslinked networks(through ionic groups, crystallinity or glassy domains). As a result, it can flow at raised temperatures[117].

(6) Semi-IPN: In semi-IPN, at least one network is not crosslinked and exists as a linear polymer in the IPN system[118]. A corresponding full-IPN can be prepared by selectively crosslinking the linear monomers.

2.4.3 The Advantages of IPN Hydrogels

The wide applications of various hydrogels types may be limited by their weak mechanical properties. For instance, PAAm hydrogels showed relatively low values of elastic modulus despite their good swelling capacity and biocompatibility[119]. A number of ways have been developed to enhance the strength of hydrogels including using a hydrophobic crosslinker in the preparation[120], and chemical grafting[121]. But they all change the original chemical structure of the polymer network. Thus the original properties of the hydrogels may be sacrificed, such as hydrophilicity, stimulus-

responsiveness, or oxygen permeability.

A new way to improve the mechanical property while maintaining the original properties of each component is through interpenetrating polymer network(IPN). The use of interpenetrating network has the advantages of combining properties from two polymer networks since there is no chemical bonding between them and each can retain its own properties while the overall performance of the IPN hydrogel can be tuned by varying the proportions of each network[122].

IPN hydrogels have been widely investigated to show improved mechanical properties[65, 123], improved biocompatibility[124], faster response to stimuli and more controlled drug release[125]. The hydrophilicity /hydrophobicity and stimuli-responsiveness of IPNs can be controlled by proper selection of the polymer components and by varying their composition.

In terms of preparing desirable self-inflating tissue expanders, IPNs may provide a way for delayed and controlled expansion by introducing a hydrophobic secondary network into the existing primary network. The swelling rate as well as equilibrium swelling ratio can be manipulated by selectively choosing the polymer components and changing their compositions.

2.5 Widely Studied IPN hydrogels

Various natural and synthetic polymers can be used to prepare IPN systems. Natural polymers such as cellulose, gelatine, chitosan are advantageous in their natural abundant source, biocompatibility, biodegradability, and nontoxicity[24], while polymers such as acrylamide, PVA, PAA, PLGA, PVP, HEMA are easy to be modified or manipulated for the desirable properties[126].

IPN systems have been prepared with various combinations of natural and synthetic polymers because of the uniqueness of preserving original individual properties and

obtaining synergistic properties in an IPN system[127, 128]. The intriguing part of preparing IPN hydrogels is to find better combinations of polymer networks that would provide better properties without sacrificing the original ones. For example, CA(cellulose acetate)/PVP IPN hydrogels showed a higher tensile strength and elongation at break compared to PVP/PMMA IPN hydrogels at the same water content[129]. CA/PVP IPN hydrogels also shows a higher water content(82%) than PHEMA(39%) while having a similar tensile strength at the swollen state[129].

2.5.1 PNIPAAm based IPN hydrogels

PNIPAAm is well known for its thermal responsiveness with a lower critical solution temperature(LCST) at around 32℃[130]. Copolymerization with monomers such as acrylic acid can provide an additional pH sensitivity[131], but the temperature sensitivity may be compromised because of the incorporation of pH-sensitive components[132]. Thus IPN may provide a way to maintain or even improve the original properties of hydrogels. PVA/PNIPAAm semi-IPN hydrogels were prepared and shown to have faster response to temperature changes compared to conventional PNIPAAm hydrogels[133, 134]. The semi-IPN hydrogels could lose over 95% water within 1 min while NIPAAm hydrogel only lost around 50% water in 2h above the LCST. The incorporation of PVA also increased the swelling capacity because of an increased hydrophilicity. Chitosan-PNIPAAm hydrogels were prepared[135] which showed increased drug loading ability because of the interaction between the anionic drug(diclofenac) and the amino groups of chitosan. They also showed a sustained drug release over 8h because of the deswelling of PNIPAAm network at 37 ℃. Both properties were not observed in single crosslinked PNIPAAm network[136] or chitosan network[135]. IPN hydrogels composed of a hydrophilic PNIPAAm and a hydrophobic PMMA were prepared, which showed better mechanical properties without sacrificing

the thermal sensitivity[113]. However, the swelling ratio was decreased from 17 to 11 when PMMA content was increased from 0 to 11.8%. Cellulose/PNIPAAm hydrogels were prepared which showed enhanced compressive modulus(58kPa) than pure cellulose hydrogel(48kPa) and PNIPAAm hydrogel(12kPa) at the swollen state[137]. However, PNIPAAm based IPN hydrogels are not qualified as tissue expanders because they are thermally responsive, which means they swell under their LCST(around 32℃) and collapse(not swelling) above that. Thus they are unable to swell when implanted in human body where the normal body temperature is around 37℃.

2.5.2 PVP based IPN Hydrogel

PVP is a non-ionic, highly hydrophilic polymer, which has been widely used in medicine, pharmaceuticals, cosmetics, foods, and other fields due to its good solubility, excellent miscibility with other polymers, non-toxicity, and biocompatibility[138]. PVP is considered a suitable component for the preparation of IPN or semi-IPN hydrogels. Semi-IPN hydrogels were prepared with crosslinked sodium alginate-g-poly(sodium acrylate) network and PVP linear polymer chains. The semi-IPN showed excellent pH sensitivity with a 7 folds increase in the swelling ratio when pH was changed from 2 to 6[139]. Incorporation of 15% PVP could improve the swelling ratio from 7.5 to around 10 but 20%PVP decreased Q to 8.5 due to an increase in chain entanglements. PVP/PAA semi-IPN hydrogels were prepared with excellent pH sensibility from 2.25 to 4 at 37℃ and improved swelling capacity compared to pure PVP hydrogel[140]. Chitosan/NVP IPN hydrogels showed an EWC of 93% in 24h and chitosan/(NVP/HEMA) IPN hydrogels showed that of 75% in 48h, exhibiting good swelling capacity[141]. They also showed good biocompatibility with human keratinocytes.

2.5.3 Chitosan based IPN Hydrogels

Chitosan has been widely investigated in the biomedical field because of its bio-adhesiveness, non-toxicity, biodegradability, and biocompatibility[142], making it a suitable choice in the preparation of IPN hydrogel for biomedical applications. Chitosan based IPN hydrogels have been extensively studied in oral drug delivery because they have excellent drug loading ability and capability of absorbing body fluids to swell[143]. Chitosan is biodegradable but the IPN structure can provide the insolubility in body fluids[143]. Chitosan has been prepared with various polymers to form IPN hydrogels with environmental responsiveness, such as pH sensitivity with poly-acrylamide[144] and PVP[145], or thermal sensitivity like N-isopropylacrylamide[146]. Chitosan/PAA IPN hydrogels were prepared by UV irradiation and maintained a high EWC in the range of 57.5% to 72.9%, compared to chitosan(59.5%) and PAA(76%)[147]. The tensile strength of the swollen IPN hydrogels lied in the range of 0.5-1.5MPa while pure PAA hydrogels could not even support themselves. The improved tensile strength was a result of polyelectrolyte complex formation between amino groups in chitosan and carboxyl groups in PAA.

However, the chitosan hydrogel is fragile and thus is always crosslinked by glutaraldehyde to increase its mechanical strength[148]. Glutaraldehyde is toxic and may hinder its application as biomaterials. Also, chitosan depolymerizes under acidic conditions, which may limit its use as drug delivery carriers[143].

2.5.4 IPNs with Biocompatible, Hydrophobic Polymers

In the 1960s, PGA(polyglycolide) was used to prepare completely biodegradable sutures[149]. Since then, biodegradable polyesters such as PGA, PLA(polylactic acid), PCL and poly(D,L-lactide-co-glycolide)(PLGA) have been widely used in the

biomedical field[150].

PLA, PGA and PLGA have been extensively studied as scaffolds for cartilage tissue engineering[151] and controlled drug delivery vehicles[152]. They are being pursued not only because they are FDA approved biocompatible polymers, but also because one can simply manipulate the swelling abilities[153], mechanical properties[154] or degradation periods[151] by simply varying the ratio of lactide to glycolide, as shown in Table 2.3.

Table 2.3 Various properties of PLGA with different lactide to glycolide ratios (reproduced from[151])

Polymer	Modulus (GPa)	Elongation (%)	Solvent	Cristallinity (%)	Degradation Time (Weeks)	Applications	Reference
Polyglycolide/ Polyglactine	7.0	15–20	Hexafluoroispropanol	45–55	6–12	Suture anchors, meniscus repair, medical devices, drug delivery, orbital floor	[31–33]
Poly(L-lactide)	2.7	-	Benzene, THF, dioxane	37	12–18	Fracture fixation, interference screws, suture anchors, meniscus repair	[33–35]
Poly(D,L-lactide)	-	3–10	Methanol, DMF	Amorphous	11–15	Orthopaedic implants, drug delivery	[32,33,36]
Poly(D,L-lactide-*co*-glycolide) 85/15	2.0	3–10	Ethyl acetate, chloroform, acetone, THF	Amorphous	5–6	Interference screws, suture anchors, ACL reconstruction	[33,34,37,38]
Poly(D,L-lactide-*co*-glycolide) 75/25	2.0	3–10	Ethyl acetate, chloroform, acetone, DMF, THF	Amorphous	4–5	Plates, mesh, screws, tack, drug delivery	[32,33,36]
Poly(D,L-lactide-*co*-glycolide) 50/50	2.0	3–10	Ethyl acetate, chloroform, acetone, DMF, THF	Amorphous	1–2	Orthopaedic implants, drug delivery	[36,38]
Poly (L-lactide-*co*-glycolide) 10/90	-						[39,40]

PCL is another FDA approved polyester with nontoxic degradation products[155] and high potential as a biomaterial for tissue regeneration[156]. These hydrophobic, biocompatible polymers are potential candidate components for preparing IPN hydrogels because they can bring hydrophobicity to a hydrophilic network and then tune the swelling rate and equilibrium swelling ratio by varying their weight fractions. Thus a hydrogel tissue expander with controlled expansion could be obtained.

Semi-IPN hydrogels composed of PEG methacrylate and PLGA were prepared and showed a more controlled release of t-PA(tissue-type plasminogen activator)[157]. The released amount for 40%PLGA in the semi-IPN hydrogel was 25ug after 1 days while for 0% PLGA hydrogel the released amount was 55ug. Semi-IPN hydrogels composed

of crosslinked poly(3-hydroxyundecenoate)(PHU) and PLGA showed an increased tensile strength with increased PLGA content[158]. Semi-IPN with 10wt% and 20%PLGA showed a tensile strength of 0.66MPa and 1.14MPa, respectively, while PHU only showed 0.46kPa. Degradation was accelerated with the incorporation of PLGA because of the acidic degradation products of PLGA.

PEGDA/PLA semi-IPN hydrogels showed controlled protein drug release by varying PEG/PLA ratio[159]. Drug release decreased around 30% after 1 day with the incorporation of 50% PLA. However, the swelling ratio was also decreased from 4.4 to 2.6 when PLA content was increased from 0% to 50%.

PVA/PCL semi-IPN porous scaffolds showed doubled compressive modulus with the incorporation of 30%PCL, compared to PVA control sample[160]. However, the swelling ratio was decreased from around 14 for PVA to 4 for 30%PLA and 2 for 70%PLA.

2.5.5 Other IPN Hydrogels

PAAm/MC(methylcellulose) semi-IPN hydrogels were prepared with controlled hydrophilicity by varying PAAm and MA compositions[161]. Semi-IPN with 3.6% PAAm showed rapid expansion of around 68 within 10 hours, while increased PAAm content decreased the swelling rate, the equilibrium swelling ratio and extended the swelling period, as shown in Figure 2.13.

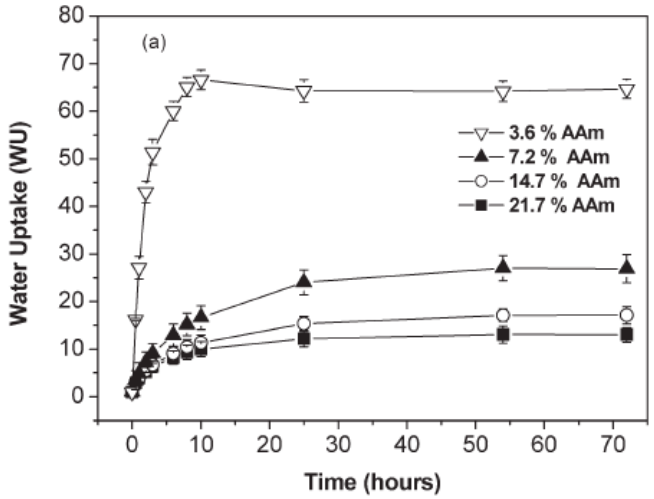

Figure 2.13 Water uptake as a function of time for PAAm/MC semi-IPN hydrogels in distilled water at 25℃ with different AAm compositions(reproduced from [161]).

PAA/CMC(carboxymethyl cellulose) semi-IPN hydrogels were prepared with a range of swelling ratio of 5 to 18 depending on the monomer ratios[162]. The swelling ratio first increased with either PAA or CMC content. However, when CMC content exceeded 1.5g or AA content exceeded 14.5mM in the preparation solution, the swelling ratio decreased with further increase in either content. This was explained by the increased entanglements and polymer density at over-high AA or CMC content, leading to a decreased mesh size of the hydrogel network.

IPN hydrogels composed of a hydrophobic poly(methyl methacrylate)(PMMA) or poly(ethyl acrylate)(PEA) as the first network and a hydrophilic poly(2-hydroxyethyl acrylate)(PHEA) as the second network were prepared and the swelling behaviour and tensile modulus were found to be dependent on the glass transition temperature of the first network[163]. PMMA (Tg of 110℃) was glassy while PEA(Tg of -10℃) was in a rubbery state at the experimental temperature. Pure PHEA showed a swelling ratio of 1.6 and a tensile modulus of 25.12MPa. PMMA/PHEA IPN showed a decreased swelling ratio in the range of 0.08 to 0.8 and modulus of 0.25GPa to 2.5GPa when PMMA weight fraction was increased from 0.13 to 0.64. However, PEA/PHEA showed

no obvious changes with increased PEA weight fraction. It was concluded that the restriction of the first hydrophobic network on the water absorption of the second hydrophilic network depends on the state (glassy or rubbery) of the first network.

2.6 Natural Skin Tissue

The swelling behaviour of hydrogels can be affected by the local ions and pH value of the swelling medium as has been discussed in section 2.2.9. Thus it is important to find out the actual swelling behaviour of hydrogel tissue expanders in vivo in an animal test. Besides, it is essential to find out whether the hydrogel can effectively generate tissue growth and whether the expanded tissue has the same quality as natural skin tissue.

The natural skin tissue has three main layers: epidermis, dermis and hypodermis (subcutaneous layer). Epidermis is composed of a keratinized stratified squamous epithelium. Dermis is a tough supporting and nourishing layer of fibroelastic and dense connective tissue. The dermis layer is composed of the papillary layer with fine fibres and the reticular layer with densely packed coarse fibres[164]. It also accommodates blood vessels, hair follicles, sweat glands and other structures. Hypodermis, the subcutaneous layer, is a looser connective tissue than the dermis and contains variable amounts of adipose tissue. The structure of the skin is shown in Figure 2.14. The properties of human skin tissue vary with age, for example, the Young's modulus has been tested to be 0.42MPa for the young and 0.85MPa for the old and also shown an increase with age[165].

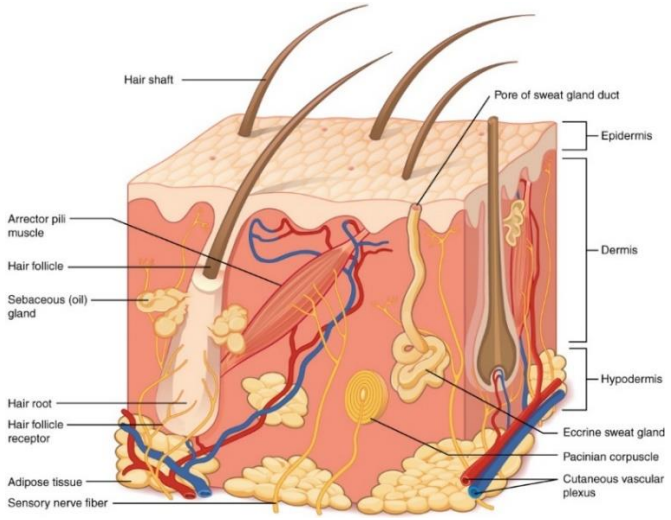

Figure 2.14 Schematic of the structure of natural skin tissue[166]

The histology of the expanded skin tissue will be analysed to see whether the expanded tissue has the same quality with the natural skin tissue. A typical histological section of normal human skin is shown in Figure 2.15. It shows a natural skin tissue with collagen fibres and sparse fibroblasts in the dermis layer. Collagen fibres are randomly oriented at the relaxed state, which is described as wavy[164]. Collagen fibres provides resistance to the stretch and tension from different directions[167]. Fibroblasts are capable of synthesizing responsible collagens, elastic and reticular fibres and the necessary components of the extracellular matrix.

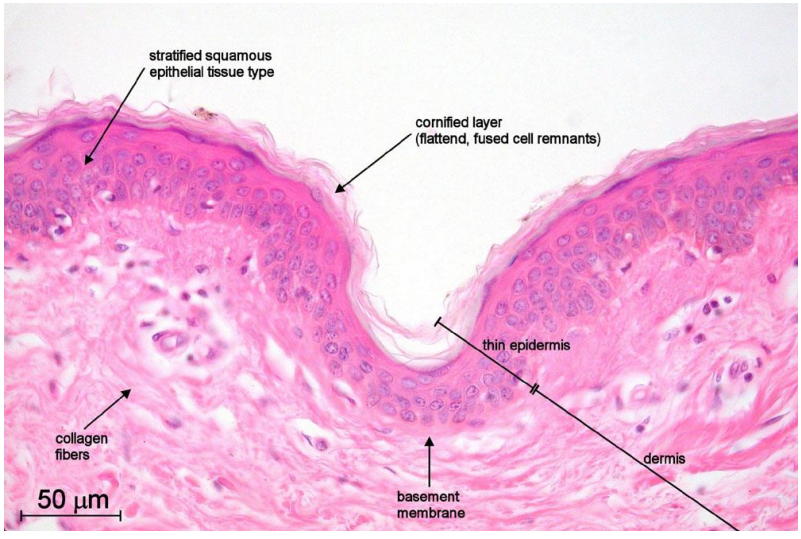

Figure 2.15 A typical histological section of normal human skin[168]

Controlled expansion will result in tissue growth with the histology similar to the natural skin tissue as shown in Figure 2.16, while over-rapid expansion will cause tissue necrosis. The histology of sheep skin tissue expanded by an uncoated VP/MMA hydrogel is shown in Figure 2.16. Skin ulceration is observed and the epithelial cells show pyknotic nuclei which indicates cell death. The dermis layer is filled with inflammatory cells with a number much larger than in the natural skin tissue. Skin ulceration and serious infection is also shown in AAc hydrogels implanted in a rat model[99].

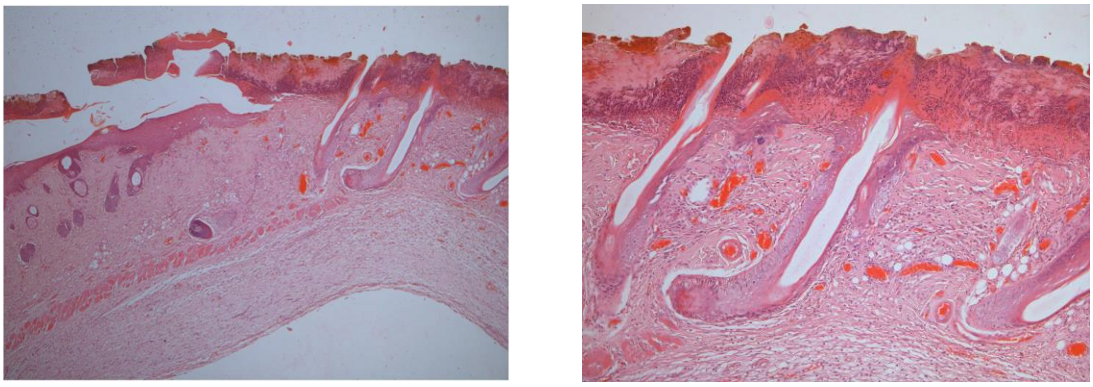

Figure 2.16 Histology of skin expanded by uncoated VP/MMA tissue expander

Thus it is important to show that the expanded tissue by a hydrogel has the same quality with natural skin tissue under histology analysis.

2.7 Summary

Hydrogels are physically or chemically crosslinked polymer networks that are able to imbibe and maintain a large amount of water. Wide ranges of hydrogels have been examined as potential candidates for replacement of soft tissue, drug delivery and release, tissue engineering scaffolds and other biomedical applications. The swelling behaviour of a hydrogel depends on its hydrophilicity/hydrophobicity(monomer ratios), the crosslinker content, the irradiation intensity and the ions and pH of the swelling medium. The higher content of the hydrophobic component results in less available binding sites for water molecules. The increase in crosslinker content or irradiation intensity generally decreases the mesh size of a hydrogel, resulting in less free volume for water molecules. A decrease in the ion concentration difference between the hydrogel network and the swelling medium causes a decrease in the osmotic pressure. In each case, a slower swelling rate and equilibrium swelling ratio will be obtained.

Their major disadvantage, i.e. their relatively low mechanical strength, can be overcome either by crosslinking, by formation of interpenetrating polymer networks (IPNs), or by crystallization. Among many of these attempts to improve wet strength, the IPN structure has been noted by many researchers because of its uniqueness of preserving the original properties of individual components. But as with other hydrogels, the increase in the mechanical properties of IPN hydrogels always comes at the expense of swelling capacity because the incorporation of a second polymer network increases the apparent overall cross-linking density [65, 123, 147, 169].

To be used as a desirable tissue expander, hydrogels should possess both the swelling capacity and the mechanical integrity at the swollen state. However, this remains a dilemma in the development of all kinds of hydrogels because of the plasticizing effect of water molecules.

Several examples of IPN hydrogels with controlled expansion have been illustrated [157, 159-161, 163], which are achieved by controlling the monomer ratios of a hydrophilic network and a hydrophobic one. Thus it is possible to design a IPN hydrogel tissue expander by introducing a hydrophobic, biodegradable polymer network(such as PLGA, PLA, PCL) penetrating into a pre-existing hydrophilic primary network(such as VP/MMA, HEMA, PAA based hydrogels). The hydrophobic secondary network will prevent the primary network(VP/MMA) from swelling too fast and thus avoid tissue necrosis. The equilibrium swelling ratio can be controlled by varying the weight fractions of the secondary polymer network. The molecular level inter-penetrating of the IPN structure will provide an inherent controlled swelling and saves the trouble of preparing a membrane or coating. Thus IPN tissue expander may be the solution of preparing self-inflating hydrogels with the ability to be crafted. And this study will focus on the preparation of IPN hydrogel tissue expanders with a proper selection of various primary networks and secondary networks. The primary goal is to prepare a desirable tissue expander with controlled expansion and the ability to be crafted by surgeons.

Animal tests need to be done to see the actual performance of the IPN hydrogel tissue expanders in vivo. The histology of natural human skin tissue has been shown in Section 2.6 and it is desirable that the expanded tissue has the same quality as the natural skin tissue.

Chapter 3: VP/MMA-PLGA IPN Hydrogel Preparation and Characterization

3 VP/MMA-PLGA IPN Hydrogel Preparation and Characterization

3.1 Introduction

The major limitation concerning self-inflating tissue expanders is their over-rapid expansion rate which will lead to tissue necrosis instead of tissue growth[13]. VP/MMA hydrogel is the primary osmotic tissue expander right now because of its biocompatibility, good swelling capacity and mechanical integrity during expansion. However, the expansion of VP/MMA reaches the equilibrium state within 2 days and uncoated VP/MMA has been shown to cause tissue necrosis in vivo[170]. A schematic of the swelling ratio of VP/MMA as a function of time is shown in Figure 3.1.

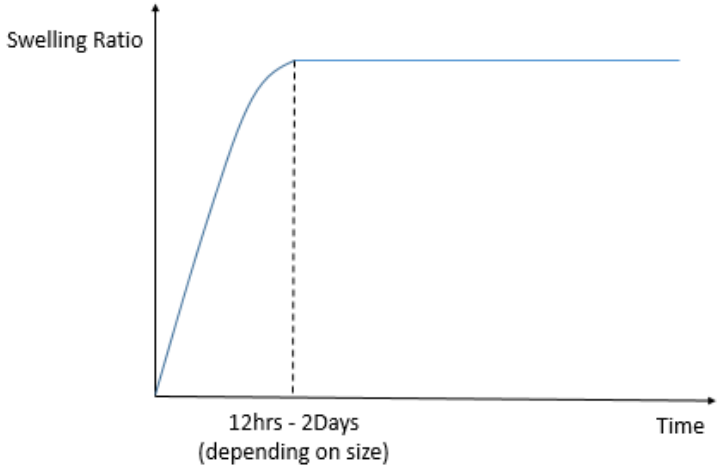

Figure 3.1 Schematic of the swelling ratio of VP/MMA as a function of time

In a desirable situation, the expansion should not initiate until a few days later, leaving enough time for the incision to heal. Moreover, the total expansion period should be in the range of 1 to 2 months, with adequate stretching for the generation of new skin cells. A schematic of the swelling ratio of a desirable tissue expander as a function of time is shown in Figure 3.2. It should be noted that only a large piece of tissue growth needs months to complete without causing tissue necrosis. For small tissue expansion, only days are needed as long as it does not cause tissue necrosis.

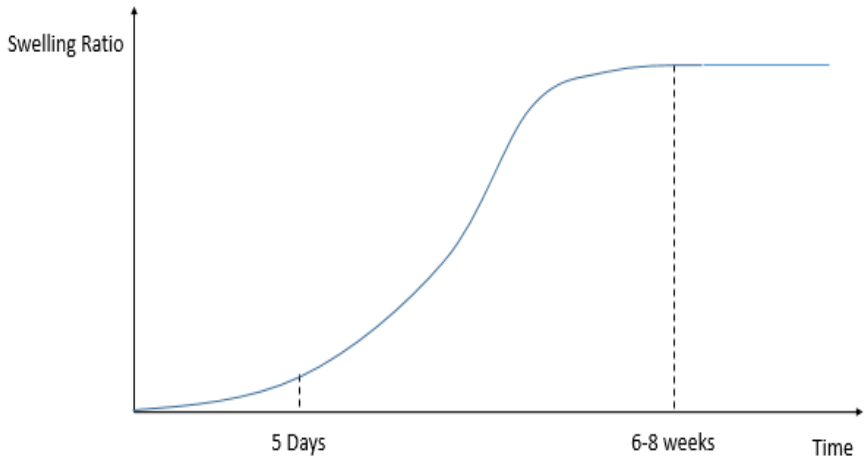

Figure 3.2 Schematic of the swelling ratio of a desirable tissue expander as a function of time

Coatings or semi-permeable silicone membranes have been applied on VP/MMA hydrogels to slow down the swelling rate[13, 170]. However, in clinical surgeries, a desirable tissue expander should be able to be crafted by surgeons to best fit into the void space on the patients. Unfortunately, coatings or membranes will be damaged upon cutting, which will result in a local burst of expansion leading to tissue necrosis.

Several examples of IPN hydrogels with controlled expansion have been shown in the literature review [157, 159-161, 163], thus it is worth looking into the preparation of IPN hydrogels as tissue expanders. IPN structure provides entanglements on a molecular level[101], endowing the hydrogel with an inherent controlled expansion and the ability to be crafted as well.

This chapter describes the preparation and characterization of VP/MMA-PLGA IPN hydrogel (will be abbreviated as PLGA IPN hereafter) tissue expanders composed of VP/MMA as the primary network and PLGA as the secondary network. PLGA IPN with varied PLGA or BIS(N, N'-methylenebisacrylamide, crosslinker) weight fractions will be prepared and their swelling behaviours, thermal and mechanical properties, and the internal structures revealed by SEM and SANS will be demonstrated.

Numerous studies have shown that by increasing the hydrophobicity or the crosslinker content, the corresponding EWC of a hydrogel would decrease, as shown in Section

2.2.5.1 and 2.2.5.2. But few studies have compared the effects of those two variables. In this study, PLGA IPN was prepared with varied PLGA weight fraction as well as varied crosslinker content to see which one is more important in controlling the swelling behaviour.

The objective of this chapter is to see:

1. What is the swelling behaviour and mechanical properties (swollen state) of PLGA IPN compared to VP/MMA? And what is the reason for the differences?
2. How does the incorporation of a secondary PLGA network change the internal structure of VP/MMA network?
3. How does BIS content affect the swelling behaviour of PLGA IPN?
4. PLGA weight fraction and BIS content, which one is more important affecting the swelling behaviour of PLGA IPN?
5. Can we achieve controlled swelling of PLGA IPN?

3.2 Experimental

3.2.1 Materials

VP/MMA xerogels(VP : MMA weight ratio 9:1) crosslinked with alkyl methacrylate (0.2wt%) as the crosslinker and azobisisobutyronitrile(AIBN)(0.2wt%) as the initiator were purchased from Polymeric Science Ltd (New Ash Green, UK). PLGA (50:50 lactic: glycolic acid) was purchased from Evonik Corporation(Birmingham Laboratories, US). The glass transition temperature, the weight average molecular weight (M_w) and polydispersity index (PDI) of PLGA is 30.5°C, 20kDa, and 2.0, respectively(according to Evonik Corporation). Acryloyl chloride, triethylamine, anhydrous ethyl acetate, n-hexane, and dichloromethane (DCM), BIS, deuterated water (D_2O) and deuterated chloroform($CDCl_3$) were purchased from Sigma-Aldrich (UK).

3.2.2 PLGA acrylation

PLGA needs to be acrylated first in order to be crosslinked in the presence of VP/MMA to form a full-IPN hydrogel. 8g PLGA was dissolved in a mixture of 120ml ethyl acetate and 5mM triethylamine in a round-bottom flask in an ice bath. 5mM acryloyl chloride was added dropwise under nitrogen and the mixture was left to react under 70°C for 3 hours and then left to cool under room temperature. The solution was filtrated 3 times to remove the residue triethylamine hydrochloride. N-hexane was then added to the filtrate to precipitate the functionalized PLGA. The precipitated PLGA was dried under vacuum under 40°C for 3 days. Figure 3.3 shows the schematic of the modification process of PLGA.

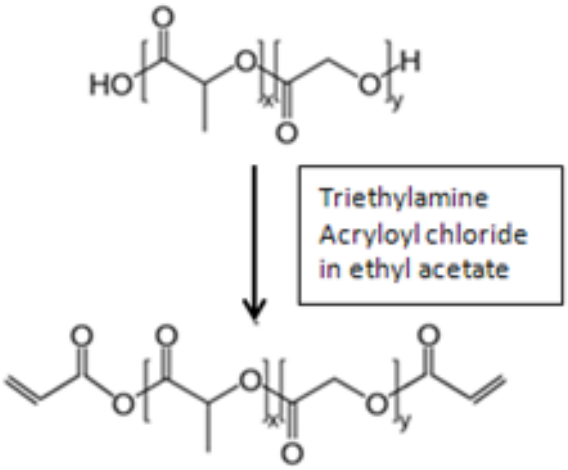

Figure 3.3 Schematic of the modification process of PLGA

3.2.3 Preparation of PLGA IPN

The acrylate end-capped PLGA was dissolved in DCM at three different concentrations, 0.025g/ml, 0.05g/ml, and 0.1g/ml. IPN with different PLGA weight fractions were denoted as vmplga0.025, vmplga0.05, vmplga0.1, respectively. VP/MMA discs with 7mm in diameter and 2.5mm in height were immersed in the solution, which was shaken in a water bath at 37°C for 3 days until VP/MMA reached the maximum swollen state. 0.2wt%(based on mass of PLGA) of the crosslinker BIS and 0.2wt%(based on

mass of PLGA) of the initiator AIBN was added and the solution was kept in the water bath at 37°C for another 2 days to induce the crosslinking of PLGA penetrating through the hydrogel base. Samples were then taken out, air dried under room temperature for 5 days and then dried under vacuum at 50°C for another 5 days to remove any residual solvent. Figure 3.4 shows the schematic of the PLGA IPN preparation process.

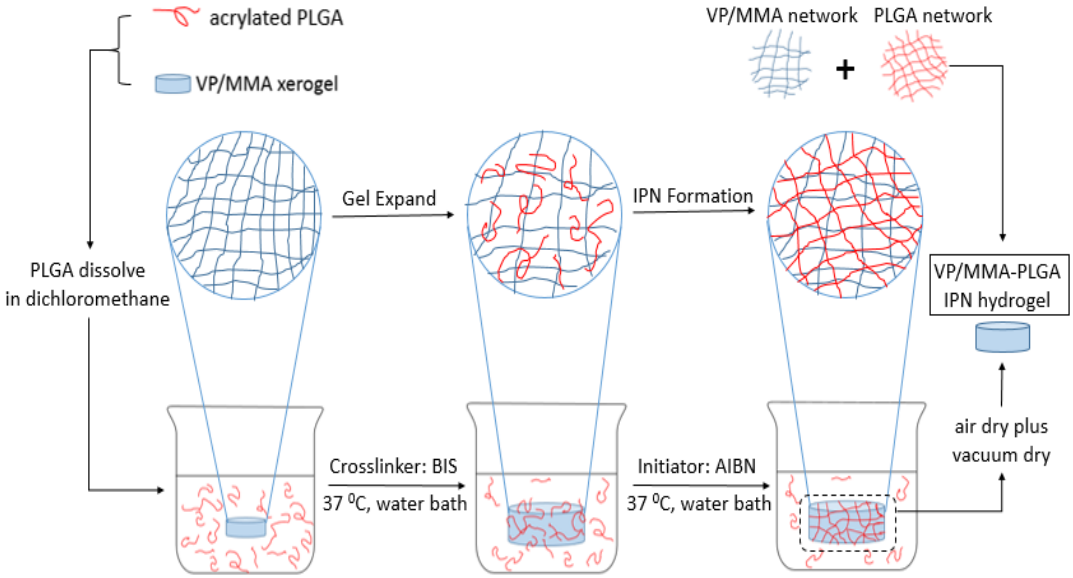

Figure 3.4 Schematic of the preparation of VP/MMA-PLGA IPN hydrogel

PLGA weight fraction in the dry PLGA IPN is calculated using equation(3.1), where m_{vmplga}, m_{vm} is mass of dry PLGA IPN and mass of VP/MMA xerogel disc used during preparation, respectively:

$$PLGA\ weight\ fraction = \frac{m_{vmplga} - m_{vm}}{m_{vmplga}} \times 100\% \quad (3.1)$$

According to experimental experiences, vmplga0.025, vmplga0.05, vmplga0.1 samples correspond to PLGA weight fractions of 20-30%, 40-50% and 60-70% in dry PLGA IPN, respectively.

43.9% and 62.8%PLGA IPN with 0.2wt%(based on PLGA monomer) and 2wt% crosslinker (BIS) were also prepared to find out the influence of crosslinker content on the swelling behaviour of the IPN hydrogels.

3.2.4 Nuclear Magnetic Resonance (NMR)

The presence of acrylation of PLGA was examined by Nuclear Magnetic Resonance ^{1}H NMR (1-dimensional proton magnetic resonance). NMR identifies the functional groups or unique structure of a compound. Different functional groups have different resonance frequencies due to the difference in the magnetic environment experienced by the nuclei[171]. And compared to FTIR (infrared spectroscopy), NMR has a higher resolution. VP/MMA or VP/MMA-PLGA IPN hydrogels cannot be analysed by NMR because they won't be dissolved in any solvents and solids requires an additional machine but provides only very broad bands with no resolved structure[171].

10mg/ml solution of original PLGA as well as the functionalized PLGA with acrylate end groups in deuterated chloroform($CDCl_3$) were tested under a Varian Mercury-300 ^{1}H NMR at room temperature. The acrylate end groups have a unique resonance frequency. The absence and presence of the resonant signals from acrylate groups before and after the functionalization process should be able to verify the successful acrylation of PLGA.

3.2.5 Differential Scanning Calorimetry (DSC)

Differential scanning calorimetry (DSC) is a widely used technique to detect the glass transition temperature (T_g) of a polymer. Figure 3.5 shows the schematic of how a DSC machine works. There are two pans, one contains the polymer and the other is empty as the reference pan. Each pan is set on top of a heater and the heating rate is the same for both pans. The difference in the heat output of the two heaters against temperature will be measured by the computer, which shows the heat absorbed by the polymer. Glass transition refers to the reversible transition of a polymer from a hard and brittle state to a rubbery state, which can be detected by monitoring the heat flow during the heating process. An increase in the heat flow (or heat capacity) of the polymer indicates its glass

transition process which usually covers a temperature range.

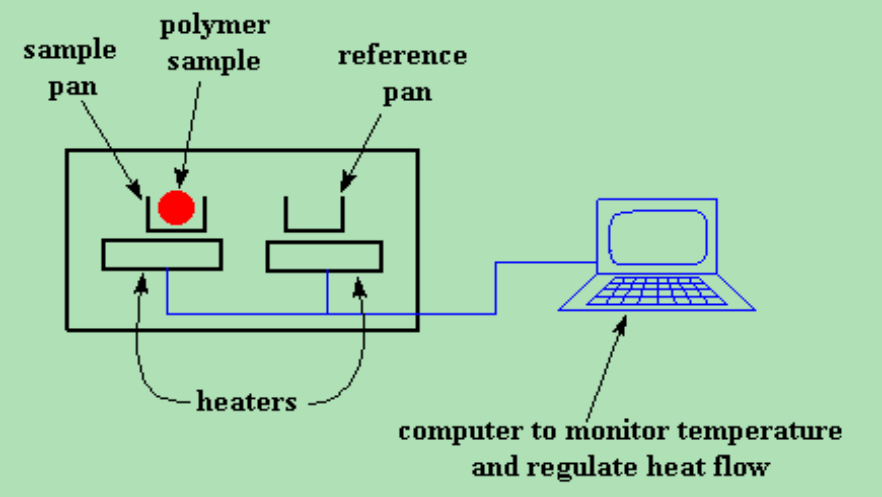

Figure 3.5 Schematic of DSC(reproduced from [172])

T_g of original PLGA, acrylated PLGA and PLGA IPN (dry state) were determined by differential scanning calorimetry (Pyris Diamond Hyper DSC) with a heating rate of 100°C /min over a temperature range of -100 to 200°C. Samples weighing within 5-10mg were analysed in aluminium pans, using an empty pan as the reference. The purge gas was helium at a flow rate of 50ml/min. A combination of heating, cooling and heating a second cycle was used in the measurements to improve the resolution.

The measurement of T_g can show phase separation in IPN hydrogels, indicating the existence of two individual polymer networks[109]. Moreover, T_g of PLGA will be compared with T_g of PLA and PCL (to be discussed in Chapter 4) to see if T_g of the secondary polymer network has any effect on the swelling behaviour of the IPN hydrogels.

T_g is extracted by the computer using the method shown in Figure 3.6 and the relative values will be shown on the specific DSC graphs. The black dashed lines are the extrapolated lines or tangent lines of the linear(almost) sections of the curve before, during and after the glass transition. The intersections are marked as onset point and end point. The difference in heat capacity ΔC_p can be calculated using the equation below

and T_g is the temperature corresponding to the half-height of the heat capacity increase.

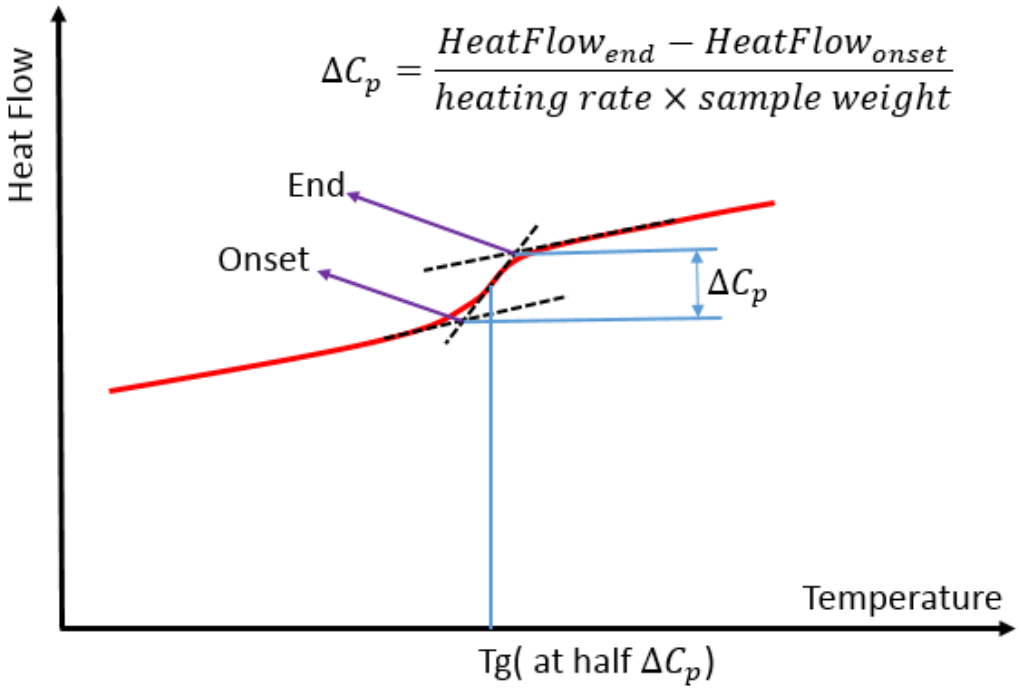

Figure 3.6 Schematic of Tg extracted from the DSC curve

3.2.6 Compression Test

Compression tests were performed on swollen samples using a Perkins Elmer DMA 7e dynamic mechanical analyser. Due to the deficiency of the DMA machine, it is only able to record the stress and strain at a set compression force rate and a maximum force. PLGA IPN and VP/MMA swollen discs were placed in the centre of the plate and compressed under a rate of 100mN/min and a maximum load of 6000mN, as shown in Figure 3.7. Compressive modulus E is calculated as the gradient of the curve in the strain range of 12%-14%. This range of strain is chosen because of these considerations:

1. The machine calculated the strain by measuring the change in the sample height. However, the sample surface is not totally flat and the machine will record from its highest point. Thus the initial region of the curve may not be reliable.
2. This range seems linear indicating elastic deformation.

Figure 3.7 Dynamic Mechanical Analysis

It is important for tissue expanders to maintain their mechanical integrity during expansion, especially when implanted under the subcutaneous layer of human skin. The compressive modulus E is also useful for the calculation of hydrogel structure parameters (such as effective crosslinking density, Flory-Huggins interaction parameter) which will be used to help explain the swelling behaviour of PLGA IPN.

3.2.7 Small Angle Neutron Scattering (SANS)

SANS is a neutron scattering technique that investigates the internal structure of a material on the nanometre to micrometre scale. SANS has been widely used in analysing the inhomogeneity in polymer solutions and hydrogels and also providing information about the shape, size and interactions of the scattering bodies[173]. Thus it is useful to apply SANS on PLGA IPN to see how the incorporation of PLGA network affects the VP/MMA network. SANS also provides a way to see if the polymer system is purely phase separated or not by fitting with the corresponding model.

Incident neutrons interact with a sample and a neutron detector measures the scattered neutron intensities, as shown in Figure 3.8.

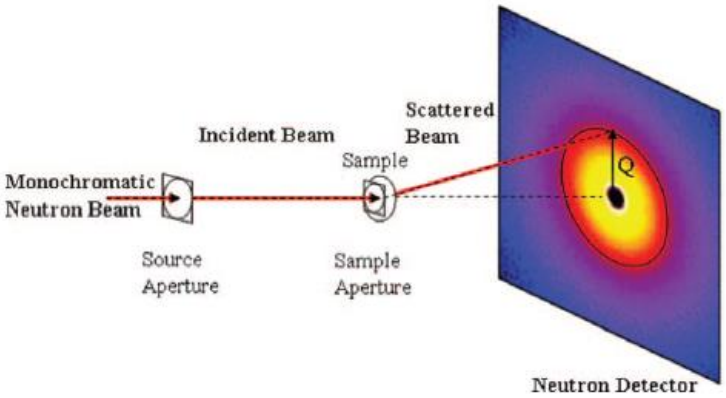

Figure 3.8 Schematic of SANS (reproduced from[173])

The scattering vector Q is defined in equation(3.2), where θ is the scattered angle and λ is the incident neutron wavelength:

$$Q = \frac{4\pi \sin\frac{\theta}{2}}{\lambda} \tag{3.2}$$

SANS signal is composed of a constant incoherent scattering(background) and a Q dependent coherent scattering, while only the latter contains useful information about the polymer structure. The coherent scattering cross section $\frac{d\sum Q}{d\Omega}$ (cm^{-1}) is described in equation(3.3), where ∅ is the volume fraction, $\Delta\rho^2$ is the contrast, P(Q) is the form factor related to size and shape of the scattering bodies and S(Q) is the structure factor showing interparticle correlation[173].

$$\frac{d\sum Q}{d\Omega} = \emptyset\Delta\rho^2 V_p P(Q) S(Q) \tag{3.3}$$

The contrast $\Delta\rho^2$ is the square of scattering length density(SLD) difference between polymer and solvent. SANS signal exists only when there is contrast.

VP/MMA and PLGA IPN with varied PLGA weight fractions were immersed in deuterated water until equilibrium state. Samples were swollen to the equilibrium state and cut into slices around 1mm thick and held in a sealed aluminium foil envelope to prevent dehydration. SANS was carried out on the Sans2d small-angle diffractometer at the ISIS Pulsed Neutron Source(STFC Rutherford Appleton Laboratory, Didcot, UK). A

collimation length of 4m and incident wavelength range of 1.75 – 16.5A was employed. Data were measured simultaneously on two 1 m^2 detectors to give a Q range of 0.004 – 1.00A^{-1}, which means a length scale($2\pi/Q$) between 6-1570A is probed. The small-angle detector was positioned 4m from the sample and offset vertically 60 mm and sideways 100 mm. The wide-angle detector was position 2.4m from the sample, offset sideways by 980 mm and rotated to face the sample. The beam diameter was 8 mm. Each raw scattering data set was corrected for the detector efficiencies, sample transmission and background scattering and converted to scattering cross-section data using Mantid software. These data were placed on an absolute scale (cm^{-1}) using the scattering from a standard sample(a solid blend of hydrogenous and per-deuterated polystyrene).

SANS data is interpreted using various models composing of various form factors and structure factors[174]. SANS data is always combined with data from other techniques such as SEM to help choose the appropriate model to evaluate the structural information. Here several models related to this work are illustrated. The scattered intensity I(Q) actually means the differential cross section $\frac{d\sum Q}{d\Omega}$ in those models[174].

1. DAB Model (Debye-Anderson-Brumberger Model)

The DAB Model[175] describes I(Q) as a function of Q in equation(3.4), where ξ is the correlation length and A, B are constants. DAB is used to characterize a system totally phase separated. ξ measures the average distance between regions of phase 1 and phase 2.

$$I(Q) = \frac{A}{(1+Q^2\xi^2)^2} + B \tag{3.4}$$

2. Lorentzian Model

The Lorentzian Model[174] is described in equation(3.5), where C, B are constants, m

is the Porod exponent. For polymer chains in a good solvent, m=5/3, and for chains in theta solvent m=2. Deviation from this model plot at the low Q range($Q < 0.01A^{-1}$) shows non-homogeneity in the scattering sample[174].

$$I(Q) = \frac{C}{1+(Q\xi)^m} + B \tag{3.5}$$

3. Correlength Model

The Lorentzian Model may not be adequate to describe a SANS data, especially when there is inhomogeneity at the low Q range[176]. Thus the Correlength Model is proposed[176] in equation(3.6), where $\frac{A}{Q^n}$ describes the Porod scattering from clusters(aggregates), and $\frac{C}{1+(Q\xi)^m}$ describes polymer/solvent interactions, i.e. thermodynamics, A, C, B are constants, n and m are fitting exponents:

$$I(Q) = \frac{A}{Q^n} + \frac{C}{1+(Q\xi)^m} + B \tag{3.6}$$

Exponent m is related to the excluded volume parameter[29]. m=5/3 shows a self-avoiding walk corresponding to swollen chains, while m=2 shows pure random walk in theta conditions and m=3 shows self-attracting walk corresponding to collapsed (not swelling) chains[176].

4. GaussLorentz Model

The GaussLorentz Model[177] is constructed for a typical single-network gel structure and composed of a first term(Gauss term) describing the static correlations and the second term(Lorentzian term) describing the dynamic correlations, as shown in equation(3.7). Ξ and ξ are static and dynamic correlation length, respectively. Ξ characterizes the average distance between static heterogeneities and ξ characterizes the correlation length of fluctuating polymer chains. $I_G(0)$ and $I_L(0)$ are the linear coefficients of each term.

$$I(Q) = I_G(0)exp\left(-\frac{Q^2\Xi^2}{2}\right) + \frac{I_L(0)}{1+Q^2\xi^2} \quad (3.7)$$

5. GelFit Model

The above GaussLorentz Model has a limiting Q dependence of -2 in the Lorentzian term. The GelFit Model[178] is a more generalized implementation of the GaussLorentz Model and is described in equation(3.8), where D is the fractal dimension of the system. The GelFit Model equals the GaussLorentz Model when D=2(theta conditions).

$$I(Q) = I_G(0)exp\left(-\frac{Q^2\Xi^2}{2}\right) + \frac{I_L(0)}{\left(1+\left[\left(\frac{D+1}{3}\times Q^2\xi^2\right)\right]\right)^{D/2}} \quad (3.8)$$

It should be noted that exponent m in the Correlength Model has the same meaning as the fractal dimension D shown in the GelFit Model. The fractal dimension D shows the behaviour of the polymer chains in the solvent and is well illustrated in Figure 3.9:

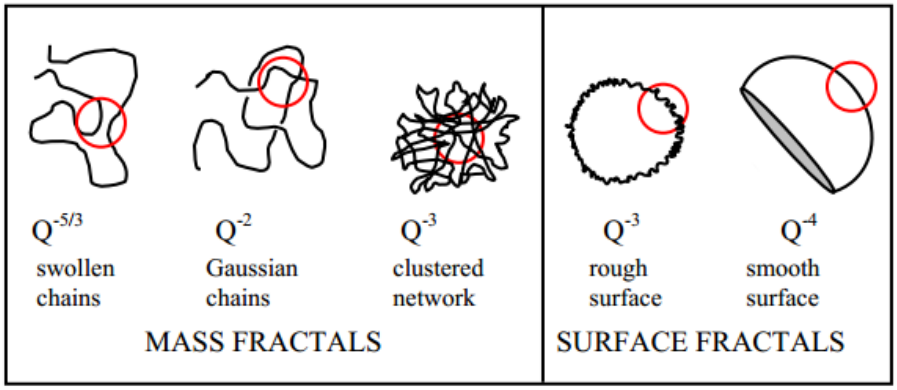

Figure 3.9 Fractal Dimensions(reproduced from[174])

SANS data of PLGA IPN were analysed using software Sasview with the above mentioned models. Data was fitted in the Q range of 0.004~0.7A^{-1} to avoid the statistically noisy data at the very extremes of the datasets. For each fitting, Sasview will give a Chi2/Npts value showing the goodness of the fit. Chi2/Npts is calculated using a least squared fitting algorithm. The smaller the Chi2/Npts value, the better the fitting.

3.2.8 Scanning electron microscope (SEM)

SEM is widely used to detect the surface morphology of a sample. SEM measurements of VP/MMA and PLGA IPN will show how the incorporation of PLGA changes the microstructure of VP/MMA and also provide information about how the IPN is formed. VP/MMA and PLGA IPNs were studied using field emission scanning electron microscope(Zeiss Nvision 40). Freeze-dried samples were cut in cross section, mounted on a double sided tape on aluminium spin stubs and sputter coated with gold using E 5400 Sputter Coater(Bio-Rad, Polaron Division). SEM images were recorded under the accelerating voltage of 2kV and 0.2k-6k magnification.

3.2.9 Swelling Behaviour in distilled water

The swelling behaviour tests of VP/MMA and PLGA IPNs were performed in distilled water at 37°C. Disc shape samples were taken out at specified time intervals and the excess surface water was removed by filter paper. The gels were measured in the diameter and height with a caliper(Absolute Digimatic Calier, Mitutoyo, Japan) and weighed by an electronic balance (ABS analytical balance, Kern Scale Tehnic, UK) until a constant volume and mass was reached. Samples were tested in triplicate and the average value was calculated. Distilled water was replaced daily.

For tissue expanders, volume swelling ratio is focused rather than mass swelling ratio as volume expansion rate and ratio are much more important. Volume swelling ratio Q_v is described in equation(3.9), where V_t and V_0 stand for sample volume at time t, and before the immersion, respectively:

$$Q_v = \frac{V_t - V_0}{V_0} \times 100\% \tag{3.9}$$

Q_v is plotted as a function of time. Initial swelling rate R_i is one of the important properties of tissue expanders because over-rapid initial swelling rate will lead to wound dehiscence and tissue necrosis. The initial volume swelling rate R_i(%/h) is

calculated as the slope of the initial linear region of the curve and swelling period T_e(h) is read from the curve as the time taken to reach the equilibrium state.

Equilibrium volume swelling ratio Q_∞ is defined in equation(3.10), where V_∞ is the sample volume at the equilibrium state:

$$Q_\infty = \frac{V_\infty - V_0}{V_0} \times 100\% \tag{3.10}$$

The equilibrium water content (EWC) is expressed in equation(3.11), where M_o and M_∞ are the mass of hydrogel before the immersion and at equilibrium, respectively:

$$EWC = \frac{M_\infty - M_o}{M_\infty} \tag{3.11}$$

Q_v is plotted as a function of time to show the overall expansion process. Q_∞ is plotted as a function of PLGA weight fraction to see if the equilibrium swelling ratio can be controlled by controlling PLGA weight fraction.

Polymer volume fraction φ_s (at equilibrium state) is defined using equation(3.12):

$$\varphi_s = \frac{V_0}{V_\infty} \times 100\% \tag{3.12}$$

Density of the hydrogel (at equilibrium state) is defined using equation(3.13):

$$\rho = \frac{M_\infty}{V_\infty} \tag{3.13}$$

3.3 Results

3.3.1 Nuclear Magnetic Resonance

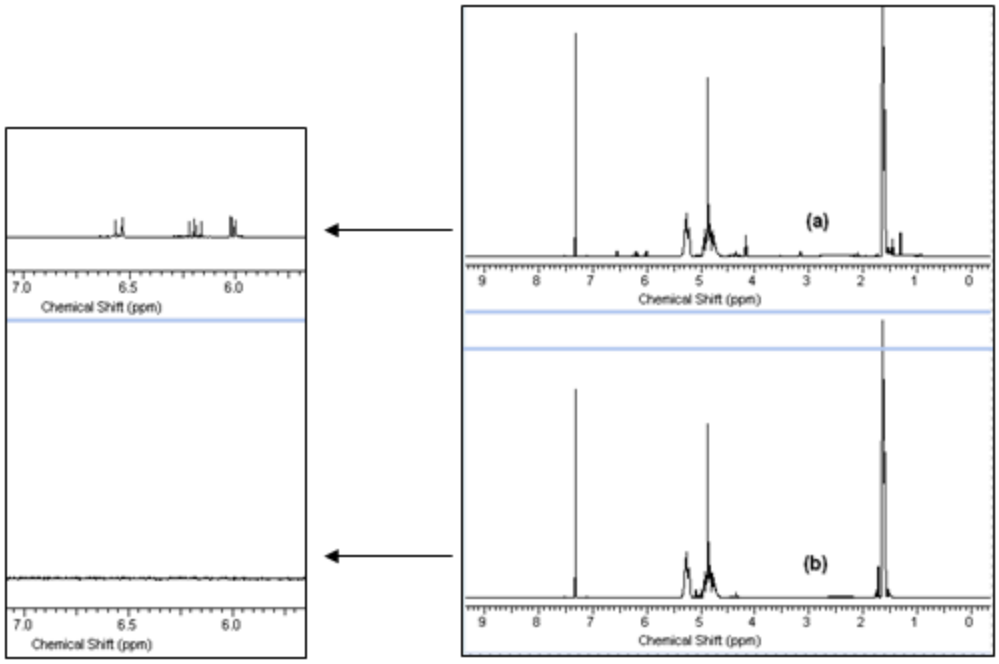

Figure 3.10 ^{1}H-NMR spectrum of (a) functionalized PLGA (b) and original PLGA

The ^{1}H-NMR spectrum of the functionalized PLGA (a) and original PLGA(b) are shown in Figure 3.10. Figure 3.10(a) and Figure 3.10(b) share several peaks from the main structure of PLGA. The peaks around 1.6 ppm correspond to the methyl groups (-CH_3), while the peaks around 5.1-5.3ppm correspond to the methine groups(-CH) in the lactide repeat units[179]. The peaks observed around 4.9ppm belong to the methylene groups (-CH_2) of the glycolide units[179]. The presence of the peaks at around 5.93ppm, 6.19ppm and 6.5ppm owing to the vinyl end groups[180] in Figure 3.10(a) demonstrates the existence of acrylate end groups in functionalized PLGA, which are not observed in original PLGA. The successful acrylate end-capping enables PLGA to be crosslinked into a biodegradable polymer network in the presence of a primary VP/MMA hydrogel network, forming a full-IPN hydrogel.

3.3.2 Differential Scanning Calorimetry

The glass transition temperature of the original PLGA is 37 °C according to the data information provided by the manufacturer. T_g of the original PLGA was tested and its DSC spectrum is shown in Figure 3.11. No obvious peak but a broad endothermic peak was observed and the extracted T_g is 22.7 °C.

DSC spectrum of the acrylated PLGA is shown in Figure 3.12. Again a very broad endothermic peak is observed and the extracted T_g is 21.2°C. This shows that there is no significant difference in the glass transition temperature before and after the acrylation of PLGA.

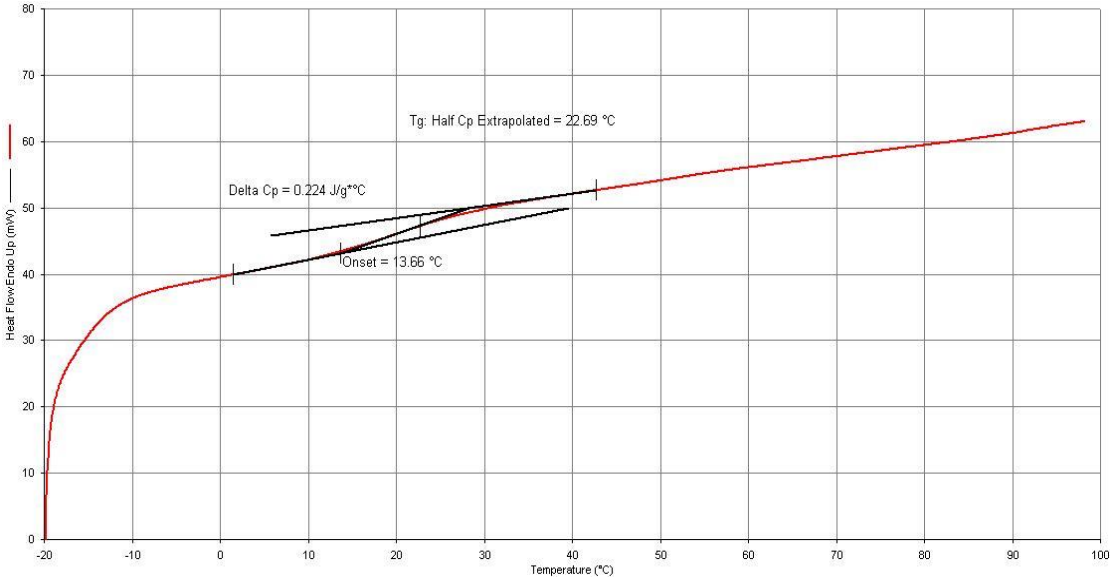

Figure 3.11 DSC spectrum of original PLGA

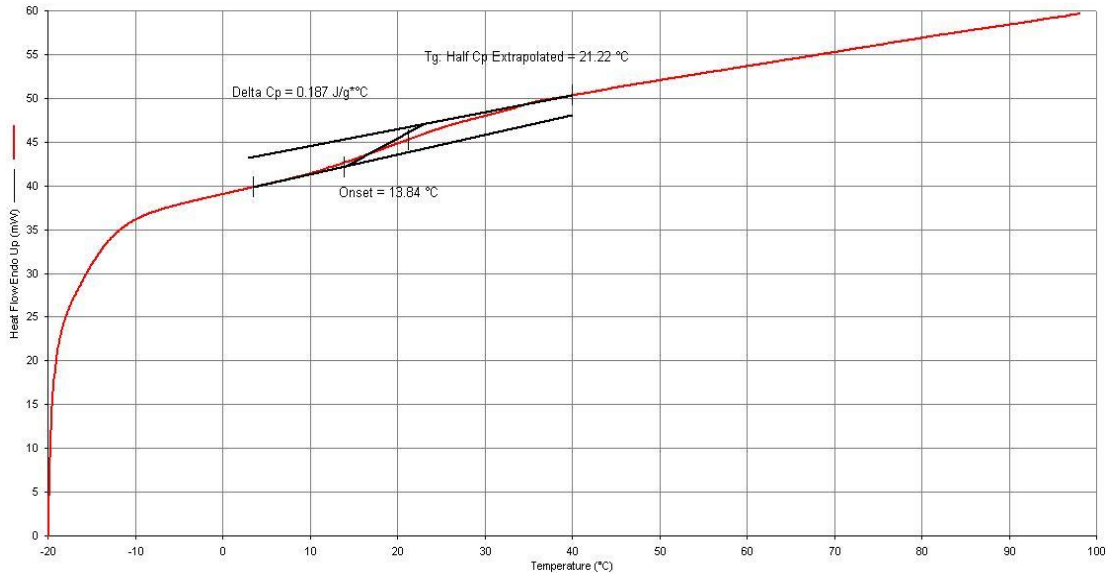

Figure 3.12 DSC spectrum of acrylated PLGA

The glass transition of PLGA IPN(dry state) is shown in Figure 3.13. The red line stands for the first heat cycle and the black one stands for the second one. No obvious endothermic peak was observed in both cycles. There is evidence of sample instability at temperatures higher than 130°C, which is again observed in the second cycle. The only detectable T_g is extracted from the very broad region around 20°C. T_g obtained in the first cycle is 16.88°C while T_g obtained from the second cycle is 16.95°C. This T_g is believed to be owing to the glass transition of PLGA. The glass transition of VP/MMA is not observed in both cycles. The meaning of the values shown in Figure 3.13 has been illustrated in Section 3.2.5.

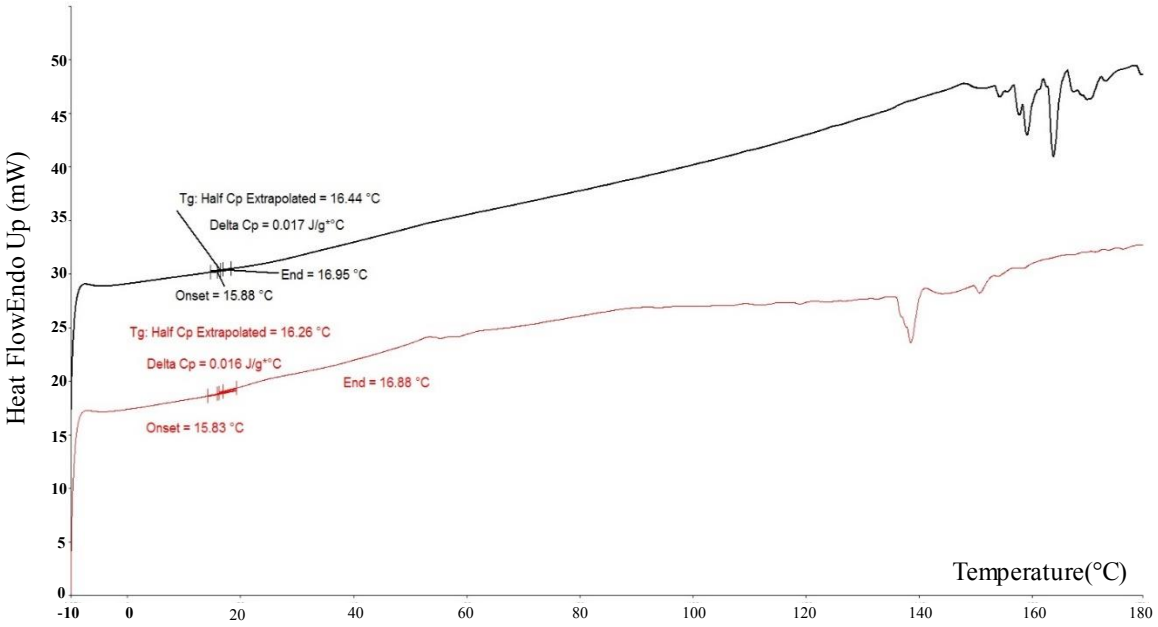

Figure 3.13 DSC spectrum of PLGA IPN (dry state).

3.3.3 Compression Test

Figure 3.14 shows the typical stress (Pa)-strain (%) curves for VP/MMA and PLGA IPN with varied PLGA weight fractions(calculated using equation(3.1)). The compressive modulus E was calculated as the slope of the curves in the strain range of 12%-14%. All the samples showed elastic deformations up to 50% of strain and no fractures were observed. During the compression, there must be some loss of water of

the hydrogel although it is not visible. Thus the compressive modulus calculated might be higher than the actual modulus as loss of water contributes to the stiffness of the hydrogel.

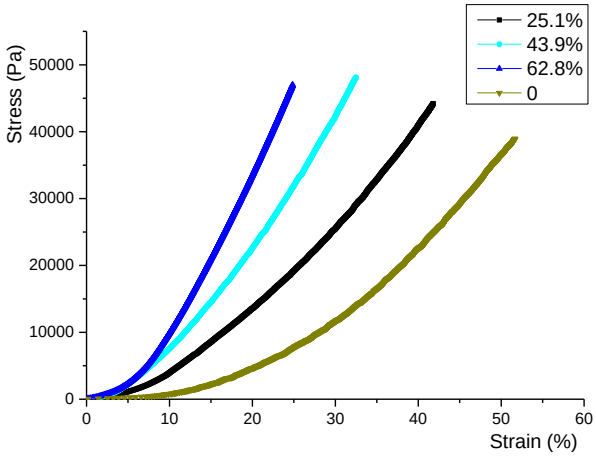

Figure 3.14 The stress-strain curves of PLGA IPNs and VP/MMA (swollen state)

The compression modulus E is summarized in Table 3.1:

Table 3.1 The compressive modulus of VP/MMA and PLGA IPNs

PLGA weight fraction (%)	E(10^5 Pa)
0	0.32
25.1	0.88
43.9	1.44
62.8	2.28

Figure 3.15 plots E as a function of PLGA weight fraction, which shows a linear relationship.

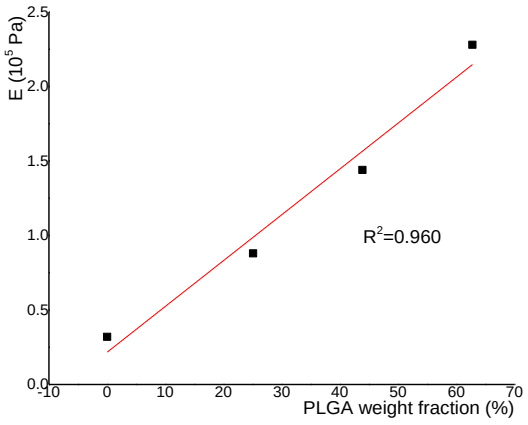

Figure 3.15 Compressive modulus E as a function of PLGA weight fraction

3.3.4 Small-angle Neutron Scattering

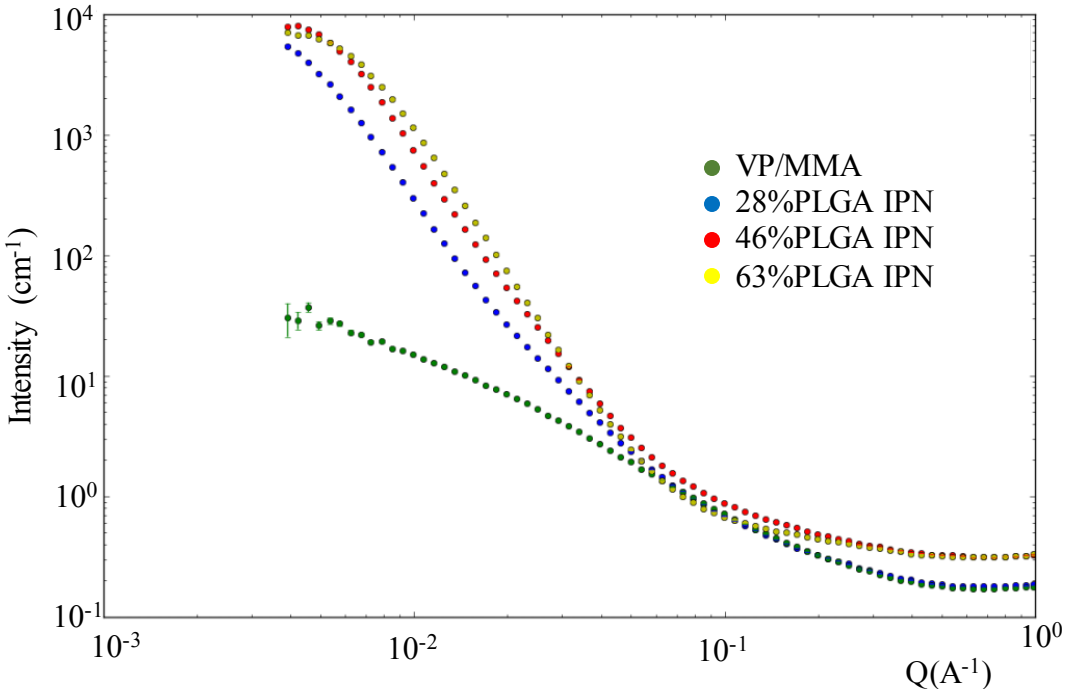

Figure 3.16 SANS spectra of VP/MMA and PLGA IPNs(swollen state), VP/MMA(green), 28%PLGA IPN(blue), 46%PLGA IPN (red), 63%PLGA IPN (yellow).

Figure 3.16 shows the scattering intensity I(Q) as a function of scattering vector Q of VP/MMA and PLGA IPN with varied PLGA weight fractions. No scattering peaks were observed. There is not much difference between the SANS spectra of PLGA IPN with different PLGA weight fractions. Compared with VP/MMA, PLGA IPNs show a higher scattering intensity (more often described as excess scattering) at the low Q range, especially when $Q<0.01\ A^{-1}$. No significant difference is observed for all the samples when scattering vector $Q>0.1\ A^{-1}$.

3.3.5 Scanning Electron Microscope

Figure 3.17 shows SEM images of the swollen VP/MMA hydrogels at the equilibrium state. VP/MMA shows a porous network structure with smooth surfaces. There are some areas where the polymer is more concentrated, as shown in Figure 3.17(a). A range of pore sizes was observed, for example, small pores (pore size < 2μm) as shown

in Figure 3.17(c), medium size pores (pore size ~ 10µm) as shown in Figure 3.17(d) and large pores (pore size >40µm) as shown in Figure 3.17(e).

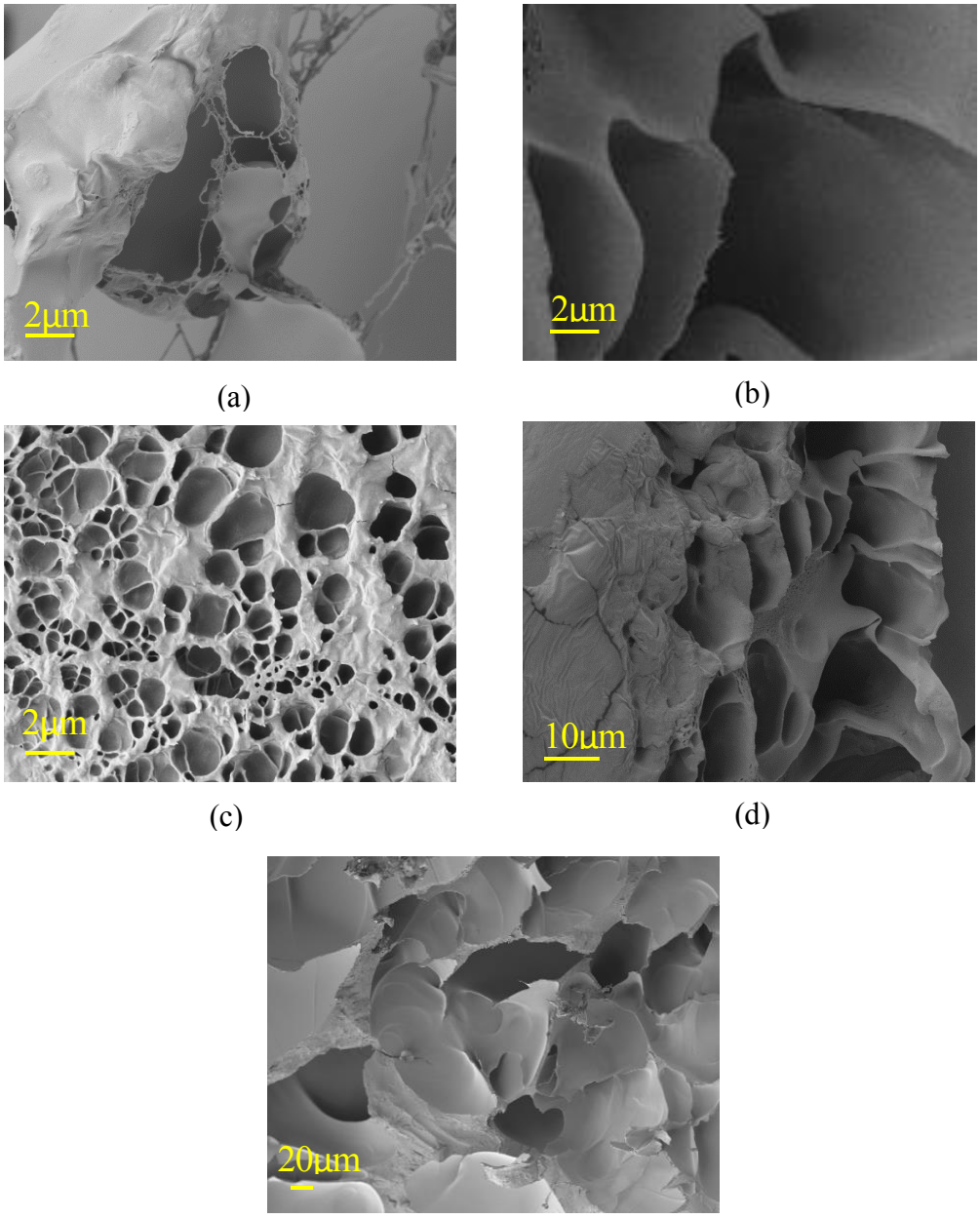

(a) (b) (c) (d) (e)

Figure 3.17 SEM images of VP/MMA

Figure 3.18 shows the SEM images of 25.1%PLGA IPN at the equilibrium state, which shows a porous network. Collapsed cells can also be observed as shown in Figure Figure 3.18(c). This could be a result of freeze-drying which may fail to preserve the original structure of the hydrogel at some places. 25.1%PLGA IPN has rougher surfaces

and thicker pore walls(Figure 3.18(a)) compared to VP/MMA(Figure 3.17(b)). Overall, the pore sizes of 25.1%PLGA IPN and VP/MMA are comparable but 25.1%PLGA IPN shows a more compact structure than VP/MMA.

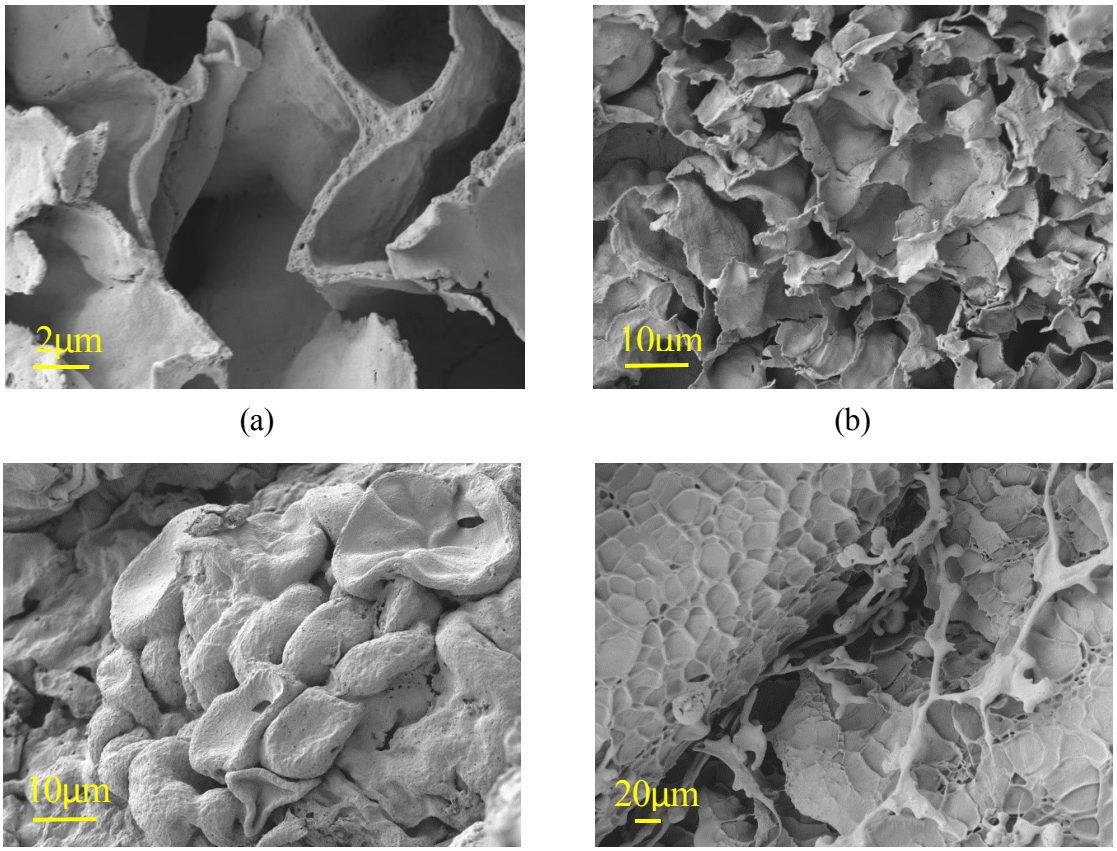

(a) (b)

(c) (d)

Figure 3.18 SEM images of 25.1%PLGA IPN

Figure 3.19 shows the SEM image of 43.9%PLGA IPN and 62.8%PLGA IPN. No porous structure was detected. Figure 3.19(a) shows collapsed balloons for 43.9%PLGA IPN and Figure 3.19(b) shows a compact structure with large aggregates and rough surfaces for 62.8%PLGA IPN.

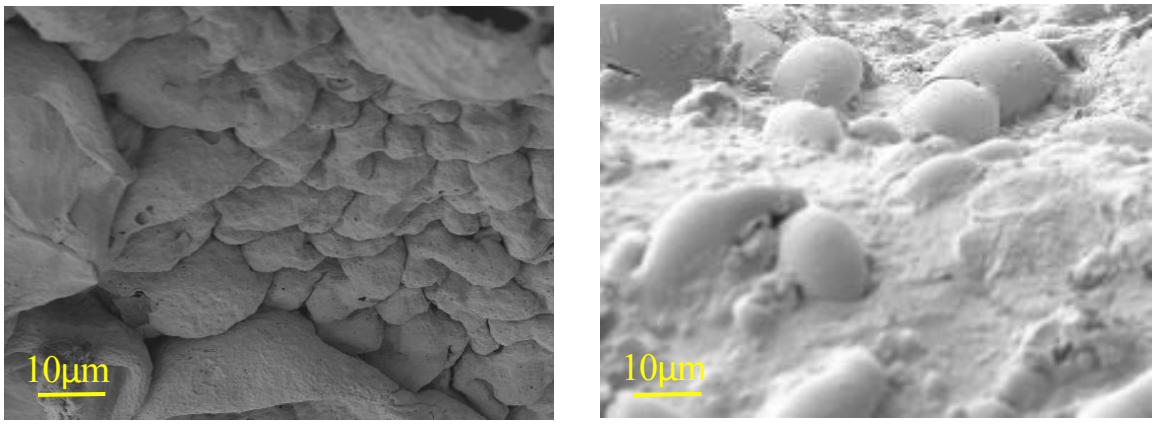

(a) 43.9% PLGA IPN (b) 62.8% PLGA IPN

Figure 3.19 SEM images of 43.9%PLGA IPN and 62.8%PLGA IPN

3.3.6 Swelling Behaviour

Figure 3.20 shows the volume swelling ratio Q_v of VP/MMA and PLGA IPNs as a function of time. For all the hydrogels, Q_v quickly increases up to a certain level at the initial state and then levels off. Q_v of VP/MMA reaches 90% of its maximum swelling within the first 10 hours. Q_v of PLGA IPN is slower and it takes longer to reach the equilibrium state, which is more obvious with higher PLGA weight fractions.

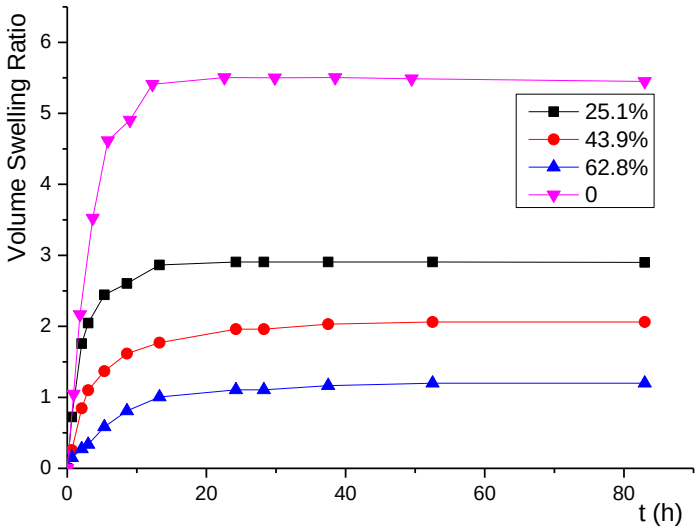

Figure 3.20 Swelling Behaviours of VP/MMA-PLGA IPN hydrogels in distilled water

Table 3.2 Swelling Parameters of VP/MMA and PLGA IPN

	Initial swelling rate R_i (%/h)	Equilibrium Swelling Ratio(100%)	Swelling Period(h)	EWC(%)
VP/MMA	96.0	5.5	12	85.6
25.1%PLGA IPN	68.4	3.0	18	75.3
43.9%PLGA IPN	37.4	2.1	40	66.9
62.8%PLGA IPN	10.6	1.2	60	55

Table 3.2 summarizes the initial swelling rate R_i, the equilibrium swelling ratio Q_∞, the swelling period, and the EWC of VP/MMA and PLGA IPNs. R_i and Q_∞ is largely decreased with the increase in PLGA weight fraction, while the time taken to reach the equilibrium state increases with the increase in PLGA weight fraction.

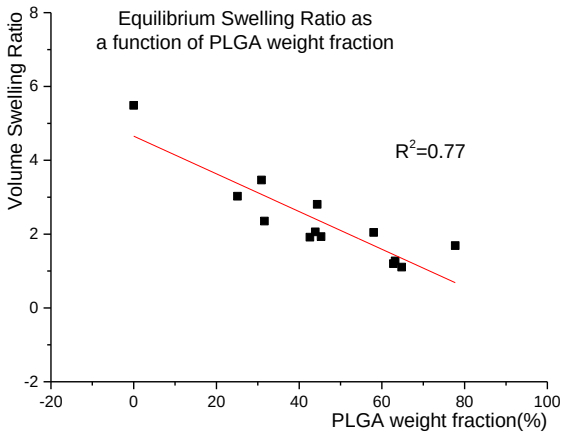

Figure 3.21 Equilibrium swelling ratio as a function of PLGA weight fraction

Figure 3.21 shows the equilibrium volume swelling ratio as a function of PLGA weight fraction. Q_∞ decreases almost linearly with PLGA weight fraction with R^2 of 0.77.

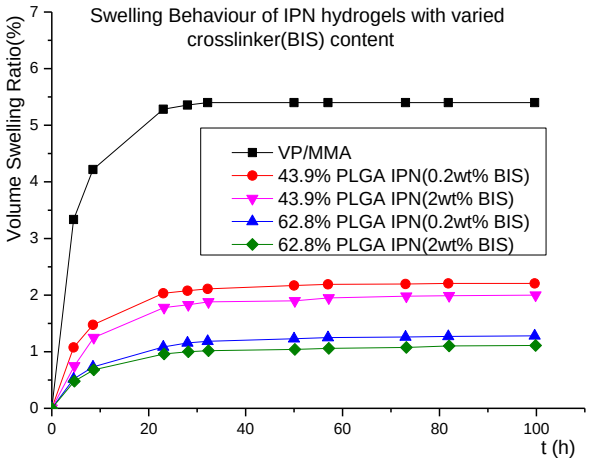

Figure 3.22 Swelling behaviour of PLGA IPN with varied crosslinker content

Figure 3.22 shows the swelling behaviour of 43.9%PLGA IPN and 62.8%PLGA IPN with 0.2wt% and 2wt% crosslinker content. Changing the crosslinker content has not produced a big influence on the swelling behaviour of PLGA IPN, although PLGA IPN with 2wt% crosslinker does show a slightly lower equilibrium swelling ratio than that with 0.2wt% crosslinker at the same PLGA weight fraction.

3.4 Discussion

3.4.1 Differential Scanning Calorimetry

Because of the absence of covalent crosslinks between individual networks in an IPN system, two T_g values have long been observed. Two T_g values were observed in PEG/chitosan IPN hydrogel[111], one at 42°C (corresponding to PEG) and another at 130°C (corresponding to chitosan). These T_g values were slightly lower than those of individual components, which was thought to be the result of a limitation on reorientation and crystallinity of due to the interference from the other network. Two T_g values at 61°C and 160°C were also observed for PNIPAAm/PNAS(poly(N-acryloxysuccinimide)) IPN hydrogels[181], while T_g of PNIPAAm and PNAS were observed at 59°C and 140°C, respectively. The shift in T_g values was thought to be a result of chain entanglements in the IPN system, requiring a higher temperature to promote chain mobility.

Thus for IPN hydrogels, two T_g values corresponding to each individual network can be observed but shifts may happen due to the entanglements between the component networks. T_g of VP/MMA has been reported to be 161°C[86] and T_g of PLGA was 21°C according to Figure 3.12. However, T_g of PLGA IPN was only observed around 17°C (Figure 3.13), which corresponds to the glass transition of PLGA. No obvious glass transition was observed for VP/MMA and fluctuations in the heat flow were present at temperatures above 130°C in both heat cycles. The instability above 130°C and the decreased T_g of PLGA is believed to be a result of residue solvent acting as a plasticizer in the IPN system. As described in Section 3.2.3, the incorporation of PLGA into VP/MMA network is though solvent absorption. And there must be residue solvent left which cannot be extracted under the mild drying conditions(for the preservation of the original shapes and structures of the bulk hydrogels). Changing the shape of the bulk

hydrogels from cylinders to plates had been observed to help evaporate the solvent because of a larger specific surface area but there was still some solvent trapped in the centre.

For hydrogels, water (moisture) absorbed from the air, solvent residues left during preparation can act as a plasticizer. It is well known that T_g of amorphous solids can be predicted using equation (3.14)[182], where $T_{g\,mix}$, T_{g1}, T_{g2} are the glass transition temperature of the mixture, component one and component two, respectively. $\emptyset_1$ and $\emptyset_2$ are their corresponding volume fraction. Thus a component with a low T_g will decrease the T_g of the mixture, which is then called a plasticizer and that with a high T_g will do the opposite.

$$T_{g\,mix} = \emptyset_1 T_{g1} + \emptyset_2 T_{g2} \tag{3.14}$$

Water has a reported T_g of -137°C(136K)[183], which makes it a highly potential plasticizer for many polymers[184]. In our case, residue DCM, with a melting point at -97°C and boiling point of 40°C, is very likely to behave like a plasticizer in the IPN hydrogels, unfastening the polymeric structure, and disrupting the inter-chain secondary bondings(like hydrogen bonding). As a result, less energy(lower temperature) is needed to promote chain mobility, leading to a decreased T_g observed around 17°C and no obvious glass transition for VP/MMA.

3.4.2 Compression Test

The incorporation of PLGA into the VP/MMA network results in reinforcement of the swollen hydrogel as confirmed by increased compressive modulus E shown in Table 3.1. The compressive stress-strain curves of VP/MMA and PLGA IPN hydrogels resemble most with that of a closed-cell foam. Both open and closed cell foam have an initial elastic region mainly caused by cell edge bending and a final densification region which figures a rapidly increasing stress[185]. The difference is that the elastic collapse

plateau (caused by elastic buckling) is always absent in a closed cell foam. In this thesis, plateau region is absent while stress rises with strain with increasing slope. This is thought to be a result of the compression of the fluid within the cells which causes an additional restoring force[185]. SEM images also indicate the closed-cell foam structures.

The same as the plateau region, the initial linear region is not clear neither in the stress-strain curves of VP/MMA and PLGA IPN hydrogels. The linear region is not clear probably because of the following reasons: 1. The sample surfaces were not completely flat, thus the initial region may not be reliable. 2. The strain rate used in this thesis is too small(on the order of 10^{-5}-10^{-4}/s). As has been reported, the initial linear region and the plateau region become more differentiated only at higher strain rates[186].

Still, we consider a closed-cell foam where a fraction Φ of the solid is contained in the cell edges(thickness t_e), and the remaining fraction 1-Φ is in the cell faces with a thickness t_f. Φ is introduced because in some cases solid material is drawn into the cell edges during preparations, leaving a thin cell face. According to Gibson and Ashby, E of a closed-cell foam is the sum of four contributions[185]: 1. Cell wall bending; 2. Cell edge bending; 3. The compression of the cell fluid; 4. Cell faces stretching, as shown in Figure 3.23.

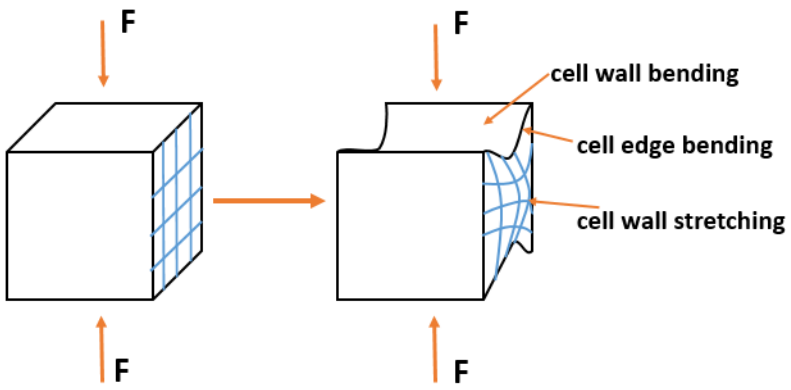

Figure 3.23 Schematic of the compression of a closed-cell foam

Young's modulus E of the closed-cell foam can be described using equation(3.15)[185], where E_s is the modulus of the solid material forming the cell faces, ρ is the density of the foam, ρ_s is the density of the cell wall solid material, P_0 is the initial water pressure inside the hydrogels, and v^* is the Poisson's ratio which is often taken as 1/3. The first term in equation(3.15) describes the contribution from cell wall bending, the second term from cell edge bending, the third from cell face stretching and the fourth from the compression of the cell fluid[185]. The cell wall bending The contribution of cell wall bending, $(1-\emptyset)^3\left(\frac{\rho}{\rho_s}\right)^3$, is always ignored because in most cases solid material is drawn into the cell edges during preparations, leaving a thin cell face thus cell wall bending is negligible. Moreover, if $\frac{\rho}{\rho_s}$ is small, it is also negligible. But this contribution should not be ignored if the cell faces are not significantly thinner than cell edges and when $\frac{\rho}{\rho_s}$ becomes large enough.

In the case of a dry polymer foam, $\frac{\rho}{\rho_s}$ equals the polymer volume fraction φ_s as shown in equation(3.16). However, the compression test were done on swollen hydrogel samples that contains large amounts of water. If we calculate $\frac{\rho}{\rho_s}$ with consideration of the weight of water, it loses its original meaning and value in this equation. The calculations do not make any sense neither. Thus for a hydrated hydrogel sample, φ_s is more appropriate to be used than $\frac{\rho}{\rho_s}$ when modelling the modulus thus equation(3.17) is used in this thesis.

$$\frac{E}{E_s} \approx (1-\emptyset)^3\left(\frac{\rho}{\rho_s}\right)^3 + \emptyset^2\frac{\rho}{\rho_s}^2 + (1-\emptyset)\frac{\rho}{\rho_s} + \frac{P_0(1-2v^*)}{E_s\left(1-\frac{\rho}{\rho_s}\right)} \tag{3.15}$$

$$\frac{\rho}{\rho_s} = \frac{\frac{M_{foam}}{V_{foam}}}{\frac{M_{foam}}{V_{solids\ in\ foam}}} = \frac{V_{solids\ in\ foam}}{V_{foam}} = \varphi_s(of\ a\ dry\ polymer\ foam) \tag{3.16}$$

$$\frac{E}{E_s} \approx (1-\emptyset)^3(\varphi_s)^3 + \emptyset^2{\varphi_s}^2 + (1-\emptyset)\varphi_s + \frac{P_0(1-2v^*)}{E_s(1-\varphi_s)} \quad (3.17)$$

It is clear that E is related to the polymer volume fraction φ_s. The higher the polymer volume fraction, the higher the modulus. With the increasing weight fraction of PLGA in the hydrogels, φ_s is increased as shown in Table 3.3(calculated using equation(3.12) from the swelling behaviour data). The more PLGA in the hydrogel, the higher the φ_s, and the higher the modulus. According to most reports, increasing the polymer volume fraction increases the modulus and plateau stress, and decreases the final strain at densification[185, 187, 188]. The decrease in E can also be explained by a lower equilibrium water content as a result of higher hydrophobicity brought by PLGA. As has been stated in Section 3.4.1, water acts as a plasticizer in the hydrogels lowering the glass transition temperature thus requiring less energy for the same deformation.

In the case of a dry porous polymer scaffold, the modelling using equation(3.15) would be simple as Es and $\emptyset$ would be fixed and P_0 is the atmosphere pressure. However, for VP/MMA and PLGA IPN hydrogels, not only φ_s, but also E_s is changing with increasing PLGA weight fraction. Determining $\emptyset$ and P_0 also need complex experiments. The stress-strain curves do not show a clear initial elasticity region nor the collapse plateau region. Thus the collapse stress, which is taken as the intercept of the extrapolations of the initial slope and the plateau stress cannot be known or compared with modelled values. Still, when plotted as a function of φ_s, E shows a power law relationship with an exponent of 1.9, as shown in Figure 3.24. The exponent corresponds to the second term in equation(3.17). Thus the cell edge bending might be the main contribution to the elastic modulus of VP/MMA and PLGA IPN hydrogels. This result is not surprising as most reports have confirmed the cell edge bending to contribute most to the modulus[185].

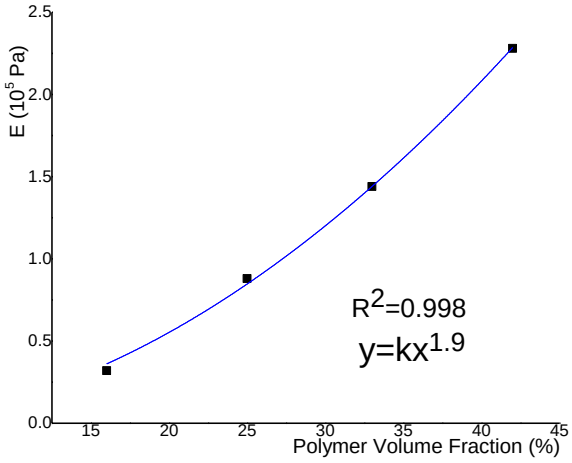

Figure 3.24 Compressive modulus E as a function of polymer volume fraction

It should be noted that this modelling may not be statistically liable because more samples are needed for a better result. More importantly, in this case, unlike the other polymer foams, E_s, modulus of the cell wall material, is actually changing because of a difference in PLGA and VP/MMA compositions(will be further discussed below).

To decrease the impact of the increase in polymer volume fraction, a normalized modulus E_n is defined here as E multiplied by the porosity(=1 $-\varphi_s$). Please note that E_n does not have a specific meaning, and is just shown to see the relative increase in modulus without the effect of the increased φ_s. A more commonly used term, the specific modulus E_d, defined as modulus divided by density, is also calculated. Those values are summarized in Table 3.3 and the red figures show the percent increase from the previous one. For example, 0.88 shows a 175% increase from 0.32.

Table 3.3 Specific modulus of VP/MMA and PLGA IPN

PLGA weight fraction (%)	E(10^5 Pa)	Density(g/ cm^3)	E_d(10^{-1}N/g)	φ_s	E_n (10^5 Pa)
0	0.32	1.19	0.27	0.16	0.27
25.1	0.88(+175%)	1.25	0.70(+159%)	0.25	0.66(+144%)
43.9	1.44(+63.6%)	1.26	1.14(+62.8%)	0.33	0.96(+45.4%)
62.8	2.28(+58.3%)	1.29	1.77(+55.3%)	0.42	1.32(+37.5%)

As can be seen from Table 3.3, the percent increase in modulus with the PLGA weight fraction is decreased by normalizations using density or polymer volume fraction. Thus the increase in φ_s does contribute to the increased modulus but it is not the only reason as the modulus is still increasing with PLGA weight fraction after the normalizations. Thus it comes to the point when we have to consider the change in E_s, the modulus of the cell wall material.

It is clear from equation(3.17) that the overall modulus of the hydrogels also depends on E_s. Those cell walls can be porous themselves and in this case, they are inter-penetrating polymer networks. A direct measurement of the cell wall modulus is difficult due to the small size of the cell member[185], but the influence with the incorporation of PLGA into the networks can be discussed as follows. Figure 3.25 shows the idealized schematic of the structures in the cell walls of VP/MMA and PLGA IPN hydrogels.

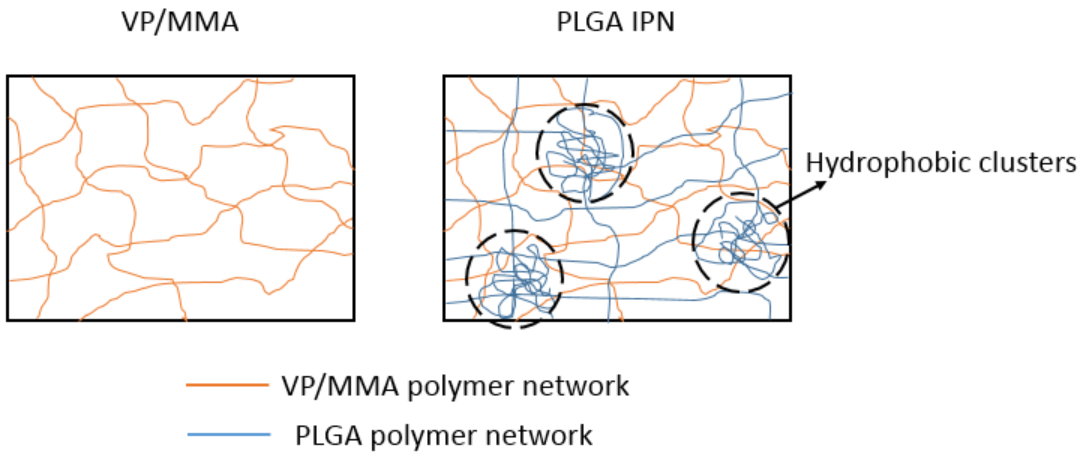

Figure 3.25 Schematic of the structures in the cell walls of VP/MMA and PLGA IPN hydrogels

When PLGA is incorporated into the single VP/MMA network, a much denser network is formed as shown in Figure 3.25. And PLGA is hydrophobic, thus its polymer chains tend to aggregate into clusters because of the attractions between non-polar groups(hydrophobic bonding)[43]. This effect is enhanced by the presence of water in

an attempt to minimize contact with water molecules[43]. These hydrophobic clusters act as physical-crosslinks, preventing chain displacements over a larger range of loading, thus leading to an increased E. The SANS data(will be discussed in Section 3.4.3) confirms the formation of clusters or aggregates which is increasing with PLGA weight fraction. The increased hydrophobic bonding contributes to the effective crosslinking density, which will be shown in Table 3.7. Thus a higher PLGA weight fraction leads to a more rigid polymer network constructing the cell walls, meaning a higher E_s. According to equation(3.17), this leads to a higher overall modulus E of the swollen hydrogels. Hydrophobic bonding has been widely reported to enhance the mechanical properties of hydrogels. These hydrophobic nanodomains formed serve as physical crosslinks and contributes to the effective crosslinking density and energy dissipation[189]. The more detailed characterizations of these hydrophobic nanodomains have been done using small angle X-ray scattering[190] and ^{13}C NMR[191].

All in all, both the polymer volume fraction φ_s and the modulus of the cell wall solid material E_s increase with PLGA weight fraction, leading to a higher modulus E of the swollen hydrogels according to equation(3.17).

It should be noted that hydrogels are viscoelastic[192], thus their mechanical properties are dependent on strain rate or time. The loading rate used in this thesis is 100mN/min and the corresponding strain rate is on the order of 10^{-5}-10^{-4}/s, which is in a quasi-static state. The hydrogels, when implanted under the subcutaneous layer of skin, are subjected to a different strain rate and dynamic loading due to the restoring force of the skin tissue and external impact as well. Thus the performance of the hydrogels in real situations might not be the same as in this compression test. It has been widely reported that the compressive modulus increases with strain rate and the plateau stress also

rises[185, 186, 193]. Actually the initial linear region and the plateau region will be much more evident at higher strain rates than lower strain rates[186]. And a yield point may not be obvious at low strain rates but will appear or become more pronounced at higher strain rates[185]. PLGA has been reported to have a higher compressive modulus and yield strength with increased strain rate[194]. It is expected that VP/MMA and PLGA IPN would have a higher modulus with increased strain rate, but it probably won't change the fact that the modulus is still increasing with PLGA weight fraction. Still, DMA(dynamic mechanical analysis)would be helpful analysing the viscoelastic behaviour of these hydrogels, including creep behaviour and stress relaxation behaviour. The change of storage and loss modulus with temperature would also provide more information about the structural change with the incorporation of PLGA. These may provide more details which would help build up a mechanical model and also better predict the mechanical performance in real situations when implanted under the skin. They may also elucidate more on the mechanism of how PLGA increases the modulus of the hydrogels and whether those hydrophobic clusters provide a better energy dissipation, as some reports suggested[189, 195]. Besides the strain rate dependence of the solid cell wall material, the cell fluid may be expelled during compression, requiring an additional work done against the viscosity of the fluid which may introduce a new strain-rate dependence[185].

E shows a good linear relationship with PLGA weight fraction, with R^2 of 0.96 as shown in Figure 3.15. This means the compressive modulus of swollen IPN hydrogels can be predicted with PLGA weight fraction before the implantation, which will be useful in the clinical surgeries.

3.4.3 Small Angle Neutron Scattering

The SANS spectrum of VP/MMA has no discernible features, which means a relatively

homogeneous structure with randomly oriented polymer chains. The presence of a very broad shoulder at low Q range ($Q<0.01A^{-1}$) means the mesh size is fairly uniform[196]. SANS data of VP/MMA and PLGA IPN was fitted with the models shown in Section 3.2.7 using Sasview software. The Chi2/Npts(goodness of fit) is summarized in Table 3.4:

Table 3.4 Chi2/Npts values of SANS data of VP/MMA and PLGA IPN fitted with different models

Model	VP/MMA	28%PLGA IPN	46%PLGA IPN	63%PLGA IPN
DAB	697.0	2089.6	1059.5	431.3
Lorentzian	4.1	830.8	611.6	249.5
Correlength	3.4	22.8	48.7	4.5
GaussLorentz	8.7	819.1	2001.7	2526.7
GelFit	3.9	158.1	195.1	100.6

Table 3.4 shows that the SANS spectrum of VP/MMA and PLGA IPN cannot be adequately described by DAB Model which characterizes a two-phase system. For VP/MMA, this is because of the covalent bonds between VP and MMA. For PLGA IPN, this is intermediate evidence that there exists some molecular level interpenetrating between the two networks and the IPN hydrogels prepared in this thesis are inter-penetrated networks and not just phase-separated systems.

Correlength Model seems to fit better than Lorentzian Model for the interpretation of the SANS data. As has been illustrated in Section 3.2.7, the difference between those two models is that Correlength Model includes an additional term characterizing the clusters at the low Q range ($Q<0.01A^{-1}$) which corresponds to large length scale ($>600A$) clusters or aggregates. For VP/MMA, the Chi2/Npts value shows no significant difference between those two models, while for PLGA IPN, Correlength Model shows a much lower Chi2/Npts value. This indicates that VP/MMA has a relatively more homogeneous network while PLGA IPN has more inhomogeneities at the large length scale.

As can be seen in Figure 3.16, the excess scattering at low Q range ($Q<0.01A^{-1}$) of

PLGA IPN is only the latter part or tail of the low Q feature, while the rest is beyond the limit of SANS equipment (6-1570A). Thus it is difficult to assign the size of the large aggregates which are probably larger than 1570A.

GaussLorentz Model is good enough to describe VP/MMA, showing a Chi2/Npts of 8.7. However, it is not adequate for the characterization of PLGA IPN, as shown by the sharply increased Chi2/Npts value with PLGA loading. The reason is that GaussLorentz Model has a limiting Q dependence of -2 in the Lorentzian term, regardless of the fractal dimension of the scattering body. Gelfit Model solves this limitation by introducing a fractal related Q dependence, thus showing an acceptable Chi2/Npts for characterizing SANS data of PLGA IPN.

SANS data of VP/MMA can be adequately described by any of the above models except for the DAB Model. However, SANS data of PLGA IPN can only be adequately described by Correlength Model and GelFit Model, i.e. models that incorporate terms to account for inhomogeneities(clusters) at the low Q range, and for the fractal dimension. Correlength Model seems to be the most appropriate one to characterize the SANS data, and the fitting curves are showing in Figure 3.26 and the corresponding fitting parameters are summarized in Table 3.5.

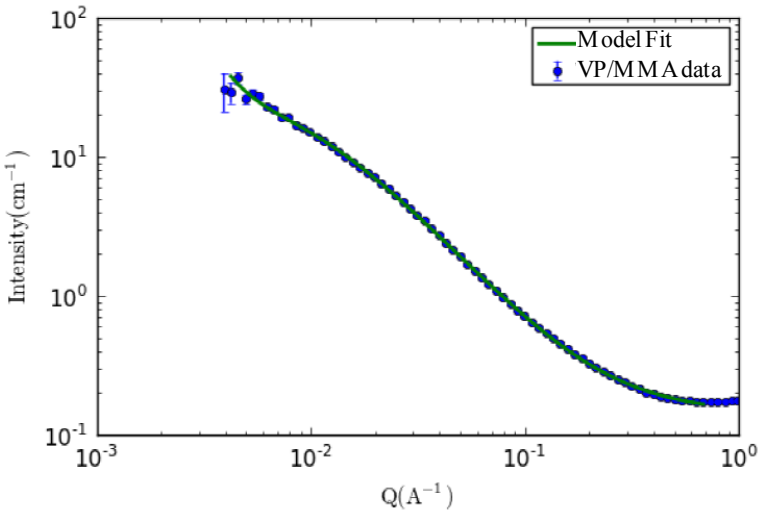

(a) VP/MMA fitted with Correlength Model

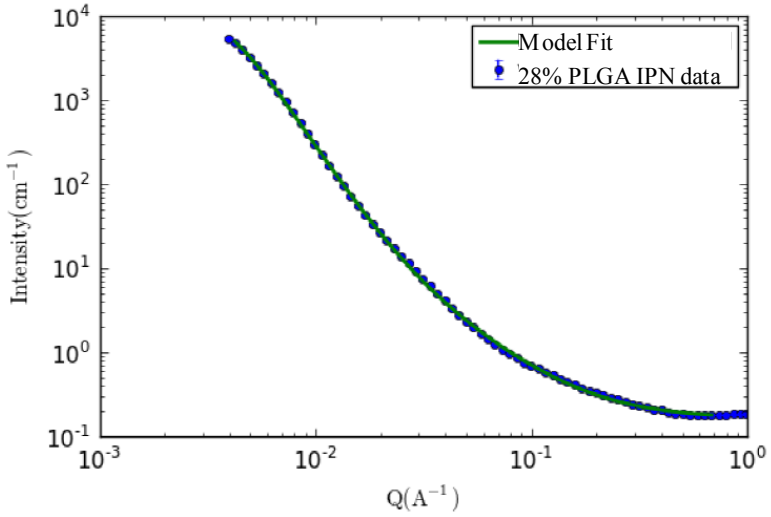

(b) 28% PLGA IPN fitted with Correlength Model

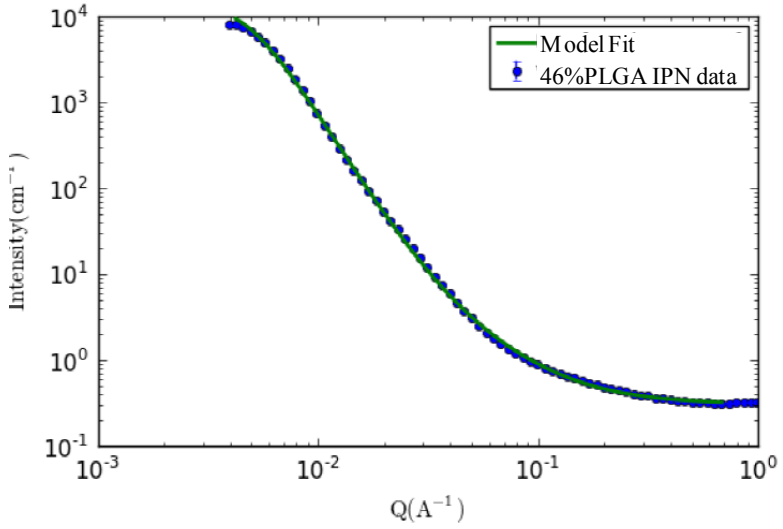

(c) 46% PLGA IPN fitted with Correlength Model

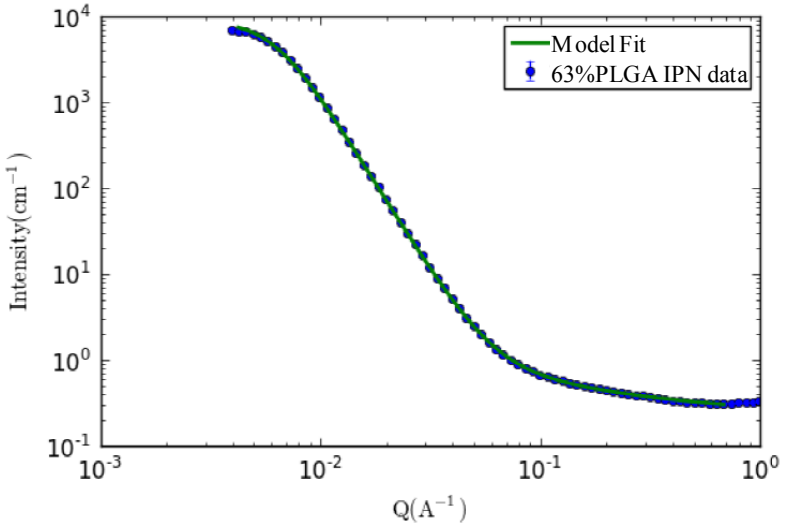

(a) 63% PLGA IPN fitted with Correlength Model

Figure 3.26 SANS spectrum fitted with Correlength Model (a)VP/MMA (b)28%PLGA IPN (c)46%PLGA IPN (d) 63%PLGA IPN

Table 3.5 Charactering parameters of SANS data fitted with Correlength Model

	VP/MMA	28%PLGA IPN	46%PLGA IPN	63%PLGA IPN
m	1.7	3.9	4.1	4.1
Correlation Length(A)	99	262	207	160

The exponent m shows the interaction between polymer chains and the solvent (see Section 3.2.7). VP/MMA has an exponent of 1.7, which means most of VP/MMA polymer chains are fully swollen in the solvent (self-avoiding walk). For PLGA IPN, the exponent is largely increased to around 4, which means that polymer chains are highly constrained in the solvent. As has been stated in Section 3.2.7, m corresponds to the fractal dimension of the scattering object. Thus the incorporation of PLGA changes the fractal dimension of the hydrogel from mass fractal to surface fractal. This is probably due to the segregation of PLGA chains which do not dissolve in D_2O and tend to stick to each other and form clusters to minimize their contact with the solvent molecules. 28%PLGA IPN shows m of 3.9, indicating rough surfaces. 46%PLGA IPN and 63%PLGA IPN shows m over 4, indicating extremely strong aggregation of PLGA domains.

The correlation length shows the average distance between entanglements[174]. And in the case of a hydrogel, ξ shows the mesh size. ξ has been long predicted to scale with the volume fraction φ_s of a swollen hydrogel[197], as shown in equation(3.18) and (3.19):

$$\xi \sim {\varphi_s}^{-3/4} \quad when\ \varphi_s \leq 0.01 \tag{3.18}$$

$$\xi \sim {\varphi_s}^{-1/2} \quad when\ \varphi_s \geq 0.01 \tag{3.19}$$

It should be noted that φ_s is related to the equilibrium swelling ratio in equation (3.20):

$$Q_\infty = \varphi_s^{-1/3} - 1 \tag{3.20}$$

Thus a smaller correlation length corresponds to a higher volume fraction φ_s, and a lower equilibrium swelling ratio.

ξ derived from the Correlength Model is plotted as a function of $\varphi_s^{-1/2}$ of the swollen hydrogels in Figure 3.27. In this study, the volume fraction of all the swollen hydrogels is larger than 0.01, thus equation (3.19) is used for the plotting.

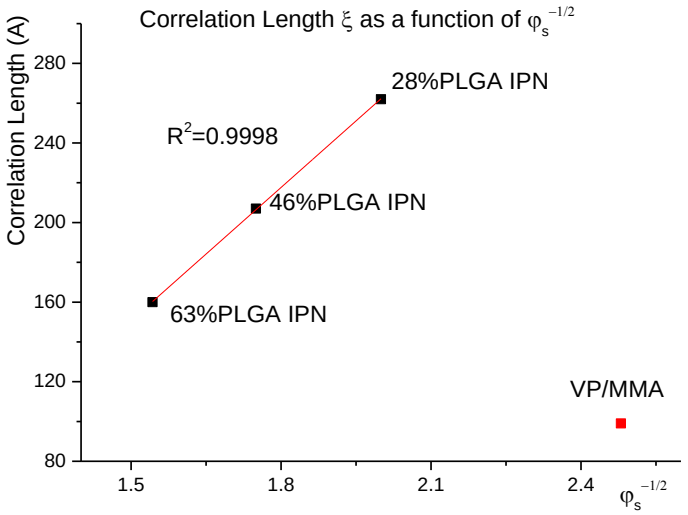

Figure 3.27 ξ of the Correlength Model as a function of the volume weight fraction $\varphi_s^{-1/2}$ of the swollen hydrogels

Figure 3.27 shows that the correlation length of PLGA IPN with varied PLGA weight fractions fits well with the scaling law. This shows that the experimental data from the

swelling behaviour and SANS is well described by the scaling law. SANS verifies that for PLGA IPN, a higher PLGA weight fraction results in a decrease in the effective mesh size(correlation length), which means more effective crosslinks per unit volume and less effective space for water diffusion and less free volume for water molecules to reside in. This contributes to the decreased water diffusion rate(swelling rate) with increased PLGA weight fraction.

However, it can also been seen that ξ of VP/MMA shows a huge deviation from the scaling law. This is probably due to the significant difference in the internal structure between VP/MMA and PLGA IPN. As has been stated above, VP/MMA has a much more homogeneous structure than PLGA IPN, whose SANS data can be described by most of the models used for hydrogels. For PLGA IPN, SANS data is collected together from both VP/MMA and PLGA networks. Thus ξ of PLGA IPN shows an averaged effective mesh size of the whole structure, including the concentration fluctuations caused by PLGA clusters. Thus ξ of VP/MMA and PLGA IPN might not be comparable, but comparing between the PLGA IPN with varied PLGA weight fractions will.

To summarize, the following observations can be obtained from the SANS analysis:

1. PLGA IPN hydrogels are not just phase-separated systems as their SANS data does not fit at all with DAB model which is built up to describe phase separated systems.
2. VP/MMA shows a relatively more homogeneous network while PLGA IPN can only be adequate characterized by models that include characterizing terms for clusters at the low Q range($Q<0.01A^{-1}$) and for fractal dimensions. Correlength Model and Gelfit Model are adequate to describe VP/MMA and PLGA IPN, while the former is still much better with the lowest Chi2/Npts values.

3. The incorporation of PLGA into VP/MMA changes the fractal dimension from mass fractal to surface fractal. Adding only 26% PLGA dramatically changes the physical structure of the hydrogel network, as can be seen from the significant changes in the model parameters between VP/MMA and 26%PLGA IPN. VP/MMA shows fully swollen polymer chains in the solvent, while PLGA IPN shows a more constrained structure with more rough surfaces and greater segregation of hydrophobic domains in the pore walls(cell faces).
4. SANS proves that for PLGA IPN, increased PLGA weight fraction results in a decreased effective mesh size. The decreased mesh size contributes to the decreased swelling rate as shown in Table 3.2. The experimental values of the correlation length and the polymer volume fraction in the swollen hydrogels fit well with the scaling law.

3.4.4 Scanning Electron Microscopy

Figure 3.17 shows that VP/MMA has a fairly uniform porous network structure with smooth surface although there are some areas where the polymer is more concentrated than the others. The pore size of VP/MMA network lies in the range of 2μm to 40μm, as shown in Figure 3.17.

25.1%PLGA IPN shows a porous network similar to that of VP/MMA, but with rougher surfaces and thicker walls. The pore size varies in a similar range compared to VP/MMA but the structure becomes more compact with more irregular shaped aggregates on the surfaces. The compactness and aggregates are more obvious with increased PLGA weight fraction. Thus it can be speculated that the functionalized PLGA monomer is absorbed into and stays on the surface of the porous network of VP/MMA hydrogel, then an in situ polymerization is carried out in the presence of the crosslinker and initiator. Because of the difference in microenvironments and the

immiscibility between PLGA and VP/MMA, PLGA tends to form aggregated domains with variable sizes and shapes. Higher PLGA weight fraction increases the entanglements and the aggregation, resulting in the increased compactness and more clusters.

The hydrophobic, crosslinked PLGA network and PLGA aggregates formed in the cell walls act as a barrier for water diffusion. Thus a decreased diffusion coefficient can be expected, which will be calculated in Section 3.4.5.2.

3.4.5 Swelling Behaviour

Table 3.2 shows the initial swelling rate, the equilibrium swelling ratio and EWC is decreasing with PLGA weight fraction, while the swelling period increases with PLGA weight fraction. The decreased swelling rate and extended swelling period can effectively reduce the rate of tissue necrosis and the absence of any coatings or membranes endows the IPN hydrogels the ability to be crafted by surgeons. Figure 3.21 shows a decreasing linear relationship between the equilibrium volume swelling ratio and PLGA weight fraction with R^2 of 0.77. Thus by controlling the PLGA weight fraction during preparation, we can predict the equilibrium volume swelling ratio of the IPN hydrogels before the implantation. This will provide an advantage for controlling the possible area of tissue growth in the plastic and reconstructive surgeries. However, the equilibrium swelling ratio is much less than that of a single VP/MMA network, which may limit the application of PLGA IPN hydrogels(will be further discussed in Section 3.4.6).

The swelling rate and equilibrium swelling ratio can be affected by the monomer ratio(hydrophobicity/hydrophilicity), crosslinker content, intensity of irradiation and other reasons, as has been discussed in Section 2.2.5. In this study, the crosslinker content and the swelling medium remain unchanged. Thus the change in the swelling

behavior is believed to be the result of change in monomer ratio, i.e. increased hydrophobicity of the hydrogel with increased PLGA weight fraction.

The hydrophobicity of a material is characterized by its water contact angle via Young's equation and VP is regarded as a highly hydrophilic polymer, as shown in Section 2.2.5.1. The contact angle of PLGA has been tested to be 69.6° ± 4.3°[198]. The contact angle of VP/MMA (9:1) has not been reported, but that of VP and MMA alone has been shown to be 5°[40] and 71.5°[41], respectively. Thus in PLGA IPN, PLGA is the hydrophobic component and VP/MMA(9:1) is the hydrophilic component. When PLGA weight fraction increases, the hydrophobicity of the hydrogel network increases and hence less binding sites are available for water molecules. Moreover, hydrophobic components act as a steric hindrance preventing water molecules from binding with the hydrophilic sites, leading to a further decreased water content. The less binding sites and the steric hindrance from hydrophobic PLGA are responsible for the decreased equilibrium water content(EWC) with increased PLGA weight fraction. And as has been discussed in Section 3.4.2, the incorporation of PLGA into the VP/MMA network increases E_s, the modulus of the cell water material. Thus when immersed in water, it is more difficult for water molecules to penetrate through the cell walls and expand the whole network, leading to a decreased initial swelling rate. The more rigid cell walls also need more time for the polymer chains to be relaxed, which extends the swelling period as a result.

The following analysis is a routine process for analysing hydrogels, including the calculations of necessary parameters that support this explanation that hydrophobicity is the cause for the difference in swelling behaviour between VP/MMA and PLGA IPN hydrogels.

3.4.5.1 Swelling Kinetics

It is important to understand the mechanism of water diffusion into the IPN hydrogels as it provides information about the parameters controlling the swelling rate. An over-rapid swelling rate of a tissue expander causes tissue necrosis instead of tissue growth[170]. The water diffusion mechanism of VP/MMA and PLGA IPN is determined using equation(3.21)[34], where M_t is the water uptake at time t and M_∞ is the water uptake at the equilibrium state, k is a constant and n is the diffusion exponent describing Fickian or anomalous swelling mechanism. The plots of equation(3.21) is shown in Figure 3.28.

$$\frac{M_t}{M_\infty} = kt^n \tag{3.21}$$

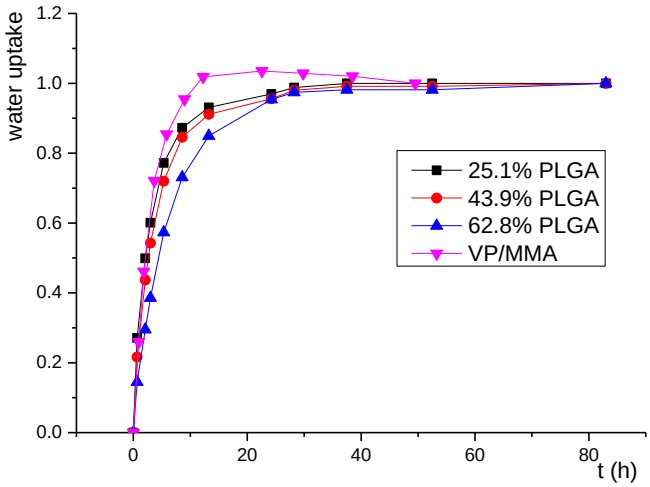

Figure 3.28 Water uptake M_t/M_∞ as a function of time

Equation (3.22) shows the natural logarithm of equation (3.21). The value of n and k can be calculated as the gradient and the intercept of the curves shown in Figure 3.29.

$$In(M_t/M_\infty) = Ink + nInt \tag{3.22}$$

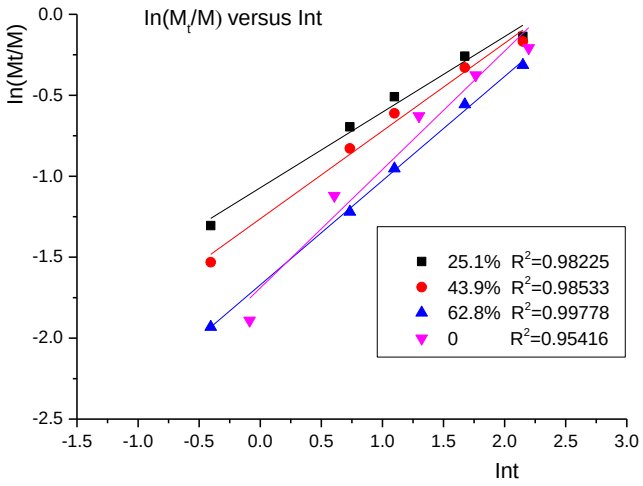

Figure 3.29 Natural logarithm of water uptake as a function of Int

This is performed in triplicate and the mean value of diffusion exponent n is obtained and summarized in Table 3.6. For cylindrical shapes, an n value between 0.4 and 0.5 corresponds to Fickian diffusion, whereas n between 0.5 and 1 indicates non-Fickian diffusion[199]. VP/MMA has an exponent n of 0.72, indicating an anomalous diffusion. 25.1% and 43.9%PLGA IPN have n values around 0.5 which characterize Fickian diffusion and a diffusion-controlled process. 62.8%PLGA IPN has the exponent of 0.64, characterizing an anomalous diffusion where water penetration is partially controlled by viscoelastic relaxation of the polymer chains[200].

Table 3.6 The diffusion exponents and diffusion mechanism of VP/MMA and PLGA IPN

PLGA weight fraction	Diffusion Exponent n	Diffusion Mechanism
0	0.72	Anomalous
25.1%	0.47	Fickian
43.9%	0.51	Fickian
62.8%	0.64	Anomalous

The difference in diffusion mechanism has been illustrated in Section 2.2.4. VP/MMA shows anomalous diffusion which means the rate of water diffusion(R_{diff}) and that of polymer chain relaxation(R_{relax}) are comparable. For IPN hydrogels, the diffusion mechanism is transferred from Fickian to non-Fickian as PLGA weight fraction increases. 25.1% and 43.9%PLGA IPN show Fickian diffusion behaviour, which means

their polymer chains still possess a high mobility to allow immediate penetration of water into the hydrogel($R_{diff} < R_{relax}$). While 62.8%PLGA IPN shows an anomalous diffusion which means its polymer chains are more constrained and hence water diffusion rate and polymer relaxation rate are comparable ($R_{diff} \approx R_{relax}$).

The transfer of diffusion mechanism from Fickian to non-Fickian in IPN hydrogels has been reported. PVA (poly(vinyl alcohol))-guar gum IPN microspheres changed its drug release mechanism from Fickian to anomalous when crosslinker (glutaraldehyde) content is increased by 3 times[201]. This was thought to be due to a decreased chain mobility as a result of increased crystallinity(as determined by DSC) brought by increased crosslinker content. Water diffusion mechanism of crosslinked PHEMA hydrogel have been widely reported to change from Fickian to anomalous when crosslinker content was increased up to a certain level(12.4mol%)[202, 203]. This was also believed to a result of increased crosslinker content that contributed to the rigidity of the network. The diffusion mechanism of acrylamide/styrene-PVA IPN hydrogel became more relaxation controlled when the content of hydrophobic styrene was increased from 4.3mM to 13mM[200].

For PLGA IPN, crosslinker content remains the same for all the hydrogels. But the increase in PLGA weight fraction will bring more hydrophobic bonding acting as physical crosslinks as has been discussed in Section 3.4.2. Thus the effective crosslinking density is increased, leading to a restricted chain mobility and change in diffusion mechanism. The more restricted chain mobility is also indicated by the increased compressive modulus with increased PLGA weight fraction shown in Table 3.1. The decreased chain mobility will contribute to a decreased diffusion coefficient, which will be calculated in Section 3.4.5.2.

3.4.5.2 Diffusion Coefficient

The diffusion coefficient D shows the rate at which the diffusing substance is transported through a cross-section of a system. For cylindrical hydrogel samples, one of the most widely used methods is the short time approximation method assuming the surface concentration is constant and the values of M_t/M_∞ is less than 0.6[34] as shown in equation (3.23), where M_t and M_∞ are the amount of water absorbed at time t and at equilibrium, respectively. D is the diffusion coefficient and r is the diameter.

$$\frac{M_t}{M_\infty} = \frac{4}{r}\sqrt{\frac{D}{\pi}} * \sqrt{t} \tag{3.23}$$

Ideally, D should be calculated using equation (3.24), considering different hydrogel has different diffusion exponent n[204]:

$$\frac{M_t}{M_\infty} = 4\left[\frac{Dt}{\pi r^2}\right]^n \tag{3.24}$$

However, the diffusion coefficients of VP/MMA and PLGA IPN calculated using equation (3.24) make no sense nor show any trend. Thus short time approximation using equation (3.23) is used instead for the calculation of D. Table 3.7 shows D values calculated using equation (3.23):

Table 3.7 Diffusion Coefficient of VP/MMA and IPN hydrogels

PLGA weight fraction	D(10^{-7}cm^2/s)
0	17.02
25.1%	9.86
43.9%	8.66
62.8%	4.94

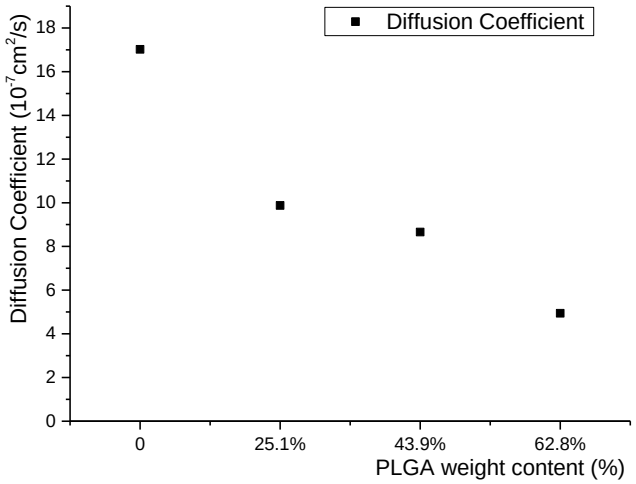

Figure 3.30 The diffusion coefficients of PLGA IPN with varied PLGA weight fraction

Figure 3.30 shows the diffusion coefficient as a function of PLGA weight fraction. The decrease in D is also believed to a result of increased hydrophobicity brought by PLGA. The amine groups of VP/MMA tend to form hydrogen bonds with water molecules, but the methyl side groups of PLGA, which is energetically unfavorable for water molecules to bind, act as diffusional barriers and steric hindrance(blocking access to a reactive site by nearby groups) as well[43]. Thus the decreased diffusion coefficient is a result of increased hydrophobicity and steric hindrance.

In addition, the mechanical analysis (Section 3.4.2) and the diffusion mechanism (Section 3.4.5.1) both confirm the more restricted chain mobility with increased PLGA weight fraction. This means chain relaxation takes more time and more energy is needed for the water molecules to penetrate in. This also contributes to the decreased diffusion coefficient.

3.4.5.3 Structure Characterization Parameters

The molecular mass between two neighbouring crosslinks for neutral networks, M_c, can be calculated from the swelling data using equation (3.25)[205], where φ_s is the polymer volume fraction at the equilibrium state, V_1 is the molar volume of water, ρ is

the density of the dry hydrogel, $\boldsymbol{\chi}$ is the Flory-Huggins interaction parameter and f is the functionality of the crosslinking agent:

$$M_C = -\frac{\rho V_1 (\varphi_s^{1/3} - 2\varphi_s f^{-1})}{[In(1-\varphi_s)+\varphi_s+\chi\varphi_s^2]} \tag{3.25}$$

The effective crosslinking density γ_e can be calculated using the swelling data and the compressive modulus using equation (3.26) and (3.27), where E is the compressive modulus, R is the universal gas constant, T is the absolute temperature:

$$E = RT\gamma_e {\varphi_s}^{1/3} \tag{3.26}$$

$$\ln(1-\varphi_s) + \varphi_s + \chi{\varphi_s}^2 + \gamma_e V_1 \left({\varphi_s}^{\frac{1}{3}} - 2\varphi_s f^{-1}\right) = 0 \tag{3.27}$$

Table 3.8 summarizes the calculated structure parameters.

Table 3.8 Structure Characterization Parameters of the hydrogels with different PLGA weight fractions

PLGA weight fraction	0	25.1%	43.9%	62.8%
G(10^5 Pa)	0.32	0.88	1.44	2.28
${\varphi_s}^{1/3}$	0.54	0.63	0.69	0.75
γ_e(mol/m^3)	24.3	57.4	85.7	124.8
φ_s	0.16	0.25	0.33	0.42
$\boldsymbol{\chi}$	0.56	0.60	0.64	0.70
$\boldsymbol{\rho}$ (g/cm^3)	1.19	1.25	1.26	1.29
M_C (10^4 g/mol)	4.90	2.18	1.47	1.03

Figure 3.31 shows the Flory-Huggins interaction parameter χ as a function of PLGA weight fraction. χ is increasing with PLGA weight fraction and deviating from 0.5 as well. The ability of polymer networks to absorb water depends the interaction between water molecules and polymer chains. According to the Flory-Huggins theory, χ takes higher values if there is a weaker interaction between polymer and water. Thus a more hydrophobic network has a higher χ. The increase in χ supports the explanation that hydrophobicity of the IPN hydrogels is increasing with PLGA weight fraction, leading to a decreased initial swelling rate, diffusion coefficient, equilibrium swelling ratio and EWC.

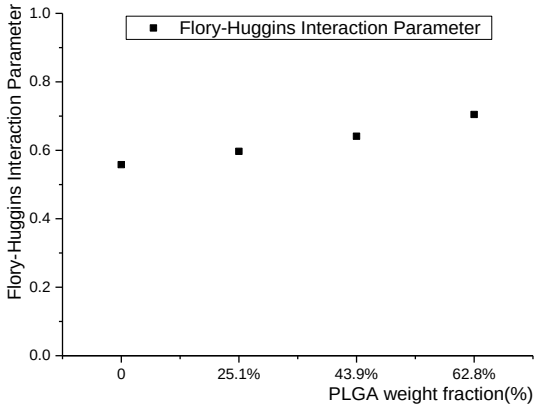

Figure 3.31 Flory-Huggins Interaction Parameter as a function of PLGA weight fraction

γ_e is the effective crosslinking density, which not only includes chemical crosslinking but also physical crosslinking like hydrophobic interactions[206]. The effective crosslinking density must be measured, since it normally differs from the theoretical crosslinking density characterized by the mole fraction of crosslinker in the monomers[207]. Figure 3.32 shows γ_e increases with the increase in PLGA weight fraction. Since the molecular weight of PLGA and crosslinker content remains the same for all IPN hydrogel, the increase in the effective crosslinking density means more physical crosslinking generated by the hydrophobic interactions of PLGA domains. The increase in γ_e corroborates the increase of compressive modulus of the swollen hydrogels (Table 3.1).

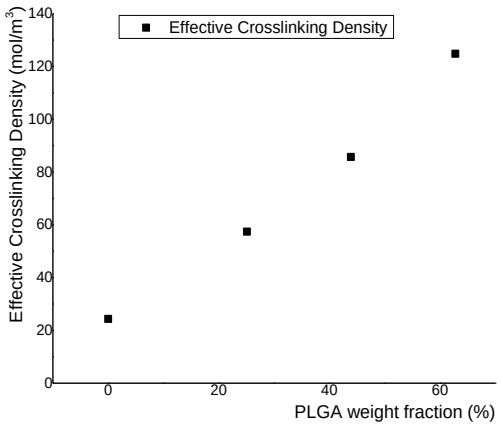

Figure 3.32 The effective crosslinking density as a function of PLGA weight fraction

γ_e has been widely observed to increase with the composition of the hydrophobic component in a hydrogel network. γ_e of VP/MMA copolymer hydrogels increased from 0.97mol/m^3 to 34.04mol/m^3 when MMA weight fraction was increased from 5% to 30% while the crosslinker content remained as 0%[206]. This was due to the increased hydrophobic bonding between MMA domains acting as physical crosslinks. Higher MMA weight fraction also led to a decreased EWC and increased Young's modulus. When the molecular weight of VP/MMA and PLGA is fixed, the decreased average molecular weight between two consecutive crosslinks, M_C and the increased effective crosslinking density γ_e indicate a decreased average distance between two effective crosslinks (mesh size), which has been confirmed by SANS.

3.4.5.4 Hydrophobicity vs Crosslinker Content

EWC can be controlled by the monomer ratios[38] which change the hydrophilicity/hydrophobicity of a hydrogel or by crosslinker content which changes the mesh size of a hydrogel[49].

Figure 3.20 and Figure 3.22 shows the swelling behaviour of PLGA IPN with varied PLGA weight fraction and varied crosslinker content, respectively. 43.9% and 62.8%PLGA IPN shows similar swelling curves when the crosslinker content is increased from 0.2wt% to 2wt%. Figure 3.33 shows the comparison between the effects of PLGA weight fraction and crosslinker content on the equilibrium swelling ratio.

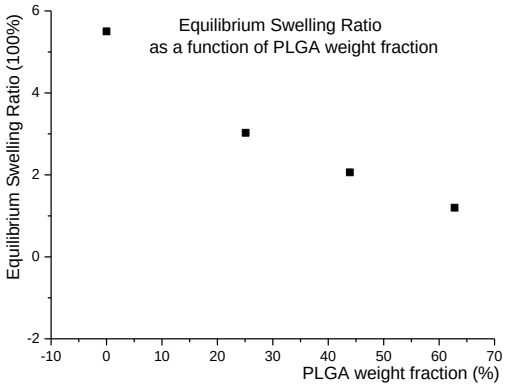

(a) Q_∞ as PLGA weight fraction

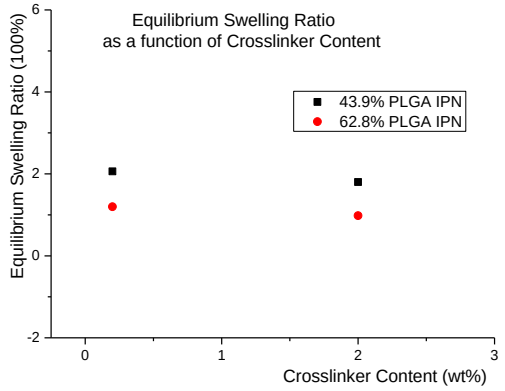

(b) Q_∞ as crosslinker content

Figure 3.33 Equilibrium Swelling Ratio as a function of (a)PLGA weight fraction (b)crosslinker content

Figure 3.33 shows that change in PLGA weight fraction creates a much steeper decrease in the equilibrium swelling ratio than change in crosslinker content. When PLGA weight fraction is increased by 2.5 folds, Q_∞ decreases by 66.7%. When crosslinker content is increased by 10 folds, Q_∞ of 43.9%PLGA IPN and 62.8%PLGA decrease only by 10%-20%. Thus for PLGA IPN hydrogels, controlling the monomer ratio, i.e. hydrophilicity/hydrophobicity of the polymer network seems more important than the crosslinker content in controlling the swelling behavior.

However, the swelling behaviour of the IPN hydrogels also depends on the properties of VP/MMA network. Since the VP:MMA monomer ratio and the crosslinker content used for the preparation of VP/MMA remains the same in this study, it is hard to conclude

that the hydrophilicity/hydrophobicity is more important than crosslinker content in controlling the swelling behaviour of PLGA IPN hydrogels.

Although it has not been systematically compared, most studies illustrated in Section 2.2.5.1 and 2.2.5.2 show a much more significant decrease in EWC with the increase in the ratio of the hydrophobic component than with the increase in crosslinker content. However, Corkhill[43] brought it into attention that this depended on different hydrophobic components as well. PHEMA hydrogels with increased crosslinker content as well as increased weight fraction of MMA or styrene were prepared and their EWC and free water content (tested by DSC) were plotted, as shown in Figure 3.34.

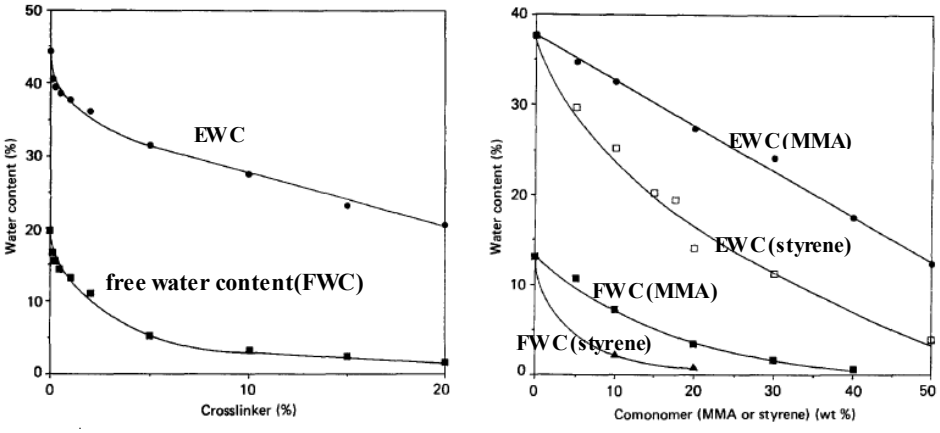

Figure 3.34 EWC and free water content of PHEMA hydrogels with increased crosslinker content(left) and increased MMA or styrene weight fraction(right)(reproduced from[43])

According to Figure 3.34, increasing crosslinker content from 0 to 20% decreases EWC from 45% to 21%, while increasing MMA and styrene weight fraction from 0 to 20% decreases EWC from 38% to 27% and 14%, respectively. Thus EWC decreased by 53.3%, 28.9%, 63.2% for the same increase in crosslinker content, MMA weight fraction and styrene weight fraction, respectively. Styrene has been reported to have a water contact angle of 91°[208], which makes it more hydrophobic than MMA (71.5°)[41]. Thus it depends on the individual properties of the hydrophobic component and the crosslinker in controlling the swelling behaviour of hydrogels.

In PLGA IPN hydrogels, tuning PLGA weight fraction seems to be more effective than crosslinker content(for crosslinking PLGA) in controlling the overall swelling behaviour. Increased PLGA weight fraction affects the swelling behaviour of the IPN hydrogels mainly by providing less binding sites for water molecules and acting as steric hindrance (providing an energetically unfavourable environment for water to bind with any hydrophilic component). The increased PLGA weight fraction also produces more hydrophobic bonding in the hydrogel network, which contributes to the more restricted mobility of the polymer chains. The increased hydrophobicity and decreased chain mobility lead to a decreased diffusion coefficient, initial swelling rate and equilibrium swelling ratio and an increased swelling period.

Thus, we can conclude that the weight fraction of PLGA is crucial in controlling the expansion rate and equilibrium swelling ratio of VP/MMA-PLGA IPN hydrogels.

3.4.6 Limitations of the PLGA IPN hydrogels

It can be noted that the equilibrium swelling ratio is largely decreased with the incorporation of PLGA network, which may limit the application of these IPN hydrogels to surgeries that require only a small piece of grown tissue, such as anophthalmia, eyelid, ear, lip or nose reconstruction. The decreased equilibrium swelling ratio is expected, as the hydrophobicity is increased with the incorporation of PLGA. Ideally, with the degradation of PLGA, the hydrogel will become less and less hydrophobic and absorb more water and finally expand to its maximum capacity as a single VP/MMA hydrogel will do. However, the expansion of PLGA IPN hydrogels can only reach a proportion of the maximum expansion of a same size VP/MMA hydrogel. This is thought to be a problem with PLGA which cannot be effectively degraded in distilled water nor untangled from the VP/MMA network and diffuse out of the

network. If PLGA remains in the network, it will stop water molecules from binding with the polar groups on VP/MMA network chains and refuse to accommodate free water molecules. However, even when immersed in PBS for months(not shown here, PBS is supposed to degrade PLGA), the hydrogel did not reach the swelling capacity of a same-size VP/MMA and as PLGA degraded, the gel became softer but no more expansion was observed. This could be attributed to two reasons: 1. The expansion may be offset by the existence of various ions in the PBS solution; 2. VP/MMA network could have already pre-expanded when immersed in DCM to incorporate PLGA networks. This pre-expansion could not be eliminated during the drying process. Thus the pre-expanded VP/MMA only has limited swelling capacity left. Thus if PLGA IPN could be prepared in a way that does not include pre-expansion in some solvent, the VP/MMA network may retain its swelling capacity. PLGA nanoparticles could be a good choice to start with if we want to avoid pre-solvent absorption. And PLGA nanoparticles may be better controlled to create a more homogeneous system and also more effectively degrade or diffuse out of the system.

The swelling period of these PLGA IPN hydrogels is longer than VP/MMA hydrogels, however, still much lower than the desirable period(weeks or months). This is the consequence of not having a coating or membrane. PLGA may slow down the water molecules from binding with the hydrophilic groups of VP/MMA, but cannot stop it. No hydrogels at present have been reported to have a swelling period over weeks or months long, unless with membranes or coatings. Thus it may still remain a problem if we want to extend the swelling period but also need the hydrogels to be able to be crafted without damaging its properties.

It might be confusing that the decreased swelling rate can also be achieved by pre-expanding VP/MMA hydrogel, and using the levelled off latter half for tissue

expansion. As shown in Figure 3.35, the swelling process of VP/MMA starting from point A is similar to that of PLGA IPN starting from point O. But the mechanical properties of VP/MMA will be steeply decreased at point A due to the water plasticizing effect, which may not be able to sustain the surgical operations. The mechanism is also different. For VP/MMA, it is mostly absorbing free water after point A as binding water gets saturated, according to Section 2.2.4. For PLGA IPN, it is slowly absorbing binding water from point O and later free water because of less binding sites and the steric hindrance from hydrophobic PLGA chains(will be further discussed below). Thus although the PLGA IPN has less swelling capacity, it is still valuable in skin reconstructions where only limited grown tissue is needed, such as anophthalmia, nose, lip or eyelid reconstruction. And for small tissue expansion, the swelling period does not have to be weeks long as long as it does not cause tissue necrosis.

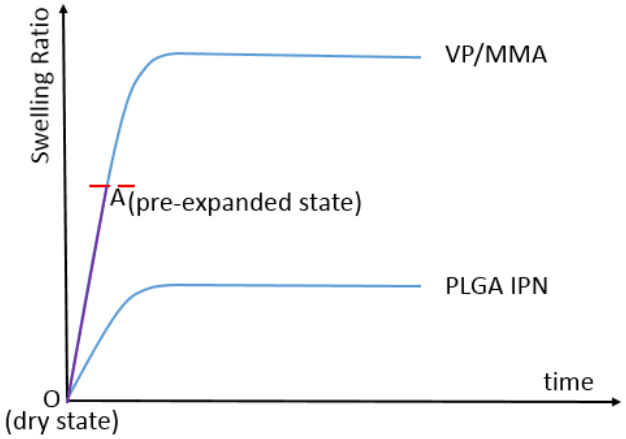

Figure 3.35 Schematic of the swelling process of PLGA IPN and VP/MMA

3.4.7 IPN structure

Identifying an inter-penetrating polymer network structure does not have a well-constructed nor accepted way. Sperling emphasized that one network must be crosslinked in the presence of another and there are no covalent bonds between them[105]. However, the interpenetrating on the molecular level is an ideal situation,

and actually only limited penetration could be achieved due to phase separation[104]. In this thesis, acrylated PLGA is crosslinked in the presence of a crosslinked VP/MMA network. Thus the preparation method meets the definition. DSC is supposed to show two individual glass transition temperatures, which indicates that there are no covalent bonds between PLGA network and VP/MMA network and both retain its own properties. However, T_g of VP/MMA is not evident because of the effect of residue DCM left in the gel. With that being said, it is believed that T_g of VP/MMA will become evident if DCM can be totally extracted. As will be shown in Chapter 4, the preparation of VP/MMA-PCL semi-IPN will be in an anhydrous state and its DSC spectrum shows two individual glass transitions. Thus DSC analysis supports the definition that there are no chemical reactions between those two networks. However, two T_g values can also indicate phase separation. SEM cannot differentiate between these two networks nor show any interpenetration on the molecule level, but SANS can evaluate the molecule level structure. The SANS analysis show that the spectra of PLGA IPN hydrogels cannot be described by the DAB model, which is built up for phase separation networks. This indicates that the IPN hydrogels are not just phase-separated networks.

To summarize, the PLGA IPN hydrogels prepared in this thesis can be defined as IPN structure as they satisfy the definition and are not just phase separated system as indicated by SANS.

3.5 Summary

VP/MMA-PLGA IPN hydrogels have been successfully prepared with varied PLGA weight fractions. The initial swelling rate and equilibrium swelling ratio decrease, while the swelling period increases with the increase in PLGA weight fraction. This is believed to be the result of increased hydrophobicity brought by the PLGA network.

PLGA affects the water absorption by reducing the available binding sites for water molecules and also acting as steric hindrance preventing water molecules from binding with any hydrophilic components. Increased PLGA weight fraction also restricts chain mobility because of the increased hydrophobic bonding acting as physical crosslinks. Together the increased hydrophobicity and more restricted chain mobility lead to a decrease in the swelling rate, diffusion coefficient, equilibrium swelling ratio and EWC. The decreased swelling rate comes at the expense of decreased equilibrium swelling ratio, which may limit the application of PLGA IPN hydrogels to surgeries that do not require a large piece of generated skin.

The higher polymer volume fraction and increased E_s(modulus of cell walls) due to hydrophobic bonding are responsible for the increased compressive modulus of the swollen hydrogels.

SANS shows that the IPN hydrogels are not just phase-separated systems as they do not fit in the DAB Model. It also shows that the incorporation of PLGA largely changes the internal structure of the hydrogel, generating much more inhomogeneity characterized by large length scale clusters. The CorreLength Model shows a decreased effective mesh size with increased PLGA weight fraction in PLGA IPN, which can be well described by the scaling law. SANS and SEM analysis indicate that PLGA goes through an in situ polymerization after being absorbed onto the surface of VP/MMA porous network and PLGA crosslinked into variable sizes and shapes due to the difference in the microenvironment. The PLGA network acts as a hydrophobic barrier for water diffusion and hydrogen bonding, resulting in the decreased swelling rate and equilibrium swelling ratio.

Increasing crosslinker content has also been shown to decrease the equilibrium swelling ratio of PLGA IPN, but at a much smaller extent than PLGA weight fraction. Thus in

the preparation of PLGA IPN hydrogels, changing PLGA weight fraction is much more effective than changing the crosslinker content(for crosslinking PLGA) in controlling the swelling behaviour.

The equilibrium volume swelling ratio(Figure 3.21) and the compressive modulus(Figure 3.15) at the swollen state can be controlled by controlling PLGA weight fraction. Thus by tailoring PLGA weight fraction in the preparation of the IPN hydrogels, we are now able to slow down the swelling rate and predict the possible area of tissue growth and mechanical performance of the tissue expanders before implantation. These IPN hydrogels have limited swelling capacities but their expansions are controlled and they are the only expanders at present without a coating or membrane, which means they can be easily crafted by surgeons to fit the desirable void volume on the patients.

Chapter 4: IPN Hydrogel with Alternative Secondary Networks

4 IPN hydrogels with alternative secondary networks

4.1 Introduction

While Chapter 3 discussed the preparation and characterization of VP/MMA-PLGA IPN hydrogel(abbreviated as PLGA IPN), this chapter is concerned with alternative secondary polymer networks to replace PLGA and their properties on the swelling behaviour of IPN or semi-IPN hydrogels. Biodegradable polyesters, PLA and PCL (polycaprolactone) have been chosen because of their hydrophobicity, biodegradability and biocompatibility (Section 2.5.4).

This chapter looks into the following aspects:

1. Is it possible to prepare IPN hydrogels with PLA or PCL?
2. What's the swelling behaviour of VP/MMA-PLA IPN hydrogel (abbreviated as PLA IPN) and VP/MMA-PCL semi-IPN hydrogel (abbreviated as PCL semi-IPN)?
3. How does T_g, hydrophobicity, and crosslinking condition of the secondary polymer network affect the swelling behaviour?
4. What's the most important property of the secondary polymer network that affects the swelling behaviour?

PLGA, PLA, and PCL vary mainly in 3 ways:

1. Glass transition temperature: T_g of PLGA was shown to be 21°C (Section 3.3.2), while that of PLA and PCL is 33.5°C and -60°C(will be verified in section 4.4.2), respectively.
2. Hydrophobicity: The hydrophobicity difference is attributed to their different chemical structure. The chemical structure of PLGA, PLA and PCL are shown in Figure 4.1, Figure 4.2 and Figure 4.3, respectively. PLA is more hydrophobic

than PGA because of the presence of methyl side groups in PLA units which create a steric barrier for water binding. Thus PLA is more hydrophobic than PLGA. PCL is even more hydrophobic and generally is highly crystalline[209, 210]because its linear backbone readily packs into extensive crystallites.

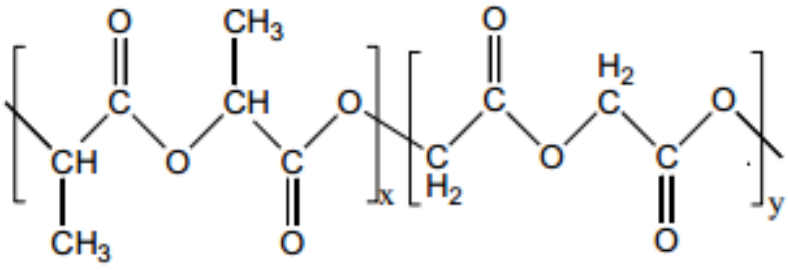

Figure 4.1 Chemical structure of PLGA

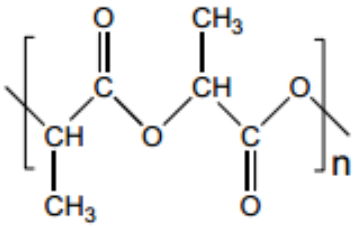

Figure 4.2 Chemical structure of PLA

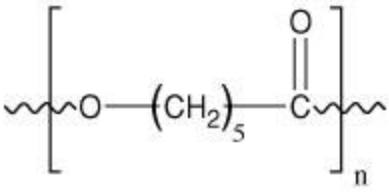

Figure 4.3 Chemical structure of PCL

The hydrophobicity order of PLGA, PLA and PCL has been verified by their water contact angles. The water contact angle of PLGA has been reported to be around 69.6°[198]. The water contact angle of PLA has been reported to be around 81°-82°[211, 212] and that of PCL in the range of 117°-134°[213, 214]. Thus the hydrophobicity order should be:

$$PLGA < PLA < PCL$$

3. Crosslinking condition: PLA IPN was prepared the same way as PLGA IPN because PLGA and PLGA share the similar chemical structure. However, PCL

can't be acrylated because of a lack of –OH end groups. PCL IPN will be prepared by crosslinking VP/MMA in the presence of PCL monomer. According to the definition of IPN (Section 2.4.1), it is defined as semi-IPN hydrogel as PCL is not crosslinked.

The swelling behaviour of PLGA IPN, PLA IPN, and PCL semi-IPN will be compared and the influence of the difference in their T_g, hydrophobicity and crosslinking condition on the swelling behaviour will be revealed.

PLA IPN and PCL semi-IPN will also be assessed using mechanical compression tests and differential scanning calorimetry. SEM will be used to show the internal morphology of those hydrogels.

4.2 Experimental

4.2.1 Materials

VP/MMA copolymeric xerogels with 9:1 VP to MMA weight ratio were purchased from Polymeric Science Ltd (New Ash Green, UK). PLA (poly D,L-lactic acid) was purchased from Evonik Corporation, Birmingham Laboratories, US. The glass transition temperature, the weight average molecular weight (M_w) and polydispersity index (PDI) of PLA were 46°C, 20kDa, and 1.8, respectively. PCL was purchased from Sigma-Aldrich, with average molecular weight of 45000g/mol, melting point of 60°C. Vinyl-pyrrolidone(VP), methyl methacrylate(MMA), allyl methacrylate, acryloyl chloride, triethylamine, anhydrous ethyl acetate, n-hexane, and dichloromethane (DCM), N,N'-Methylenebisacrylamide (BIS), azobisisobutyronitrile (AIBN), Deuterated chloroform ($CDCl_3$) were purchased from Sigma-Aldrich(UK).

4.2.2 PLA acrylation

PLA needs to be acrylated first in order to be crosslinked in the presence of VP/MMA

to form a full-IPN. The acrylation process of PLA is the same as described for PLGA in 3.2.2.

4.2.3 Preparation of PLA IPN

The preparation of PLA IPN is the same as described for PLGA IPN in 3.2.3. IPN hydrogels with different PLA weight fraction were denoted as vmpla0.025, vmpla0.05, vmpla0.1, respectively. 0.2wt%(based on weight of PLA) of the crosslinker BIS and 0.2wt%(based on weight of PLA) of the initiator AIBN were used for PLA crosslinking, the same amount as for PLGA. PLA weight fraction is calculated using equation (4.1), Where $m\%$, m_{vmpla}, m_{vm} stands for the weight fraction of PLA in PLA IPN(dry), the mass of PLA IPN(dry), and the mass of the original VP/MMA xerogel disc, respectively:

$$m\% = \frac{m_{vmpla} - m_{vm}}{m_{vmpla}} \times 100\% \quad (4.1)$$

Using equation 4.1, vmpla0.025, vmpla0.05, vmpla0.1 samples correspond to a PLA weight fraction of around 30%, 50% and 70% in the IPN hydrogels, respectively.

4.2.4 Preparation of PCL semi-IPN

VP/MMA polymer network was crosslinked in the presence of PCL monomers. 0.9g vinyl-pyrrolidone and 0.1g methyl methacrylate monomers (weight ratio 9:1) were blended with 0.3g PCL at 70°C for 1h which is above the melting point of PCL(60°C). Allyl methacrylate (0.2 wt%) and AIBN (0.2wt%), based on the weight of VP and MMA monomers were then added as the crosslinking agents. The mixture was blended to homogeneity and thermally polymerised in a polypropylene tube. The monomers were initiated at 35°C for 12 hours and gel network was formed at 80°C for 12h. The weight fraction of PCL is calculated using equation (4.2):

$$m\% = \frac{m_{pcl}}{m_{pcl} + m_{vp} + m_{mma} + m_{crosslinking\ agents}} \times 100\% \quad (4.2)$$

Using equation (4.2), PCL weight fraction is $\frac{0.3g}{0.3g+0.9g+0.1g+0.012g} = 22.9\%$

PCL semi-IPN with higher PCL weight fractions was not prepared because of the high viscosity of PCL monomer in its molten state.

4.2.5 Preparation of VP/MMA

VP/MMA xerogel rods were used in the previous chapter which were purchased from Polymeric Science Ltd (New Ash Green, UK) but their preparation method was unknown. To serve as an absolute control sample to PCL semi-IPN, VP/MMA hydrogel was prepared in the lab using the same method as shown in Section 4.2.4 just without adding PCL. 0.9g VP and 0.1g MMA monomers (weight ratio 9:1) were blended under room temperature for 10 minutes. Allyl methacrylate(0.2wt%) and AIBN(0.2wt%) were then added as the crosslinking agents. The mixture was blended to homogeneity and thermally polymerised in a polypropylene tube. The monomers were initiated at 35°C for 12 hours, and then at 80°C for 12h.

4.3 Characterization

4.3.1 Nuclear Magnetic Resonance (NMR)

The acrylation process of PLA was verified by Nuclear Magnetic Resonance (NMR). 10mg/ml solution of the original PLA and the functionalized PLA in deuterated chloroform ($CDCl_3$) were tested under a Varian Mercury-300 ^1H NMR at room temperature. As described in 3.3.1, acrylate end groups have their unique resonance frequencies. The absence and presence of the resonant signals from acrylate groups before and after the functionalization process should be able to verify if PLA is successfully acrylate end-capped.

4.3.2 Differential scanning calorimetry (DSC)

The determination of the glass transition temperature shows the phase separation in the

IPN system and serves as evidence for the co-existence of component networks in the IPN hydrogel. Moreover, T_g of PLA and PCL will be compared with T_g of PLGA to see if T_g of the secondary polymer network has any effect on the swelling behaviour of the IPN hydrogels. T_g of dry PLA IPN and PCL semi-IPN were determined by differential scanning calorimetry (Pyris Diamond Hyper DSC) with a heating rate of 100 °C /min over a temperature range of -100 to 200°C. Samples weighing within 5-10mg were analysed in aluminium pans, using an empty pan as the reference. The purge gas was helium at a flow rate of 50ml/min. A combination of heating, cooling and heating a second time was used to improve the resolution. T_g is extracted the same way as described in Section 3.2.5.

4.3.3 Compression Test

The same as described in Section 3.2.6, the compression tests were performed on the fully swollen samples using a Perkins Elmer DMA 7e dynamic mechanical analyser. The compression rate was 100mN/min and the maximum load was 6000mN. Compressive modulus E is calculated as the gradient of the curve in the strain range of 12%-14%.

4.3.4 Scanning Electron Microscope (SEM)

Microstructure of PLA IPN and PCL semi-IPN (swollen, freeze-dried) were studied using field emission scanning electron microscope(Zeiss Nvision 40). Freeze-dried samples were mounted on a double sided tape on aluminium spin stubs and sputter coated with gold using E 5400 Sputter Coater(Bio-Rad, Polaron Division). SEM images were recorded under the accelerating voltage of 2kV and 0.2K-6k magnification.

4.3.5 Swelling Behaviour

Swelling behaviour tests were carried out in distilled water at 37 °C, exactly the same as described in Section 3.2.9. All the samples were performed in triplicate and the average

value was calculated. The distilled water was replaced daily. The initial volume swelling rate, equilibrium swelling ratio, swelling period, EWC, polymer volume fraction and density of PLA IPN and PCL semi-IPN were characterized exactly the same way as described for PLGA IPN in Section 3.2.9.

4.4 Results

4.4.1 Nuclear Magnetic Resonance

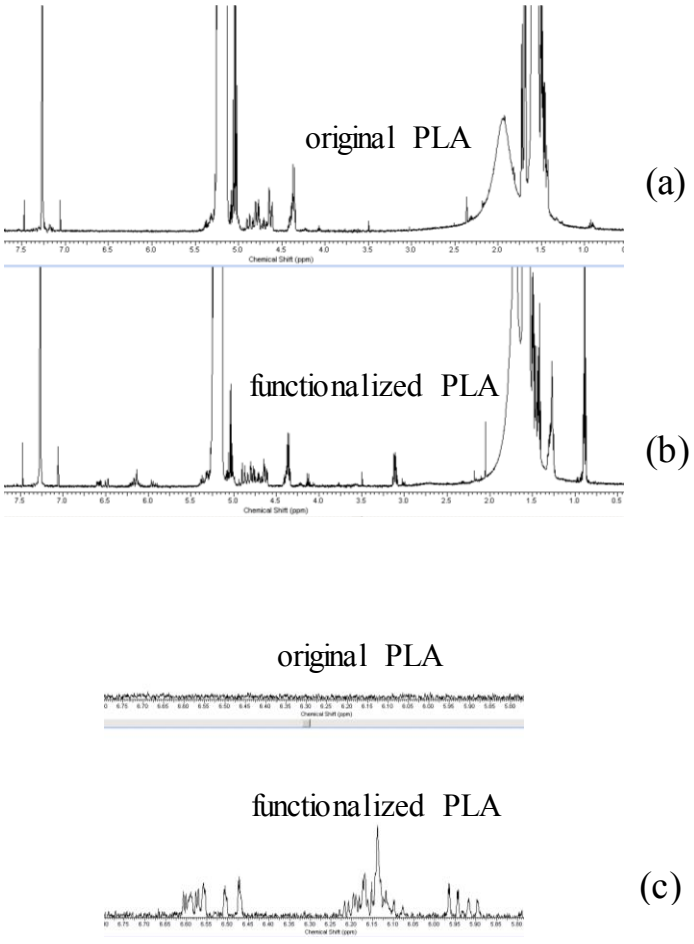

Figure 4.4 ^{1}H-NMR spectrum of (a)original PLA (b)functionalized PLA (c)the magnified image of the absence and presence of the functional groups before and after acrylation.

The ^{1}H-NMR spectrum of the original PLA(a) and the functionalized PLA(b) and the magnified image of the functional groups(c) are shown in Figure 4.4. The ^{1}H-NMR spectrum of both PLA share several peaks from the main structure of PLA. The peaks

around 1.6 ppm correspond to the methyl groups (-CH_3), while the peaks around 5.1-5.3ppm correspond to the methine groups(-CH) in the lactide repeat units[179]. No peaks are observed at around 4.9 ppm (the methylene groups) in Figure 4.4 because there are no glycolide units[179]. The presence of the peaks at around 5.93ppm, 6.19ppm and 6.5ppm owing to the vinyl end groups[180] in Figure 4.4(b) demonstrates the existence of acrylate end groups in functionalized PLA, which are not observed in Figure 4.4(a). The successful acrylate end-capping enables PLA to be crosslinked into a biodegradable polymer network in the presence of a primary VP/MMA hydrogel network, forming a full IPN.

4.4.2 Differential Scanning Calorimetry

T_g of the original PLA is 46°C according to the data information provided by the manufacturer. T_g of the acrylated PLA was tested under DSC and shown in Figure 4.5. The extracted T_g is 33.54°C.

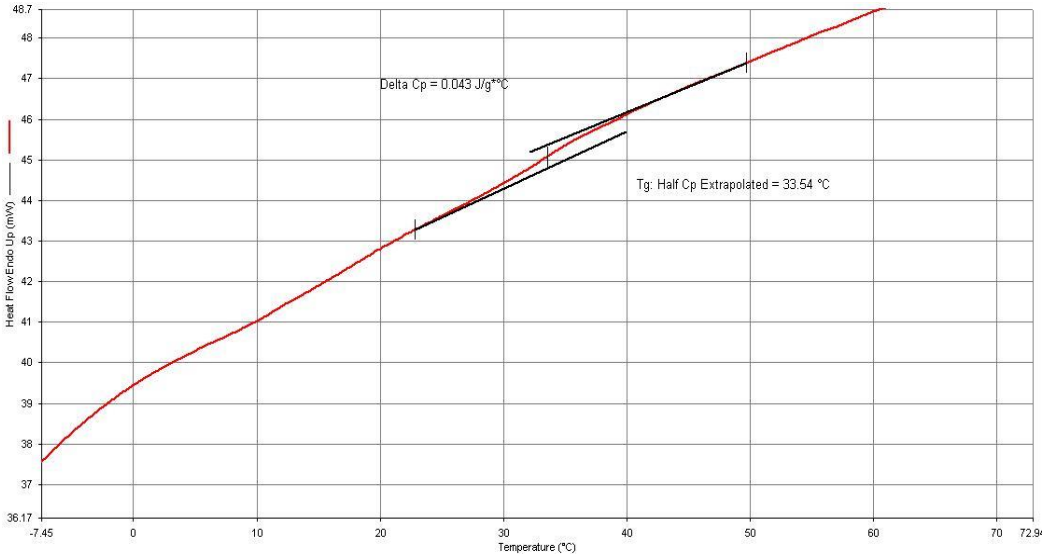

Figure 4.5 DSC spectrum of acrylated PLA

DSC spectrum of PLA IPN (dry state) is shown in the Figure 4.6. The red line stands for the first heat cycle and the black one stands for the second cycle. In the first cycle, there was a broad glass transition observed at 22.67°C, which is believed to be the glass

transition of PLA. Sample instability was observed at temperatures above 110 °C, which was eliminated in the second cycle. The glass transition of PLA shifted to 39.23°C in the second cycle and no obvious glass transition of VP/MMA was observed.

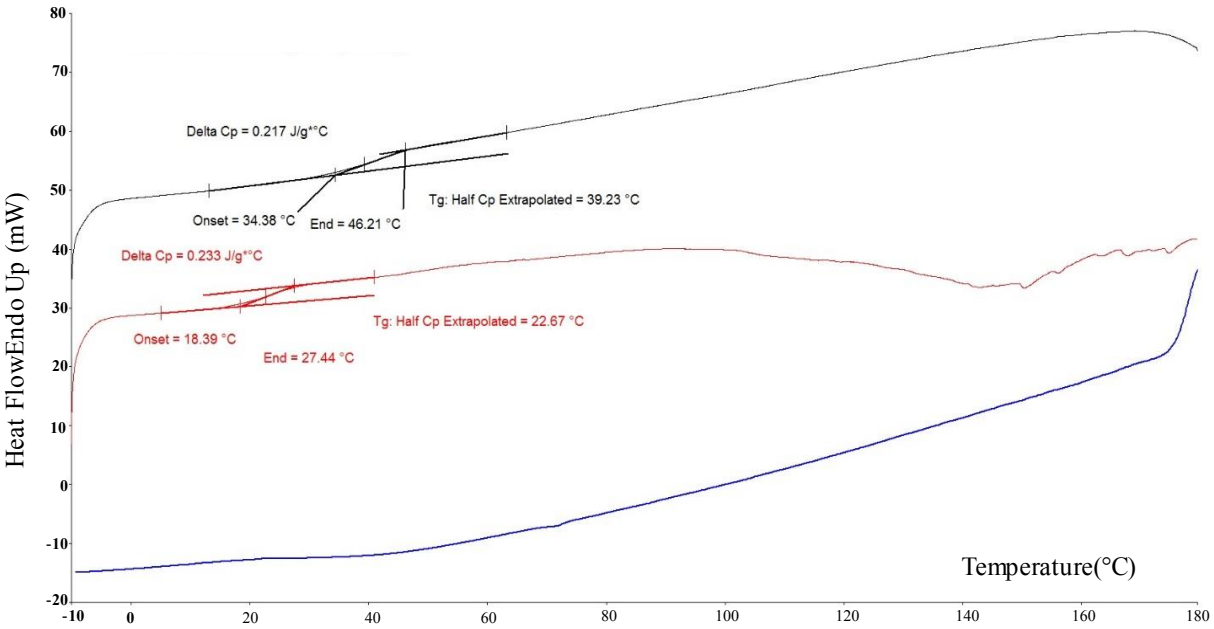

Figure 4.6 DSC spectrum of PLA IPN (dry state)

As the contrast sample of PCL semi-IPN, VP/MMA xerogel prepared in the lab was tested under DSC. Its DSC spectrum is shown in Figure 4.7. There was evidence of sample instability at high temperatures (above 130°C) in the first cycle. The glass transition was clear in the second cycle. A broad glass transition was observed and the T_g extracted is 131.8°C.

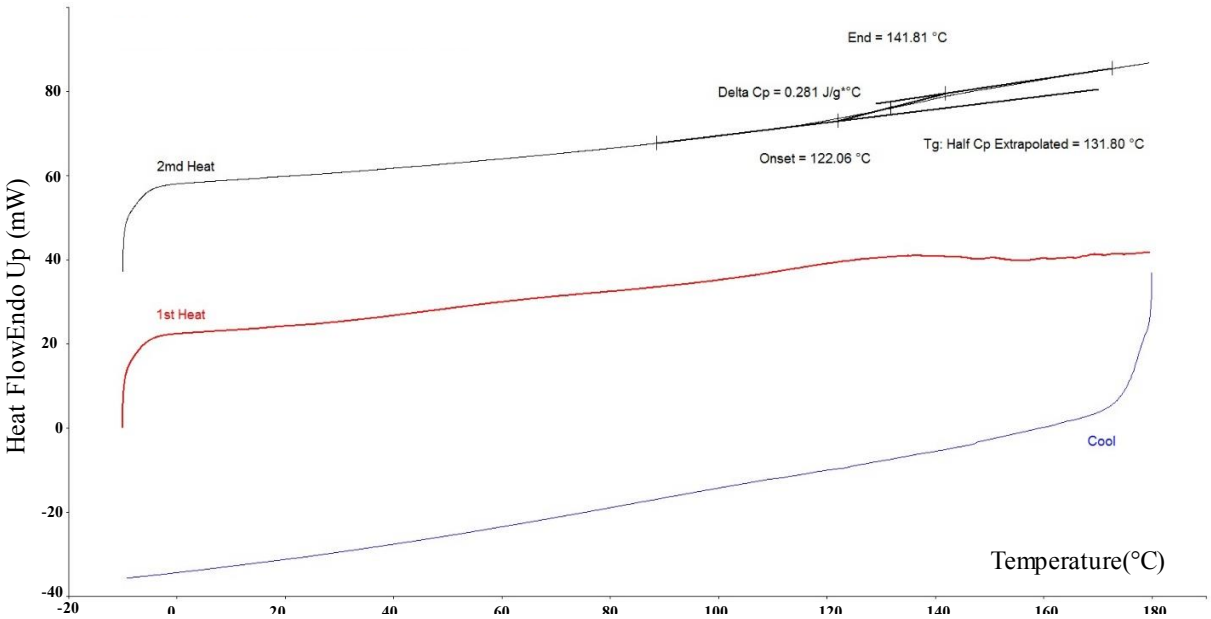

Figure 4.7 DSC spectrum of the VP/MMA xerogel prepared in the lab

The DSC spectrum of PCL semi-IPN(dry) is shown in Figure 4.8. The glass transition of PCL was not very clear in the 1st heat cycle but was observed in the 2nd heat cycle at around -60°C. A peak around 60°C was observed in both heat cycles. The glass transition of VP/MMA was not very clear in the 1st heat cycle but was observed in the 2nd cycle, at 146.21°C.

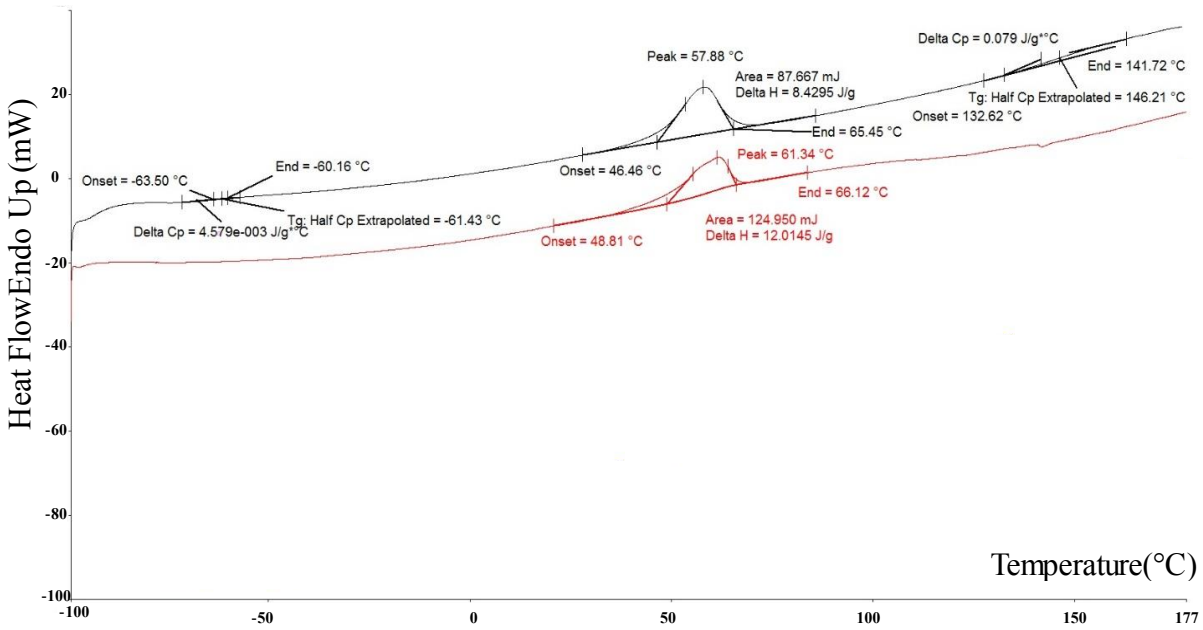

Figure 4.8 The DSC spectrum of PCL semi-IPN (dry state)

4.4.3 Compression Test

Figure 4.9 shows the stress-strain curve of PLA IPN with varied PLA weight fractions. The compressive modulus E is shown in the Table 4.1(a) and compared with that of PLGA IPN(Table 4.1(b)).

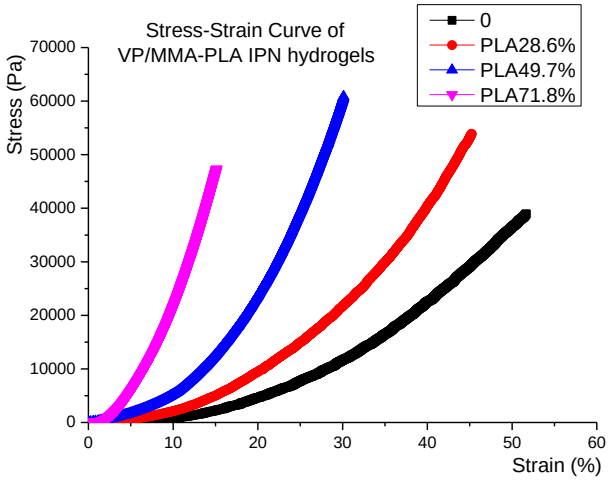

Figure 4.9 Stress-strain curves of VP/MMA and PLA IPN

Table 4.1 The compressive modulus of the IPN hydrogels with different PLA(a) and PLGA(b) weight fractions

PLA weight fraction (%)	G(10^5 Pa)
0	0.32
28.6	0.67
49.7	1.57
71.8	5.2

(a)

PLGA weight fraction (%)	G(10^5 Pa)
0	0.32
25.1	0.88
43.9	1.44
62.8	2.28

(b)

As can be seen from Table 4.1(a), E of PLA IPN is increasing with increasing PLA weight fraction. This is similar with PLGA IPN, whose compressive modulus also increases with PLGA weight fraction.

The stress-strain curves of swollen VP/MMA (prepared in the lab) and PCL semi-IPN are shown in Figure 4.10. The extracted E is summarized in Table 4.2. PCL semi-IPN shows a much higher E than VP/MMA. At the similar weight fraction, PCL semi-IPN has a higher compressive modulus compared to PLGA IPN (0.88×10^5Pa) and PLA IPN (0.67×10^5Pa).

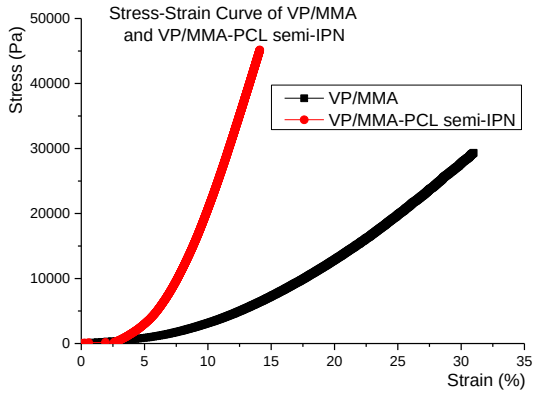

Figure 4.10 Stress-Strain curve of VP/MMA and PCL semi-IPN

Table 4.2 Compressive Modulus of VP/MMA and PCL semi-IPN

PCL weight fraction (%)	E(10^5 Pa)
0	0.79
22.9	6.2

4.4.4 Scanning Electron Microscopy

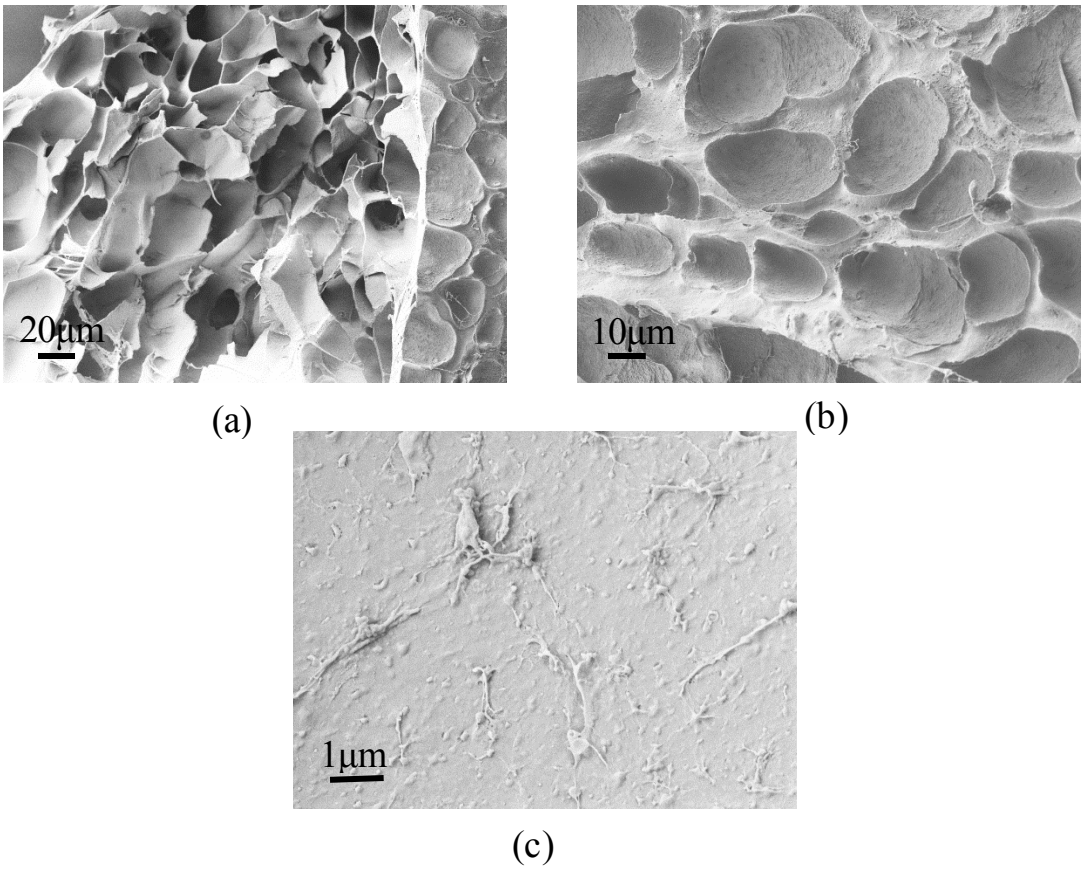

Figure 4.11 SEM images of 30%PLA IPN (swollen state, freeze-dried)

Figure 4.11 shows the SEM images of 30%PLA IPN (PLA weight fraction 30%,

swollen state, freeze-dried). 30%PLA IPN shows porous network, which is similar as PLGA IPN (see Chapter 3.3.5). The pore size ranges from around 10μm to 40um. Small spheres or irregular aggregates were observed on the surface of the network as shown in Figure 4.11(c). The same as PLGA IPN, PLA IPN also shows rough surfaces compared to VP/MMA.

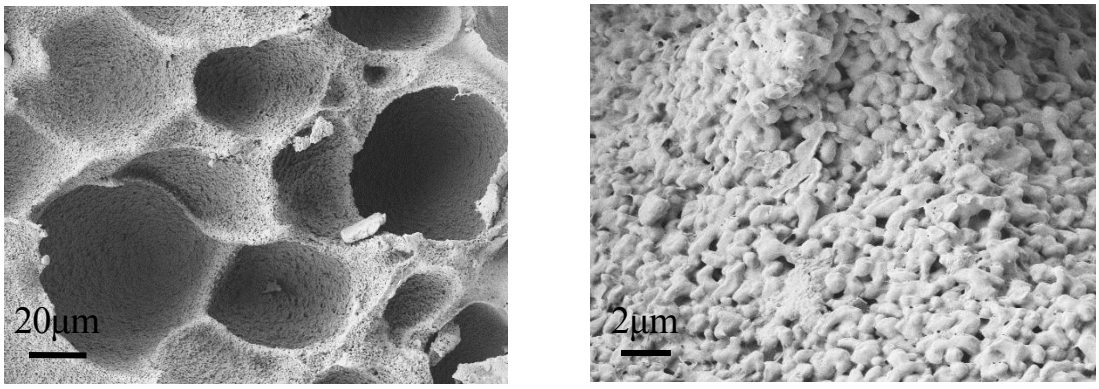

Figure 4.12 SEM images of 50%PLA IPN(swollen state, freeze-dried)

Figure 4.12 shows the SEM images of 50%PLA IPN. Large pores and rough surfaces were detected as shown in Figure 4.12(a). Figure 4.12(b) takes a closer look at the surface and round and irregular aggregates were detected, which are more compact than 30A%PLA IPN shown in Figure 4.11(c).

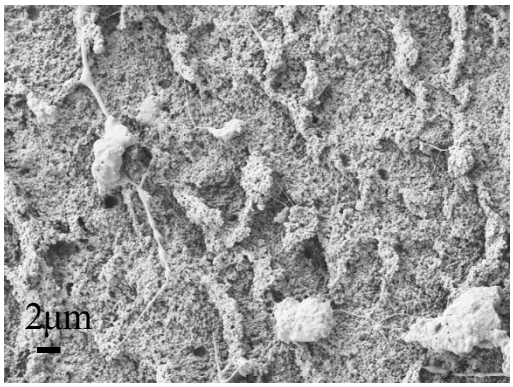

Figure 4.13 SEM images of 70%PLA IPN(swollen state, freeze-dried)

Figure 4.13 shows the SEM image of 70%PLA IPN. Porous network was not detected for 70%PLA IPN. Round and irregular aggregates were found on the surfaces. Small

aggregates were packing into large aggregates and the structure is much more compact than 30%PLA IPN and 50%PLA IPN shown above.

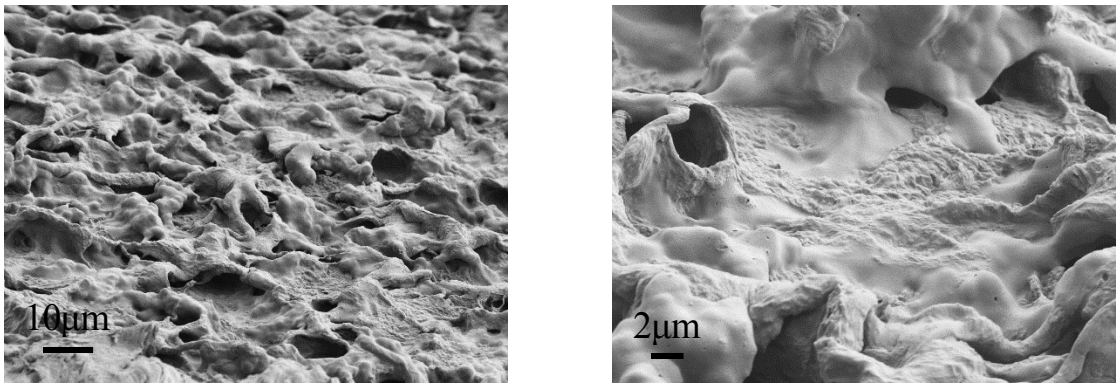

Figure 4.14 SEM images of PCL semi-IPN (22.9% PCL, swollen state, freeze-dried)

Figure 4.14 shows the SEM images of 22.9%PCL semi-IPN. There was no obvious porous network and the structure was quite compact with rough surfaces. There were some small holes on the surface with irregular sizes.

4.4.5 Swelling Behaviour

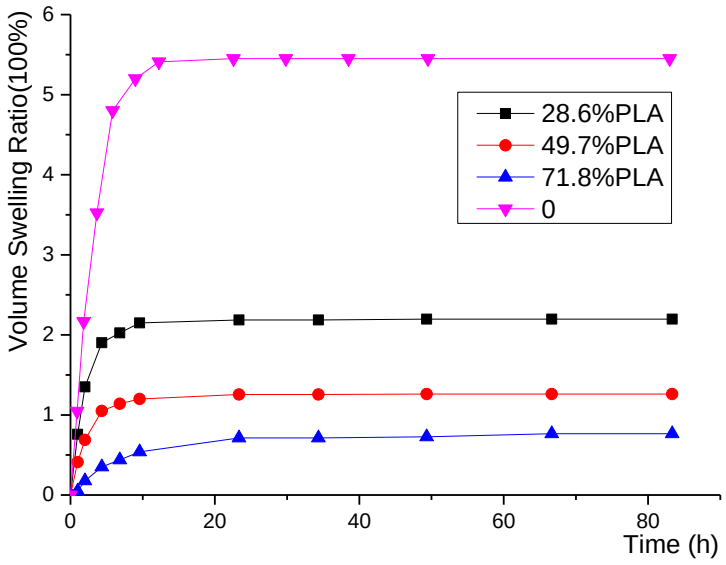

Figure 4.15 The volume swelling ratio of PLA IPN with varied PLA weight fractions as a function of time

Figure 4.15 shows the volume swelling ratio of PLA IPN as a function of time. Similar to PLGA IPN, the volume swelling ratio increases rapidly in the beginning and then levels off. The initial swelling rate(R_i), equilibrium swelling ratio(Q_∞) and swelling

period(T_e) and EWC is summarized in Table 4.3 below, which shows R_i is largely decreased with the increase in PLA weight fraction.

Table 4.3 Initial Swelling Rate, equilibrium swelling ratio, swelling period and EWC of VP/MMA and PLA IPN

	Initial swelling rate(%/h)	Equilibrium Swelling Ratio (100%)	Swelling Period(h)	EWC(%)
VP/MMA	96.0	5.5	12	85.6
28.6%PLA	42.1	2.21	20	72.7
49.7%PLA	23.2	1.25	45	57.8
71.8%PLA	8.4	0.76	80	44.3

The incorporation of PLA slows down the swelling and extends the expansion period. The equilibrium swelling ratio of VP/MMA is around 5.5. However, 28.6%PLA IPN has a Q_∞ of 2.21, 49.7%PLA IPN of 1.25 and 71.8% PLA IPN of 0.76. As stated in Section 3.3.6, 25.1%PLGA IPN can swell up to 3 times its original size, 43.9%PLGA IPN up to 2 times, and 62.8%PLGA IPN up to 1 time. Thus PLA IPN has smaller equilibrium swelling than PLGA IPN at similar weight fraction of the secondary polymer network.

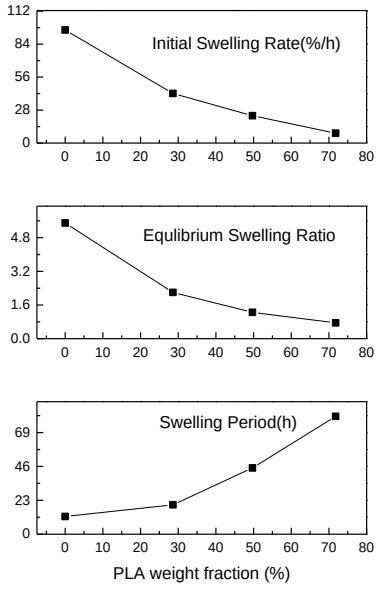

Figure 4.16 Initial swelling rate, equilibrium swelling ratio and swelling period of PLA IPN with increased PLA weight fraction

Figure 4.16 shows the initial swelling rate, equilibrium swelling ratio and swelling period of PLA IPN with increased PLA weight fraction. The initial swelling rate and equilibrium swelling ratio decreases while the swelling period increases with increase in PLA weight fraction. These three important parameters characterizing the swelling behaviour all scale with the change in PLA weight fraction.

Figure 4.17 shows the equilibrium volume swelling ratio as a function of PLA weight fraction. The same as PLGA IPN, PLA IPN has an equilibrium swelling ratio decreasing almost linearly with increasing PLA weight fraction.

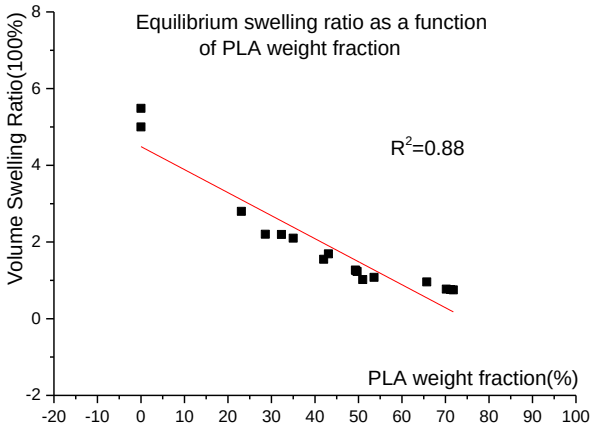

Figure 4.17 Volume swelling ratio of PLA IPN as a function of PLA weight fraction

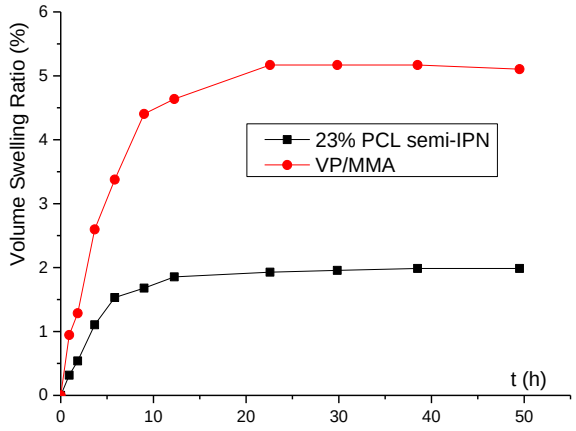

Figure 4.18 The volume swelling ratio of VP/MMA and PCL semi-IPN as a function of time

Figure 4.18 shows the volume swelling ratio of PCL semi-IPN and VP/MMA (prepared

in the lab) as a function of time. VP/MMA prepared in the lab shows similar swelling curve with the one bought from Polymer Science Ltd. And the equilibrium swelling ratio of both VP/MMA hydrogels is around 5. The initial swelling rate(R_i), equilibrium swelling ratio(Q_∞) and swelling period(T_e) and EWC of VP/MMA (prepared in the lab) and PCL semi-IPN is shown in Table 4.4.

Table 4.4 The initial swelling rate, equilibrium swelling ratio and swelling period and EWC of VP/MMA(prepared in the lab) and PCL semi-IPN

	Initial Swelling Rate(%/h)	Equilibrium Swelling Ratio (100%)	Swelling Period(h)	EWC (%)
VP/MMA (prepared in the lab)	68	5.2	22	85.2
PCL semi-IPN	29.7	1.98	38	67.9

The incorporation of an uncrosslinked PCL network decreases the initial swelling rate and equilibrium swelling ratio and extends the swelling period.

4.5 Discussion

4.5.1 Differential Scanning Calorimetry

No obvious peak was observed in the DSC spectrum of PLA IPN. A broad endothermic peak was observed at low temperature and the extracted T_g was 22.67 °C in the first cycle and 39.23°C in the second one. There was evidence of sample instability or evaporation at temperatures higher than 110°C, which was only observed in the first heat cycle. This could be a result of residue dichloromethane or absorbed water evaporating at high temperatures. T_g in the region of 20-40°C is believed to show the glass transition of PLA. Because of the residue dichloromethane acting as a plasticizer, T_g was decreased to 22.67°C in the first heat cycle and was increased back to 39.23°C in the second one. The glass transition of VP/MMA was unclear in both heat cycles, which is believed to be the result of residue dichloromethane that had still not been removed.

Just as PLGA IPN, the preparation of PLA IPN went through an expansion process in dichloromethane and not all the solvents could be extracted during the drying process for the preservation of the original shapes and structures of the bulk hydrogels. Thus, the residue dichloromethane acts as a plasticizer, unfastening the polymer structure, disrupting the inter-chain secondary bonding, thus lowering the energy needed to promote chain mobility, decreasing T_g and causing the glass transition of VP/MMA to be unclear.

The glass transition of PCL semi-IPN showed much less sample instability at high temperatures, compared to PLGA IPN and PLA IPN. This is because the preparation of PCL semi-IPN was at an anhydrous state and no residue solvents could act as plasticizers. The glass transition of PCL and VP/MMA was clear in the second heat cycle. The glass transition around -60°C is thought to be the glass transition of PCL. The endothermic peak at 60°C shows the melting of PCL. The glass transition of VP/MMA is shown at 146°C, which is similar to the glass transition temperature of VP/MMA xerogel prepared in the lab (131.8°C, shown in Figure 4.7).

4.5.2 Compression Test

The same as PLGA IPN, PLA IPN and PCL semi-IPN both show increased compressive modulus E as their weight fraction is increased in the IPN system. The same as discussed in Section 3.4.2, first of all, the increased modulus is a result of increased polymer volume fraction φ_s in the hydrogels. Similar to PLGA IPN hydrogels, the internal structure of PLA IPN hydrogels can also be seen as closed cells, and their compressive modulus can be described by equation(3.17). Thus the higher the polymer volume fraction φ_s, the higher the modulus. PLGA and PLA have similar properties and Figure 4.19 plots the modulus E as a function of polymer volume fraction of PLGA or PLA in the hydrogels. PLGA IPN and PLA IPN were plotted together to increase the

statistically accuracy. As can be seen from Figure 4.19, E fits in a power law relationship with φ_s with the exponent of 3.2. This exponent corresponds to the first term in equation(3.17) showing the contribution of cell wall bending to the overall modulus. The fact that E can be adequately described by the cube of φ_s indicates that cell wall bending might be the main contribution to the overall elastic modulus. It has been shown in Chapter 3 that E of PLGA IPN can be adequately described by φ_s square, which corresponds to cell edge bending. Thus cell wall and edge bending may be the main contribution to the modulus of these hydrogels. But still, it should be noted that more samples and tests are needed for a more complete modelling and a more accurate result. Also, the cell wall modulus E_s, of PLA IPN, is also changing with PLA weight fraction.

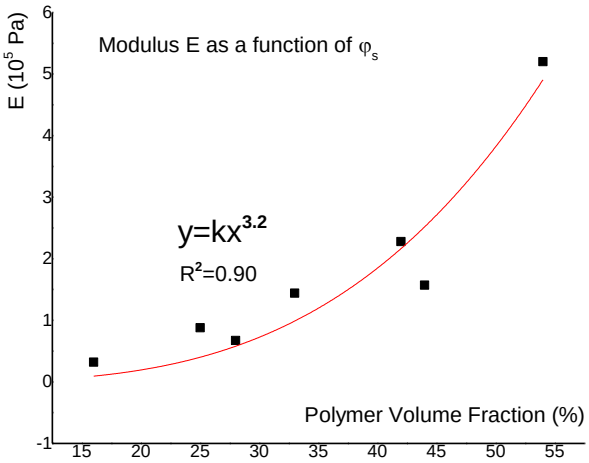

Figure 4.19 Compressive modulus E as a function of polymer volume fraction φ_s

The normalized modulus is shown in Table 4.5. E_d is E divided by density of the swollen hydrogels, and E_n is E times $(1-\varphi_s)$.

Table 4.5 Normalized modulus of PLA IPN hydrogels

PLA weight fraction (%)	E(10^5 Pa)	Density(g/cm^3)	E_d(10^{-1}N/g)	φ_s	E_n (10^5 Pa)
0	0.32	1.19	0.27	0.16	0.27
28.6	0.67(+109%)	1.24	0.54(+100%)	0.28	0.48(+77.8%)
49.7	1.57(+134%)	1.30	1.21(+124%)	0.44	0.88(+83.3%)
71.8	5.2(+231%)	1.37	3.80(+214%)	0.54	2.4(+172.7%)

The same as for PLGA IPN, the normalization by density and polymer volume fraction both help reduce the increase percent of the compressive modulus with increased PLA weight fraction. At similar weight fraction, PLA IPN shows a similar modulus value as PLGA IPN.

As can be seen from equation(3.17), E is also determined by E_s, the modulus of the cell wall solid material. And for PLA IPN, it stands for the modulus of the IPN networks consisting of VP/MMA and PLA. Bulk PLGA and PLA show similar modulus around 2GPa, with PLA exhibiting a slightly higher value[153]. Generally PLA shows a higher modulus than PLGA because the formation of PLGA copolymer disrupts the crystalline phases, leading to a lower modulus than PGA or PLA alone[215]. Also PLA is more hydrophobic than PLGA, leading to a stronger hydrophobic bonding, which increases the physical crosslinking and leads to a higher E_s. Thus E_s of PLA IPN is supposed to be higher than that of PLGA IPN. And according to equation(3.17), E of PLA IPN is then supposed to be higher than PLGA IPN at the same φ_s. However, E of PLGA IPN and PLA IPN show similar values at similar φ_s. This could be attributed to the way of incorporating PLGA or PLA networks during the preparation of the IPN hydrogels. PLGA or PLA network is introduced into the VP/MMA network through solvent absorption. As has been discussed, DCM cannot be fully extracted during the drying process because of the fragile nature of the hydrogels. Thus the PLGA or PLA network

existing in the dry IPN gels is probably still in a half-dry state. The plasticizing effect of DCM will largely decrease the modulus of bulk PLGA or PLA and bring them to a similar value. Thus E_s of PLGA IPN and PLA IPN may be quite similar. The half-dry state of PLGA and PLA is the reason that the bulk modulus of PLGA or PLA cannot be used in the modelling. The modulus of PLGA or PLA in the cell walls of the hydrogels could be quite different from their reported values because of the plasticizing effect of DCM.

Table 4.6 Normalized modulus of PCL IPN

PCL weight fraction(%)	E(10^5 Pa)	Density(g/cm^3)	E_s(10^{-1}N/g)	φ_s	E_n (10^5 Pa)
23	6.2	1.17	5.30	0.33	4.2

PCL semi-IPN shows a much higher compressive modulus than VP/MMA, at a low PCL weight fraction (around 23%). Table 4.6 shows that after normalization by density or φ_s, the modulus of PCL semi-IPN is still much higher than PLGA IPN and PLGA IPN, at similar weight fraction. PCL has no functional groups to be crosslinked, and no crosslinker is added during the preparation. Thus the higher E cannot be a result of increased crosslinker content. PCL is a semicrystalline polymer with a glass transition temperature of -61°C, which means it has much higher chain mobility at the experimental temperature than PLGA and PLA[216]. Bulk PCL is also reported to have a lower modulus than PLGA or PLA, around 300MPa[217]. This means the modulus of the cell wall material, E_s of PCL semi-IPN is also supposed to be lower than that of PLGA IPN or PLA IPN at the similar weight fraction in the hydrogels. Thus a lower E of PCL semi-IPN is expected at the same weight fraction. However, it shows a higher compressive modulus, even higher than PLGA IPN or PLA IPN with higher φ_s. Thus E_s of PCL semi-IPN is actually higher than that of PLGA IPN or PLA IPN. This could be attributed to one or any combinations of the following reasons:

1. The high molecular weight of PCL (45kDa) which promotes physical

entanglements of the polymer chains, resulting in lower strain under the same stress and a higher E_s.

2. PCL is more hydrophobic than PLGA and PLA (see section 4.1), thus may create stronger hydrophobic bonding, resulting in a stiffer network.
3. The preparation process of PCL semi-IPN was done in an anhydrous state. Thus unlike PLGA and PLA IPN, it should not have any residue solvent(like DCM in PLGA IPN and PLA IPN) that could act as a plasticizer. Thus chain mobility is more restricted, which leads to a higher E_s.

T_g of the secondary polymer network does not seem to have much effect on the mechanical properties of the IPN hydrogels. The hydrophobicity and the polymer volume fraction of the secondary network, and the modulus of the cell wall material E_s are playing a much more prominent role in determining the compressive modulus of the IPN hydrogels.

4.5.3 Scanning Electron Microscopy

Compact structures with rough surfaces were detected for PLGA IPN, PLA IPN and PCL semi-IPN. For PLA IPN, a porous network was detected under low PLA weight fraction(30% and 50%)(Figure 4.11 and 4.12). The aggregates on the surfaces were more packed as PLA weight fraction increased. Those aggregates are believed to be crosslinked PLA domains and as PLA weight fraction increases, there are more and larger aggregates with irregular shapes. Those aggregates are formed on the surfaces of the pores and are responsible for the surface roughness. In a similar manner to PLGA IPN, it can be speculated that the functionalized PLA monomer was absorbed into the network of VP/MMA through solvent absorption, then an in situ polymerization was carried out in the presence of the crosslinker and the initiator. Because of the difference of microenvironments and the immiscibility between PLA and VP/MMA, PLA

polymerized on the surface of the VP/MMA porous network, and formed domains with variable sizes and shapes.

Figure 4.11-4.13 show an increase in the size of aggregates and compactness in the structure, corresponding to a higher polymer volume fraction of the hydrogel with increased PLA weight fraction.

It is difficult to assign a specific pore size because some pores appear as a collapsed or closed shell that may or may not have been cut or distorted during specimen preparation or freeze-drying. Thus there appears to be a wide range of pore sizes and this could be a result of inhomogeneity of the hydrogel where polymer is more concentrated than the others. Overall though, the pore size of PLGA IPN and PLA IPN are broadly similar.

However, it is obvious that PCL semi-IPN has more compact structure and much fewer and smaller pores than PLGA IPN and PLA IPN at the similar weight fraction, which indicates a higher polymer volume fraction at the fully swollen state.

4.5.4 Swelling Behaviour

4.5.4.1 Diffusion Mechanism and Structure Characterization Parameters

The water diffusion mechanism of PLA IPN and PCL semi-IPN are determined the same way as described in Section 3.4.5. Figure 4.20 shows the water uptake(M_t/M_∞) of PLA IPN and PCL semi-IPN as a function of time and their diffusion exponents as calculated using equation(4.3), where M_t is the water uptake at time t and M_∞ is the water uptake at the equilibrium state, k is a constant and n is the diffusion exponent. The diffusion exponents are summarized in Table 4.7, in comparison to PLGA IPN.

$$\frac{M_t}{M_\infty} = kt^n \tag{4.3}$$

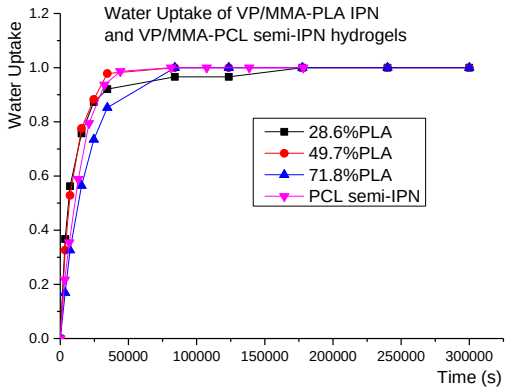

Figure 4.20 Water uptake of PLA IPN and PCL semi-IPN as a function of time

Table 4.7 Diffusion Exponents and Mechanism of PLGA IPN, PLA IPN and PCL semi-IPN

Secondary Polymer Weight Fraction	Diffusion Exponent n	Diffusion Mechanism
0	0.72	Anomalous
25.1% PLGA	0.47	Fickian
43.9% PLGA	0.51	Fickian
62.8% PLGA	0.64	Anomalous
28.6% PLA	0.47	Fickian
49.7% PLA	0.56	Anomalous
71.8% PLA	0.78	Anomalous
22.9% PCL	0.73	Anomalous

As can be seen from Table 4.7, PLGA IPN and PLA IPN both transfer from Fickian diffusion to anomalous diffusion as their weight fraction increases. 43.9%PLGA IPN shows n of 0.51 and 49.7%PLA IPN shows that of 0.56. Thus it can be interpolated that at PLGA or PLA weight fraction higher than 45%, the polymer chains will not be sufficiently mobile to permit immediate penetration of water molecules into the hydrogel network. The water diffusion rate and the polymer relaxation rate will be comparable and both control the swelling. For PCL semi-IPN, it already exhibits anomalous diffusion at a low PCL weight fraction of 22.9%.

Diffusion coefficients D were calculated the same way as described in Section 3.4.5. Table 4.8 summarized D values calculated using equation (4.4).

$$\frac{M_t}{M_\infty} = \frac{4}{r}\sqrt{\frac{D}{\pi}} * \sqrt{t} \qquad (4.4)$$

PLGA and PLA IPN show decreased D with increased PLGA or PLA weight fraction. At similar weight fraction, PLA IPN shows a lower D than PLGA IPN, while PCL semi-IPN shows the lowest D. This corroborates the hydrophobicity order: PLGA < PLA < PCL(see section 4.1). At similar weight fraction, the more hydrophobic the secondary polymer, the less hydrophilic bonding sites are available for water molecules and the stronger the steric hindrance of hydrophobic components preventing water molecules from bonding with hydrophilic components. This leads to the decrease in the diffusion coefficient.

Table 4.8 Diffusion Coefficient of VP/MMA, PLGA IPN, PLA IPN, and PCL semi-IPN

	Diffusion Coefficient D (cm^2/s)
VP/MMA	2.46×10^{-6}
25.1% PLGA	1.13×10^{-6}
43.9% PLGA	7.54×10^{-7}
62.8% PLGA	3.08×10^{-8}
28.6% PLA	7.85×10^{-7}
49.7% PLA	2.98×10^{-7}
71.8% PLA	3.01×10^{-9}
22.9% PCL	1.05×10^{-8}

Table 4.9 Structure characterization parameter of PLGA, PLA IPN hydrogels and PCL semi-IPN hydrogel

Secondary Polymer Weight Fraction	0	PLGA 25.1%	PLGA 43.9%	PLGA 62.8%	PLA 28.6%	PLA 49.7%	PLA 71.8%	PCL 22.9%
E(10^5 Pa)	0.32	0.88	1.44	2.28	0.67	1.57	5.2	6.2
$\varphi_s{}^{1/3}$	0.54	0.63	0.69	0.75	0.65	0.76	0.82	0.69
γ_e (mol/m^3)	24.3	57.4	85.7	124.8	42.3	84.8	260.4	369.0
φ_s	0.16	0.25	0.33	0.42	0.28	0.44	0.54	0.33
χ	0.56	0.60	0.64	0.70	0.61	0.70	0.81	0.63

Table 4.9 summarizes the structure characterization parameters calculated the same way as described in Section 3.4.5. γ_e is the effective crosslinking density. φ_s is the polymer volume fraction. χ is the Flory-Huggins interaction parameter. E is the modulus of the swollen hydrogel. As can be seen from Table 4.9, χ is increasing with increasing secondary polymer weight fraction, verifying the increased hydrophobicity. At similar

weight fraction, PLA IPN shows a slightly higher χ than PLGA IPN. 22.9%PCL semi-IPN has a χ value of 0.65, higher than 25.1%PLGA, 43.9%PLGA, and 28.6%PLA IPN, demonstrating higher hydrophobicity. This is in consistence with the reported hydrophobicity order of PLGA < PLA < PCL(see section 4.1).

The increase in effective crosslinking density γ_e can be a result of increased crosslinker content[49, 78] or increased weight fraction of the relatively more hydrophobic component[28, 78]. As has been stated above, for PLGA IPN and PLA IPN, crosslinker content stays fixed. And PCL is not even crosslinked in the hydrogel network, yet it shows a γ_e value of 369mol/m^3, even higher than 62.8%PLGA and 49.7%PLA IPN. This demonstrates significantly stronger physical crosslinking in PCL semi-IPN, which could be a result of the higher molecular weight of PCL, leading to a higher level of entanglements, or a stronger hydrophobic bonding forming more hydrophobic aggregates acting as physical crosslinks.

The effective crosslinking density has been widely reported to be linked with the compressive modulus of a hydrogel[38, 39, 49]. Figure 4.21 shows that E increases almost linearly with the corresponding γ_e.

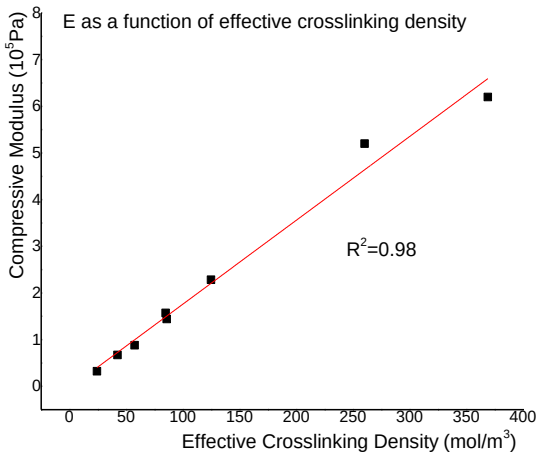

Figure 4.21 Compressive modulus as a function of effective crosslinking density

4.5.4.2 The effect of T_g, hydrophobicity, and crosslinker content on the swelling behaviour

For each individual case of PLGA IPN, PLA IPN and PCL semi-IPN, it has already been shown(Table 3.2, Table 4.3, Table 4.4) that the initial swelling rate(R_i), equilibrium swelling ratio(Q_∞) and swelling period(T_e) depend on the weight fraction of the secondary polymer network.

Here we look at IPN hydrogels with different secondary polymer networks when their weight fractions are similar in the IPN system. Figure 4.22-4.24 shows the initial swelling rate(R_i), equilibrium swelling ratio(Q_∞) and swelling period(T_e) as a function of T_g, water contact angle, and crosslinker content of the secondary polymer network, respectively. It can be seen from Figure 4.22-4.24 that R_i, Q_∞, T_e show no dependence on T_g or crosslinker content, but they are linked with the water contact angle of the secondary polymer network. R_i and Q_∞ decreases, while T_e increases with increase in water contact angle.

Thus it can be concluded that the hydrophobicity (water contact angle) of the secondary polymer network is the dominant parameter affecting the swelling behaviour of IPN and semi-IPN hydrogels. The swelling behaviour does not depend on the T_g of the secondary polymer network, nor does the compressive modulus of swollen hydrogels (see Section 4.5.2). Also, the swelling behaviour does not depend on the chemical crosslinking condition of secondary polymer network, whether it is crosslinked or not.

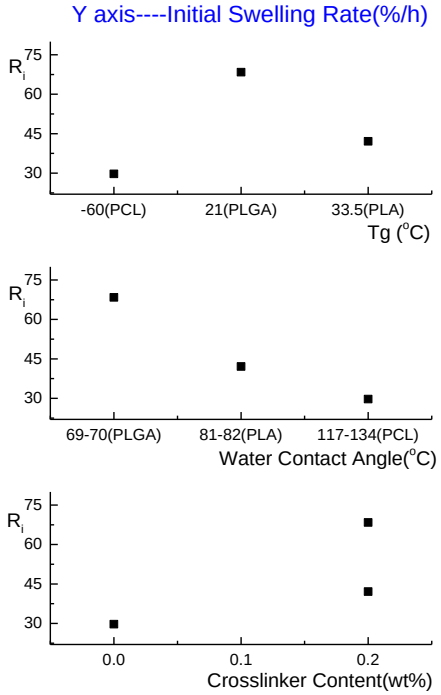

Figure 4.22 Initial swelling rate as a function of Tg, water contact angle and crosslinker content of secondary polymer network

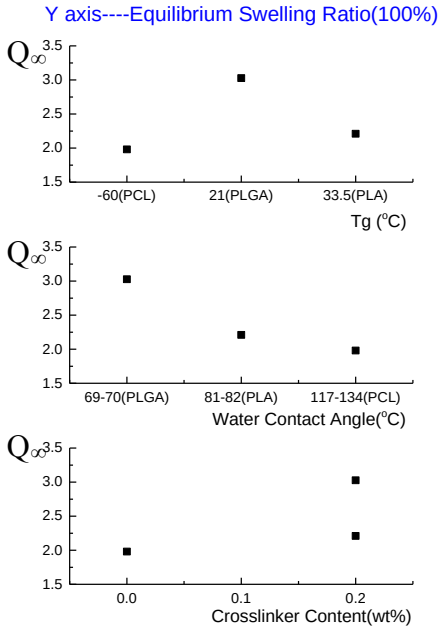

Figure 4.23 Equilibrium swelling ratio as a function of Tg, water contact angle and crosslinker content of secondary polymer network

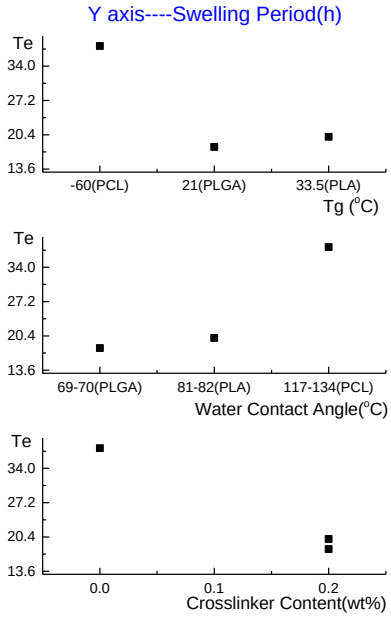

Figure 4.24 Swelling period as a function of Tg, water contact angle and crosslinker content of secondary polymer network

4.5.5 What controls the swelling behaviour?

It has been shown above that the initial swelling rate(R_i), equilibrium swelling ratio(Q_∞) and swelling period(T_e) all scale with the water contact angle and the weight fraction of the secondary polymer network. Figure 4.25 summarizes the values of R_i, Q_∞, and T_e as a function of the water contact angle and the weight fraction of the secondary polymer network. Two major observations can be read from Figure 4.25:

1. For a fixed kind of secondary polymer, R_i and Q_∞ decrease, while T_e increases with the increase in its weight fraction.
2. At similar weight fractions, secondary polymer network with higher water contact angle leads to lower R_i and Q_∞, while higher T_e

Overall, at similar weight fraction, PCL semi-IPN exhibits the lowest R_i, lowest Q_∞, and longest T_e. While PLGA IPN shows the highest R_i, highest Q_∞ and shortest T_e. PLA IPN exhibits the intermediate between those two. This verifies the reported hydrophobicity order of PLGA < PLA < PCL(see section 4.1). PCL is the most hydrophobic of the

three, which results in the least binding sites for water molecules and the highest steric hindrance to prevent them from binding with hydrophilic groups. This leads to the lowest water diffusion rate and equilibrium water content. Moreover, PCL semi-IPN shows the highest modulus (at the similar weight fraction of PLGA or PLA), which means the most restricted chain mobility. Thus it takes longer to let the water molecules plasticizing in and results in an extended swelling period to reach the equilibrium state.

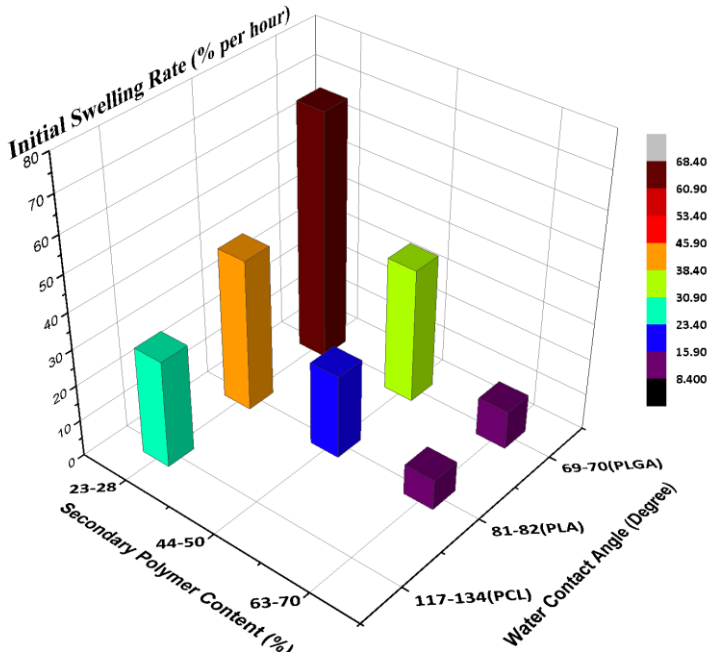

(a)

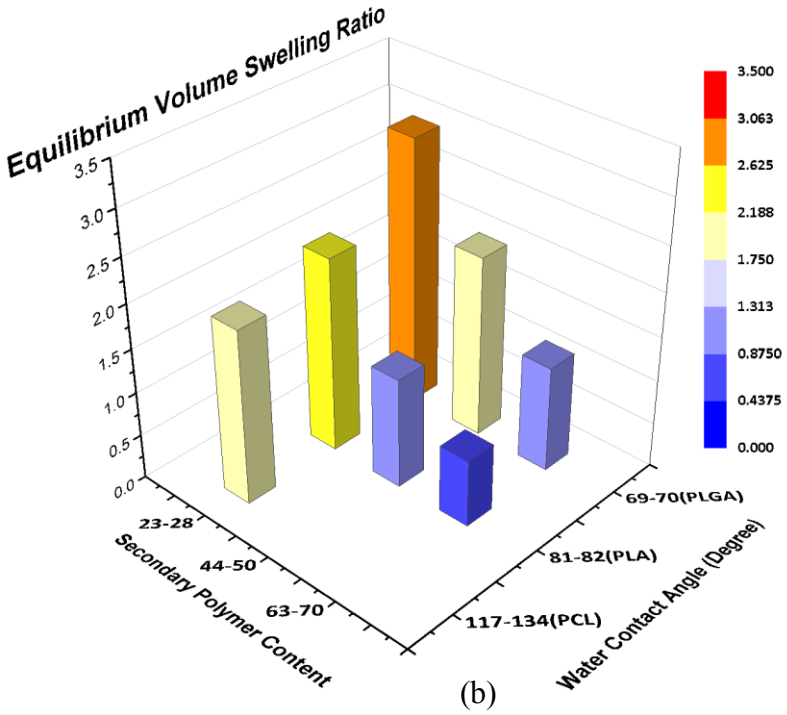

(b)

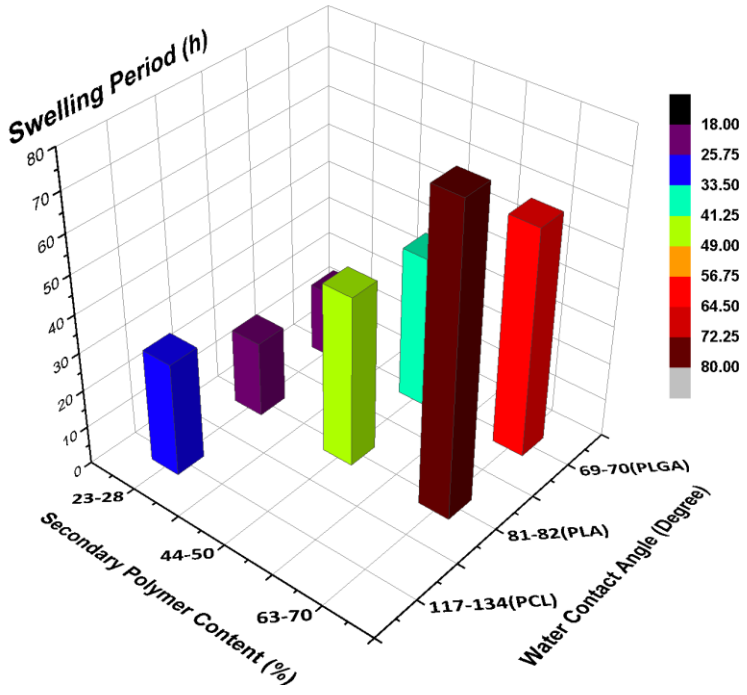

(c)

Figure 4.25 The (a) initial swelling rate (b) equilibrium swelling ratio (c) swelling period as a function of the water contact angle and weight fraction of the secondary polymer network

4.6 Summary

PLA IPN and PCL semi-IPN hydrogels have been successfully prepared in this chapter and their swelling behaviour, mechanical properties, glass transition temperature and internal morphology have been studied and compared with those of PLGA IPN.

PLA IPN and PCL semi-IPN shows similar swelling behaviour with PLGA IPN. With the incorporation of PLA or PCL, hydrogel shows a decreased initial swelling rate(R_i), equilibrium swelling ratio(Q_∞) and an increased swelling period(T_e). The same as PLGA IPN, PLA IPN and PCL semi-IPN show controlled initial swelling rate that help avoid tissue necrosis, but the equilibrium swelling ratio is sacrificed which limits the application of these IPN and semi-IPN hydrogels to reconstructions that only require a small piece of grown tissue.

Increased weight fraction of PLA or PCL leads to increased polymer volume fraction, which is responsible for the increased compressive modulus of the swollen hydrogels. At similar weight fraction, PLGA IPN and PLA IPN show similar modulus values while PCL semi-IPN shows a significant higher value. This is probably attributed to the preparation method of PLGA IPN and PLA IPN, which involves DCM absorption, that leaves PLGA and PLA in a half-dry state, and causes a significant decrease in the modulus of the cell walls(E_s).

At similar weight fraction, PCL semi-IPN shows the lowest R_i and Q_∞, with the highest T_e. PLGA IPN shows the highest R_i and Q_∞, with the lowest T_e. PLA IPN has the intermediate values between them. This corroborates the reported hydrophobicity order (Section 4.1) of

$$\text{PLGA} < \text{PLA} < \text{PCL}$$

PLGA, PLA and PCL vary in their glass transition temperature, which is 21°C, 33.5°C and -60°C, respectively. They also vary in their crosslinking condition (PLGA IPN and

PLA IPN have the same crosslinker content(0.2wt%) while PCL is not crosslinked). However, the swelling behaviour shows no dependence on either T_g or the crosslinking condition of the secondary polymer network. Instead, it is closely related to the hydrophobicity (water contact angle) and weight fraction of the secondary polymer network.

The main conclusions are:

1. When the secondary polymer network is fixed, the higher its weight fraction, the lower the initial swelling rate and equilibrium swelling ratio, the higher the time taken to reach equilibrium state.
2. At similar weight fraction, secondary polymer network with higher hydrophobicity(water contact angle) exhibits lower initial swelling rate and equilibrium swelling ratio, and higher time taken to reach equilibrium state.

Chapter 5: IPN Hydrogel with Alternative Primary Networks

5 IPN hydrogels with alternative primary networks

5.1 Introduction

While Chapter 4 investigated the alternative secondary polymer networks that can be used with VP/MMA to create IPN or semi-IPN hydrogels, this chapter is concerned with alternative primary networks to replace VP/MMA. The idea is to combine the primary network with the secondary polymer network through solvent absorption. Thus, it is crucial for the primary network to be able to swell in water as well as in at least one organic solvent that can dissolve the hydrophobic secondary polymer network. Also, it is important for the primary network to have both swelling capacity and mechanical integrity at its swollen state.

The investigation of an alternative gel base starts with the polymerization of HEMA(2-hydroxyethyl methacrylate) hydrogel. HEMA has been widely used in tissue engineering as contact lenses[90], wound dressings[91], surgical prostheses[92]. HEMA is preferred because of its excellent biocompatibility and similar properties to those of living tissues[218]. However, the swelling of HEMA is low[93]. Thus HEMA can be copolymerized with VP or sodium acrylate (SA) to increase its swelling capacity[93, 219]. This chapter looks into the following questions:

1. Is it possible to prepare bulk, crack-free HEMA, VP/HEMA, and HEMA/SA hydrogels?
2. What's the swelling behaviour of HEMA, VP/HEMA, and HEMA/SA and their mechanical properties at the swollen state?
3. Is it possible to prepare IPN hydrogels with one of the above hydrogels as the primary network and PLGA as the secondary network?

5.2 Experimental

5.2.1 Materials

2-Hydroxyethyl methacrylate(98%)(1.073g/ml), vinyl-pyrrolidone(VP)(1.04g/ml), ethylene glycol dimethacrylate(EDGMA), potassium persulfate(KPS), acrylic acid, sodium hydroxide, dichloromethane (DCM), N,N'-Methylenebisacrylamide (BIS), azobisisobutyronitrile (AIBN), tetrahydrofuran(THF), acetone, ethyl acetate, polypropylene tubes(12mm*75mm) were all purchased from Sigma Aldrich.

5.2.2 Preparation of HEMA hydrogel

Crosslinked HEMA hydrogels were prepared by thermal polymerization of an aqueous reaction mixture containing the 2-hydroxyethyl methacrylate monomer, EGDMA as the crosslinking agent, and AIBN as the initiator[220, 221]. HEMA, EGDMA(1wt% based on HEMA mass), and AIBN(1wt% based on HEMA mass), were mixed together and stirred for 1h at room temperature. The polypropylene tubes were used as the polymerization reactors. The mixture was poured into these tubes and copolymerized for 24 hours at 60°C. Hydrogels were obtained in the form of long cylinders and then cut into discs.

5.2.3 Preparation of VP/HEMA hydrogel

The copolymerization of VP/HEMA hydrogels has been widely reported[219] but few studies are concerned with the volume swelling ratio. Mixtures of VP and HEMA in the volume ratios of 9:1, 8:2, 7:3, 5:5 were blended under room temperature with 1wt%(of total weight of VP and HEMA) BIS until homogeneous solution was obtained. Samples with varied ratios of VP to HEMA will be designated as shown in Table 5.1. 1wt% AIBN was added to the reaction mixture, which was then degassed with nitrogen to remove any oxygen that could act as a chain-terminating agent. The reaction mixture was poured into polypropylene tubes and polymerization was carried out at 60°C for

24h. Bulk hydrogels with cylinder shapes were removed from the tubes and cut into discs. Table 5.1 shows the compositions of VP/HEMA hydrogels.

Table 5.1 Compositions of VP/HEMA hydrogels

Designation	Volume Ratio (VP:HEMA)	VP(μl)	HEMA(μl)	BIS(g)	AIBN(g)
VP9/HEMA1	9:1	1350	150	0.0156	0.0156
VP8/HEMA2	8:2	1200	300	0.0156	0.0156
VP7/HEMA3	7:3	1050	450	0.0156	0.0156
VP5/HEMA5	5:5	750	750	0.0156	0.0156

5.2.4 Preparation of VP/HEMA-PLGA IPN hydrogel

VP7/HEMA3, VP5/HEMA5, HEMA were cut into discs of around 6mm diameter and 3mm in height. Acrylated PLGA(0.025g/ml) was dissolved in dichloromethane(DCM) at room temperature and blended to a homogeneous solution. Each disc was added to the solution with 0.2wt%(based on the mass of PLGA) BIS and the mixture was shaken in a water bath at 37°C for 3 days until it reached the maximum swollen state. 0.2wt% AIBN(based on the mass of PLGA) was added and the mixture was kept at 37°C water bath for another 2 days. The disc was then taken out to dry in air at room temperature.

5.2.5 Preparation of HEMA/SA hydrogels

The compositions for preparing HEMA/SA hydrogels is shown in Table 5.2. SA was obtained by neutralizing acrylic acid with an aqueous sodium hydroxide solution (1.6-1.7M) at room temperature. HEMA was then added to the mixture according to the predetermined mole ratio shown in Table 5.2. 0.01g KPS and 0.01g BIS were added as the initiator and the crosslinker, respectively. The reaction mixtures were blended at room temperature until homogeneous solutions were obtained. They were then poured into polypropylene tubes and polymerization was carried out under 60°C for 24h. Cylinder hydrogels were removed from the tubes and cut into discs.

Table 5.2 Formula for the preparation of HEMA/SA hydrogels

Sample	AA(g)	NaOH(g)	HEMA(μl)	HEMA:SA (mole ratio)	BIS(g)	KPS(g)
hemaSA1	0.475	0.264	800	1:1	0.01	0.01
hemaSA2	0.0475	0.0264	800	10:1	0.01	0.01
hemaSA3	0.0237	0.0132	800	20:1	0.01	0.01
hemaSA4	0.0047	0.0026	800	100:1	0.01	0.01

The copolymerization of HEMA/SA hydrogels has been reported but the obtained hydrogels contain cracks[222]. For the preparation of bulk, crack-free HEMA/SA hydrogels, several crosslinker and initiator combinations were tried as shown in Table 5.3.

Table 5.3 Combinations of crosslinker and initiator for the preparation of HEMA/SA bulk hydrogels

	Crosslinker	Initiator
Combination 1	EGDMA	AIBN
Combination 2	BIS	AIBN
Combination 3	BIS	KPS

5.3 Characterization

5.3.1 Compression Test

The same as described in Section 3.2.6, the compression tests were performed on the fully swollen samples using a Perkins Elmer DMA 7e dynamic mechanical analyser. The compression rate was 100mN/min and the maximum load was 6000mN. Compressive modulus E is calculated as the gradient of the curve in the strain range of 12%-14%.

5.3.2 Scanning Electron Microscope

Microstructure of fully swollen VP/HEMA and HEMA/SA hydrogels were studied using field emission scanning electron microscope(Zeiss Nvision 40). Freeze-dried samples were mounted on a double sided tape on aluminium spin stubs and sputter coated with gold using E5400 Sputter Coater(Bio-Rad, Polaron Division). SEM images were recorded under the accelerating voltage of 2kV and 0.2K-6k magnification.

Porosity was determined using ImageJ. For each sample, three sections were chosen and the porosity values were determined by ImageJ. The mean porosity was then calculated.

5.3.3 Swelling Behaviour

Swelling behaviour tests were performed the same way as described in Section 3.2.9. All the experiments were performed in triplicate and the average value was calculated. The distilled water was replaced daily. The initial volume swelling rate(R_i), equilibrium swelling ratio(Q_∞), and equilibrium water content(EWC) of hydrogels were characterized exactly the same way as described in Section 3.2.9.

The porosity at equilibrium swelling state can be calculated from the swelling data using equation(5.1)[223], where M_0 and M_∞ are the masses of hydrogel before immersion and at equilibrium state, respectively, ρ is the density of distilled water and V is the volume of hydrogel:

$$Porosity = \frac{(M_\infty - M_0)}{\rho V} \times 100\% \quad (5.1)$$

5.4 Results

5.4.1 Compression Test

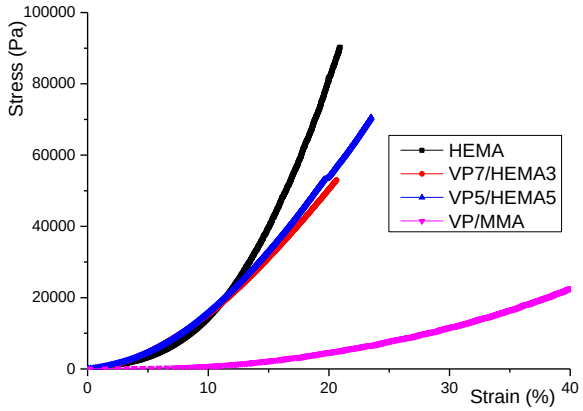

Figure 5.1 Stress-Strain curve of the swollen HEMA, VP7/HEMA3, VP5/HEMA5 and VP/MMA hydrogel

Figure 5.1 shows the stress-strain curve of the swollen HEMA and VP/HEMA

hydrogels, in comparison with VP/MMA hydrogel. E values are shown in Table 5.4.

Table 5.4 Compressive modulus of HEMA, VP/HEMA and VP/MMA hydrogels (NA: not available, hydrogel fractured during expansion)

	Compressive Modulus E (10^5Pa)
VP/MMA	0.32
VP9/HEMA1	NA
VP8/HEMA2	NA
VP7/HEMA3	3.2
VP5/HEMA5	3.6
HEMA	5.45

It can be seen from Table 5.4 that HEMA and VP/HEMA hydrogels show a higher compressive modulus compared to VP/MMA hydrogel. HEMA hydrogel shows the highest compressive modulus of 5.45×10^5Pa, and the increase in VP content decreases the compressive modulus of VP/HEMA hydrogels.

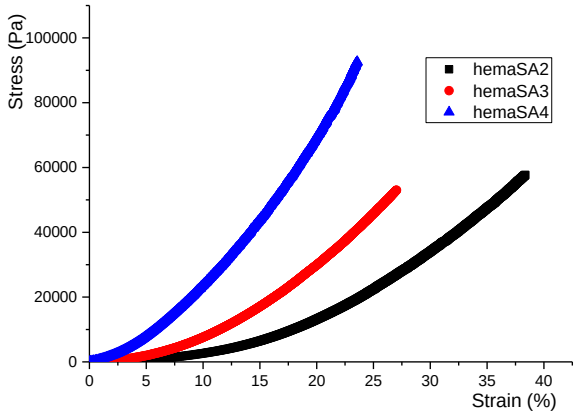

Figure 5.2 Stress-Strain curves of HEMA/SA hydrogels

Table 5.5 Compressive modulus of HEMA/SA hydrogels(NA: not available, hydrogel fractured during expansion)

	Compressive Modulus E(10^5Pa)
hemaSA1	NA
hemaSA2	0.83
hemaSA3	1.98
hemaSA4	4.12

Figure 5.2 shows the stress-strain curves of swollen HEMA/SA hydrogels and Table 5.5 summarizes the compressive modulus E. E decreases with increased SA content.

5.4.2 Scanning Electron Microscopy

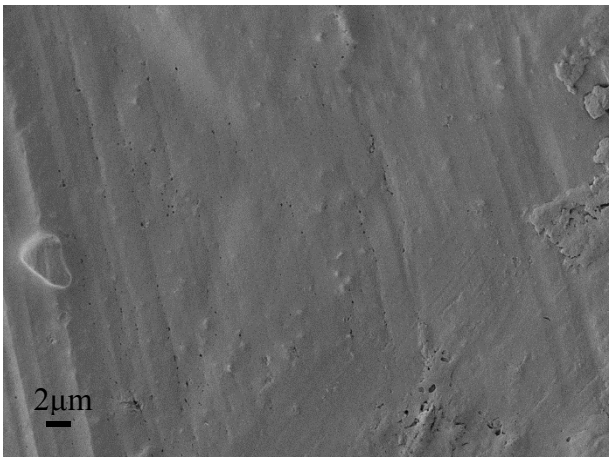

(a) HEMA

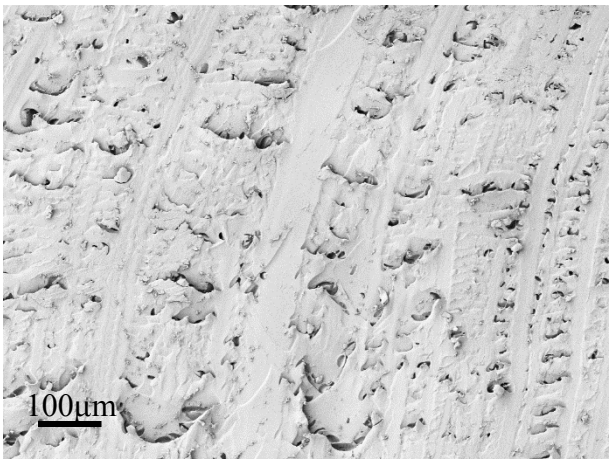

(b) VP5/HEMA5

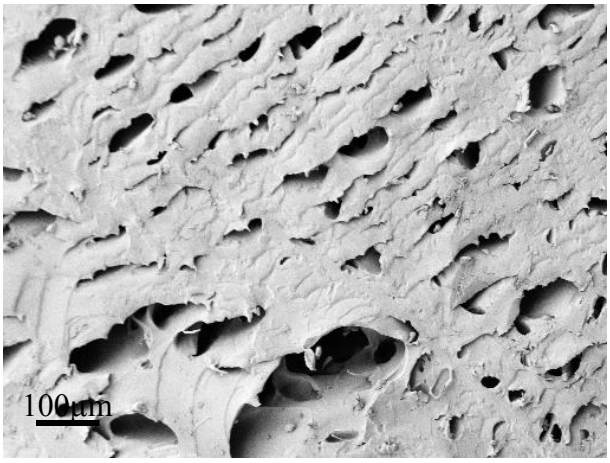

(c)VP7/HEMA3

Figure 5.3 SEM images of swollen hydrogel samples (a) HEMA (b) VP5/HEMA5 (c) VP7/HEMA3

Figure 5.3 shows the SEM images of fully swollen hydrogel samples (a)HEMA (b)VP5/HEMA5 (c)VP7/HEMA3. As can be seen from Figure 5.3(a), HEMA hydrogel

shows little pores on its surface. VP5/HEMA5 shows some separate small pores or holes with around 5µm in diameter. VP7/HEMA3 shows much more porosity and larger pore sizes (10µm-100µm) compared to VP5/HEMA5 and HEMA hydrogels.

The porosity determined using ImageJ is summarized in Table 5.6. The porosity is increasing with increasing VP content in the hydrogels.

Table 5.6 Porosity of VP/HEMA and HEMA determined using ImageJ

	Porosity (%)			
	Area 1	Area 2	Area 3	Mean
HEMA	9.7	13.2	2.2	8.4
VP5/HEMA5	7.8	15.9	18.3	14.0
VP7/HEMA3	24.3	26.0	30.6	27.0

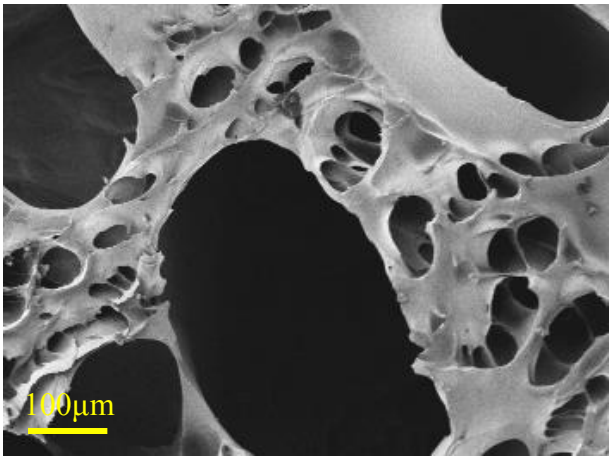

(a) hemaSA2

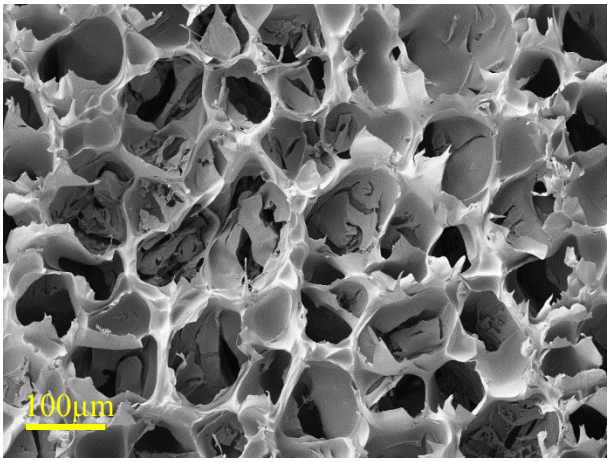

(b) hemaSA3

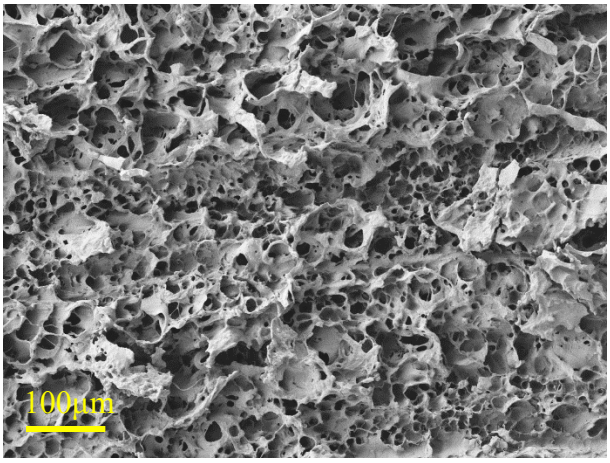

(c) hemaSA4

Figure 5.4 SEM images of (a) hemaSA2 (b) hemaSA3 (c) hemaSA4

Figure 5.4 shows the SEM images of HEMA/SA hydrogels. The pore size is increasing with increasing SA content in the hydrogels. The pore size is not evenly distributed and hydrogels with higher SA content show a higher proportion of interconnected pores and a looser network.

Table 5.7 Porosity of HEMA/SA hydrogels determined using ImageJ

	Porosity (%)			
	Area 1	Area 2	Area 3	Mean
hemaSA2	55.5	60.8	58.9	58.4
hemaSA3	37.1	38.2	41.2	38.8
hemaSA4	17.1	12.7	8.6	12.8

Table 5.7 summarizes the porosity of HEMA/SA hydrogels determined using ImageJ. The porosity is increasing with SA content in the hydrogels.

5.4.3 Swelling Behaviour

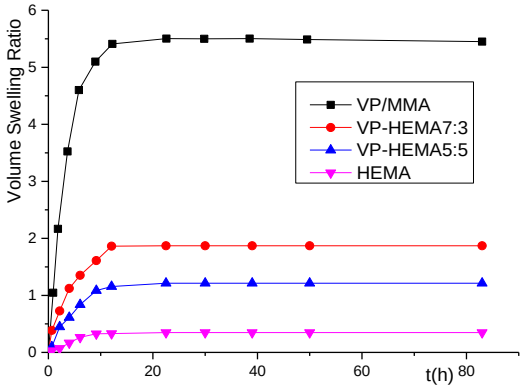

Figure 5.5 The volume swelling ratio of VP/MMA, HEMA and VP-HEMA hydrogels as a function of time

Table 5.8 Initial Volume Swelling Rate of VP/MMA and VP/HEMA hydrogels

	Initial Swelling Rate(%/h)	Equilibrium Swelling Ratio(100%)	EWC(%)
VP/MMA	96.0	5.5	85.6
VP7/HEMA3	26.4	1.8	64.3
VP5/HEMA5	15.9	1.2	53.8
HEMA	4.00	0.3	32.4

Figure 5.5 shows the volume swelling ratio as a function of time for HEMA and VP/HEMA, in comparison to VP/MMA. The initial swelling rate R_i, equilibrium swelling ratio Q_∞ and EWC of the hydrogels is summarized in Table 5.8. VP/HEMA hydrogels show a higher R_i and Q_∞ with higher VP content. R_i of VP/HEMA is far less than that of VP/MMA. VP7/HEMA3 has a R_i of 26.4% per hour, which is only around 25% of that of VP/MMA, and VP5/HEMA5 of 15.9% per hour, HEMA only of 4% per hour. EWC increases with increased VP content in the VP/HEMA hydrogels.

The swelling curves of VP9/HEMA1, and VP8/HEMA2 are not shown in Figure 5.5 because they all collapsed during expansion and broke into pieces. The swollen state of these hydrogels is shown in Figure 5.6 below. VP9/HEMA1 and VP8/HEMA2 have collapsed and lost their shape during expansion although they expanded to a larger size than VP7/HEMA3, VP5/HEMA5 and HEMA hydrogels. It can also be seen that the swollen size of VP/HEMA hydrogels is increasing with increasing VP content.

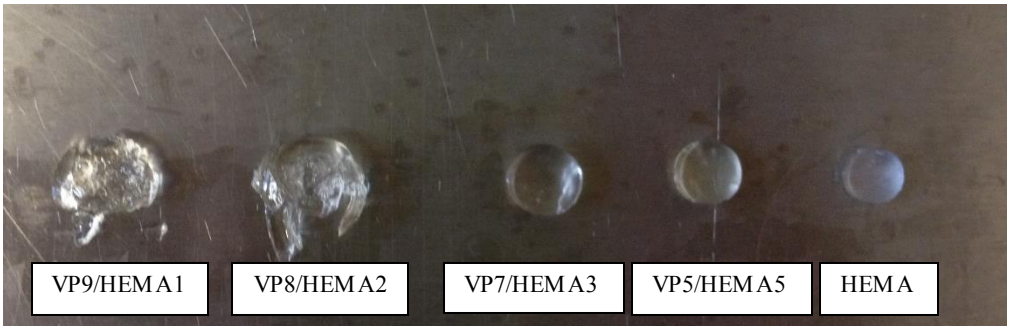

Figure 5.6 Swollen state of VP/HEMA and HEMA hydrogels

Among VP/HEMA hydrogels, the one with the highest swelling capacity without losing its mechanical integrity during expansion is VP7/HEMA3, which can swell up to 2.8 times its original size and maintain its original shape at the same time. Thus VP7/HEMA3 was tried first as the primary network to prepare IPN hydrogel with PLGA. VP7/HEMA3 hydrogel did swell in dichloromethane but when it was taken out to dry, it tended to form cracks on the surface upon contact with the air. The formation of cracks on the surfaces is shown in Figure 5.7.

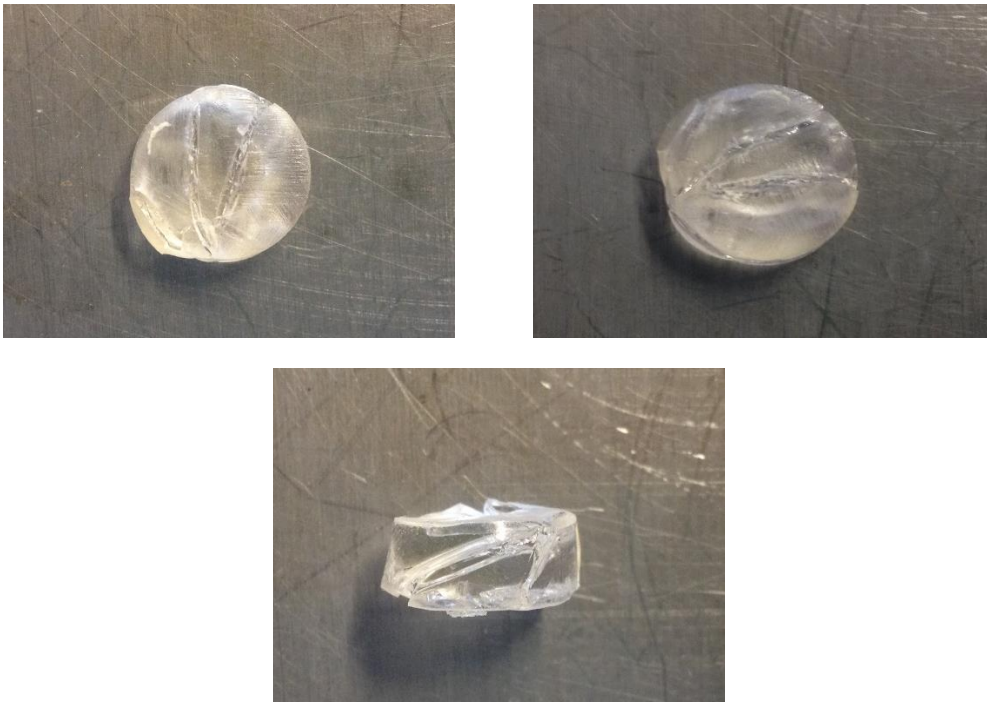

Figure 5.7 Crack formations on the surfaces of VP7/HEMA3 hydrogel after having been immersed in DCM for 3 days

HEMA/SA hydrogel was prepared with different crosslinker and initiator combinations illustrated in Table 5.3 for the successful preparation of bulk, crack-free hydrogels.

Figure 5.8 shows the appearance of the bulk hydrogels prepared using the 3 combinations described in Table 5.3.

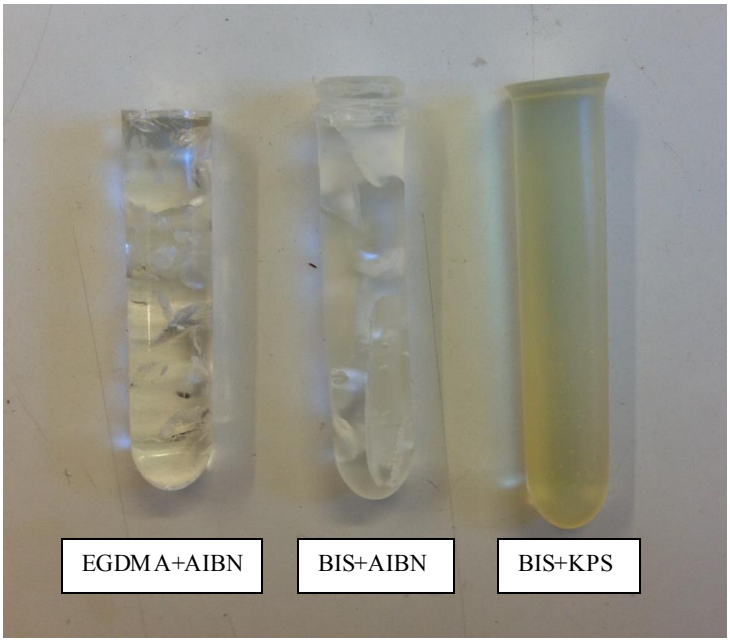

Figure 5.8 Appearance of HEMA/SA hydrogels using crosslinker and initiator combinations shown in Table 5.3

Combination 1 (EGDMA+AIBN) and combination 2 (BIS+AIBN) produced cracks and small bubbles, while combination 3 (BIS+KPS) produces homogeneous, crack-free hydrogel. Thus BIS and KPS is chosen as the crosslinker and initiator to prepare bulk HEMA/SA hydrogels.

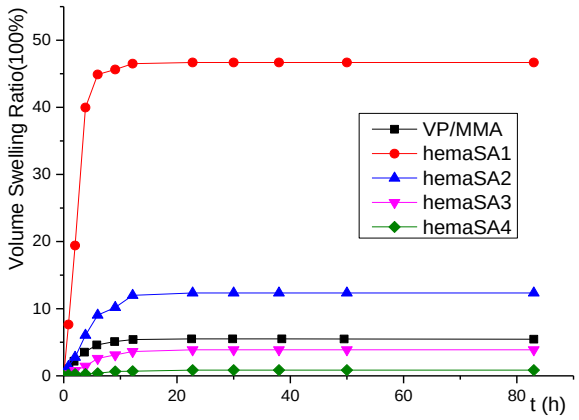

Figure 5.9 Swelling behaviour of HEMA/SA and VP/MMA hydrogels

Table 5.9 Initial Swelling Rate and EWC of HEMA/SA hydrogels

	Volume Swelling Rate(%/h)	Equilibrium Swelling Ratio (100%)	EWC(%)
hemaSA1	1050	47	96.8
hemaSA2	155.7	12.5	91.9
hemaSA3	37.6	3.8	79.6
hemaSA4	5.6	1.0	44.1

Figure 5.9 shows the swelling behaviour of HEMA/SA hydrogels with varied monomer ratios in distilled water and Table 5.9 summarizes the initial swelling rate, equilibrium swelling ratio and EWC of those hydrogels. The swelling curve of VP/MMA is also plotted as a comparison. HEMA/SA hydrogel exhibits increased R_i, Q_∞ and EWC with increased SA content.

Samples all maintained their mechanical integrity during expansion except for hemaSA1 (HEMA: SA 1:1), which started to collapse after 2h in distilled water as shown in Figure 5.10. The measurements of diameter and height were done on the remaining edges of the collapsing sample so the plotted swelling ratio might be smaller than the actual swelling ratio.

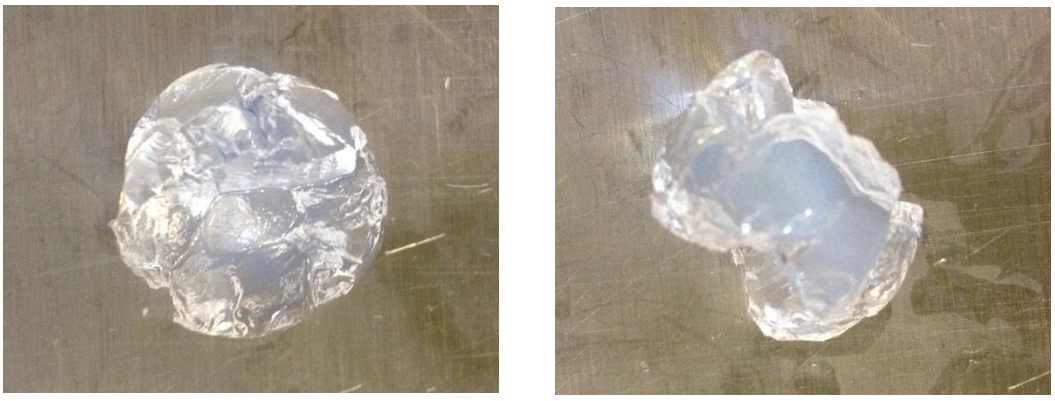

Figure 5.10 Collapsed hemaAA1 (HEMA: SA 1:1) hydrogel during expansion

5.5 Discussion

5.5.1 Compression Test

The compressive modulus E of swollen VP7/HEMA3, VP5/HEMA5 and HEMA all

shows a higher value than that of VP/MMA (see Table 5.4). E is increasing with increasing HEMA content in the hydrogel, with HEMA having the highest value of 5.45×10^5Pa.

As has been stated in Section 3.4.2, first of all the influence of polymer volume fraction of the hydrogel needs to be taken into consideration. A higher HEMA content results in a higher polymer volume fraction φ_s. According Gibson and Ashby, E increases with φ_s both in an open cell structure and a closed one[185]. The normalized modulus is shown in Table 5.10. E_d is E divided by density of the swollen hydrogels, and E_n is E times $(1-\varphi_s)$.

Table 5.10 Normalized modulus of VP/HEMA and HEMA hydrogels

	E(10^5 Pa)	Density(g/cm^3)	E_d(10^{-1}N/g)	φ_s	E_n (10^5 Pa)
VP7/HEMA3	3.2	1.16	2.76	34.8%	2.08
VP5/HEMA5	3.6	1.23	2.93	45.2%	1.97
HEMA	5.45	1.31	4.16	74.2%	1.41

The compressive modulus is still increasing with increasing HEMA content after normalization by density, but is decreasing after normalization by polymer volume fraction. This means the increase in φ_s with increased HEMA content is largely responsible for the increased modulus of the hydrogel.

The increasing in E with increasing HEMA content has been reported in VP/HEMA hydrogels[78]. The contact angle of PHEMA hydrogel has been tested to be around 60°[42], which makes it less hydrophilic than VP. Thus in VP/HEMA hydrogels, HEMA is the hydrophobic component and VP is the hydrophilic component. Thus the more HEMA in the hydrogels, the less binding sites for the water molecules which act as plasticizers. The hydrophobic bonding in HEMA hydrogels has been reported, which may be localized between the α-methyl groups of the repeating units[224]. These hydrophobic bondings act as physical crosslinks, contributing to the effective crosslinking density and hence the elastic modulus[225]. Thus a higher HEMA content

may create more hydrophobic bonding in the hydrogels, increasing the energy needed for chain mobility. The increased effective crosslinking density will be shown in Table 5.14.

Table 5.11 Normalized modulus of HEMA/SA hydrogels

	E(10^5 Pa)	Density(g/cm^3)	E_s(10^{-1}N/g)	φ_s	E_n (10^5 Pa)
hemaSA2	0.83	1.21	0.68	7.5%	0.77
hemaSA3	1.98	1.22	1.62	20.5%	1.57
hemaSA4	4.12	1.38	2.99	54%	1.89

The compressive modulus of HEMA/SA is increasing with increasing HEMA content, but is largely offset by normalization by the relative density(polymer volume fraction), as shown in Table 5.11. Thus similar as VP/HEMA hydrogels, the increased polymer volume fraction is largely responsible for the increased modulus.

As can be seen from

Figure 5.4, increasing SA content creates more open and interconnected cells in the hydrogel at the equilibrium state. The structure of HEMA/SA hydogels can be analysed as an open-cell foam. For an open cell foam, cell edge bending is the main contribution for the elastic modulus. The modulus can described in equation(5.2), where E_s is the modulus of the cell edge solid material, C_1 is the constant, φ_s is the polymer volume fraction.

$$\frac{E}{E_s} = C_1 \varphi_s^2 \tag{5.2}$$

As HEMA content increases, φ_s increases as can be seen from Table 5.11. Thus E is increasing with HEMA content. However, as has been discussed in Chapter 3, the modulus of the cell wall material, E_s, is also a variable here. According to the hydrophobic bonding theory discussed above, more HEMA may create more hydrophobic bonding that contributes to a higher E_s. Thus altogether, a higher φ_s and a higher E_s result in a higher E with HEMA content. It can be noted in

Figure 5.4(a) that even the cell edges of hemaSA2 is highly porous. The pores in the cell edges will largely decrease its resistance to elastic bending, leading to a lower modulus.

Sodium acrylate offers a higher affinity for water molecules because of the dissociated ions which increase the osmotic pressure in distilled water (will be further discussed in

5.5.3). Thus a higher SA content results in a higher EWC and more water molecules acting as a plasticizer, reducing the energy needed to promote chain mobility. Using sodium acrylate to create super-absorbent hydrogels has been widely reported, but the increase in swelling ratio all comes at the expense of the mechanical properties. For example, HEMA-sodium acrylate hydrogels were prepared and showed a higher mechanical strength with higher HEMA content but lower swelling[93]. It remains a problem to find the right balance between the swelling capacity and mechanical strength of hydrogels, especially for use as tissue expanders where both swelling capacity and mechanical strength are required.

5.5.2 Scanning Electron Microscopy

As can be seen from Figure 5.3(a), HEMA shows little porosity at the swollen state. With the increase in VP content, the morphology of the swollen VP/HEMA hydrogel shows higher porosity and an enlarged pore size. The porosity can be determined by ImageJ as shown in Table 5.6 and 5.7. The porosity can also be calculated from the swelling data using equation (5.1). Porosity values derived using those two methods are summarized in Table 5.12.

Table 5.12 Porosity of VP/HEMA hydrogels

	Porosity (%)	
	ImageJ	From swelling data
HEMA	8.4	42.4
VP5/HEMA5	14.0	66.7
VP7/HEMA3	27.0	76.1

The porosity calculated from both methods increases with increased VP content. However, the values determined from ImageJ are significantly smaller than those calculated from the swelling data. The reason could be the limitation of Image J which can only detect pore sizes in a certain range. However, the difference between those two methods is significant, indicating the existence of interconnected pores inside the

hydrogel matrix which were not fully observed on the surfaces under SEM. Determination of the porosity of hydrogels with interconnected structure is more complicated, requiring the technique of mercury intrusion porosimetry[226] or computer algorithm[227].

Table 5.13 summarizes the porosity of HEMA/SA hydrogels obtained using ImageJ and equation (5.1). Porosity determined using ImageJ is again much smaller than that from the swelling data, indicating the existence of interconnected pores as stated above.

Table 5.13 Porosity of HEMA/SA hydrogels

	Porosity(%)	
	ImageJ	From swelling data
hemaSA2	58.4	99.9
hemaSA3	38.8	97.8
hemaSA4	12.8	60.9

The change in porosity between hemaSA2, hemaSA3 and hemaSA4 corresponds to their morphology change under SEM (see Figure 5.4). The porosity of a hydrogel can be affected by various reasons, including the preparation method[228], crosslinker concent[229] and monomer ratio[42]. In this study, the preparation method and crosslinker concent remain the same for VP/HEMA and HEMA/SA hydrogels. Thus the porosity difference is a result of different monomer ratios. As has been discussed in Section 2.2.4, when water molecules enter a hydrogel network, they firstly form bound water with the polar groups of the polymer chains, then form freezing bound water and finally exist as free water after bound and freezing bound water have reached their maximum contents[27]. The more hydrophilic the polymer network, the more free water it absorbs[28]. Higher VP or SA content leads to higher hydrophilicity of the hydrogel network, providing more binding sites for water molecules and attracting more to reside in as free water, resulting in a higher equilibrium water content. Moreover, ydrogels with a higher content of hydrophilic component has been widely reported to facilitate the formation of porous network with more interconnected pores or channels

[42, 230, 231]. And more hydrophilic networks tend to form porous network faster upon contact with solvents, which contributes to their rapid solvent uptake at the initial stage[231].

5.5.3 Swelling Behaviour

It is clear that HEMA hydrogel has a low swelling and thus it needs to be copolymerized with VP and SA. HEMA shows a low equilibrium swelling ratio of 0.3, which is inadequate in swelling capacity as a tissue expander although it maintains the mechanical integrity during expansion. EWC of HEMA hydrogel is 32.4%, which is consistent with the reported value[95]. The contact angle of PHEMA hydrogel has been tested to be around 60°[42], which makes it less hydrophilic than VP. With the increase of VP content in the VP/HEMA hydrogel, the equilibrium swelling ratio is increased from 0.3 to 1.8. VP9/HEMA1 and VP8/HEMA2 are supposed to have higher equilibrium swelling ratio than 1.8 (VP7/HEMA3), but their low mechanical properties lead to collapse of the gel network during expansion, as shown in Figure 5.6. The inverse relationship between the swelling capacity and mechanical properties has been widely reported(see Section 2.2.6), which is also demonstrated in equation(5.3). γ_e is the effective crosslinking density. φ_s is the polymer volume fraction in the swollen hydrogel. E is the elastic modulus of the swollen hydrogel, R is the universal gas constant, T is the absolute temperature. Higher hydrophilicity leads to a higher swelling capacity, thus a lower φ_s and a lower E.

$$E = RT\gamma_e {\varphi_s}^{1/3} \tag{5.3}$$

Water uptake (W_t/W_∞, W_t and W_∞ is the water uptake at time t and at equilibrium, respectively) of VP/HEMA hydrogels as a function of time is shown in Figure 5.11. The diffusion exponent and diffusion mechanism are calculated using equation (5.4) and summarized in Table 5.14. k is a constant and n is the diffusion exponent.

$$\frac{W_t}{W_\infty} = kt^n \tag{5.4}$$

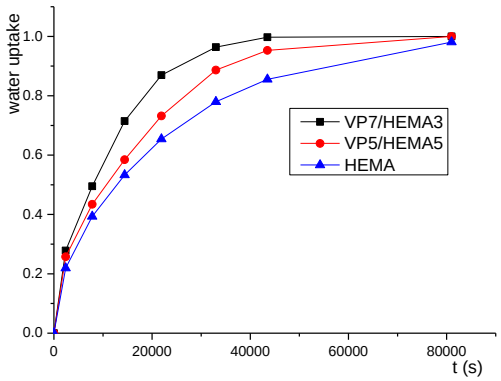

Figure 5.11 water uptake of VP/HEMA hydrogels as a function of time

Table 5.14 Diffusion Exponent and Diffusion Mechanism of VP/HEMA hydrogels

	Diffusion Exponent n	Diffusion Mechanism
HEMA	0.49	Fickian
VP5/HEMA5	0.49	Fickian
VP7/HEMA3	0.51	Fickian

It can be seen from Table 5.14 that VP7/HEMA3, VP5/HEMA5 and HEMA hydrogels all show a diffusion exponent around 0.5, indicating Fickian diffusion. The Fickian diffusion mechanism is consistent with those reported[25, 232]. Thus the water uptake of HEMA and VP/HEMA hydrogels are diffusion-controlled.

Table 5.15 Diffusion Coefficient of VP/HEMA hydrogels

	Diffusion Coefficient(10^{-7} cm^2/s)
HEMA	0.85
VP5/HEMA5	2.7
VP7/HEMA3	7.3

The diffusion coefficient D is calculated using equation (5.5) and shown in Table 5.15. Increased VP content results in increased hydrophilicity and less restriction on chain mobility which is also indicated by the decreased compressive modulus in Table 5.4. Both lead to an increase in the diffusion coefficient. This diffusion coefficient shows good consistence with the values reported[59].

$$\frac{M_t}{M_\infty} = \frac{4}{r}\sqrt{\frac{D}{\pi}} * \sqrt{t} \tag{5.5}$$

Table 5.16 Effective Crosslinking Density and Flory-Huggins interaction parameter of VP/HEMA hydrogel

	VP/MMA	VP7/HEMA3	VP5/HEMA5	HEMA
γ_e (mol/m^3)	24.3	187.8	192.8	248.7
χ	0.56	0.65	0.73	1.03

Table 5.16 shows the effective crosslinking density and Flory-Huggins Interaction Parameter calculated using equation (5.6). χ is the Flory-Huggins interaction parameter. V_1 is the molar volume of water, f is crosslinker functionality.

$$\ln(1-\varphi_s)+\varphi_s+\chi{\varphi_s}^2+\gamma_e V_1\left({\varphi_s}^{\frac{1}{3}}-2\varphi_s f^{-1}\right)=0 \qquad (5.6)$$

As shown in Table 5.16 both γ_e and χ are increasing with HEMA content. The increased χ verifies the increased hydrophobicity of the hydrogel, which is responsible for the decreased diffusion coefficient. In VP/HEMA hydrogels, HEMA is playing the role as the hydrophobic component, and reduces the available bonding sites for water molecules and acts as steric hindrance at the same time. This slows down the swelling rate and reduces the EWC as well. The increased γ_e shows more physical entanglements and hydrophobic bonding with higher HEMA content, which contributes to the increased compressive modulus as shown in Table 5.4.

Among VP/HEMA hydrogels, VP7/HEMA3 shows the highest swelling while maintaining its mechanical integrity. Thus VP7/HEMA3 was tried first to prepare IPN hydrogel with PLGA, but the formation of cracks is inevitable. VP5/HEMA5 and HEMA hydrogels were both tried, but the cracks formed immediately after they were in contact with air. The crack formation of the hydrogel may be caused by the capillary force of the solvent present in the pores on pore walls of the hydrogel network. There is a distinct critical surface tension of the solvent causing fractures and cracks in the gel. When a wet gel is taken out of the solvent to dry, solvent at the surface evaporates and the solvent front appears at the surface layer of the gel body. Zarzycki et al.[233] considered that the cracks or fracture occur in drying gels when the capillary force

exerted by the pore liquid to the pore wall exceeds the strength of the gel network. If the fine pores are regarded as capillaries of diameter D, the solvent with surface tension γ causes the capillary force ΔP defined in equation (5.7), where θ is the contact angle between the capillary wall and the solvent:

$$\Delta P = \frac{4\gamma cos\theta}{D} \tag{5.7}$$

When a wet gel is taken out to dry, the solvent on the surface layer evaporates, and accordingly, the surface layer of the gel body tends to shrink, inducing the tensile stress in the surface layer, while the inner layer does not shrink. This results in crack or fracture formation when the stress exceeds the strength of the gel. Thus, to avoid crackles, one has to suppress the capillary force acting on the walls of the pore in a wet gel body or increase the mechanical strength of the wet gel. The former can be achieved when the drying is carried out under supercritical condition (pressure or temperatures)[234] and the latter can be achieved by changing the chemical structure of the hydrogel. Further work is not discussed here because even for VP7/HEMA3 hydrogel, the equilibrium swelling ratio is only 1.8, and with the incorporation of PLGA, there will be even less swelling. This might not meet the requirements of swelling capacity as tissue expanders.

For the preparation of crack-free bulk HEMA/SA hydrogel, three combinations of crosslinker and initiator were investigated and the results are shown in Figure 5.8. Combination 1 and combination 2 turned out to be unsuccessful. The polymerization of HEMA and SA was performed in distilled water, thus a water-soluble initiator such as potassium sulfate($K_2S_2O_8$) proved to be more suitable than insoluble AIBN. Combination 3 was found to be successful in producing crack-free hydrogels.

HEMA/SA hydrogels show much higher swelling capacities than VP/MMA and VP/HEMA hydrogels and the swelling ratio is increasing with SA content. The higher

the SA content, the stronger the affinity of the gels for water. The water contact angle of HEMA/SA hydrogel was tested and shown to increase with increased HEMA content in the hydrogels[222]. This demonstrates that HEMA/SA hydrogels with higher SA content are more hydrophilic.

SA(sodium acrylate) is the neutralized product of poly(acrylic acid) and has been widely used to make superabsorbent polymers or hydrogels[100, 222]. SA based copolymers are one of the major class of ionic polymers, or polyelectrolyte gels with charge covalently bonded to the polymer chain. They can swell much more than HEMA hydrogel because of the dissociated counterions($-COO^-$, Na^+) which increase the osmotic pressure.

When HEMA/SA hydrogel is immersed in water, it dissociates into negative carboxylate groups and positive sodium ions. Figure 5.12 shows the schematic of HEMA/SA hydrogels in distilled water. The polymer chains in a hydrogel usually exist in the shape of randomly coiled molecules. In HEMA/SA hydrogels, the electrostatic repulsion between adjacent negative charges($-COO^-$) uncoils the polymer chains and expands the network. Upon contact with water the sodium ions are hydrated, which reduces their attraction to the carboxylate ions due to the high dielectric constant of water. They are able to move freely within the network, but cannot escape outside the gel due to the condition of overall electrical neutrality. As a result, the concentration difference of Na^+ within the gel and the outer solution (water) creates the additional osmotic pressure.

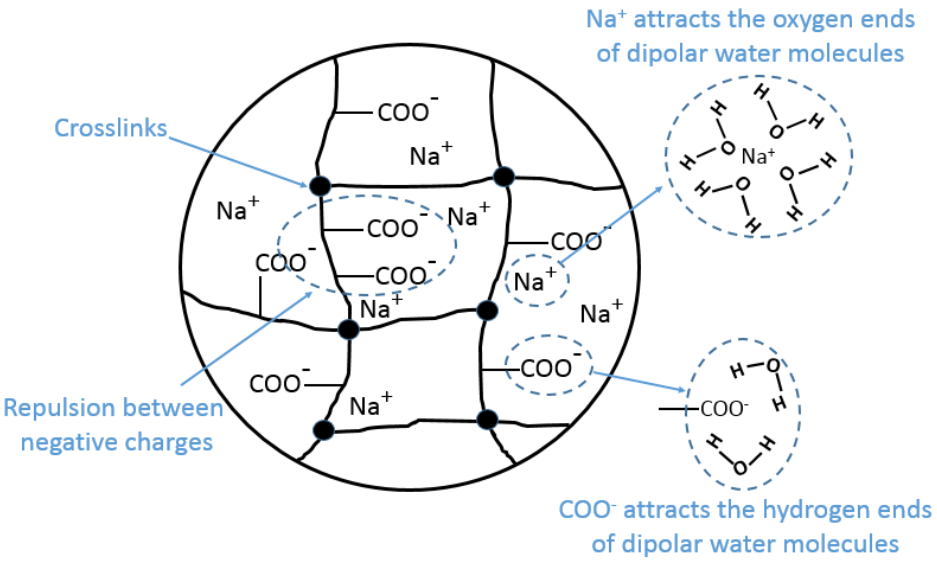

Figure 5.12 Schematic of HEMA/SA hydrogel network in distilled water

Table 5.17 shows the diffusion exponent, diffusion mechanism and diffusion coefficient of HEMA/SA hydrogels calculated using equation(5.3) and (5.4). hemaSA1 shows a diffusion exponent of 1, indicating Case II diffusion. hemaSA2-4 show the diffusion exponent in the range of 0.5-1, indicating anomalous diffusion. Diffusion exponent is shown to increase with SA content in the hydrogels. The diffusion exponent of hemaSA hydrogels is in consistence with those reported for SA based superabsorbent hydrogels. AAm(acrylamide)/SA hydrogels showed an increased diffusion exponent with increased SA content in the range of 0.65-1.03[235]. HEMA/SA hydrogels showed a diffusion exponent in the range of 0.72-0.86, indicating anomalous diffusion[236]. Diffusion coefficient D is also increasing with SA content in the hydrogels. The increased D is attributed to the increased hydrophilicity brought by the dissociated ions and higher chain mobility as indicated by the decreased compressive modulus.

Table 5.17 Diffusion exponent, diffusion mechanism, and diffusion coefficient of HEMA/SA hydrogels

	Diffusion Exponent	Diffusion Mechanism	Diffusion Coefficient (10^{-7} cm^2/s)
hemaSA1	1	Case II	21.5
hemaSA2	0.89	anomalous	15.4
hemaSA3	0.81	anomalous	3.6
hemaSA4	0.57	anomalous	0.64

Table 5.18 Effective crosslinking density γ_e and Flory-Huggins interaction parameter χ of HEMA/SA hydrogels(NA: not available, sample fractured during expansion)

	γ_e (mol/m^3)	χ
hemaSA1	NA	NA
hemaSA2	81.2	0.45
hemaSA3	137.8	0.56
hemaSA4	208.9	0.81

Table 5.18 shows the effective crosslinking density and Flory-Huggins interaction parameter of HEMA/SA hydrogels. As has been discussed above, the increased γ_e is a result of increased hydrophobic bonding with increased HEMA content. χ is shown to increase and deviate from 0.5 with increased HEMA content, signifying the increased hydrophobicity of the hydrogels.

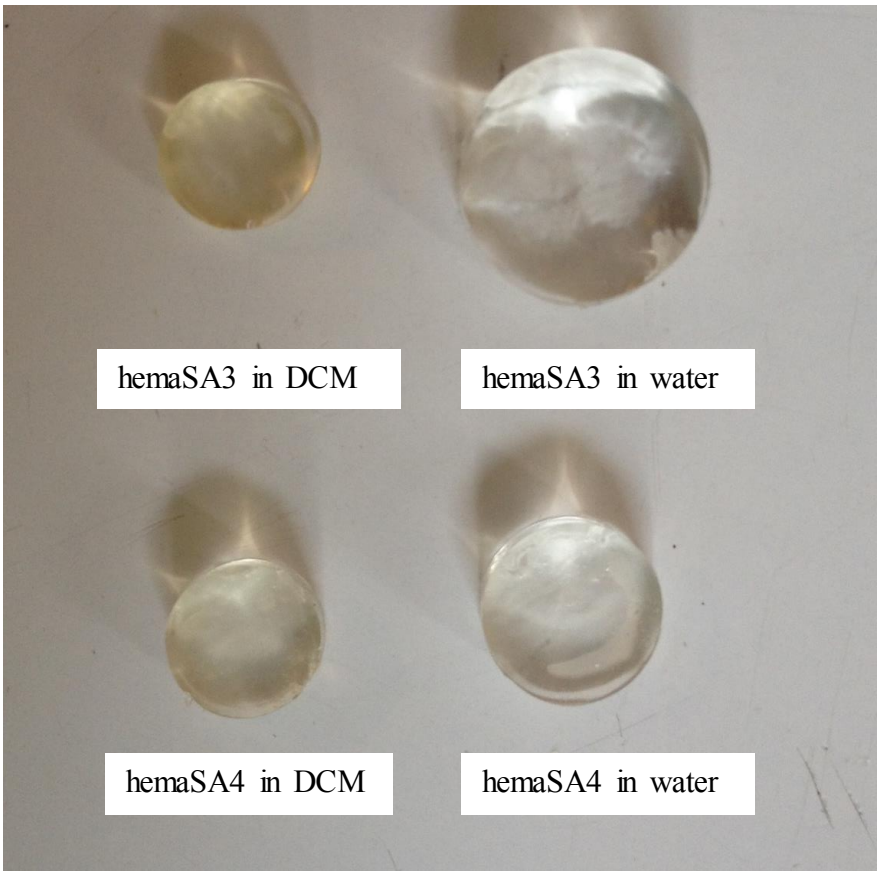

Figure 5.13 The swollen hemaSA3 and hemaSA4 hydrogels after being immersed in DCM and water(from the same original size)

hemaSA2 showed no swelling in dichloromethane(DCM), making it impossible to incorporate the secondary PLGA network to prepare IPN hydrogel. This was thought to

be the result of the high affinity of hydrophilic hemaSA2 network for polar solvents like water but much less affinity for less-polar solvents (organic solvents). Thus, HEMA/SA with higher HEMA content was prepared. However, for hemaSA3 and hemaSA4, neither showed discernible swelling in DCM, as shown in Figure 5.13(all samples from the same original size). hemaSA3 and hemaSA4 both remained their original size when immersed in DCM. While in distilled water hemaSA3 swelled up to around 5 times its original volume and hemaSA4 to around twice its original volume. hemaSA2-4 hydrogels were immersed in a variety of organic solvents that dissolve PLGA, including acetone, dichloromethane, ethyl acetate, tetrahydrofuran, but none of them showed discernible swelling in these organic solvents. The swelling of polyelectrolyte hydrogels like hemaSA hydrogels is thought to be largely linked to the polarity of the solvent. The dielectric constant of the experimented solvents is summarized in Table 5.19, which shows that PLGA only dissolves in organic solvents with dielectric constant less than 21. Unfortunately none of these organic solvents serves as a good swelling medium for HEMA/SA hydrogels.

Table 5.19 Dielectric constant of solvents used in the experiments

Solvent	Dielectric Constant ε
water	80.1
dichloromethane	8.9
ethyl acetate	6.0
tetrahydrofuran	7.6
acetone	20.7

For polyelectrolyte gels like hemaSA hydrogels, their superior swelling in polar solvents such as water originates from the electrostatic repulsion between the charges on the polymer chains and the osmotic imbalance between the interior and exterior of the gels caused by freely mobile or loosely bounded counter-ions. A high swelling degree of polyelectrolyte hydrogels has never been achieved in nonpolar organic solvents unless the polymer chains are modified with lipophilic ionic groups[237].

Common electrolyte gels remain a compact, dense state in less polar organic solvents because of the formation of a higher number of aggregates of ions and ion pairs[237, 238]. In nonpolar solvents counter ions tend to be trapped and form ion pairs, while in polar solvents they tend to form dissociated ions. In nonpolar solvent, the dissociation of ions is completely suppressed due to the low dielectric constant of the solvent and the ionic groups form tightly bound ion pairs. The ion pairs attract each other due to the dipole-dipole interactions and form so-called multiplets acting as additional physical crosslinks. A schematic of ion pair and multiplets formation in polyelectrolyte gels is shown in Figure 5.14. Some counter ions are free, others form ion pairs marked by dotted lines. Some of the ion pairs aggregates and from multiplets, as marked by letters M.

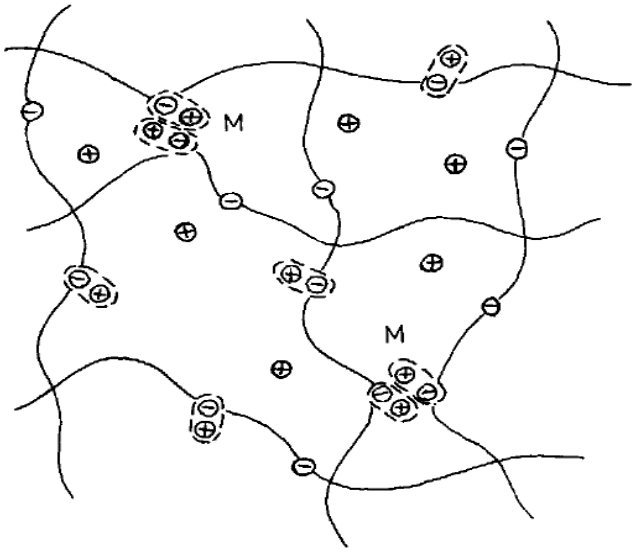

Figure 5.14 Ion pair and multiplets formation in polyelectrolyte gels(reproduced from[238])

Consider the situation in a salt-free solvent, there is an ion dissociation-association equilibrium. Some of the ions are dissociated and these groups carry the charge, others remain in the associated state, i.e. corresponding counter ions are bound and form ion pairs. The number of ion pairs u can be determined using equation (5.8)[238] where e is the elementary charge, a is the characteristic distance between the ions in an ion pair, ε

is the dielectric constant of the solvent, k is the Boltzmann constant, and T is the temperature.

$$u = \frac{e^2}{\varepsilon akT} \tag{5.8}$$

Thus for polar media like water, ε is large and u is usually less than 1, which means all the potentially charged groups are dissociated. While for non-polar media, ε is small and $u \gg 1$, which means all the counter ions form ion pairs. The formation of ion pairs and multiplets decreases the concentration of mobile ions in the gel and the corresponding osmotic pressure decrease, leading to the observed non-swelling in nonpolar organic solvents.

5.6 Summary

HEMA, VP/HEMA, HEMA/SA bulk hydrogels have been successfully made with varied monomer ratios.

HEMA shows good mechanical integrity but minimal swelling. HEMA is then copolymerized with VP and SA for higher swelling capacity but it comes at the expense of mechanical integrity during expansion.

VP7/HEMA3 shows the highest swelling in VP/HEMA hydrogels without losing its mechanical integrity. It is then prepared with PLGA to form IPN hydrogels. However, the capillary force caused during solvent evaporating exceeds the limit of the hydrogel strength, leading to fractures on the surfaces during the drying process. Supressing capillary force can be realized by drying the gels under supercritical pressure or temperature but further work is not discussed here because VP7/HEMA3 only has an equilibrium swelling ratio of 1.8 in water, which will be less with the incorporation of PLGA.

hemaSA2 and hemaSA3 shows good swelling capacity while maintaining their

mechanical strength but none of them swells in organic solvents that dissolve PLGA. hemaSA hydrogels are one of the polyelectrolyte gels and $–COO^-$ and Na^+ tend to form ion pairs and multiplets in less polar solvent instead of dissociated ions that contribute to gel swelling. Thus HEMA/SA hydrogels are not able to incorporate PLGA through solvent absorption.

For use as tissue expanders, hydrogels need to be able to swell to a large extent while retaining the mechanical integrity during expansion. However, preparing hydrogel networks with both swelling capacity and good mechanical properties remains a big problem in the research field. And to prepare IPN hydrogels with controlled and delayed swelling, the incorporation of a secondary, hydrophobic network is almost inevitable. Unless the preparation process can be completed in an anhydrous state, it is essential that primary hydrogel network is able to swell in at least one less polar solvent that dissolves the secondary network. None of the prepared hydrogels has been successful in preparing IPN hydrogels, but it provides the possibility of preparing alternative bulk hydrogels as tissue expanders and suggestions for incorporating secondary polymer network through solvent absorption. Figure 5.15 summarizes the suggestions for choosing primary and secondary networks to prepare IPN hydrogels as tissue expanders. Note that this is based on incorporating secondary network through solvent absorption. If the preparation can be performed in an anhydrous state (requiring low melting point of secondary network), there is no need for the primary network to be able to swell in non-polar solvents.

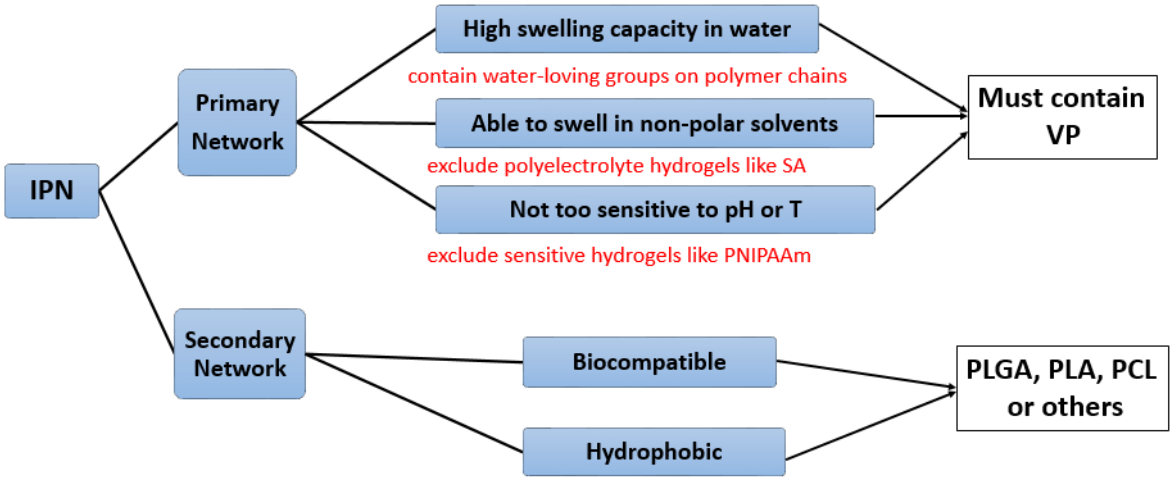

Figure 5.15 Suggestion for choosing primary and secondary network to prepare IPN hydrogels as tissue expanders

CHAPTER 6: Animal Test

6 Animal Test

6.1 Introduction

While Chapter 3 discussed the swelling behaviour of VP/MMA-PLGA IPN hydrogel (abbreviated as PLGA IPN) in distilled water, this chapter concerns with the swelling behaviour of IPN hydrogel in PBS and in vivo in a sheep model. Uncoated VP/MMA and PAA hydrogels have been shown to induce tissue necrosis in the animal study because of their over-rapid expansion rate[99, 170]. And due to the existence of ions and a different pH value in physiological conditions, it is expected that the expansion of PLGA IPN would behave differently (see Section 2.2.5.4). Also, compared to laboratory conditions, there is a limited amount of body fluids at the surgical sites available to PLGA IPN, which might restrict its swelling. Thus it is important to test the in vivo performance of PLGA IPN. This chapter looks into the following aspects:

1. The swelling behaviour of PLGA IPN in PBS and in vivo
2. Is it safe to use PLGA IPN in clinical surgeries?
3. Can PLGA IPN effectively induce tissue growth in vivo?
4. Does the expanded tissue have the same quality as natural skin tissue?

This chapter will demonstrate whether PLGA IPN is effective as a tissue expander in a living mammal and also give implications for the clinical trials of the IPN hydrogels in humans.

The structure of human skin layer has been demonstrated in Section 2.6. PLGA IPN hydrogels are implanted on sheep limb between the subcutaneous layer and the sheep tendon, as schematically shown in Figure 6.1.

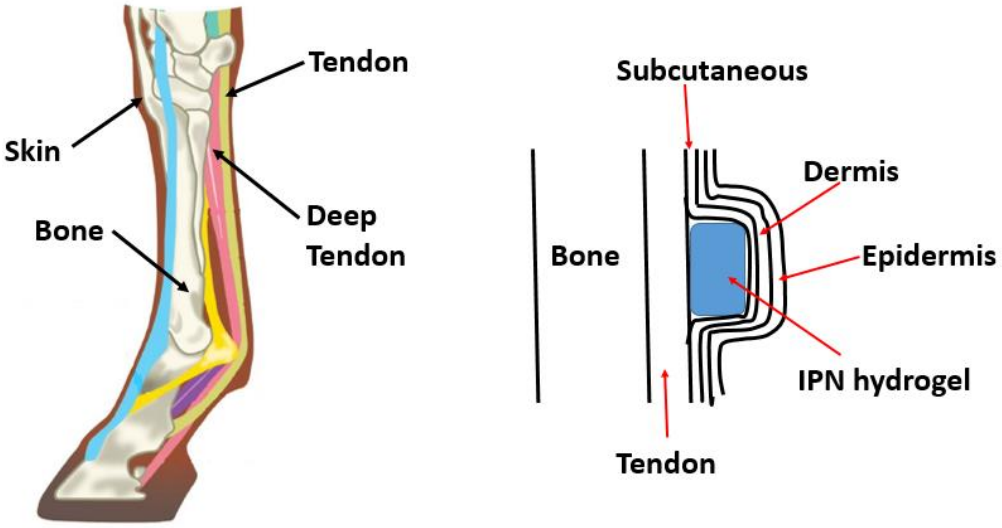

Figure 6.1 Schematic of PLGA IPN hydrogels implant position(between tendon and subcutaneous layer) in sheep limb

The histology of the expanded skin tissue will be analysed to see whether the expanded tissue has the same quality with the natural skin tissue. The thickness of the epidermis, dermis, the orientation of collagen, and the number of fibroblasts and inflammatory cells of the expanded tissue are compared with those of the natural skin tissue. A typical histological section of normal human skin has been shown in Section 2.6.

6.2 Experiments and Characterization

6.2.1 Materials

Materials used to prepare PLGA IPN were exactly the same as described in Chapter 3.2.1. Phosphate Buffer Saline tablet was obtained from Sigma Aldrich.

6.2.2 In Vitro Study (Degradation Study)

30%PLGA IPN(PLGA weight fraction in dry gel around 30%) was prepared using the materials and methods described in Chapter 3.2.3. PLGA IPNs were immersed in PBS(phosphate buffer saline solution) which is 0.01M phosphate buffer, 0.0027M potassium chloride, 0.137M sodium chloride, pH 7.4 at 37°C. At predetermined time intervals, samples were taken out and measured in the diameter and height with a

caliper(Absolute Digimatic Calier, Mitutoyo, Japan) and weighed by an electronic balance(ABS analytical balance, Kern Scale Tehnic, UK). The initial swelling rate and the equilibrium swelling ratio were calculated the same way as described in Section 3.2.9.

At 10 days, 20 days, 1 month, 1.5 month and 2 month after immersion in PBS, samples were taken out to dry in the air for 3 days and then dried in the oven for another 3 days under 40°C. After that, samples were taken out and weighed. The difference in mass before the immersion and after predetermined time intervals was calculated. Mass loss is calculated using equation(6.1), M_t and M_0 refer to dry mass of PLGA IPN after immersion in PBS for predetermined time intervals and before immersion, respectively:

$$Mass\ Loss(\%) = \frac{M_t - M_0}{M_0} \times 100\% \quad (6.1)$$

6.2.3 Device Sterilization

30%PLGA IPN samples were sterilized in sealed bags under γ-radiation at a dose of 25kGy by Swann Morton at Oxtex.

6.2.4 In Vivo Study

The in vivo study was done with the help of University of Malaya, in Kuala Lumpur, Malaysia. The sheep chosen are all male, Dorper Breed imported from Australia with average weight between 30 to 50 kilograms, bought from (Genetic Improvement and Farm Technologies Sdn Bhd).

6.2.4.1 Standard Operation Procedure

Sheep was fasted 24 hours before surgery. One hour before surgery, the sheep was weighed to calculate the amount of drugs to be used. For sedation, 100mg/ml ketamine was given via intravenous injection on sheep's jugular vein and it collapsed after a few seconds. The sheep was brought to the operation theatre. Its upper limb was shaved and

cleaned with alcohol. For induction, a needle was inserted into its cephalic vein and 10 mg/2 ml diazepam was introduced, followed by 100mg/ml ketamine, for the sheep to be more relaxed. Before intubation, soft rope was placed around each the upper and lower jaw to facilitate the mouth opening and for the head to be elevated and extended. The endotracheal tube was inserted, secured and the cuff was inflated. The inhalation anaesthetics were maintained with isoflurane.

Next, the surgical area of the sheep limb was shaved. The shaved surgical area was cleaned with alcohol swab, iodine and clean water. The surgery was done under sterile condition inside an operation theatre. Incision cut was made on the sheep limb. A tunnel, about 5 cm in length, was made to create an adequate pocket size to place the hydrogel. The tunnel was made in between subcutaneous layer of skin and on the top of tendon. PLGA IPN was then placed at the end of the tunnel. One suture was made to ensure that the hydrogel did not move from its original position. The incision cut was sutured. The surgical area was cleaned with alcohol. The macroscopic view of the sheep limb right after the implantation is shown in Figure 6.2.

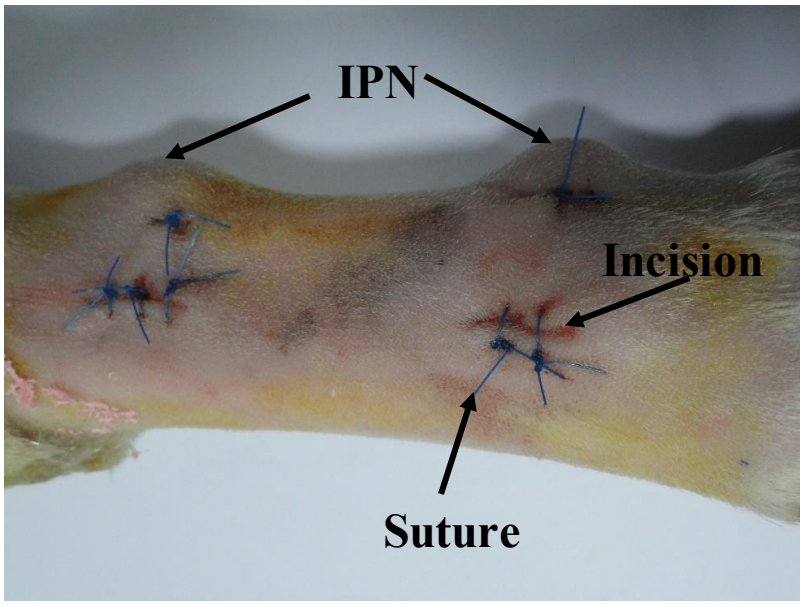

Figure 6.2 The macroscopic view of sheep limb right after implantation

A digital calliper (Mitutoyo Digimatic Coolant Proof Caliper) was used to take the

reading of height and volume of stretched skin. A lateral view photo was also taken to see the expansion progress. The sheep recovered immediately after surgery. Free access to food and water were given to the sheep. Daily measurements and lateral view photos were consistently taken from Day 0 to Day 31. Throughout the post-operative period, any sign of pain or abnormal behaviour of the sheep was monitored and recorded.

The diameter of the IPN hydrogel was measured using the caliper from different angles as shown in Figure 6.3. Each day, 4 readings were taken from those angles and the mean value was calculated.

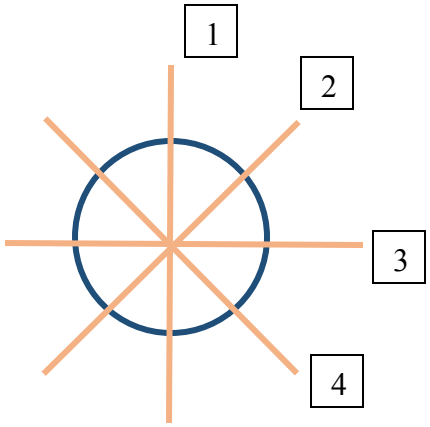

Figure 6.3 Schematic of the measurements of diameter of the implanted hydrogel

The height of PLGA IPN was measured every day including the height of the limb itself. The original height of the limb without the hydrogel was taken. And the hydrogel height during expansion should be calculated using equation (6.2):

Hydrogel Height = Value read from the calliper – the original limb height (6.2)

The height of PLGA IPN was also taken from 3 different positions and the mean value was calculated. The in vivo swelling behaviour as a function of time was drawn using the mean value calculated from daily measurements on the sheep limb.

6.2.4.2 PLGA IPN Explantation

At day 31, PLGA IPNs were explanted following the explantation protocol. A vertical and elliptical shape of incision was made on the side of the hydrogel, near the raised border of the expanded skin. The appropriate length of incision was made based on the

length of the expanded tissue area. The thick capsule surrounding the hydrogel was undermined. One small nick was made on the outer wall of capsule, followed by blunt dissection to expose the hydrogel. Hydrogel was gently pushed out from its surrounding capsule and removed. Expanded skin tissue about 2 x 2 x 0.3 cm was harvested. The remaining skin tissue was sutured back to retain its normal condition.

6.2.4.3 Histology and Analysis

The histological procedure contains the following 4 main steps:

1. ***Sample Fixation to preserve structure***: Expanded tissue was fixed with 4% buffered formalin solution. The fixation of skin tissue sample took about 48 hours at room temperature.
2. ***Sample imbedding to permit sectioning***: Expanded tissue was transferred into 70% alcohol and stored at 4°C temperature. It was washed with formalin, followed by 70% alcohol, 95% alcohol, absolute alcohol and toluene, and then infiltrated with wax. Next, tissue was embedded in paraffin wax. Tissue was placed in paraffin bath at 58°C for 15 minutes.
3. ***Sample Sectioning***: Cooled and hardened tissues were cut using a microtome (a specially designed slicing machine) with 10 serial sections, 4-5μm in thickness each. The slides were placed with paraffin sections on the warming block in a 65°C oven for 20 minutes for the wax to start melting and to bond the tissue on the glass.
4. ***Sample Staining***: Xylene was poured onto the sample, followed by absolute alcohol, 95% alcohol, 70% alcohol and tap water. Then, haematoxylin was poured, followed by tap water. 0.5 acid alcohol was used to differentiate the colour, followed by tap water again, and then by 2% potassium acetate for bluing process. Eosin was poured to counter stain, followed by 95% alcohol,

absolute alcohol and xylene.

Histology slides were analysed by a software called Pannoramic Viewer(3D Histech Kft, Budapest, Hungary). The epidermis and dermis thickness could be easily measured by pointing one point to another. As for inflammatory cells and fibroblasts count, three separate areas were chosen at the dermis region, at 40 x magnification. The cells with round shape was considered as inflammatory cells and cells with more elongated in structure was fibroblasts. Others such as the hair follicles and other skin appendages were also presented.

6.3 Results

6.3.1 In Vitro Swelling Behaviour

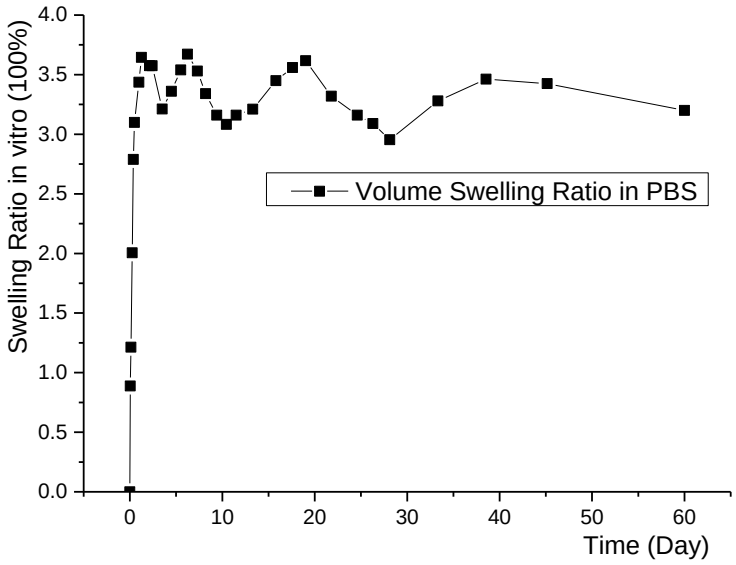

Figure 6.4 Swelling Behaviour of 30%PLGA IPN in PBS

Figure 6.4 shows the swelling behaviour of 30%PLGA IPN in vitro in PBS pH 7.4 at 37°C. PLGA IPN in PBS showed rapid swelling in the first 3 days and then went through the process of swelling being interrupted by short periods of decrease or stagnation. The swelling reached the first peak at Day 2.5 with swelling ratio at 3.64. It then shrank to 3.21 at Day 3.5 and then re-swelled to the second peak of 3.67 at Day

6.3. This deswelling-reswelling process was continued, with the third peak shown at Day 19 and the fourth shown at Day 38. The initial volume swelling rate R_i is 24.5% per hour.

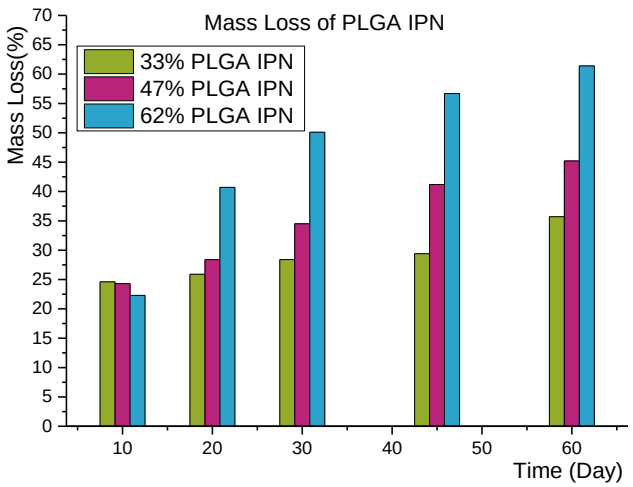

Figure 6.5 Weight loss in PBS of IPN hydrogels with varied PLGA weight fractions

Figure 6.5 shows the mass loss of PLGA IPN immersed in PBS over two months. For varied PLGA weight fraction in the IPN hydrogels, mass losses are all increasing as time goes by. After 10 days in PBS, all PLGA IPN show a weight loss in the range of 22-25%. IPN hydrogel with higher PLGA weight fraction shows a steeper weight loss over time. 33%PLGA IPN showed a weight loss of 28.4% after one month and 35.7% after two months. 47%PLGA IPN showed a weight loss of 34.5% after one month and 45.2% after two months. 62%PLGA IPN showed a weight loss of 50.1% after one month and 61.4% after two months.

6.3.2 In Vivo Swelling Behaviour

In total 8 30%PLGA IPN hydrogels were implanted and 6 ended up dissolved (collapsed or broke into pieces). Those 6 surgical sites also showed inflammation and damage to the surrounding tissue. Only 2 samples remained swelling until Day 31.

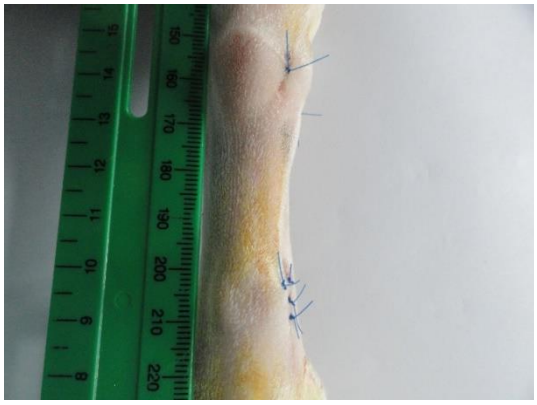

(f) After implantation

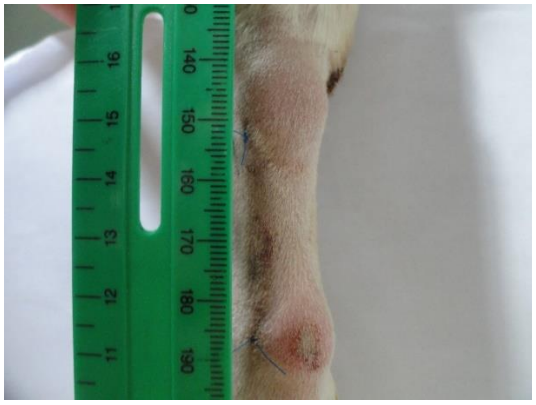

(e) Day 4

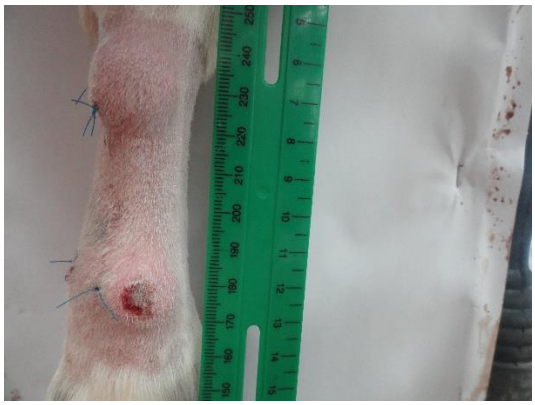

(d) Day 7

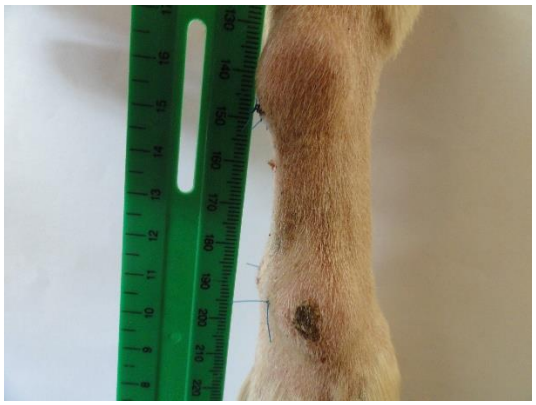

(c) Day 10

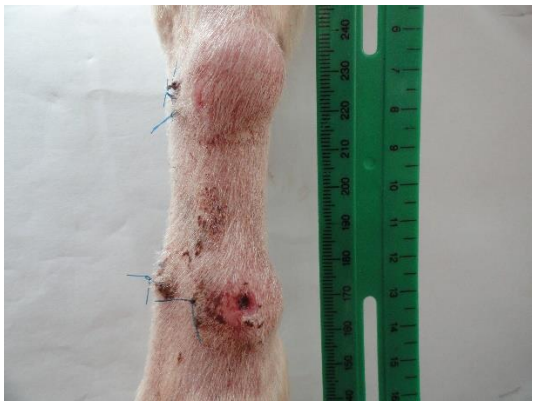

(b) Day 14

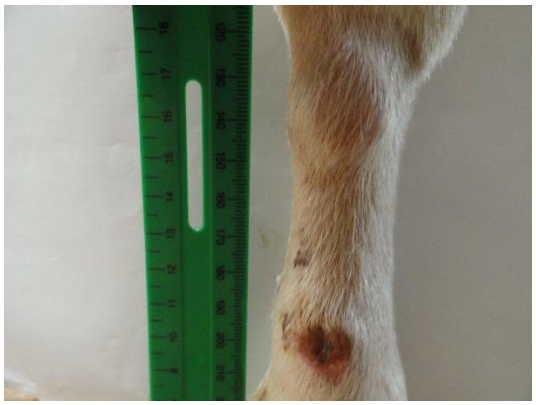

(a) Day 27

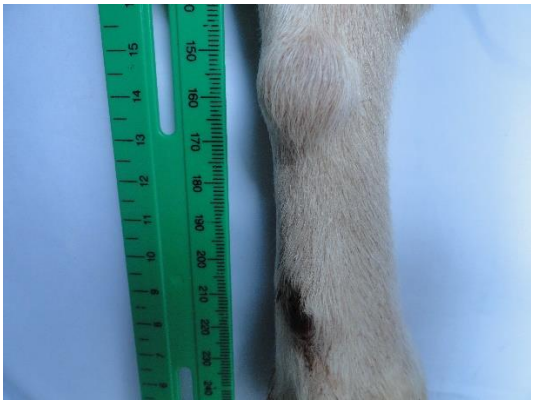

(g) Day 30

Figure 6.6 Images of the implanted PLGA IPN in sheep limb

Figure 6.6 shows the images of two implanted PLGA IPN on a sheep limb, from right after implantation to 30 days after implantation. The upper sample reached a maximum swelling in around 4 days and maintained its swelling until Day 30, while the lower one swelled up to Day 7, then deswelled and finally dissolved after Day 14. The lower one also shows inflammation and damage to the surrounding tissue, leaving the wound until Day 30. According to the daily measurements records, there was suspected pain of the sheep at Day 22-Day 25. The sheep are said to be in pain if they refused to be measured by calliper and tended to kick back when calliper is placed. Thus daily measurements of Day 22- Day25 are not available. The volume swelling ratio of the PLGA IPN in vivo as a function of time is shown in Figure 6.7.

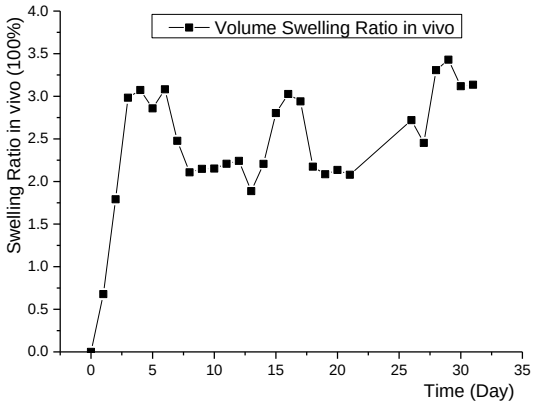

Figure 6.7 Swelling Behaviour of 30%PLGA IPN in vivo

30%PLGA IPN in vivo reached a maximum swelling ratio 4 days after implantation. After that, it experienced the process of swelling being interrupted by short periods of decrease or stagnation. It reached the first peak of 3.08 at Day4 and then deswelled to 2.1 at Day 8. The second peak was observed at Day 16 and the third at Day 29. The hydrogel was explanted on day 31 so further observation was not available. The initial volume swelling rate in vivo is 2.8% per hour.

6.3.3 Comparison of the swelling behaviour in vitro and in vivo

The swelling behaviour of 30%PLGA IPN in vitro and in vivo is compared in Figure 6.8. Both reached a maximum swelling ratio within 4 days. After reaching the first peak of swelling, both experienced the process of swelling being interrupted by short periods of decrease or stagnation.

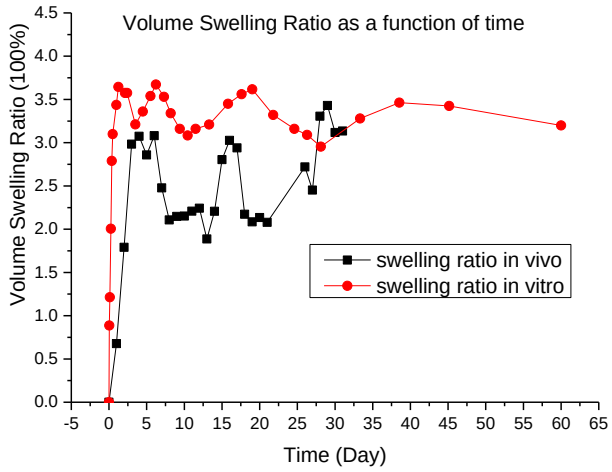

Figure 6.8 In vitro and in vivo volume swelling ratio of 30%PLGA IPN as a function of time

The initial swelling rate is 24.5%/h in vitro and 2.8%/h in vivo. The maximum swelling ratio in vivo is around 0.6 smaller than that in vitro. The time taken to reach the first peak swelling in vivo is 0.58 day longer than that in vitro. In a word, compared to in vitro swelling, in vivo swelling has smaller initial swelling rate, and maximum swelling ratio and takes longer to reach the first maximum swelling.

6.3.4 Histology Results

The histological view of the expanded tissue stained with H&E is shown in Figure 6.9, revealing normal skin layers of keratin, epidermis, and dermis. Figure 6.10 shows the control sample of the natural skin tissue. No obvious difference can be observed between those two samples. The hair follicles and sebaceous glands of the expanded tissue, which are shown in Figure 6.11 and 6.12, are well preserved and seem to be normal compared to those in the natural skin tissue.

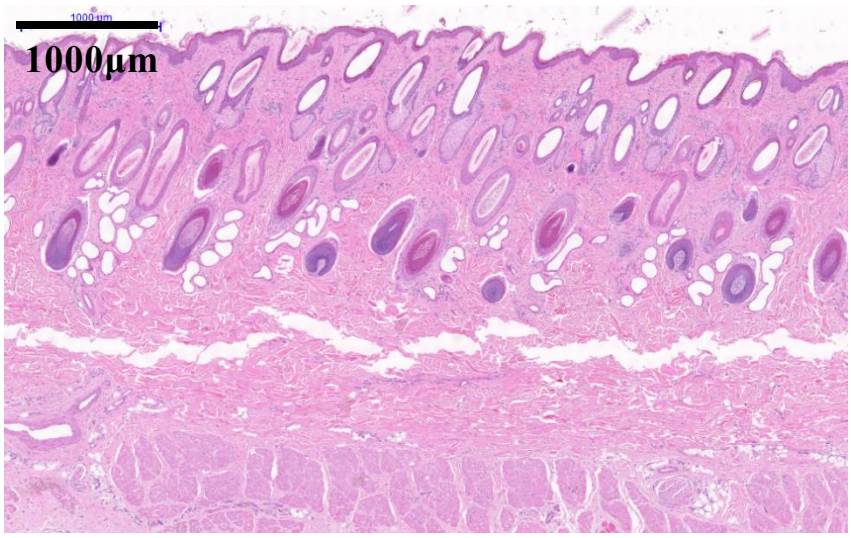

Figure 6.9 The H&E stained histologic section of the expanded tissue containing layers of keratin, epidermis and dermis

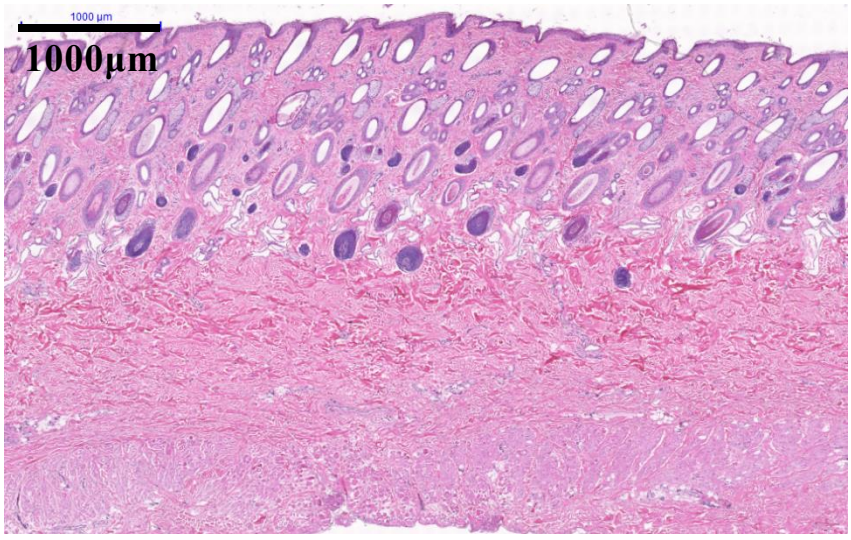

Figure 6.10 The H&E stained histologic section of natural skin tissue containing layers of keratin, epidermis and dermis

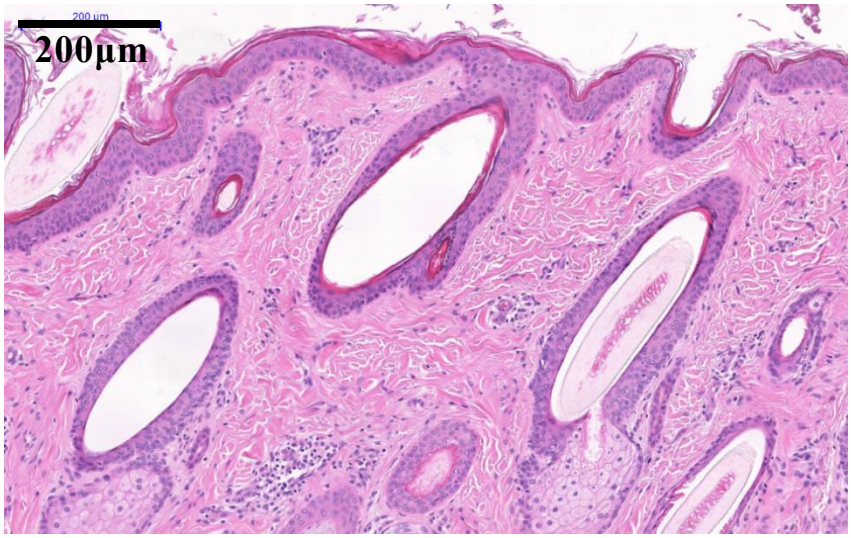

Figure 6.11 Hair Follicles of the expanded skin tissue

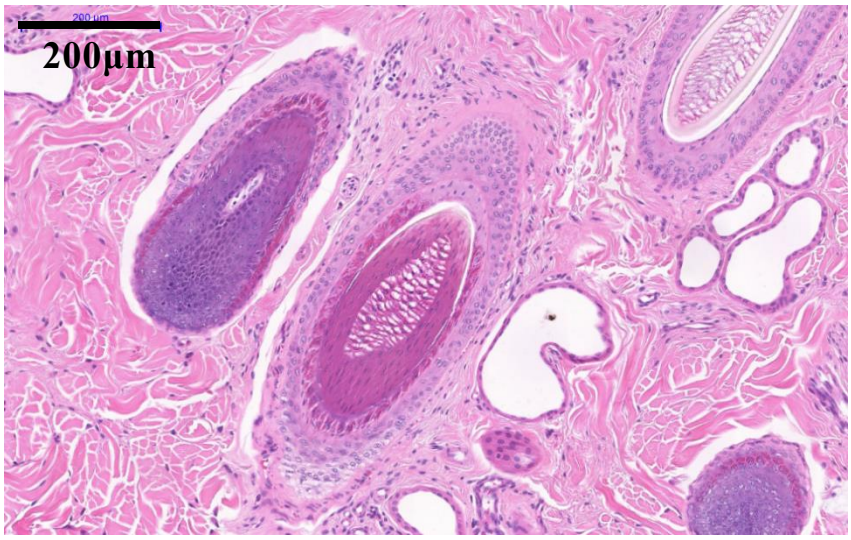

Figure 6.12 Sebaceous glands of the expanded skin tissue

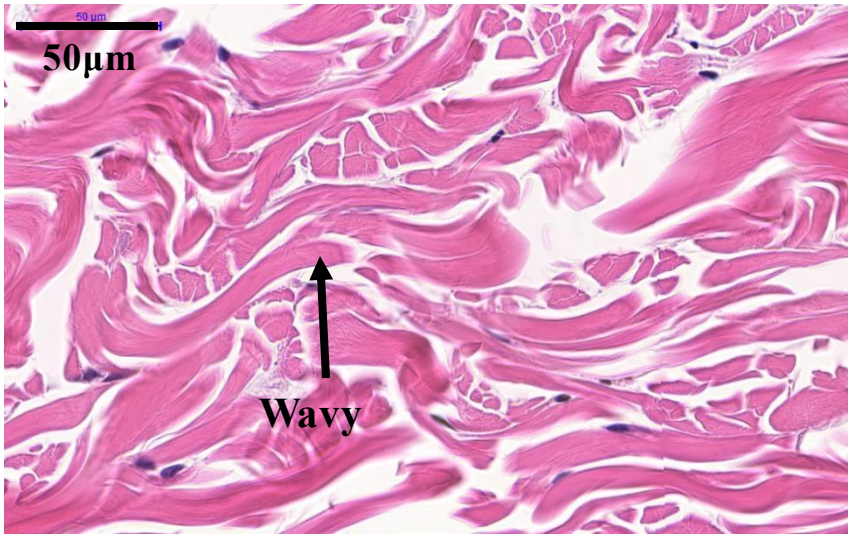

Figure 6.13 Connective tissue of natural skin tissue

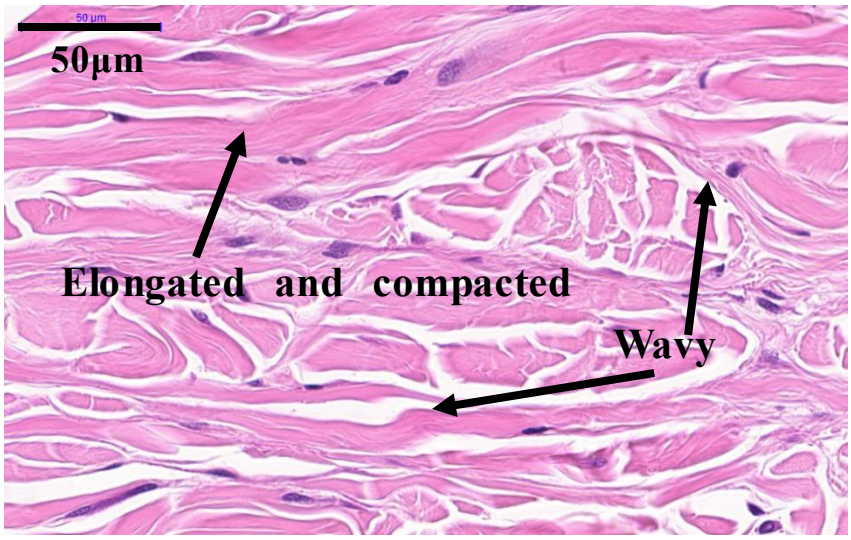

Figure 6.14 Connective tissue of the expanded skin tissue

Figure 6.13 and Figure 6.14 show the dense connective tissue in the dermis layer of the natural skin tissue and the expanded tissue. Both connective tissue show a high proportion of collagen fibers (CF) and sparse fibroblast cells. In natural skin tissue, collagen fibers are randomly oriented, which is described as wavy. In expanded tissue, a mixture of compacted and wavy collagen fibers are observed. Overall, there is not much difference between those two.

The numbers of fibroblasts and inflammatory cells are counted as shown in Figure 6.15 and compared with those from the natural skin tissue. Cells with elongated shape are

assumed to be fibroblasts (orange labels) and cells with a relatively round shape are assumed to be inflammatory cells (green labels).

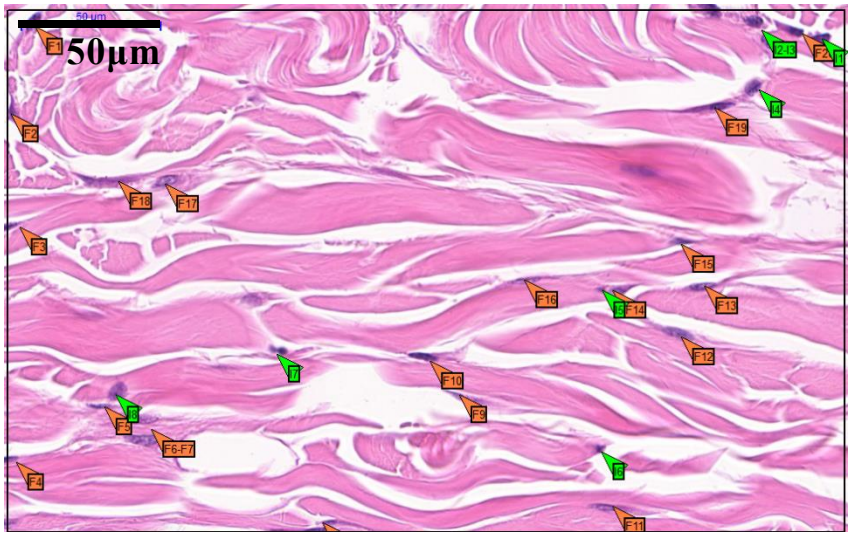

Figure 6.15 Labelling of fibroblasts (orange labels) and inflammatory cells (green labels) in one of the sections of the expanded tissue

The mean value of the thickness of the epidermis, dermis, as well as the average number of fibroblasts and inflammatory cells are summarized in Table 6.1.

Table 6.1 The mean value of the thickness of epidermis, dermis and the average number of fibroblasts and inflammatory cells of the expanded tissue and natural skin tissue

	Natural Skin Tissue	**Expanded Skin Tissue**
Epidermis Thickness	40µm	55µm
Dermis Thickness	2926µm	2849µm
Number of Inflammatory Cells	5	7
Number of Fibroblast	15	20

Overall there is not much difference in the thickness of epidermis or dermis between the expanded tissue and the natural skin tissue. Compared with natural skin tissue, the expanded tissue shows a thicker epidermis and a slightly thinner dermis. The expanded tissue also shows an increased number of fibroblasts and a similar number of inflammatory cells.

6.4 Discussion

6.4.1 In vitro swelling behaviour

The swelling ratio of PLGA IPN in PBS reached the first peak at Day 2.5 with a value of 3.64. This is smaller than the peak value of around 5.5 in distilled water. The most probable reason lies in the decreased osmotic swelling pressure because of the concentration difference of ions inside and outside the hydrogel network[239] and the restorative force from the dermis. Fluctuations in swelling ratio is observed, which is not present in the case of distilled water. Fluctuations in swelling ratio of neutral hydrogels have been observed at various extent in distilled water or PBS, but the reason is not fully revealed yet. PVA/PVP blend hydrogels showed a decrease in swelling after the first peak swelling was reached[240]. This was followed by fluctuations in swelling, which was more pronounced in hydrogels with higher PVP content. It was explained that the instability in swelling was due to the interruption of PVA crystal formation by bulky pyrrolidone rings. PVA hydrogel with PLGA nanoparticles showed fluctuations and instability in swelling in PBS[241] and the reason was not revealed. It is not possible yet to determine the cause of this effect from this work. This is left for the future work.

6.4.2 In vivo swelling behaviour

Most PLGA IPN samples are shown to be unstable in vivo. 6 out of 8 samples dissolved within 15 days after implantation, causing inflammation at the surgical sites and damage to the surrounding tissue. The collapsing in vivo could be attributed to one or combinations of the following reasons:

1. Residue DCM (dichloromethane): Due to the delicate and bulky nature of hydrogel sample, residue DCM during preparation is unavoidable. DCM acts as a plasticizer which increases the chain mobility, as has been discussed in Section

3.4.1. Thus residue DCM acts as a plasticizer in PLGA IPN. As the hydrogel expands in vivo, more fluids come in and also act as plasticizers. Finally, the hydrogel becomes unable to withstand the pressure coming from the stretched skin and collapsed. Moreover, DCM is toxic and volatile, which might cause inflammation in vivo.

2. Accidents: Sheep may rest on its lower limb, which may crush the PLGA IPN. It may also bash it against the fence because of the discomfort followed by tissue expansion. In both cases, the sample would be damaged or destroyed because of its fragile nature.
3. PLGA degradation: Most literature indicate that PLGA biodegradation doesn't involve any enzymatic activity and is purely through hydrolysis[152]. PLGA biodegrades into lactic and glycolic acids, which are metabolized and subsequently eliminated from the body as carbon dioxide and water[242]. PLGA degradation has been reported to be dependent on its composition[243, 244]. The increase in glycolic acid percentage in the oligomers accelerates the degradation because glycolic units are more hydrophilic. PLGA 50:50 was used in this study, which has been reported to exhibit faster degradation than PLGA 65:35, PLGA 75:25 or PLGA 85:15[244]. Also, PLGA 50:50 has been shown to have a significantly faster degradation in vivo as compared to in vitro due to the autocatalytic effect of the acidic environment created by its degradation products[245].

It has been discussed in Section 3.4.2 that PLGA increases the compressive modulus of the IPN hydrogels in water because of the formation of hydrophobic bonding. With PLGA degrading, hydrophobic bonding disappears and the IPN hydrogel loses its mechanical integrity. The loss of mechanical strength by PLGA degradation has been

reported. PLGA 75:25 scaffolds started to become fragile and lose their mechanical properties when PLGA rapidly degraded after 4 weeks and highly degraded samples even fractured in compressive test[246].

According to Figure 6.5, almost 25% mass loss was observed after 10 days in PBS for 33%PLGA IPN, which means 75.8% PLGA degraded within this time. This could lead to a significant decrease in the mechanical integrity of the IPN hydrogel. And it corresponds to most PLGA IPN collapsing in vivo within 15 days.

Thus PLGA degradation seems to be the most possible reason for hydrogel collapsing.

6.4.3 Comparison of the swelling behaviour in vitro and in vivo

According to Figure 6.8, IPN hydrogel shows lower initial swelling rate(2.8%/h) and smaller peak swelling value in vivo than in PBS. Similar findings were also shown for the VP/MMA hydrogel in a rat model[170]. Three reasons may be responsible for this observation:

1. The osmotic pressure is decreased because of the existence of ions in the body fluids, according to equation (2.9) (see Section 2.2.5.4).
2. There is limited body fluids available in vivo.
3. The hydrogel suffers from the restorative force from the skin.

These lead to the decreased maximum swelling ratio and extend the time needed to reach the first maximum swelling.

The fluctuations in the swelling ratio after first peak swelling is reached is observed both in vitro and in vivo. In vitro fluctuations has been reported but different hydrogels have fluctuations to different extent and it is shown to be related with the composition of the hydrogel network[240, 241]. In vivo fluctuations of hydrogels is also common in the clinical reports. For example, acrylamide, acrylic acid and N-isopropylacrylamide hydrogels implanted in a rat model showed constant fluctuations in vivo after the first

peak swelling was reached within 5 days[99].

The reasons for the fluctuations are either not elucidated or not proved. For the IPN hydrogels, further work could be done to wash the hydrogel in distilled water to eliminate unreacted monomers or crosslinker before the experiments and see if the fluctuations still exist.

6.4.4 Histology Results

Collagen fibers appear as wavy in natural skin tissue, meaning they are randomly oriented. For expanded tissue, a mixture of compacted and wavy collagen fibers are observed in Figure 6.14, indicating the collagen is reverting back to its baseline level. Because of the expansion of the hydrogel, the collagen fibers become compacted and elongated or more aligned. After full expansion, the reversion of skin back to its original pre-expansion state has been widely reported [247-249]. For IPN hydrogel, the first peak swelling was observed within 4 days and the histology samples were collected on the 31 days after implantation, thus it displays a mixture of compacted and wavy collagen fibers. Overall, there is not much difference in histology between the expanded tissue and natural skin tissue.

According to Table 6.1, there is not much difference in the thickness of epidermis or dermis between the expanded tissue and natural skin tissue. Expanded tissue shows a slightly thicker epidermis, indicating more activity of the epidermis layer in response to an expanding mass beneath the subcutaneous layer. The thickening of the epidermis layer has been widely observed [170, 248, 250, 251]. This is believed to be the increase in mitotic activity of the keratinocytes in response to epidermal tension, which has been confirmed by autoradiographic labelling[250, 252]. Epidermal tension initiates changes in keratinocyte morphology, which activate biochemical signaling cascades leading to increased mitotic activity and cell proliferation. This finally results in an increase in the

total number of keratinocytes and a net gain in epidermal surface area.

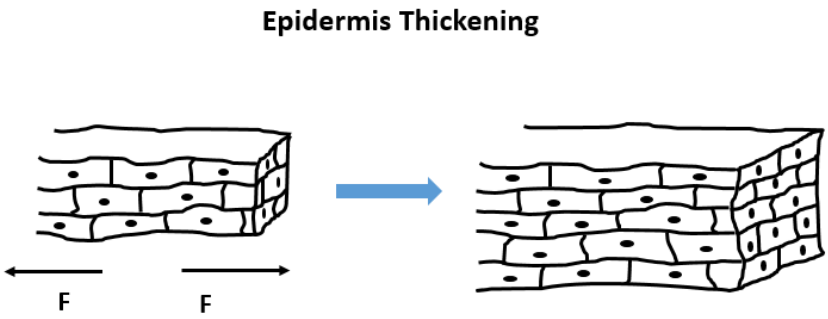

Figure 6.16 Increase in keratinocytes in response to epidermal tension F

$$\delta l = \frac{F \times l}{A \times E} \tag{6.3}$$

Figure 6.16 shows the schematic of the increase in keratinocytes in response to epidermal tension F. l is the original length of the epidermis, δl is the deformation of the epidermis, A is the cross-section area, E is the Young's modulus. According to equation (6.3), in order to minimize its deformation, the epidermis layer will replicate keratinocytes to increase the cross-section area A. This results in the epidermis thickening observed.

The dermis thickness of the expanded skin tissue is slightly smaller than that of natural skin tissue. The increase in epidermis thickness and slight decrease in dermis thickness are in accordance with other clinical reports of tissue expanders [248, 249, 253]. It is generally accepted that the thickness of the epidermis and dermis will return to their baseline level a few weeks or months after the expansion ceases.

There is an increase in the number of fibroblasts in the expanded skin tissue, indicating an increase in collagen synthesis in response to expansion. The increase in fibroblasts corresponds to the large bundles of collagen fibers shown in Figure 6.14, which represent abundant quantities of immature collagen synthesized by the observed elevated numbers of fibroblasts[254]. The number of inflammatory cells is slightly higher than that in natural skin tissue but there is no sign of significant inflammation.

This suggests that little damage is caused to the tissue by PLGA IPN expansion. Uncoated VP/MMA has been shown to have a steep expansion to over 550% in the first 3 days[170], causing skin ulceration and large amount of inflammatory cells in the dermis layer. Rapid expansion of uncoated self-inflating tissue expanders has also been shown to cause bone resorption underneath the hydrogels in a rat model[255]. In the present clinical trials, the successful self-inflating tissue expanders are all coated[170] or prepared with a perforated silicone envelop[13, 256, 257] to slow down the swelling rate and prevent serious inflammation or tissue necrosis. VP/MMA-PLGA IPN hydrogel has shown the same effect while possessing the potential to be crafted because of the absence of a coating or silicone envelop.

Overall, the cell response to the expansion is benign and there is no sign of tissue necrosis, suggesting that PLGA IPN is safe to be used clinically.

6.5 Summary

The swelling behaviour of IPN hydrogel in PBS and in vivo in a sheep model have been shown in this chapter. Both in vitro and in vivo, IPN hydrogel reached peak swelling within 4 days and showed fluctuation in swelling after first peak was reached. Compared to swelling in vitro, in vivo swelling has smaller initial swelling rate, smaller peak swelling and takes longer time to reach first peak swelling. This is believed to be the result of decreased osmotic pressure in an environment that contains ions, the limited body fluids in vivo and the restorative force from the skin.

Samples dissolved within 15 days at 6 out of 8 surgical sites, indicating weakened mechanical strength in vivo. Inflammation and tissue damage were observed where hydrogel dissolved. The residue DCM, accidental damage by the sheep could be the reasons for this collapsing but PLGA degradation induced loss in mechanical integrity seems most likely. 75.8% PLGA was observed degraded in PBS after 10 days, which

corresponds to most PLGA IPN samples dissolving in vivo within 15 days.

At surgical sites where PLGA IPN maintained the swelling until 31 days after implantation, obvious skin tissue expansion was observed without any inflammation or tissue damage.

A histological study of the successfully expanded tissue shows similar structure and cell types compared to natural skin tissue. The thickened epidermis and slightly thinner dermis are in accordance with most clinical reports of tissue expanders. Increased number of fibroblasts indicates increased activity of collagen production. No obvious inflammation or tissue damage was observed and skin appendages are well preserved.

The in vivo study shows that PLGA IPN are effective in swelling at a controlled rate that would avoid tissue damage or tissue necrosis. The histology results demonstrate that they are safe to be used clinically for growing tissue with the same quality as natural skin tissue. The big problem lies in the loss of mechanical integrity as PLGA degrades. Further work could be done to solve this problem by using PLGA with varied composition ratios to prevent PLGA from degrading too fast.

VP/MMA-PLGA IPN hydrogels have shown their biocompatibility and effectiveness in tissue expansion. They are the only kind of tissue expander at present that possesses an appropriate swelling rate for tissue expansion without the clumsiness of a silicone envelop or polymer coatings.

7 Conclusions

This study is concerned with developing a self-inflating hydrogel tissue expander with controlled expansion and the ability to be crafted by surgeons. The current solution to create controlled expansion is preparing additional coatings or semi-permeable membranes, which will be damaged upon crafting and result in a local burst of expansion leading to tissue necrosis. Thus for the first time, an interpenetrating polymer network(IPN) tissue expander has been prepared.

VP/MMA-PLGA IPN hydrogels has been successfully prepared. The incorporation of PLGA decreases the initial swelling rate from 96%/h to a range of 68.4%-10.6%, depending on PLGA weight fraction. This will save the trouble of coatings or membranes, providing an inherent low swelling rate and avoiding tissue necrosis. The swelling period can be increased from 12h to 60h with 62.8%PLGA weight fraction, providing a chronic swelling process which is good for tissue growth. The equilibrium swelling ratio can be controlled by controlling the PLGA weight fraction. The increased polymer volume fraction and hydrophobic bonding with PLGA content result in an increased compressive modulus of the swollen hydrogels.

However, the swelling capacity is largely decreased because of the hydrophobicity increased by the incorporation of PLGA network, which will limit the application of these IPN hydrogels to surgeries that only need small tissue growth, such as anophthalmia, lip, nose or eyelid reconstruction.

IPN or semi-IPN hydrogels with alternative secondary networks have been successfully prepared. VP/MMA-PLA IPN shows the initial swelling rate in the range of 42.1%/h to 8.4%/h, depending on PLGA weight fraction. VP/MMA-PCL semi-IPN shows the initial swelling rate of 29.7%/h at the PCL weight fraction of 23%. The initial swelling rate, equilibrium swelling ratio decrease, while the swelling period and compressive

modulus of the swollen hydrogels increase with the increase in PLA or PCL weight fraction. The initial swelling rate R_i, equilibrium swelling ratio Q_∞ and swelling period T_e have all been shown to scale with the hydrophobicity(water contact angle) of the secondary network, regardless of its glass transition temperature and crosslinking condition. As PCL is the most hydrophobic of the three, VP/MMA-PCL semi-IPN shows the lowest R_i and Q_∞, while the highest T_e at similar weight fraction of the secondary network.

HEMA, VP/HEMA and HEMA/SA bulk hydrogels have been successfully prepared as potential primary networks. HEMA shows a low equilibrium swelling ratio of 0.3 and VP/HEMA shows Q_∞ in the range of 1.2-1.8, which might not be enough to generate tissue expansion. HEMA/SA hydrogels shows superior swelling capacity in the range of 1-47, which is increasing with increasing SA content. But the increased swelling capacity comes at the expense of mechanical properties of the swollen hydrogels. HEMA/SA hydrogels fail to swell in non-polar solvents because of the formation of ions pairs, making it impossible to incorporate hydrophobic polymer network like PLGA through solvent absorption. Considering the existence of ions in physiological conditions and the possible pH change during expansion, the primary network hydrogel should not be electrolyte hydrogels nor pH or temperature sensitive. And for successful preparation of IPN hydrogels through solvent absorption, the primary network has to contain VP.

VP/MMA-PLGA IPN hydrogels have been studied in a sheep model. VP/MMA-PLGA IPN has been shown to be successful in inducing tissue growth with the same quality as natural skin tissue. But a problem exists as the hydrogels tend to lose their mechanical integrity as PLGA rapidly degrades in vivo within 15 days.

In conclusion, VP/MMA-PLGA IPN hydrogels have been successfully prepared for the

first time with controlled expansion and the potential to be crafted by surgeons to best fit the void volume on the patient. The biocompatibility and efficacy of the IPN hydrogels in tissue expansion has been verified by the animal test. It is the only kind of self-inflating tissue expander at present without the clumsiness of an additional coating or membrane, providing a huge advantage in the clinical surgeries. The IPN system applies to a variety of combinations of primary and secondary networks and it remains a huge amount of work to find out the best match. However, these IPN hydrogels are not perfect considering their limited swelling capacity and swelling period.

8 Future Work

The following future work is recommended to further build upon the work presented in this thesis.

1. Dynamic mechanical analysis(DMA) is needed for further investigation into the mechanical properties of these IPN hydrogels and better predict their performance in real situation when implanted under the skin.
2. While the hydrophobicity of the secondary network has been shown to be the dominant factor affecting the swelling behaviour of the IPN hydrogels, more work could be done to change the properties of the primary VP/MMA network, such as VP: MMA ratio and the crosslinker content of VP/MMA to see if there is any difference.
3. SANS has been used to probe the internal structure of VP/MMA-PLGA IPN hydrogels at the fully swollen state. More work could be done using contrast matching. For example, using contrast matching to see only the signal from PLGA network or VP/MMA network under SANS. This could provide a better view of how individual networks in an IPN system behave, which will help improve their properties. SANS can also be used to detect the states of polymer networks from the dry state to various states during expansion, which will be useful in understanding the swelling behaviour.
4. Thermal polymerization is the main method used in this study because of a lack of access to other polymerization techniques. γ-radiation could be used for the polymerization as it generally produces more and stronger crosslinks, which will help with the mechanical properties of the hydrogels at the swollen state.
5. The swelling of VP/MMA-PLGA IPN in PBS and in vivo have shown fluctuations after first peak swelling is reached. It is worth looking into this area

as it is widely observed but rarely explained in this field.

6. VP/MMA-PLGA IPN was prepared with PLGA 50:50 in this study, which has been shown to degrade too quickly and has led to the mechanically collapse in vivo. PLGA 50:50 has the fastest degradation among its series. Thus PLGA 85:15 or PLA could be used for the animal test, which is expected to improve the mechanical properties of the IPN hydrogels in vivo.
7. There are numerous combinations of primary and secondary networks that can be used to create IPN hydrogel tissue expanders. This study is built primarily upon VP/MMA primary network and polyester secondary networks. Thus a lot of potential combinations could be done in search for the desirable properties of tissue expanders.

Bibliography

1. R. E. De Filippo, A. Atala, *Stretch and Growth: The Molecular and Physiologic Influences of Tissue Expansion.* Plastic & Reconstructive Surgery, 2002. **109**(7): p. 2450-2462.
2. F. H. Silver, L. M. Siperko, G. P. Seehra, *Mechanobiology of force transduction in dermal tissue.* Skin Research and Technology, 2003. **9**(1): p. 3-23.
3. T. Takei, I. Mills, K. Arai, B. E. Sumpio, *Molecular basis for tissue expansion: clinical implications for the surgeon.* Plastic & Reconstructive Surgery, 1998. **102**(1): p. 247-258.
4. C. G. Neumann, *The expansion of an area of skin by progressive distention of a subcutaneous balloon; use of the method for securing skin for subtotal reconstruction of the ear.* Plastic & Reconstructive Surgery, 1957. **19**(2): p. 124-130.
5. C. Radovan, *Breast reconstruction after mastectomy using the temporary expander.* Plastic & Reconstructive Surgery, 1982. **69**(2): p. 195-208.
6. R. H. Schuster, S. Rotter, W. Boonn, G. Efron, *The use of tissue expanders in immediate breast reconstruction following mastectomy for cancer.* British Jounal of Plastic Surgery, 1990. **43**(4): p. 413-418.
7. L. A. Gibstein, D. L. Abramson, R. A. Bartlett, D. P. Orgill, J. Upton, J. B. Mulliken, *Tissue expansion in children: a retrospective study of complications.* Annals of Plastic Surgery, 1997. **38**(4): p. 358-364.
8. M. G. Dickson, D. T. Sharpe, *The complications of tissue expansion in breast reconstruction: a review of 75 cases.* British Jounal of Plastic Surgery, 1987. **40**(6): p. 629-635.
9. E. D. Austad, G. L. Rose, *A self-inflating tissue expander.* Plastic & Reconstructive Surgery, 1982. **70**(5): p. 588-594.
10. K. G. Wiese, *Osmotically induced tissue expansion with hydrogels: a new dimension in tissue expansion? A preliminary report.* Journal of Cranio-Maxillofacial Surgery, 1993. **21**(7): p. 309-313.
11. K. G. Wiese, D. E. Heinemann, D. Ostermeier, J. H. Peters, *Biomaterial properties and biocompatibility in cell culture of a novel self-inflating hydrogel tissue expander.* Journal of Biomedical Materials research, 2001. **54**(2): p. 179-188.
12. K. K. Gundlach, R. F. Guthoff, V. H. Hingst, M. P. Schittkowski, U. C. Bier, *Expansion of the socket and orbit for congenital clinical anophthalmia.* Plastic & Reconstructive Surgery, 2005. **116**(5): p. 1214-1222.
13. M. A. Ronert, H. Hofheinz, E. Manassa, H. Asgarouladi, R. R. Olbrisch, *The beginning of a new era in tissue expansion: self-filling osmotic tissue expander--four-year clinical experience.* Plastic & Reconstructive Surgery, 2004. **114**(5): p. 1025-1031.
14. S. Chummun, P. Addison, K. J. Stewart, *The osmotic tissue expander: a 5-year experience.* Journal of Plastic, Recontructive & Aesthetic Surgery, 2010. **63**(12): p. 2128-2132.
15. S. S. Wee, S. E. Logan, T. A. Mustoe, *Continuous versus intraoperative expansion in the pig model.* Plastic & Reconstructive Surgery, 1992. **90**(5): p. 808-814.
16. N. A. Peppas, A. G. Mikos, *Preparation methods and structure of hydrogels.* Hydrogels in Med and Pharm. CRC Press, 1986: p. 1-26.
17. L. B. Peppas, R. S. Harland, *Preparation and characterization of crosslinked hydrophilic networks.* Absorbent Polymer Technology. Elsevier Science Publishers, 1990.
18. O. Wichterle, D. Lim, *Hydrophilic Gels for Biological Use.* Nature, 1960. **185**: p.

117-118.
19. B. V. Slaughter, S. S. Khurshid, O. Z. Fisher, A. Khademhosseini, N. A. Peppas, *Hydrogels in Regenerative Medicine.* Advanced Materials, 2009. **21**(32-33): p. 3307-3329.
20. S. R. Van Tomme, W. E. Hennink, *Biodegradable dextran hydrogels for protein delivery applications.* Expert Review of Medical Devices, 2007. **4**(2): p. 147-164.
21. D. P. Chang, J. E. Dolbow, S. Zauscher, *Switchable Friction of stimulus-responsive hydrogels.* Langmuir, 2007. **23**(1): p. 250-257.
22. A. S. Hoffman, *Hydrogels for biomedical applications.* Advanced Drug Delivery Reviews, 2002. **54**(1): p. 3-12.
23. J. M. Zhu, *Bioactive Modification of Poly(ethylene glycol) Hydrogels for Tissue Engineering.* Biomaterials, 2010. **31**(17): p. 4639-3656.
24. L. Gasperini, J. F. Mano, R. L. Reis, *Natural polymers for the microencapsulation of cells.* Journal of the Royal Society Interface, 2014. **11**(100): p. 1-19.
25. P. Ghi, D. J. T. Hill, A. K. Whittaker, *Water sorption by poly(tetrahydrofurfuryl methacrylate-co-2-hydroxyethyl methacrylate). I. A mass-uptake study.* Journal of Polymer Science Part B: Polymer Physics, 2000. **38**(14): p. 1939-1946.
26. X. H. Lu, X. Cheng, Y. S. Sun, *Study on the swelling behaviour of copolymer hydrogel.* Chinese Journal of Polymer Science, 1986. **2**: p. 134-141.
27. Y. K. Sung, D. E. Gregonis, M. S. John, J. D. Andrade, *Thermal and pulse NMR analysis of water in poly(2-hydroxyethyl methacrylate).* Journal of Applied Polymer Science, 1981. **26**(11): p. 3719-3728.
28. M. B. Ahmad, M. B. Huglin, *States of water in poly(methyl methacrylate-co-N-vinyl-2-pyrrolidone) hydrogels during swelling.* Polymer, 1994. **35**(9): p. 1997-2000.
29. P. J. Flory, *Principles of Polymer Chemistry.* Cornell University Press: Ithaca, New York, 1953.
30. E. V. Farahani, J. H. Vera, D. G. Cooper, M. E. Weber, *Swelling of ionic gels in electrolyte solutions.* Industrial & Engineering Chemistry Research, 1990. **29**(4): p. 554-560.
31. T. P. Davis, M. B. Huglin, *Effect of crosslinker on properties of copolymeric N-vinyl-2-pyrrolidone/methyl methacrylate hydrogels and organogels.* Macromolecular Chemistry and Physics, 1990. **191**(2): p. 331-343.
32. Y. Li, T. Tanaka, *Kinetics of swelling and shrinking of gels.* The Journal of Chemical Physics, 1990. **92**(2): p. 1365-1371.
33. J. Singh, M.E. Weber, *Kinetics of one-dimensional gel swelling and collapse for large volume change.* Chemical Engineering Science, 1996. **51**(19): p. 4499-4508.
34. P. L. Ritger, N. A. Peppas, *A simple equation for description of solute release I. Fickian and non-fickian release from non-swellable devices in the form of slabs, spheres, cylinders or discs.* Journal of Controlled Release, 1987. **5**(1): p. 23-36.
35. T. I. Croll, A. J. O' Connor, G. W. Stevens, J. J. White, *Controllable Surface Modification of Poly(lactic-co-glycolic acid) (PLGA) by Hydrolysis or Aminolysis I: Physical, Chemical, and Theoretical Aspects.* Biomacromolecules, 2004. **5**(2): p. 463-473.
36. V. Dupres, T. Camesano, D. Langevin, A. Checco, P. Guenoun, *Atomic force microscopy imaging of hair: correlations between surface potential and wetting at the nanometer scale.* Journal of Colloid and Interface Science, 2004. **269**(2): p. 329-335.
37. E. A. Vogler, *Structure and reactivity of water at biomaterial surfaces.* Advances in Colloid and Interface Science, 1998. **74**(1-3): p. 69-117.
38. T. P. Davis, M. G. Huglin, *Effect of composition on properties of copolymeric N-*

vinyl-2-pyrrolidone/methyl methacrylate hydrogels and organogels. Polymer, 1990. **31**(3): p. 513-519.
39. T. P. Davis, M. B. Huglin, *Studies on Copolymeric Hydrogels of N-Vinyl-2-pyrrolidone with 2-Hydroxyethyl Methacrylate.* Macromolecules, 1989. **22**: p. 2824-2829.
40. W. N. A. Bergius, L. R. Hutchings, N.M. Sarih, R.L. Thompson, M. Jeschke, R. Fisher, *Synthesis and characterisation of end-functionalised poly(N-vinylpyrrolidone) additives by reversible addition-fragmentation transfer polymerisation.* Polymer Chemistry, 2013. **4**(9): p. 2815-2827.
41. F. Ran, S. Q. Nie, Y. Lu, C. Cheng, D. S. Wang, S. D. Sun, C. S. Zhao, *Comparison of surface segregation and anticoagulant property in block copolymer blended evaporation and phase inversion membranes.* Surface and Interface Analysis, 2012. **44**(7): p. 819-824.
42. Y. K. Son, Y. P. Jung, J. H. Kim, *Preparation and Properties of PEG-modified PHEMA Hydrogel and the Morphological Effect.* Macromolecular Research, 2006. **14**(3): p. 394-399.
43. P. H. Corkhill, A. M. Jolly, C. O. Ng, B. J. Tighe, *Synthetic hydrogels: 1. Hydroxyalkyl acrylate and methacrylate copolymers - water binding studies.* Polymer, 1987. **28**(10): p. 1758-1766.
44. A. Moshaverinia, N. Roohpour, S. Ansari, M. Moshaverinia, S. Schricker, J. A. Darr, U. Rehman, *Effects of N-vinylpyrrolidone(NVP) containing polyelectrolytes on surface properties of conventional glass-ionomer cements(GIC).* Dental Materials, 2009. **25**: p. 1240-1247.
45. A. M. Atta, A. Azim, *Effect of crosslinker functionality on swelling and network parameters of copolymeric hydrogels.* Polymers for Advanced Technologies, 1998. **9**(6): p. 340-348.
46. A. Takahashi, H. Hisatomi, *Hydrophilic monomers suppress the adsorption of plasma protein onto a poly(vinylidene fluoride) membrane.* Molecular Medicine Reports, 2009. **2**: p. 749-752.
47. P. H. Sellenet, B. C. Allison, B. M. Applegate, J. P. Youngblood, *Hydrophilized pyridinium bactericidal polymers.* Polymer Preprints, 2005. **46**(2): p. 1240-1241.
48. Y. Wang, J. H. Ma, S. G. Yang, J. Xu, *PDMAA/Clay nanocomposite hydrogels based on two different initiations.* Colloids and Surfaces A: Physicochemical and Engineering Aspects, 2011. **390**(1-3): p. 20-24.
49. T. P. Davis, M. B. Huglin, D. C. F. Yip, *Properties of poly(N-vinyl-2-pyrrolidone) hydrogels crosslinked with ethyleneglycol dimethacrylate.* Polymer, 1988. **29**(4): p. 701-706.
50. Lee, R. A. Haldon and B. E., *Structure and permeability of porous films of poly(hydroxy ethyl methacrylate).* British Polymer Journal, 1972. **4**(6): p. 491-501.
51. V. Panic, B. Adnadjevic, S. Velickovic, J. Jovanovic, *The effects of the synthesis parameters on the xerogels structures and on the swelling parameters of the poly(methacrylic acid) hydrogels.* Chemical Engineering Journal, 2010. **156**(1): p. 206-214.
52. N. A. Peppas, S. R. Lustig, *The Role of Cross-links, Entanglements, and Relaxations of the Macromolecular Carrier in the Diffusional Release of Biologically Active Materials.* Annals of the New York Academy of Sciences, 1985. **446**: p. 26-40.
53. M. T. Lugo, N. A. Peppas, *Molecular Design and in Vitro Studies of Novel pH-Sensitive Hydrogels for the Oral Delivery of Calcitonin.* Macromolecules, 1999. **32**(20): p. 6646-6651.
54. E. S. Lee, S. W. Kim, S. H. Kim, J. R. Cardinal, H. Jacobs, *Drug release from hydrogel devices with ratecontrolling barriers.* Journal of Membrane Science, 1980. **7**(3): p. 293-303.

55. H. L. Abd El-Mohdy, S. Ghanem, *Biodegradability, antimicrobial activity and properties of PVA/PVP hydrogels prepared by γ-irradiation.* Journal of Polymer Research, 2009. **16**(1): p. 1-10.
56. H. L. Abd El-Mohdy, H. A. Abd El-Rehim, *Radiation synthesis of kappa-carrageenan/acrylamide graft copolymers as superabsorbents and their possible applications.* Journal of Polymer Research, 2009. **16**(1): p. 63-72.
57. J. H. Lee, D. G. Bucknall, *Swelling Behavior and Network Structure of Hydrogels Synthesized Using Controlled UV-Initiated Free Radical Polymerization.* Journal of Polymer Science Part B: Polymer Physics, 2008. **46**(14): p. 1450-1462.
58. K. A. Aquino, *Sterilization by Gamma Irradiation.* Gamma Radiation, Prof. Feriz Adrovic (Ed.), 2012, ISBN: 978-953-51-0316-5, InTech.
59. J. H. Lee, *Development of an anisotropic swelling hydrogel for tissue expansion: control over the degree, rate and direction of hydrogel swelling.* Dissertation, Georgia Institute of Technology, 2008.
60. E. Karadag, D. Saraydin, S. Cetinkaya and O. Guven, *In vitro swelling studies and preliminary biocompatibility evaluation of acrylamide-based hydrogels.* Biomaterials, 1996. **17**(1): p. 67-70.
61. Q. Xing, K. Yates, C. Vogt, Z. C. Qian, M. C. Frost, F. Zhao, *Increasing Mechanical Strength of Gelatin Hydrogels by Divalent Metal Ion Removal.* Scientific Reports, 2014. **4**: p. 1-10.
62. T. Huang, H. G. Xu, K. X. Jiao, L. P. Zhu, H. R. Brown, H. L. Wang, *A Novel Hydrogel with High Mechanical Strength: A Macromolecular Microsphere Composite Hydrogel.* Advanced Materials, 2007. **19**(12): p. 1622-1626.
63. B. Xu, H. J. Li, Y. Y. Wang, G. Z. Zhang, Q. S. Zhang, *Nanocomposite hydrogels with high strength cross-linked by titania.* The Royal Society of Chemistry, 2013. **3**(20): p. 7233-7236.
64. K. Haraguchi, T. Takehisa, *Nanocomposite Hydrogels: A Unique Organic–Inorganic Network Structure with Extraordinary Mechanical, Optical, and Swelling/De-swelling Properties.* Advanced Materials, 2002. **14**(16): p. 1120-1124.
65. J. P. Gong, Y. Katsuyama, T. Kurokawa, Y. Osada, *Double-Network Hydrogels with Extremely High Mechanical Strength.* Advanced Materials, 2003. **15**(14): p. 1155-1158.
66. Y. Okumura, K. Ito, *The Polyrotaxane Gel: A Topological Gel by Figure-of-Eight Cross-links.* Advanced Materials, 2001. **13**(7): p. 485-487.
67. B. H. Cipriano, S. J. Banik, R. Sharma, D. Rumore, W. Hwang, R. M. Briber, S. R. Raghavan, *Superabsorbent Hydrogels That Are Robust and Highly Stretchable.* Macromolecules, 2014. **47**(13): p. 4445-4452.
68. H. Omidian, J. G. Rocca, K. Park, *Elastic, superporous hydrogel hybrids of polyacrylamide and sodium alginate.* macromolecular Bioscience, 2006. **6**(9): p. 703-710.
69. B. Nair, *Final Report On the Safety Assessment of Polyvinylpyrrolidone (PVP).* International Journal of Toxicology, 1998. **17**(4): p. 97-130.
70. H. A. Ravin, A. M. Seligman, And J. Fine, *Polyvinyl Pyrrolidone as a Plasma Expander-Studies on Its excretion, Distribution and Metabolism.* The New England Journal of Medicine, 1952. **247**: p. 921-929.
71. S. Aroua, E. G. V. Tiu, M. Ayer, T. Ishikawa, Y. Yamakoshi, *RAFT synthesis of poly(vinylpyrrolidone) amine and preparation of a water-soluble C60-PVP conjugate.* Polymer Chemistry, 2015. **6**(14): p. 2616-2619.
72. Rehab, M. B. Huglin and M., *Mechanical and thermodynamic properties of butyl acrylate-N-vinylpyrrolidone hydrogels.* Polymer, 1987. **28**(13): p. 2200-2206.
73. O. Guven, M. Sen, *Preparation and characterization of poly(n-vinyl 2-pyrrolidone) hydrogels.* Polymer, 1991. **32**(13): p. 2491-2495.

74. S. Benamer, M. Mahlous, A. Boukrif, B. Mansouri, S. L. Youcef, *Synthesis and characterisation of hydrogels based on poly(vinyl pyrrolidone).* Nuclear Instruments and Methods in Physics Research Section B: Beam Interactions with Materials and Atoms, 2006. **248**(2): p. 284-290.
75. B. K. Mishra, M. Datt, A. K. Banthia, *Synthesis and Characterization of Pectin/PVP Hydrogel Membranes for Drug Delivery System.* AAPS PharmSciTech, 2008. **9**(2): p. 395-403.
76. L. C. Lopergolo, A. B. Lugao, L. H. Catalani, *Direct UV photocrosslinking of poly(N-vinyl-2-pyrrolidone) (PVP) to produce hydrogels.* Polymer, 2003. **44**(20): p. 6217-6222.
77. M. L. Zhai, H. F. Ha, F. Yoshii, K. Makuuchi, *Effect of kappa-carrageenan on the properties of poly(N-vinyl pyrrolidone)/kappa-carrageenan blend hydrogel synthesized by γ-radiation technology.* Radiation Physics and Chemistry, 2000. **57**(3-6): p. 459-464.
78. T. P. Davis, M. B. Huglin *Studies on copolymeric hydrogels of N-vinyl-2-pyrrolidone with 2-hydroxyethyl methacrylate.* Macromolecules, 1989. **22**(6): p. 2824-2829.
79. M. W. Peterseim, M. E. Wilson, *Bilateral intraocular lens implantation in the pediatric population.* Ophthalmology, 2000. **107**(7): p. 1261-1266.
80. P. D. Dalton, L. Flynn and M. S. Shoichet, *Manufacture of poly(2-hydroxyethyl methacrylate-co-methyl methacrylate) hydrogel tubes for use as nerve guidance channels.* Biomaterials, 2002. **23**(18): p. 3843-3851.
81. V. Sankar, T. S. Kumar, K. P. Rao, *Preparation, Characterization and Fabrication of Intraocular Lens from Photo initiated Polymerised Poly(methyl methacrylate).* Trends in Biomaterials and Artificial Organs, 2004. **17**(2): p. 24-30.
82. J. L. Bohnert, T. A. Horbett, B. D. Ratner and F. H. Royce, *Absorption of Proteins From Artificial Tear Solutions to Contact Lens Materials.* Investigate Ophthalmology & Visual Science, 1988. **29**(3): p. 362-373.
83. P. D. Dalton, L. Flynn, M. S. Shoichet, *Manufacture of poly(2-hydroxyethyl methacrylate-co-methyl methacrylate) hydrogel tubes for use as nerve guidance channels.* Biomaterials, 2002(23): p. 18.
84. I. Calderara, R. Gougeon, L. Delmotte, V. Lemee, D. J. Lougnot, *NMR study of the structure and properties of poly(MMA-co-VP) crosslinked hydrogels.* Journal of Polymer Science Part A: Polymer Chemistry, 1997. **35**(17): p. 3619-3625.
85. M. Kita, Y. Ogura, Y. Honda, S. H. Hyon, Y. Ikada, *Evaluation of polyvinyl alcohol hydrogel as a soft contact lens material.* Graefes Arch Clin Exp Ophthalmol, 1990. **228**(6): p. 533-537.
86. M. C. Swan, D. G. Bucknall, T. E. Goodacre, J. T. Czernuszka, *Synthesis and properties of a novel anisotropic self-inflating hydrogel tissue expander.* Acta Biomaterialia, 2011. **7**(3): p. 1126-1132.
87. L. Rees, P. Morris and P. Hall, *Osmotic tissue expanders in cleft lip and palate surgery: a cautionary tale.* Journal of Plastic, Reconstructive & Aesthetic Surgery, 2008. **61**(1): p. 119-120.
88. T. Anwander, M. Schneider, W. Gloger, R. H. Reich, T. Appel, M. Marini, M. Wenghoefer, M Merkx, S. Berge, *Investigation of the expansion properties of osmotic expanders with and without silicone shell in animals.* Plastic & Reconstructive Surgery, 2007. **120**(3): p. 590-595.
89. M. A. Ronert, H. Hofheinz, E. Manassa, H. Asgarouladi, R. R. Olbrisch, *The beginning of a new era in tissue expansion: self-filling osmotic tissue expander-four-year clinical experience.* Plastic & Reconstructive Surgery, 2004. **114**(5): p. 1025-1031.
90. S. Tonge, L. Jones, S. Goodall, B. Tighe, *The ex vivo wettability of soft contact lenses.* Current Eye Research, 2001. **23**(1): p. 51-59.

91. P. H. Corkhill, C. J. Hamilton and B. J. Tighe, *Synthetic hydrogels VI. Hydrogel composites as wound dressings and implant materials.* Biomaterials, 1989. **10**(1): p. 3-10.
92. M. F. Refojo, F. L. Leong, *Poly(methyl acrylate-co-hydroxyethyl acrylate) hydrogel implant material of strength and softness.* Journal of Biomedical Materials Research, 1981. **15**(4): p. 497-509.
93. H. Omidian, *Swelling and Mechanical Properties of Modified HEMA-based Superporous Hydrogels.* Journal of Bioactive and Compatible Polymers, 2010. **25**(5): p. 483-497.
94. J. M. Seidel, S. M. Malmonge, *Synthesis of PolyHEMA Hydrogels for Using as Biomaterials. Bulk and Solution Radical-Initiated Polymerization Techniques.* Materials Research, 2000. **3**(3): p. 79-83.
95. A. K. Bajpai, M. Shrivastava, *Water sorption dynamics of a binary copolymeric hydrogel of 2-hydroxyethyl methacrylate (HEMA).* Journal of Biomaterial Sciences. Polymer Edition, 2002. **13**(3): p. 237-256.
96. J. Q. Wang, W. H. Wu, *Swelling behaviors, tensile properties and thermodynamic studies of water sorption of 2-hydroxyethyl methacrylate/epoxy methacrylate copolymeric hydrogels.* European Polymer Journal, 2005. **41**(5): p. 1143-1151.
97. M. C. Darnell, J. Y. Sun, M. Mehta, C. Johnson, P. R. Arany, Z. G. Suo, D. J. Mooney, *Performance and biocompatibility of extremely tough alginate/polyacrylamide hydrogels.* Biomaterials, 2013. **34**(33): p. 8042-8048.
98. D. Saraydin, S. U. Saraydin, E. Karadag, E. Koptagel, O. Guven, *In vivo biocompatibility of radiation crosslinked acrylamide copolymers.* Nuclear Instruments and Methods in Physics Research Section B: Beam Interactions with Materials and Atoms, 2004. **217**(2): p. 281-292.
99. J. Varga, L. Janovak, E. Varga, G. Eros, I. Dekany, L Kemeny, *Acrylamide, Acrylic Acid and N-Isopropylacrylamide Hydrogels as Osmotic Tissue Expanders.* Skin Pharmacology and Physiology, 2009. **22**(6): p. 305-312.
100. X. Y. Ma, R. L. Wei, J. W. Cheng, J. P. Cai, J. Zhou, *Synthesis and characterization of pectin/poly (sodium acrylate) hydrogels.* Carbohydrate Polymers, 2011. **86**(1): p. 313-319.
101. B. Suthar, H. X. Xiao, D. Klempne, K. C. Frisch, *A review of kinetic studies on the formation of interpenetrating polymer networks.* Polymers of Advanced Technologies, 1996. **7**(4): p. 221-233.
102. L. H. Sperling, *Recent advances in interpenetrating polymer networks.* Polymer Engineering & Science, 1985. **25**(9): p. 517-520.
103. H. L. Frisch, D. Klempner, K. C. Frisch, *A topologically interpenetrating elastomeric network.* Polymer Letters, 1969. **7**(11): p. 775-779.
104. Sperling, L. H., *Introduction to Physical Polymer Science.* John Wiley & Sons. Inc. Publication, 2006.
105. L. H. Sperling, *Interpenetrating Polymer Networks: An Overview.* American Chemical Society, 1994. **1**: p. 3-38.
106. Aylsworth, *US Patent 1, 111, 284*, 1914.
107. J. R. Millar, *Interpenetrating polymer networks. Styrene–divinylbenzene copolymers with two and three interpenetrating networks, and their sulphonates.* Journal of the Chemical Society, 1960. **263**(0): p. 1311-1317.
108. H. L. Frisch, *A Topologically Interpenetrating Elastomeric Network.* Polymer Letters, 1969. **7**(11): p. 775-779.
109. L. H. Sperling, D. W. Friedman, *Synthesis and mechanical behavior of interpenetrating polymer networks: Poly(ethyl acrylate) and polystyrene.* Journal of Polymer Science Part A-2: Polymer Physics, 1969. **7**(2): p. 425-427.
110. S. J. Kim, S. J. Park, M. S. Shin, Y. H. Lee, N. G. Kim, S. I. Kim, *Thermal characteristics of IPNs composed of polyallylamine and chitosan.* Journal of

Applied Polymer Science, 2002. **85**(9): p. 1956-1960.
111. S. J. Lee, S. S. Kim, Y. M. Lee, *Interpenetrating polymer network hydrogels based on poly(ethylene glycol) macromer and chitosan.* Carbohydrate Polymers, 2000. **41**(2): p. 197-205.
112. E. S. Dragan, *Design and applications of interpenetrating polymer network hydrogels. A review.* Chemical Engineering Journal, 2014. **243**: p. 572-590.
113. X. Q. Lu, M. L. Zhao, J. Q. Li, H. F. Ha, *Radiation preparation and thermo-response swelling of interpenetrating polymer network hydrogel composed of PNIPAAm and PMMA.* Radiation Physics and Chemistry, 2000. **57**(3): p. 477-480.
114. J. J. Wang, F. Liu, *Enhanced adsorption of heavy metal ions onto simultaneous interpenetrating polymer network hydrogels synthesized by UV irradiation.* Polymer Bulletin, 2013. **70**(4): p. 1415-1430.
115. J. S. Lee, J. H. Shin, B. K. Kim, Y. S. Kang, *Modification of aqueous polyurethanes by forming latex interpenetrating polymer networks with polystyrene.* Colloid and Polymer Science, 2001. **279**(10): p. 959-965.
116. K. F. Mueller, S. J. Heiber, *Gradient-IPN-modified hydrogel beads: Their synthesis by diffusion–polycondensation and function as controlled drug delivery agents.* Journal of Applied Polymer Science, 1982. **27**(10): p. 4043-4064.
117. D. L. Siegfried, D. A. Thomas, L. H. Sperling, *Thermoplastic interpenetrating polymer network composition and process. US 4468499A, 1984*.
118. E. S. Dragan, M. M. Lazar, M. V. Dinu, F. Doroftei, *Macroporous composite IPN hydrogels based on poly(acrylamide) and chitosan with tuned swelling and sorption of cationic dyes.* Chemical Engineering Journal, 2012. **204-206**: p. 198-209.
119. J. Baselga , I. Hernandez-Fuentes , I. F. Pierola , M. A. Llorente, *Elastic properties of highly crosslinked polyacrylamide gels.* Macromolecules, 1987. **20**(12): p. 3060-3065.
120. S. Atzet, S. Curtin, P. Trinh, S. Bryant, B. Ratner, *Degradable poly(2-hydroxyethyl methacrylate)-co-polycaprolactone Hydrogels for Tissue Engineering Scaffolds.* Biomacromolecules, 2008. **9**(12): p. 3370-3377.
121. R. Tripathi, B. Mishra, *Development and Evaluation of Sodium Alginate–Polyacrylamide Graft–Co-polymer-Based Stomach Targeted Hydrogels of Famotidine.* AAPS PharmSciTech, 2012. **13**(4): p. 1091-1102.
122. L. H. Sperling, *Interpenetrating polymer networks and related materials.* Journal of Polymer Science: Macromolecular Reviews, 1977. **12**(1): p. 141-180.
123. H. Park, D. Kim, *Swelling and mechanical properties of glycol chitosan/poly(vinyl alcohol) IPN-type superporous hydrogels.* Journal of Biomedical Materials Research. Part A, 2006. **78**(4): p. 662-667.
124. S. P. Zhao, D. Ma, L. M. Zhang, *New semi-interpenetrating network hydrogels: synthesis, characterization and properties.* Macromolecular Bioscience, 2006. **6**(6): p. 445-451.
125. A. Lohani, G. Singh, S. S. Bhattacharya, A. Verma, *Interpenetrating Polymer Networks as Innovative Drug Delivery Systems.* Journal of Drug Delivery, 2014: p. 1-11.
126. B. Dhandayuthapani, Y. Yoshida, T. Maekawa, D. S. Kumar, *Polymeric Scaffolds in Tissue Engineering Application: A Review.* International Journal of Polymer Science, 2011: p. 1-19.
127. R. Boppana, R. V. Kulkarni, S. S. Mutalik, C. M. Setty, B. Sa, *Interpenetrating network hydrogel beads of carboxymethylcellulose and egg albumin for controlled release of lipid lowering drug.* Journal of Microencapsulation, 2010. **27**(4): p. 337-344.
128. L. Pescosolido, T. Vermonden, J. Malda, *In situ forming IPN hydrogels of*

calcium alginate and dextran-HEMA for biomedical applications. Acta Biomaterialia, 2011. **7**(4): p. 1627-1633.
129. Nagaoka, S., *Mechanical Properties of Composite Hydrogels.* Polymer Journal, 1989. **21**: p. 847-850.
130. M. R. Guilherme, R. Silva, E. M. Girotto, A. F. Rubira and E. C. Muniz, *Hydrogels based on PAAm network with PNIPAAm included: hydrophilic–hydrophobic transition measured by the partition of Orange II and Methylene Blue in water.* Polymer, 2003. **44**(15): p. 4213-4219.
131. G. H. Chen, A. S. Hoffman, *Temperature-induced phase transition behaviors of random vs. graft copolymers of N-isopropylacrylamide and acrylic acid.* Macromolecular Rapid Communications, 1995. **16**(3): p. 175-182.
132. M. K. Yoo, Y. K. Sung, Y. M. Lee, C. S. Cho, *Effect of polyelectrolyte on the lower critical solution temperature of poly(N-isopropyl acrylamide) in the poly(NIPAAm-co-acrylic acid) hydrogel.* Polymer, 2000. **41**(15): p. 5713-5719.
133. J. T. Zhang, S. X. Cheng and R. X. Zhuo, *Poly(vinyl alcohol)/poly(N-isopropylacrylamide) semi-interpenetrating polymer network hydrogels with rapid response to temperature changes.* Colloid and Polymer Science, 2003. **281**(6): p. 580-583.
134. J. T. Zhang, R. Bhat and K. D. Jandt, *Temperature-sensitive PVA/PNIPAAm semi-IPN hydrogels with enhanced responsive properties.* Acta Biomaterialia, 2009. **5**(1): p. 488-497.
135. C. A. Lorenzo, A. Concheiro, A. S. Dubovik, N. V. Grinberg, T. V. Burova, V. Y. Grinberg, *Temperature-sensitive chitosan-poly(N-isopropylacrylamide) interpenetrated networks with enhanced loading capacity and controlled release properties.* Journal of Controlled Release, 2005. **102**(3): p. 629-641.
136. R. B. Iglesias, R. Coronilla, A. Concheiro, C. A. Lorenzo, *Preparation of chitosan beads by simultaneous cross-linking/insolubilisation in basic pH: Rheological optimisation and drug loading/release behaviour.* European Journal of Pharmaceutical Sciences, 2005. **24**(1): p. 77-84.
137. C. Y. Chang, K. Han, L. Zhang, *Structure and properties of cellulose/poly(N-isopropylacrylamide) hydrogels prepared by IPN strategy.* Polymers for Advanced Technologies, 2011. **22**(9): p. 1329-1334.
138. B. V. Robinson, F. M. Sullivan, J. F. Bozelleca, S. L. Schwartz, *A critical review of the kinetics and toxicology of polyvinylpyrrolidone (Povidone) (1st ed.). Lewis Publishers. 1990.*
139. W. B. Wang, A. Q. Wang, *Synthesis and swelling properties of pH-sensitive semi-IPN superabsorbent hydrogels based on sodium alginate-g-poly(sodium acrylate) and polyvinylpyrrolidone.* Carbohydrate Polymers, 2010. **80**(4): p. 1028-1036.
140. S. P. Jin, M. Z. Liu, F. Zhang, S. L. Chen, A. Z. Niu, *Synthesis and characterization of pH-sensitivity semi-IPN hydrogel based on hydrogen bond between poly(N-vinylpyrrolidone) and poly(acrylic acid).* Polymer, 2006. **47**(5): p. 1526-1532.
141. L. T. Ng, S. Swami, *IPNs based on chitosan with NVP and NVP/HEMA synthesised through photoinitiator-free photopolymerisation technique for biomedical applications.* Carbohydrate Polymers, 2005. **60**(4): p. 523-528.
142. D. K. Singh, A. R. Ray, *Graft copolymerization of 2-hydroxyethylmethacrylate onto chitosan films and their blood compatibility.* Journal of Applied Polymer Science, 1994. **53**(8): p. 1115-1121.
143. P. K. Suresh, S. K. Suryawani and D. Dewangan, *Chitosan-based Interpenetrating Polymer Network(IPN) Hydrogels: A Potential Multicomponent Oral Drug Delivery Vehicle.* International Journal of Comprehensive Pharmacy, 2011. **2**(8): p. 1-8.
144. K. Rao, V. K. Naidu, S. Subha, M. Sairam, T. M. Aminabhavi, *Novel chitosan-*

based pH-sensitive interpenetrating network microgels for the controlled release of cefadroxil. Carbohydrate Polymers, 2006. **66**(3): p. 333-344.
145. M. V. Risbud, A. A. Hardikar, S. V. Bhat and R. R. Bhonde, *pH-sensitive freeze-dried chitosan–polyvinyl pyrrolidone hydrogels as controlled release system for antibiotic delivery.* Journal of Controlled Release, 2000. **68**(1): p. 23-30.
146. X. C. Chen, H. Song, T. Fang, J. X. Bai, J. Xiong, H. J. Ying, *Preparation, characterization, and drug-release properties of pH/temperature-responsive poly(N-isopropylacrylamide)/chitosan semi-IPN hydrogel particles.* Journal of Applied Polymer Science, 2010. **116**(3): p. 1342-1347.
147. J. W. Lee, S. Y. Kim, S. S. Kim, Y. M. Lee, K. H. Lee and S. J. Kim, *Synthesis and characteristics of interpenetrating polymer network hydrogel composed of chitosan and poly(acrylic acid).* Journal of Applied Polymer Science, 1999. **73**(1): p. 113-120.
148. M. Kawase, N. Michibayashi, Y. Nakashima, N. Kurikawa, K. Yagi, T. Mizoguchi, *Application of glutaraldehyde-crosslinked chitosan as a scaffold for hepatocyte attachment.* Biological & Pharmaceutical Bulletin, 1997. **20**(6): p. 708-710.
149. E. E. Schmitt, R. A. Polistina, *Surgical Sutures. US Pat 3297033*, 1967.
150. J. C. Middleton, A. J. Tipton, *Synthetic biodegradable polymers as orthopedic devices.* Biomaterials, 2000. **21**(23): p. 2335-2346.
151. J. M. Moran, D. Pazzano, L. J. Bonassar, *Characterization of Polylactic Acid–Polyglycolic Acid Composites for Cartilage Tissue Engineering.* Tissue Engineering, 2003. **9**(1): p. 63-70.
152. H. K. Makadia, S. J. Siegel, *Poly Lactic-co-Glycolic Acid (PLGA) as Biodegradable Controlled Drug Delivery Carrier.* Polymers for Advanced Technologies, 2011. **3**(3): p. 1377-1397.
153. P. Gentile, V. Chiono, I. Carmagnola, P. V. Hatton, *An Overview of Poly(lactic-co-glycolic) Acid (PLGA)-Based Biomaterials for Bone Tissue Engineering* International Journal of Molecular Sciences, 2014. **15**: p. 3640-3659.
154. Z. Pan, J. D. Ding, *Poly(lactide-co-glycolide) porous scaffolds for tissue engineering and regenerative medicine.* Interface Focus, 2012. **2**(3): p. 366-377.
155. H. Y. Kweon, M. K. Yoo, I. K. Park, T. H. Kim, H. C. Lee, H. S. Lee, J. S. Oh, T. Akaike, C. S. Cho, *A novel degradable polycaprolactone networks for tissue engineering.* Biomaterials, 2003. **24**(5): p. 801-808.
156. M. C. Azevedo, R. L. Reis, M. B. Claase, D. W. Grijpma, J. Feijen, *Development and properties of polycaprolactone/hydroxyapatite composite biomaterials.* Journal of Materials Science: Materials in Medicine, 2003. **14**(2): p. 103-107.
157. Y. J. Park, J. F. Liang, Z. Q. Yang, V. C. Yang, *Controlled release of clot-dissolving tissue-type plasminogen activator from a poly(l-glutamic acid) semi-interpenetrating polymer network hydrogel.* Journal of Controlled Release, 2001. **75**(1-2): p. 37-44.
158. H. W. Kim, C. W. Chung, Y. B. Kim, Y. H. Rhee, *Preparation and hydrolytic degradation of semi-interpenetrating networks of poly(3-hydroxyundecenoate) and poly(lactide-co-glycolide).* International Journal of Biological Macromolecules, 2005. **37**(5): p. 221-226.
159. C. D. Brown, P. S. Stayton, A. S. Hoffman, *Semi-interpenetrating network of poly(ethylene glycol) and poly(D,L-lactide) for the controlled delivery of protein drugs.* Journal of Biomaterials Science. Polymer Edition, 2005. **16**(2): p. 189-201.
160. N. Mohan, P. D. Nair, *Polyvinyl alcohol-poly(caprolactone) Semi IPN scaffold with implication for cartilage tissue engineering.* Journal of Biomedical Materials Research Part B: Applied Biomaterials, 2008. **84B**(2): p. 584-594.
161. F. A. Aouada, M. G. Moura, W. T. L. Silva, E. C. Muniz and L. H. C. Mattoso,

Preparation and characterization of hydrophilic, spectroscopic, and kinetic properties of hydrogels based on polyacrylamide and methylcellulose polysaccharide. Journal of Applied Polymer Science, 2011. **120**(5): p. 3004-3013.
162. A. K. Bajpai, A. Mishra, *Ionizable interpenetrating polymer networks of carboxymethyl cellulose and polyacrylic acid: Evaluation of water uptake.* Journal of Applied Polymer Science, 2004. **93**(5): p. 2054-2065.
163. G. G. Ferrer, M. S. Sanchez, J. L. G. Ribelles, F. R. Colomer, I. C. Cortazar and A. Vidaurre, *Influence of the nature of the porous confining network on the sorption, diffusion and mechanical properties of hydrogel IPNs.* European Polymer Journal, 2010. **46**(4): p. 774-782.
164. W. Montagna, *The Structure and Function of Skin.* New York: Academic Press, 1956.
165. P. G. Agache, C. Monneur, J. L. Leveque, J. De Rigal, *Mechanical properties and Young's modulus of human skin in vivo.* Archives of Dermatological Research, 1980. **269**(3): p. 221-232.
166. Anatomy&Physiology. By OpenStax College [CC BY 3.0 (http://creativecommons.org/licenses/by/3.0)], via Wikimedia Commons, 2013.
167. T. Gibson, R. M. Kenedi, J. E. Craik, *The mobile micro-architecture of dermal collagen: A bio-engineering study.* British Journal of Surgery, 1965. **52**(10): p. 764-770.
168. G. T. Overney, *Human Histology for Amateur Microscopists.* Micscape, online magazine, Microscopy UK copyright, 2002.
169. M. N. Prabhakar, U. S. Rao, P. K. Babu, M. C. S. Subha, K. C. Rao, *Interpenetrating Polymer Network Hydrogel Membranes of PLA and SA for Control Release of Penicillamine Drug.* Indian Journal of Advances in Chemical Science, 2013. **1**(4): p. 240-249.
170. Z. Radzi, *Development of Anisotropic Self-Inflating Tissue Expanders for Clinical Applications.* Thesis. University of Oxford. , 2014.
171. Friebolin, H., *Basic One- and Two-Dimensional NMR Spectroscopy.* 5th Edition. Publisher: Weinheim: Wiley-VCH. ISBN 9783527327829, 2011.
172. *Copyright Polymer Science Learning Center, Department of Polymer Science, The university of Southern Mississippi, 2005.*
173. Hammouda, B., *SANS from Polymers—Review of the Recent Literature.* Polymer Reviews, 2010. **50**(1): p. 14-39.
174. B. Hammouda, *Probing Nanoscale Structures-The SANS Toolbox.* available online at http://www.ncnr.nist.gov/staff/hammouda/the_SANS_toolbox.pdf, 2009.
175. P. Debye, H. R. Anderson, H. Brumberger, *Scattering by an Inhomogeneous Solid. II. The Correlation Function and Its Application.* Journal of Applied Physics, 1957. **28**(6): p. 679-683.
176. B. Hammouda, D. L. Ho, S. Kline, *Insight into Clustering in Poly(ethylene oxide) Solutions.* Macromolecules, 2004. **37**(18): p. 6932-6937.
177. G. Evmenenko, E. Theunissen, K. Mortensen, H. Reynaers, *SANS study of surfactant ordering in κ-carrageenan/cetylpyridinium chloride complexes.* Polymer, 2001. **42**(7): p. 2907-2913.
178. M. Shibayama, T. Tanaka, C. C. Han, *Small angle neutron scattering study on poly(N‐isopropyl acrylamide) gels near their volume‐phase transition temperature.* The Journal of Chemical Physics, 1992. **97**(9): p. 6829-6841.
179. P. Lan, W. Wang, *H-NMR Spectroscopy Analysis of Homo and Copolymers of L-lactic Acid.* Journal of Fiber Bioengineering and Informatics, 2009. **2**(2): p. 137-140.
180. P. T. Knight, K. M. Lee, T. Chung, P. T. Mather, *PLGA−POSS End-Linked Networks with Tailored Degradation and Shape Memory Behavior.*

Macromolecules, 2009. **42**(17): p. 6596-6605.
181. A. Ortega, E. Bucio, G. Burillo, *New Interpenetrating Polymer Networks of N-isopropylacrylamide/N-acryloxysuccinimide: Synthesis and Charaterization.* Polymer Bulletin, 2008. **60**: p. 515-524.
182. B. C. Hancock, G. Zografi, *The Relationship Between the Glass Transition Temperature and the Water Content of Amorphous Pharmaceutical Solids.* Pharmaceutical Research, 1994. **11**(4): p. 471-477.
183. N. Giovambattista, C. A. Angell, F. Sciortino, H. E. Stanley, *Glass-Transition Temperature of Water: A Simulation Study.* Physical Review Letters, 2004. **93**(4): p. 1-4.
184. M. I. Beck, I. Tomka, E. Waysek, *Physico-chemical characterization of zein as a film coating polymer: A direct comparison with ehtyl cellulose.* Interational Journal of Pharmaceutics, 1996. **141**(1-2): p. 137-150.
185. L. J. Gibson, M. F. Ashby, *Cellular Solids: Structure and Properties, second ed. Cambridge University Press, Cambridge.* 1997.
186. J. Zhang, M. F. Ashby, *CPGS Thesis, Engineering Department, Cambridge, UK.* 1988.
187. L. J. Gibson, M. F. Ashby, *The mechanics of three-dimensional cellular materials.* Proc. R. Soc. Lond, 1982. **382**(43-59).
188. L. J. Gibson, *Biomechanics of cellular solids.* Journal of Biomechanics, 2005. **38**: p. 377-399.
189. J. K. Hao, R. A. Weiss, *Viscoelastic and Mechanical Behavior of Hydrophobically Modified Hydrogels.* Macromolecules, 2011. **44**(23): p. 9390-9398.
190. J. Tian, T. A. P. Seery, R. A. Weiss, *Physically Cross-Linked Alkylacrylamide Hydrogels: Phase Behavior and Microstructure.* Macromolecules, 2004. **37**(26): p. 9994-10000.
191. K. Yokota, A. Abe, S. Hosaka, I. Sakai, H. Saito, *A ^{13}C Nuclear Magnetic Resonance Study of Covalently Cross-Linked Gels. Effect of Chemical Composition, Degree of Cross-Linking, and Temperature to Chain Mobility.* Macromolecules, 1978. **11**(1): p. 95-100.
192. M. Ahearne, Y. Yang, A. J. El Haj, K. Y. Then, K. K. Liu, *Characterizing the viscoelastic properties of thin hydrogel-based constructs for tissue engineering applications.* Journal of the Royal Society Interface, 2005. **2**(5): p. 455-463.
193. A. D. Mulliken, M. C. Boyce, *Mechanics of the rate-dependent elastic-plastic deformation of glassy polymers from low to high strain rates.* International Journal of Solids and Structures, 2006. **43**: p. 1331-1356.
194. M. A. Slivka, N. C. Leatherbury, K. Kieswetter, G. G. Niederauer, *Porous, Resorbable, Fiber-Reinforced Scaffolds Tailored for Articular Cartilage Repair.* Tissue Engineering, 2001. **7**(6): p. 767-780.
195. S. Rose, A. Dizeux, T. Narita, D. Hourdet, A. Marcellan, *Time dependence of dissipative and recovery processes in nanohybrid hydrogels.* Macromolecules, 2013. **46**: p. 4095-4104.
196. E. M. Saffer, M. A. Lackey, D. M. Griffin, S. Kishore, G. N. Tew, S. R. Bhatia, *SANS Study of Highly Resilient Poly(ethylene glycol) Hydrogels.* Soft Matter, 2014. **10**(12): p. 1905-1916.
197. C. F. Schmidt, M. Baermann, G. Isenberg, E. Sackmann, *Chain dynamics, mesh size, and diffusive transport in networks of polymerized actin: a quasielastic light scattering and microfluorescence study.* Macromolecules, 1989. **22**(9): p. 3638-3649.
198. M. A. Graf, *Feasibility Study of the Modification of PLGA Thin Layers.* Semester Thesis, Swiss Federal Institute of Technology Zurich, Department of Materials Science, Laboratory for Surface Science and Technology, 2001.
199. D. Saraydin, E. Karadag, O. Guven, *The releases of agrochemicals from*

radiation induced acrylamide/crotonic acid hydrogels. Polymer Bulletin, 1998. **41**(5): p. 577-584.
200. S. Shukla, A. K. Bajpai, J. Bajpai, *Swelling Controlled Delivery of Antibiotic from a Hydrophilic Macromolecular Matrix with Hydrophobic Moieties.* Macromolecules Research, 2003. **11**(4): p. 273-282.
201. K. S. Soppimath, A. R. Kulkarni, T. M. Aminabhavi, *Controlled release of antihypertensive drug from the interpenetrating network poly(vinyl alcohol)-guar gum hydrogel microspheres.* Journal of Blomaterials Science. Polymer Edition, 2000. **11**(1): p. 27-43.
202. C. C. R. Robert, P. A. Buri, N. A. Peppas, *Effect of degree of crosslinking on water transport in polymer microparticles.* Journal of Applied Polymer Science, 1985. **30**(1): p. 301-306.
203. S. H. Gehrke, D. Biren, J. J. Hopkins, *Evidence for Fickian water transport in initially glassy poly(2-hydroxyethyl methacrylate).* J. Biomater. Sci. Polymer Edn, 1994. **6**(4): p. 375-390.
204. N. A. Peppas, A. G. Mikos, *Analysis of Fickian and non-Fickian drug release from polymers.* Pharmaceutica acta Helvetiae, 1985. **60**(4): p. 110-111.
205. P. J. Flory, J. Rehner, *Statistical mechanics of crosslinked polymer networks I. Rubberlike elasticity.* The Journal of Chemical Physics, 1943. **11**(11): p. 512-520.
206. L. M. Muratore, K. Steinhoff, T. P. Davis, *Self-reinforcing hydrogels comprised of hydrophobic methyl methacrylate macromers copolymerised with either N-vinyl-2-pyrrolidone or 2-hydroxyethyl acrylate.* Journal of Materials Chemistry, 1999. **9**: p. 1687-1691.
207. Y. Liu, M. B. Huglin, *Effective crosslinking densities and elastic moduli of some physically crosslinked hydrogels.* Polymer, 1995. **36**(8): p. 1715-1718.
208. A. Augsburg, K. Grundke, K. Poschel, H. J. Jacobasch, A. W. Neumann, *Determination of contact angles and solid surface tensions of poly(4-X-styrene) films.* Acta Polymerica, 1998. **49**(8): p. 417-426.
209. R. M. Ho, Y. W. Chiang, C. C. Lin, B. H. Huang, *Crystallization and Melting Behavior of Poly(ε-caprolactone) under Physical Confinement.* Macromolecules, 2005. **38**: p. 4769-4779.
210. A. Rohadi, R. Endo, S. Tanimoto, S. Sasaki, S. Nojima, *Effects of Molecular Weight and Crystallization Temperature on the Morphology Formation in Asymmetric Diblock Copolymers with a Highly Crystalline Block.* Polymer Journal, 2000. **32**(7): p. 602-609.
211. R. M. Rasal, *Surface and Bulk Modification of Poly(lactic Acid).* Publisher ProQuest, 2009, Contributor Clemson University. Chemical and Biomolecular Engineering.
212. A. V. Janorkar, *Surface modification of poly(L-lactide) films by grafting hydrophilic polymers and branched architectures.* E-Theses. Copyright The University of Hong Kong Libraries.
213. S. G. Hong, G. H. Kim, *Electrospun micro/nanofibrous conduits composed of poly(ε-caprolactone) and small intestine submucosa powder for nerve tissue regeneration.* Journal of Biomedical Materials Research Part B: Applied Biomaterials, 2010. **94**(2): p. 421-428.
214. P. Kaewkong, P. Uppanan, B. Thavornyutikarn, W. Kosorn, W. Janvikul, *Chondrocyte Infiltration and ECM Production on Surface-Treated PCL Scaffolds: Alkaline Hydrolysis versus Plasma Treatment.* International Journal of Boiscience, Biochemistry and Bioinformatics, 2013. **3**(5): p. 429-432.
215. K. A. Athanasiou, C. M. Agrawal, F. A. Barber, S. S. Burkhart, *Orthopaedic applications for PLA-PGA biodegradable polymers.* Arthroscopy: The Journal of Arthroscopic & Related Surgery, 1998. **14**(7): p. 726-737.
216. M. A. Woodruff, D. W. Hutmacher, *The return of a forgotten polymer:*

polycaprolactone in the 21st century. Progress in Polymer Science, 2010. **35**(10): p. 1217-1256.
217. B. D. Ulery, L. S. Nair, C. T. Laurencin, *Biomedical Applications of Biodegradable Polymers.* J Polym Sci B Polym Phys, 2011. **49**(12): p. 832-864.
218. S. Brahim. D. Narinesingh, A. Guiseppi-Elie, *Synthesis and Hydration Properties of pH-Sensitive p(HEMA)-Based Hydrogels Containing 3-(Trimethoxysilyl)propyl Methacrylate.* Biomacromolecules, 2003. **4**(3): p. 497-503.
219. B. Ahmad, S. Bashir, S. Nisa, M. B. Huglin, *Chemically Crosslinked N-Vinyl-2-Pyrrolidone/2-Hydroxyethyl Methacrylate (VP/HEMA) Copolymer for the Controlled Release of Cyclic Oligopeptide.* Turk J Chem, 2004. **28**: p. 279-285.
220. H. Studenovska, M. Slouf, F. Rypacek, *Poly(HEMA) hydrogels with controlled pore architecture for tissue regeneration applications.* Journal of Materials Science: Materials in Medicine, 2008. **19**(2): p. 615-621.
221. B. Podkoscielna, A. Bartnicki, B. Gawdzik, *New crosslinked hydrogels derivatives of 2-hydroxyethyl methacrylate: Synthesis, modifications and properties.* eXPRESS Polymer Letters, 2012. **6**(9): p. 759-771.
222. B. M. Shin, J. H. Kim, D. J. Chung, *Synthesis of pH-responsive and adhesive super-absorbent hydrogel through bulk polymerization.* Macrmolecular Research, 2013. **21**(5): p. 582-587.
223. K. Sohail, I. U. Khan, Y. Shahzad, T. Hussain, N. M. Ranjha, *pH-sensitive polyvinylpyrrolidone-acrylic acid hydrogels: Impact of material parameters on swelling and drug release.* Brazilian Journal of Pharmaceutical Sciences, 2014. **50**(1): p. 173-184.
224. M. F. Refojo, *Hydrophobic Interaction in Poly(2-hydroxyethyl Methacrylate) Homogeneous Hydrogel.* Journal of Polymer Science, 1967. **5**: p. 3103-3113.
225. T. P. Davis, M. B. Huglin, *Some mechanical properties of poly(2-hydroxyethyl methacrylate) gels swollen in water/1,4-dioxane mixtures.* Die Makromolekulare Chemie, Rapid Communications, 1988. **9**(1): p. 39-43.
226. S. G. Levesque, R. M. Lim, M. S. Shoichet, *Macroporous interconnected dextran scaffolds of controlled porosity for tissue-engineering applications.* Biomaterials, 2005. **26**(35): p. 7436-7446.
227. J. K. Kim, M. J. Yaszemski, L. C. Lu, *Three-Dimensional Porous Biodegradable Polymeric Scaffolds Fabricated with Biodegradable Hydrogel Porogens.* Tissue Engineering: Part C, 2009. **15**(4): p. 583-594.
228. N. Annabi, J. W. Nichol, X. Zhong, C. D. Ji, S. Koshy, A. Khademhosseini, F. Dehghani, *Controlling the Porosity and Microarchitecture of Hydrogels for Tissue Engineering.* Tissue Engineering: Part B, 2010. **16**(4): p. 371-383.
229. H. Chavda, C. Patel, *Effect of crosslinker concentration on characteristics of superporous hydrogel.* International Journal of Pharmaceutical Investigation, 2011. **1**(1): p. 17-21.
230. Y. Y. Huang, T. W. Chung, T. W. Tzeng, *Drug release from PLA/PEG microparticulates.* International Journal of Pharmaceutics, 1997. **156**(1): p. 9-15.
231. Y. Zhang, C. C. Chu, *Biodegradable dextran-polylactide hydrogel networks: their swelling, morphology and the controlled release of indomethacin.* Journal of Biomedical Materials Research, 2002. **59**(2): p. 318-328.
232. D. J. T. Hill, M. C. H. Lim, A. K. Whittaker, *Water diffusion in hydroxyethyl methacrylate(HEMA)-based hydrogels formed by γ-radiolysis.* Polymer International, 1999. **48**(10): p. 1046-1052.
233. J. Zarzycki, M. Prassas, J. Phalippou, *Synthesis of glasses from gels: the problem of monolithic gels.* Journal of Materials Science, 1982. **17**(11): p. 3371-3379.
234. S. Sakka, *Handbook of sol-gel science and technology. 1. Sol-gel processing*.

Springer Science & Business Media, 2005.
235. E. Karadag, D. Saraydin, *Swelling of Superabsorbent Acrylamide/Sodium Acrylate Hydrogels Prepared using Multifunctional Crosslinkers.* Turk J Chem, 2002. **26**: p. 863-875.
236. W. F. Lee, Y. H. Lin, *pH-Reversible Hydrogels. IV. Swelling Behavior of the 2-Hydroxyethyl Methacrylate-co-Acrylic Acid-co-Sodium Acrylate Copolymeric Hydrogels.* Journal of Applied Polymer Science, 2001. **81**: p. 1360-1371.
237. T. Ono, T. Sugimoto, S. Shinkai, K. Sada, *Lipophilic polyelectrolyte gels as super-absorbent polymers for nonpolar organic solvents.* Nature Materials, 2007. **6**: p. 429-433.
238. A. R. Khokhlov, E. Y. Kramarenko, *Polyelectrolyte/Ionomer behavior in polymer gel collapse.* Macromolecular Theory and Simulations, 1994. **3**(1): p. 45-59.
239. N. V. Gupta, H. G. Shivakumar, *Investigation of Swelling Behavior and Mechanical Properties of a pH-Sensitive Superporous Hydrogel Composite.* Iranian Journal of Pharmaceutical Research, 2012. **11**(2): p. 481-493.
240. J. Thomas, A. Lowman, M. Marcolongo, *Novel associated hydrogels for nucleus pulposus replacement.* Journal of Biomedical Materials research Part A, 2003. **67A**(4): p. 1329-1337.
241. K. L. Spiller, S. J. Laurencin, A. M. Lowman, *Characterization of the behavior of porous hydrogels in model osmotically-conditioned articular cartilage systems.* Journal of Biomedical Materials Research Part B: Applied Biomaterials, 2009. **90B**(2): p. 752-759.
242. G. Crotts, T. G. Park, *Protein delivery from poly(lactic-co-glycolic acid) biodegradable microspheres: Release kinetics and stability issues.* Journal of Microencapsulation, 1998. **15**(6): p. 699-713.
243. R. A. Miller, J. M. Brady, D. E. Cutright, *Degradation rates of oral resorbable implants (polylactates and polyglycolates): Rate modification with changes in PLA/PGA copolymer ratios.* Journal of Biomedical Materials Research, 1977. **11**(5): p. 711-719.
244. J. M. Anderson, M. S. Shive, *Biodegradation and biocompatibility of PLA and PLGA microspheres.* Advanced Drug Delivery Reviews, 1997. **28**(1): p. 5-24.
245. L. C. Lu, S. J. Peter, M. D. Lyman, H. L. Lai, S. M. Leite, J. A. Tamada, S. Uyama, J. P. Vacanti, R. Langer, A. G. Mikos, *In vitro and in vivo degradation of porous poly(dl-lactic-co-glycolic acid) foams.* Biomaterials, 2000. **21**(18): p. 1837-1845.
246. L. Wu, J. Ding, *In vitro degradation of three-dimensional porous poly(D,L-lactide-co-glycolide) scaffolds for tissue engineering.* Biomaterials, 2004. **25**(27): p. 5821-5830.
247. G. H. Sasaki, *Intraoperative sustained limited expansion (ISLE) as an immediate reconstructive technique.* Clinics in Plastic Surgery, 1987. **14**(3): p. 563-573.
248. E. D. Austad, K. A. Pasyk, K. D. Maclatchey, G. W. Cherry, *Histomorphologic evaluation of guinea pig skin and soft tissue after controlled tissue expansion.* Plastic & Reconstructive Surgery, 1982. **70**(6): p. 704-710.
249. K. A. Pasyk, L. C. Argenta, C. Hassett, *Quantitative analysis of the thickness of human skin and subcutaneous tissue following controlled expansion with a silicone implant.* Plastic & Reconstructive Surgery, 1988. **81**(4): p. 516-523.
250. A. J. Francis, R. Marks, *Skin stretching and epidermopoiesis.* British Journal of Experimental Pathology, 1977. **58**(1): p. 35-39.
251. C. A. Squier, *The stretching of mouse skin in vivo: effect on epidermal proliferation and thickness.* The journal of Investigative Dermatology, 1980. **74**(2): p. 68-71.
252. E. D. Austad, S. B. Thomas, K. Pasyk, *Tissue expansion: dividend or loan?* Plastic & Reconstructive Surgery, 1986. **78**(1): p. 63-67.

253. K. A. Pasyk, E. D. Austad, K. D. Mcclatchey, G. W. Cherry, *Electron microscopic evaluation of guinea pig skin and soft tissues "expanded" with a self-inflating silicone implant.* Plastic & Reconstructive Surgery, 1982. **70**(1): p. 37-45.
254. S. R. Baker, *Fundamentals of expanded tissue.* Head & Neck, 1991. **13**(4): p. 327-333.
255. C. Stuehmer, M. Rucker, P. Schumann, K. H. Bormann, Y. Harder, B. Sinikovic, N. C. Gellrich, *Osseous alterations at the interface of hydrogel expanders and underlying bone.* Journal of Cranio-Maxillofacial Surgery, 2009. **37**(5): p. 258-262.
256. H. J. Uijlenbroek, Y. Liu, J. F. He, C. Visscher, M. A. Van Waas, D. Wismeyer, *Expanding soft tissue with Osmed tissue expanders in the goat maxilla.* Clinical Oral Implant Research, 2011. **22**(1): p. 121-128.
257. P. Abrahamsson, S. Isaksson, G. Andersson, *Guided bone generation in a rabbit mandible model after periosteal expansion with an osmotic tissue expander.* Clinical Oral Implants Research, 2011. **22**(11): p. 1282-1288.